Numerical modelling based on the multiscale homogenization theory. Application in composite materials and structures

Doctoral Thesis

by

Hiram Badillo Almaraz

Advisor: Dr. Sergio H. Oller Martinez

Thesis submitted to the Department of
Strength of Materials and Structural Engineering
in partial fulfillment of the requirements for the degree of

Doctor of Engineering
(Structural Analysis)

at the
Technical University of Catalonia

Barcelona, March 2012

Acta de qualificació de tesi doctoral

Curs acadèmic: 2011-2012

Nom i cognoms

HIRAM BADILLO ALMARAZ

DNI / NIE / Passaport

X5409377F

Programa de doctorat

ANALISIS ESTRUCTURAL

Unitat estructural responsable del programa

DEPARTAMENT DE RESISTÈNCIA DE MATERIALS I ESTRUCTURES A L'ENGINYERIA (RMEE)

Resolució del Tribunal

Reunit el Tribunal designat a l'efecte, el doctorand / la doctoranda exposa el tema de la seva tesi doctoral titulada

NUMERICAL MODELLING BASED ON THE MULTISCALE HOMOGENIZATION THEORY. APPLICATION IN COMPOSITE MATERIALS AND STRUCTURES.

Acabada la lectura i després de donar resposta a les qüestions formulades pels membres titulars del tribunal, aquest atorga la qualificació:

☐ APTA/E ☐ NO APTA/E

(Nom, cognoms i signatura)		(Nom, cognoms i signatura)
President/a		Secretari/ària
(Nom, cognoms i signatura)	(Nom, cognoms i signatura)	(Nom, cognoms i signatura)
Vocal	Vocal	Vocal

_____, _____ d'/de _____ de _____

El resultat de l'escrutini dels vots emesos pels membres titulars del tribunal, efectuat per l'Oficina de Doctorat, a instància de la Comissió de Doctorat de la UPC, atorga la MENCIÓ CUM LAUDE:

☐ SI ☐ NO

(Nom, cognoms i signatura)	(Nom, cognoms i signatura)	(Nom, cognoms i signatura)
Vicerectora de Recerca Presidenta de la Comissió de Doctorat	Cap de l'Oficina de Doctorat Secretària de la Comissió de Doctorat	Secretari/ària del tribunal o membre UPC del tribunal, coordinador o responsable administratiu del programa

Barcelona, _____ d'/de _____ de _____

A mi mamá.
Por ser un ejemplo
de integridad y de fortaleza,
por su amor incodicional
y por ser un ejemplo de vida.

A la memoria de mi padre.
Quien se que está
orgulloso de verme terminar
esta etapa de mi vida.

If we knew what it was we were doing,
it would not be called research,
would it?

Albert Einstein

Acknowledgments

I would like to thank my advisor, Sergio Oller, for his guidance and knowledge transmitted during the duration of this project. For his patience, respect and kindness that showed to me all the time. I would like to thank him especially for his great optimism in the hardest times when nothing seemed to fit.

Special thanks to Eugenio Oñate, for giving me the opportunity to collaborate with him and to learn from him, but above all, for his friendship. My most sincere gratitude and deeply appreciation.

Many thanks to Carlos Labra for his great support on the programming part of this thesis. His role was vital in the assembling of the intricate computational tool elaborated as part of this research.

Thanks also to Xavier Martinez for the thoughtful discussions and the valuable comments he always had about the topic. For letting me use his perturbation method to adapt it onto my research. His support is greatly acknowledged.

To Professor Miguel Cervera for his help on the topic of strain softening. His clarifying ideas were very helpful to fully understand this problem.

Thanks to the fantastic group of people that I've meet during my stay in Barcelona. To Patricia Ruiz, Beniamino Russo, Marina Xicola, Ruben Hernández, Keyla Valle, Nikolaos Galanis, Elli Kartsakli, Oscar Flores, Cristina Heras, Luca Pelà, Rene Brunner, Gregory Savona, Marc Cabeza and Flaminio Minerva. For the great moments that we have had together during all this time. For being my family while I was here.

To rest of the TG team. To Elena Franco, Alejandra García, Miguel Dieguez, Isidro Rivera, Sergio Ferrer, Juan Gaudiano, Miriam Cortes, Ma. Luisa Tapia, Bruno Fernandes and Dominic Villanueva. For making that year when we lived at TG the best year of my life.

To my friends and colleagues at the UPC and CIMNE. To Roberto Lopez, Abel Coll, Pooyan Dadvand, Enrique Escolano, Giovana Gavidia, Claudio Zinggerling, Angel Priegue, Enrique Ortega, Jose Manuel González, Sergio Valero and Josep Lagunas. For all the conversations (and good times) in which work was not the main discussion topic.

To all my brothers and sisters. For encouraging me to continue when things were upside down. Finishing this work wouldn't have been possible without their help and support.

I would like to thank Rosa Ma. Olea, secretary of the RMEE department. For her kindness and willingness to help. Specially for making more bearable the bureaucratic process to present this thesis.

Most of the developments included in this work were possible by the support of several institutions such as the Spanish Government, through the Ministerio de Ciencia y Tecnología ('DELCOM', Ref. MAT2008-02232/MAT), CIMNE (International Center for Numerical Methods in Engineering) and FPU fellowship grant awarded by the Universitat Politècnica de Catalunya (UPC). All these supports are gratefully acknowledged

Abstract

Most of the materials that surround us can be considered as composite materials since nearly all of them, regardless of whether they were man engineered or were naturally formed, are composed by several phases or constituents at certain spatial scale. Based on this fact it can be stated that what determines if a material is considered as homogeneous or as heterogeneous is the scale to which the material is being referenced with.

Within the context of continuum mechanics it is possible nowadays to analyze almost any homogeneous material that has been subjected to some kind of action getting results approximate enough to reality by using numerical methods such as the finite element method, which is based on physical and mathematical concepts developed within the scope of computational mechanics. However, when dealing with composite materials or structures composed by two or more materials, each material that is part of the composite will behave in a characteristic manner according to the physical and chemical properties that govern its behavior. Several methods have emerged over the last decades trying to solve the problem of analyzing composite materials following multi-scale techniques. Among these procedures the homogenization method is one of the most commonly used techniques to estimate or predict the constitutive response at the macroscopic level of the composite based of an analysis performed on a subscale (also known as micro scale).

The majority of the homogenization techniques developed so far are valid only for composites that have a periodic distribution over the entire domain of the structure such that they can be represented by one element representative of the volume (or unit cell) of the composite. However, in some cases the structure or composite may be formed by more than one type of periodic domain distribution, making the existing homogenization techniques not suitable to analyze this type of cases in which more than one recurrent configuration appears. To overcome this problem in this thesis a multi-domain homogenization technique has been proposed and developed based on the solution of a two-scale method, according to the standard continuum mechanics formulations.

Contents

List of Figures

Chapter 1

Introduction

Within the context of solid mechanics, engineering materials can be grouped based on their atomic configuration according to the predominant type of bonding and spatial arrangement of their constituents into four categories: metals and alloys, intermetallics, ceramics and glasses, and polymers (plastics). The type of bonding is an essential factor that influences the physical and mechanical properties and that makes each class of materials unique. Hence, all the materials that fit in these four categories can be defined as homogeneous materials from an engineering point of view.

In the scope of continuum mechanics great efforts have been devoted to represent the behavior of homogeneous materials, by using physical and mathematical concepts, in a sufficient approximated manner. This knowledge has been applied in the field of computational mechanics to obtain the mechanical response of materials when they are subjected to some kind of action, whether external or internal, through several numerical methods, like for example the finite element method [129]. The overall sum of these concepts makes it nowadays possible to analyze almost any sort of homogeneous material getting results approximate enough to what happens in reality.

However, for the case of heterogeneous materials which are formed by the arrangement of two or more components, the combination of the phases occurs without a chemical reaction, in contrast to the cases where this merging produces a new homogeneous material, as it takes place for example, in the case of alloys. As a result, each material that is part of the compound will behave in a characteristic manner according to the physical and chemical properties that govern their behavior. Therefore, the direct application of methods like the finite element method (FEM) is not the most appropriate or effective, since in a conventional FEM analysis the behavior of each component material has to be expressed by a specific constitutive law with particular parameters, this means that the model structure has to be discretized in a way that the size of the finite element is equal at least than the size of the components of the composite. This restriction requires generating a complex discretized model with a large number of finite elements that may

be difficult to achieve and in most of the cases it may demand an extremely expensive computational effort, making the conventional FEM analysis much more difficult to carry out, and in some cases, unfeasible to perform, therefore a more suitable strategy must be implemented to analyze composite materials and to characterize their performance and fracture criterions.

1.1 Background and motivation

Several approaches have been developed to mathematically represent and model composites as heterogeneous materials. Constitutive models have been developed for a large number of composites to asses the global behavior of the compound by obeying the thermodynamic laws in the linear and the non-linear range. The constitutive equations for the so called macro-models have been developed for composites with different arrangements such as materials with long and short fibers, fibers laminated with one or more directions, rolled-laminated with one or more layers, etc. However, these models can not be generalized, since the constitutive relationships were made on a particular composite material and cannot be extrapolated to other composites, therefore they are restricted by this limitation.

Over the last decades various methods have emerged as alternative to the models developed explicitly for a particular composite. From these methods the mixing theory and the homogenization method stand out from the rest since they deal with the problem of modeling composites in a different manner than when using other formulations which consider the composite as a single material with properties inherited from its constituents.

The homogenization theory deals with the problem of analyzing composite materials from an internal point of view of the structure, i.e. the information of the behavior of the whole composite is obtained through a micromechanical study of the properties of the individual components and the interaction between them. The properties are obtained through a subscale (referred as micro scale) level on a representative volume element (RVE) of the composite (also known as unit cell). Several homogenization techniques have been developed through the years, among them: the effective medium approach [26], the self-consistent method [51], the variational boundary method, which provides upper and lower limits of the total stiffness [50, 96], the method of assembly of spheres [49] and the asymptotic homogenization method [7, 103]. The complex task that is required to represent the physical and mechanical microstructural behavior of composites makes that the use of the unit cell to represent the internal structure of the composite altogether with the stable computational methods to be very convenient in most of the cases, in comparison to the rest of procedures developed so far.

In the field of homogenization methods that use the unit cell or RVE approach there is a technique for the computation of composites materials and structures known as multiscale homogenization methods, also known as global-local analysis. This proposal arose

because most of the homogenization methods present a problem when the constitutive behavior becomes non-linear, and a closed form constitutive relation at the macroscopic level is difficult to achieve. The multi-scale modeling procedures do not result in closed form general constitutive equations, since they compute the stress-strain ratio at each point of integration of the macro scale. The stress-strain relationship is obtained by performing a detailed modeling of the internal structure of the composite at the micro scale of the compound. Among the main features of these procedures it was found that: a) the multi-scale methods do not require any constitutive assumption at the macro level; b) are suitable for arbitrary behavior of materials, even physically non-linear response and time-dependency; c) they can provide the possibility to introduce detailed micro structural information, including physical and geometric evolution of the microstructure on the macroscopic analysis; and d) may allow the use of any modeling technique in computing the response at the micro scale, for example, the finite element method, the Voronoi cell method, or numerical methods based on fast Fourier transforms, among others.

More recent works in the homogenization field include computing the response of the composite using a second-order scheme based on the incorporation of the gradient of the macroscopic deformation [58], using artificial neural networks to obtain the numerical response of composites [70], or using a reduced multiple scale eigendeformation-based reduced order homogenization method, which provides considerable computational cost saving in comparison to the direct homogenization method [125].

On the other hand, the mixing theory treats the composite as a homogeneous material which takes into account the behavior of the different constituents according to their proportion in the volume of the composite [120]. The conventional formulation admits that all the composite constituents are subjected to the same strains [42, 92, 93]. New proposals have been made recently in this field which include allowing different strain deformations at different stages [89] and combining the mixing theory with the anisotropy theory by mapping spaces for composite reinforced with fibers [14].

In more recent works, one of the main drawbacks of the mixing theory is addressed by replacing the condition which enforces a parallel distribution of the constituents in the composite for a serial-parallel model, where the iso-strain condition in the fiber direction and the iso-stress condition in the parallel direction is enriched by including a formulation to compute the transverse and shear stiffness in the serial/parallel mixing theory [98]. The micro-mechanical interaction among components is incorporated in an improved formulation of the serial/parallel mixing theory to model delamination and compression failure due to fiber buckling by [71].

From the two theories exposed in the above paragraphs, the mixing theory may result more practical from the point of view of the computational cost, since homogenization is a rather expensive computational process. However, although great advances have been made in this method in terms of including the micro-structural interaction, there are still

some limitations in the formulations proposed recently, such as the inability to model complex arrangements of the internal structure, as in the case when voids are present in the composite domain. Therefore this thesis will be focused on developing a technique of solution for the analysis of composite materials based on the homogenization approach.

Nevertheless, the existing homogenization techniques available present a limitation since most of them are based on the assumption that the entire domain of the composite is represented by one periodic or quasi-periodic distribution as the one shown in Figure 1.1a, being this a limitation since composites may present distributions like the one presented in Figure 1.1b, where two fields of periodic distributions exist within the same domain of the composite, making the existing homogenization techniques not suitable for the analysis of this type of internal structures. Therefore, a different approach has to be followed to exploit the advantages that the homogenization technique offers in the analysis of composite materials in order to analyze structural arrangements that are characterized by more then one periodic distribution.

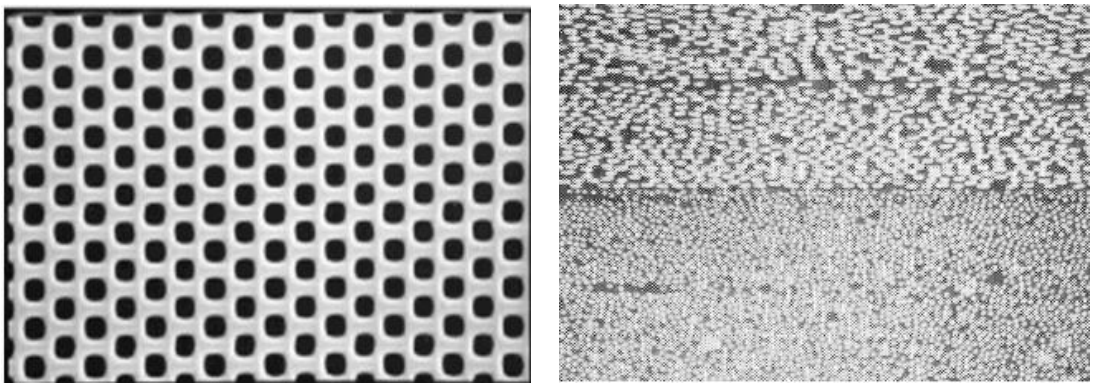

(a) (b)

Figure 1.1: Examples of heterogeneous materials with different micro-structural composites domains: (a) Composite material with one micro-structural periodic distribution; (b) Composite material with two micro-structural periodic distributions

1.2 Objectives of this work

This research is focused on developing a homogenization method using a two-scale first-order approach to find reliable estimates of the linear and non-linear overall response of composite materials and structures that can be defined as periodic or quasi-periodic, according to the internal distribution of the components of the structure. The main objective of this thesis is to take this formulation further in order to develop a homogenization technique to analyze composites or structures which contain more than one periodic distribution over the entire domain of the continuum. In order to achieve this goal, a multi-domain decomposition homogenization approach is proposed. This approach consists in assigning

one different unit cell to each of the different subperiodic domains that forms part of the internal structure of the composite. Each cell may differ in the number of components, may have different physical configurations and different material properties as well. The methodology is focused to be extensible to the solution of composite structures exploiting the same principles that govern the composite material analysis.

The theoretical principles used in multi-scale homogenization are expressed and applied to assemble a computational tool based on two nested boundary value problems represented by a finite element code in two scales: a) one global scale, which treats the composite as an homogeneous material and deals with the boundary conditions, the loads applied and the different periodic (or quasi-periodic) subdomains that may exist in the composite; and b) one local scale, which obtains the homogenized response of the unit cell and that deals with the geometry distribution and with the material properties of the constituents.

Among of the most difficult tasks to compute the response of a composite material is to obtain the non-linear constitutive tensor of the compound since it changes for each load increment and for each iteration of the analysis once the structure has entered in the non-linear range. For this reason, one of the aims of this study is to propose an adequate method to compute the homogenized non-linear tangent constitutive tensor for each unit cell once that the threshold of nonlinearity has been surpassed.

One of the main drawbacks of multi-scale homogenization techniques, is that the computational process is rather expensive, thus a serial computational process would not be the most appropriate to follow. Therefore, among the aims of this research is that in the implementation of the computational tool a parallelization approach must be followed in order to overcome the time-consuming process that homogenization implies.

The final objective of this thesis is to prove that the numerical tool developed is capable of solving composite materials and structures with one or more periodic quasi-periodic internal distributions independently of the material properties and of the geometrical arrangement of the constituents in a reliable way. In order to demonstrate that the formulation proposed works adequately, various examples are solved and their response is compared to benchmark solutions obtained by the FEM.

1.3 Outline

In Chapter 2 the state of the art of the modeling techniques for composite materials is presented. In this chapter a thorough review is made of the main developments of the methods that deal with the analysis of composite materials. The chapter starts with a full description of analytical, semi-analytical and purely numerical methods are presented and described making use of the most outstanding articles found in the literature review until this date. The literature review is mainly dedicated to explain the evolution of the different

multi-scale homogenization techniques starting with the effective medium approximation of Eshelby and following on until what we know nowadays as the multi-scale homogenization. The chapter also includes a review of the mixing theory since this due to the importance of the method and its close relationship with homogenization. The different multi-scale computational techniques found to date based on the homogenization theory are fully described. The main advantages and limitations of each method are pointed out.

Chapter 3 presents the basis of the mathematical approach for solving composites in terms of homogenized variables using a multi-domain decomposition approach. The method is developed within a two-scale framework following a mathematical formulation of first-order. The problem of homogenization is stated based on the relationship between the strains at the macroscopic scale with the transformation experienced by the periodicity vectors that are contained on a structural scale much smaller called micro scale. The application of the periodic boundary conditions in the micro scale is fully described as well as the determination of the average stress measures. The computation of the homogenized linear-elastic and non-linear constitutive tensors of the composite obtained by means of perturbations methods are explained in detail. The problems that may originate the local effects in the global response of the composite when applying the multi-domain decomposition method are discussed thoroughly.

In Chapter 4 the numerical implementation of the homogenization method is presented following a two-scale framework. The numerical implementation is carried out by means of two different programs, one that deals with the macroscopic or global scale and another one that deals with the micro or local scale. Both codes are based on the finite element code PLCd [19]. The nested solution scheme of the finite element implementation is thoroughly described, including the numerical implementation of the procedure to obtain the homogenized constitutive tensors and the description of the approach used for the parallelization routine of the computational tool.

Chapter 5 present an analysis of the effect of softening in two-scale homogenization following a smeared cracked approach. Mesh objectivity is discussed first within the classical FE formulation in one scale and then the concepts exposed are extrapolated into the two-scale homogenization framework. The importance of the element characteristic length in a multi-scale analysis is highlighted in the computation of the specific dissipated energy when strain-softening occurs. The problem of objectivity is addressed by modifying the softening law implemented at the microscale by normalizing it with respect to the element characteristic length at the macroscale.

In Chapter 6 various examples are presented in order to evaluate and explore the capabilities of the computational approach presented in this research. Several aspects have been studied, such as analyzing different composite arrangements that include different types of materials, composites that present softening after the yield point is reached (e.g. damage and plasticity) in composites with one and with several periodic domains using

different unit cell configurations. A comparison of the computational effort of the two-scale homogenization method with respect to the classical one-scale FE method is performed on each of the examples presented. Furthermore, the effectiveness of the method proposed to compute the non-linear tangent tensor of the composite as well as the efficiency of the parallelization process are exposed in one of the examples presented. The main focus of this chapter is to demonstrate the applicability of the extended homogenization proposal and its advantages over the existing homogenization techniques.

Finally in Chapter 7, the main findings of this study are given in terms of a brief summary and in terms of recommendations and conclusions. Future lines of study and future developments are given in this chapter as well.

This page is intentionally left blank.

Chapter 2

Modeling strategies for analyzing composite materials. State of the art

The concept of analyzing composite materials as we know it nowadays came up only until the second half of the twentieth century. Before that date, the analysis and design of this type of materials was carried out mostly by the use of empirical formulas obtained by means of laboratory tests which resembled the behavior of the composite in an acceptable way to some extent in accordance with the existing limitations. The first attempts to analyze composite structures in a more rigorous manner, made use of effective properties which are defined simply in terms of the averages of various quantities over the system (i.e. the components or phases of the composite), however with the appearance of new numerical methods and new computational tools, altogether with the increasingly use of new composite materials in the aviation, automobile, naval and civil industries and in the manufacture of structures which have a significant mechanical performance it has become vital to obtain the response of composites not only in an approximate manner, but to fully understand their linear and nonlinear behavior to predict when and how the damage will occur and the effects that it will produce.

Several numerical and mathematical methods have been developed in recent years to achieve this task in order to take into account the individual properties of the constituents and their geometrical arrangement. In the following paragraphs analytical, semi-analytical and purely numerical methods are presented and described making use of the most outstanding articles found in the literature review until this date. The literature review presented in this chapter it is mainly dedicated to explain the evolution of the different multi-scale homogenization techniques since the research presented in this thesis is developed based on this theory, starting with the effective medium approximation of Eshelby, and following on until what we know nowadays as the multi-scale homogenization. Nevertheless, the review starts with a concise description of the mixing theory, due to the

importance that this branch has on the modeling strategies for analyzing composite materials and because this theory is in some sense some sort of homogenization.

Different multi-scale computational techniques to obtain the numerical response of composite materials based on the homogenization theory are fully described. The main advantages and limitations of each method are pointed out.

2.1 Mixing Theory

The mixing theory arose from the study of two or more interacting continua proposed by Truesdell and Toupin [120]. The theory is established on the principle of interaction between the components of the composite known as the classical theory of mixtures.

Some of the earliest works that applied and further developed this theory are found in Truesdell [119] for linear systems; in Adkins [1] and in Green and Adkins [41] who elaborated general non-linear constitutive equations; in Green and Naghdi [42] who proposed a dynamical theory of the flow relative to two continua; in Bowen and Wiese [9] where a thermo mechanical theory of a diffusing mixture of elastic materials is presented; and in Ortiz and Popov [92] where general constitutive equations are obtained for unreinforced concrete idealized as a composite material.

The classical theory of mixtures is basically based on the assumption that each component contributes in the behavior of the composite in the same proportion as their volumetric proportion allowing the combination of materials which are governed by different constitutive laws and in the assumption that all the component materials which form part of a solid point of the composite have the same deformation as expressed by (2.1).

$$\varepsilon_{ij} = (\varepsilon_{ij})_1 = (\varepsilon_{ij})_2 = \cdots = (\varepsilon_{ij})_n \tag{2.1}$$

where ε_{ij} and $(\varepsilon_{ij})_n$ represent the deformation of the composite and of the $n-th$ component of the composite material, respectively.

The last statement, however, poses a strong limitation in the use of this theory for predicting the behavior of composite materials when they enter in the non-linear range since each component may be experiencing different deformation stages for a given load step. To address this problem, several formulations have emerged from the classical theory of mixtures in order to consider the nonlinearity of each of the components of the composite.

2.1.1 Modifications to the classical theory of mixtures

Among the schemes proposed to modify the classical theory of mixtures there are: the modified classical theory using a serial-parallel model [91, 82], the generalized theory of

mixtures [88], the classical theory of mixtures for large strains [13], the generalized theory of mixtures for large strains [88] and a modification of the theory of mixtures for short reinforcements [14], among others.

Classical theory of mixtures using a serial-parallel model

The modification of the classical theory of mixtures expressed in small strain deformations using a serial-parallel model proposed by Oller et al. [91] and Oñate et al. [82] to represent the behavior of the composite whose constituents are involved in a combination of a serial-parallel behavior implies an automatic adjustment of the properties of the composite taking into account each component and their topological distribution, which allows having different strains in every component that forms part of each point of the solid. The fundamental hypothesis of this generalization of the theory of mixtures is based on the definition of the strain field of the whole as a weighted sum of the contributions of the components in series and parallel as expressed in Equation (2.2).

$$\varepsilon_{ij} = (1 - \aleph)\varepsilon_{ij}^{par} + \aleph\, \varepsilon_{ij}^{ser} \tag{2.2}$$

where ε_{ij}^{ser} and ε_{ij}^{par} represents the serial and parallel strain deformations respectively and $\aleph$ is the coupling parameter that relates the serial-parallel deformation behavior. This parameter varies among 0 and 1 and it indicates the preferred direction of the material behavior at one point and which is associated to the principal stress direction. However, this model has the inconvenient that in order to obtain the value of $\aleph$ a calibration must be made through experimental results.

Generalized theory of mixtures

The generalized theory of mixtures [88] proposes a modification of the serial-parallel classical theory to make possible the resolution of any composite with reinforced matrix, without the limitation required by the classical theory imposed by the deformation compatibility. On the other hand, this new approach automatically adjusts the closure equation of the composite material, this means that it allows to establish the relationship between the deformation in the composite and the deformation in each of the components. This compatibility equation provides the link between the hypotheses of parallel behavior with the hypotheses of behavior in series. For this reason it is called the serial-parallel generalized compatibility hypothesis and can be expressed as:

$$(\varepsilon_{ij})_c = \underbrace{(1 - \chi_c) \cdot I_{ijkl}\, \varepsilon_{kl}}_{(\varepsilon_{ij}^{par})_c} + \underbrace{\chi_c \cdot [(\phi_{ijkl})_c \cdot (\varepsilon_{kl} - \varepsilon_{kl}^{p}) + (\varepsilon_{kl}^{p})_c]}_{(\varepsilon_{ij}^{ser})_c} \tag{2.3}$$

Equation (2.3) can be defined as well as:

$$(\varepsilon_{ij})_c = [(1 - \chi_c) \cdot I_{ijkl} + \chi_c \cdot (\phi_{ijkl})_c] : \varepsilon_{kl} - \chi_c(\widehat{\varepsilon}_{kl}^{p})_c \tag{2.4}$$

where $(\widehat{\varepsilon}^{p}_{kl})_c$ is a plastic strain deformation defined for operational purposes with no physical meaning, obtained from the mean plastic deformation of the composite distributed among its members according to their relationships of stiffness $(\phi_{ijkl})_c(\varepsilon^{p}_{kl})$ and the real plastic deformation of the component $(\varepsilon^{p}_{kl})_c$. While $(\varepsilon_{ij})_c$ is the strain in the c-th component, which can be decomposed into their parallel $(\varepsilon^{par}_{ij})_c$ and series share $(\varepsilon^{ser}_{ij})_c$, while ε_{kl} corresponds to the total deformation that occurs in the composite. In this case the serial-parallel coupling parameter is defined as $0 \leq [\chi_c = sin\alpha_\chi] \leq 1$, with the angle α_χ defined as $0 \leq [\alpha_\chi = (x^{f}_{Loc}, x^{\sigma}_{1})] \leq \pi/2$ which corresponds to the angle that there is between the orientation of the higher principal stress (x^{σ}_{1}) with respect to the fiber orientation (x^{f}_{Loc}). This parameter value is equal to 0 for pure parallel behavior and 1 for pure serial behavior.

Classical theory of mixtures expressed in large strains

The mixing theory of basic substances based on a large strain hypothesis [13] assumes that the atomic diffusion in the absence of deformations is identical for all components of the composite as in the classical theory of mixtures for small strains. The hypothesis must be verified in the referential configuration as in the spatial configuration for each phase. The hypothesis maintains that the substances are involved in the response of the composite in proportion to the volume they occupy in the total volume. The hypothesis emphasizes the relationship between the volume of a component in the spatial and referential configuration, which is given by the determinant of the deformation gradient.

To obtain the constitutive equation for the reference and the spatial configurations, the problem is divided into an elastic problem in small strains and in a problem in large plastic strains, in which the free energy is uncoupled in elastic and inelastic energy. The solution is given by an iterative procedure and it starts by computing the strain increments at the reference configuration and then through tensor transport operations the strain tensor is obtained in the updated configuration. The integration of the constitutive equation for each phase of the composite is obtained in the updated configuration as well. Each of these phases may have different types of constitutive behavior (plasticity, damage, etc.), which in turn may be isotropic or anisotropic. Once the stress state of each component is obtained the stresses and the constitutive tensor of the composite are computed according to the classical mixing theory. The stresses and the tangent elastoplastic constitutive tensor are pulled back to the reference configuration. Finally the internal forces are computed and the balance with the external forces applied is verified until convergence of the method is obtained.

Generalized theory of mixtures expressed in large strains

The generalized theory of mixtures made in large strains [88] provides a conceptual extension of the definitions made for the classical theory of mixtures in large strains. The formulation begins from the hypothesis of non-compliance of the compatibility of deformations expressed in Equation (2.1). The constitutive equations are obtained in the reference

and the updated configuration following a formulation similar to that for the classical theory of mixtures in large strains, with and essential difference which lies in the definition of the strains in each configuration, since it is not unique for all the components. According to this definition, the stresses of the composite in the referential configuration **S** are computed according to Equation (2.5).

$$\mathbf{S} = \sum_{c=1}^{n} k_c[(1-\chi_c)\cdot\mathbf{I}_4 + \chi_c\cdot(\Phi)_c]^T : [(\mathbf{C}^S)_c : [(1-\chi_c)\cdot\mathbf{I}_4 + \chi_c\cdot(\Phi)_c] : (\mathbf{E}^e)_c] \quad (2.5)$$

In the updated configuration, the Kirchoff stresses τ are given by Equation (2.6) .

$$\begin{aligned} \boldsymbol{\tau} &= \sum_{c=1}^{n} k_c[(1-\chi_c)\cdot\mathbf{I}_4 + \chi_c\cdot(\phi)_c]^T : [(\mathbf{c}^\tau)_c : [(1-\chi_c)\cdot\mathbf{I}_4 + \chi_c\cdot(\phi)_c] : (\mathbf{e}^e)_c] \\ &= J\,\boldsymbol{\sigma} \end{aligned} \quad (2.6)$$

where k_c is the volumetric participation of the c-th component obtained in function of the Jacobian J, $\mathbf{I}_4$ is the fourth order identity tensor, $(\Phi)_c$ and $(\phi)_c$ are the serial behavior factor for the referential and the updated configurations respectively, $(\mathbf{C}^S)_c$ and $(\mathbf{c}^\tau)_c$ represent the real anisotropic tangent constitutive tensor for the c-th component for each configuration, $(\mathbf{E}^e)_c$ and $(\mathbf{e}^e)_c$ are the elastic deformations of each phase in the reference and updated configurations respectively and $\boldsymbol{\sigma}$ is the Cauchy stress tensor.

The rest of the procedure to compute the response of the composite is similar to the one explained in the classical theory of mixtures for large strains in the preceding paragraphs.

Theory of mixtures for composites with short length fibers

The classical mixing theory formulation is oriented towards composites reinforced with long fibers, in which the kinematic condition of the classical or generalized formulation is met. However, for the case of short length reinforcements as the aspect ratio of the fiber decreases, the status of the fiber-matrix compatibility is no longer fulfilled due to local effects. This means that the compatibility condition expressed in Equation (2.1) is not satisfied due to the different strains that occur between the matrix and fibers.

One way to incorporate the contribution of the short fiber reinforcement to the theory of mixtures is by introducing the average stress along the fiber as shown in Equation (2.7).

$$\begin{aligned} \overline{\sigma}_f &= C_f^\sigma \left[1 - \frac{tanh(\beta\frac{l}{2})}{(\beta\frac{l}{2})}\right] Em \\ &= \widetilde{C}_f^\sigma E_m \end{aligned} \quad (2.7)$$

where C_f^σ is the Young's modulus of the reinforcement, E_m is the longitudinal strain of the matrix component, $\overline{\sigma}_f$ is the average Young's modulus of the reinforcement or homogenized module and the parameter β is given by Equation (2.8).

$$\beta = \sqrt{\frac{G_c}{C_f^\sigma} \frac{2\pi}{A_f \, ln\left(\frac{r'}{r}\right)}} \tag{2.8}$$

where G_c is the transverse elastic modulus of the composite, A_f is average cross section of the reinforcement and r' is the mean distance between the reinforcing fibers.

The definition of an average Young's modulus of the reinforcement which is function of the length of the fibers and of the geometrical parameters of the composite and that has a magnitude smaller than the real one, makes clear that its participation on the composite mechanical properties depend not only on the intrinsic properties of the reinforcement, but also on the overall properties of the matrix-reinforcement assemblage. This concept, based on the homogenization of the tension along the fiber expressed in Equation (2.7) can be extended to a two or tri dimensional plane through simplification, giving as a result the following approximate constitutive tensor for short-fiber reinforcement.

$$\widetilde{\mathbf{C}}_f^S = \mathbf{C}_f^S \left[1 - \frac{tanh(\beta \frac{l}{2})}{(\beta \frac{l}{2})}\right] \tag{2.9}$$

where $\mathbf{C}_f^S$ is the orthotropic constitutive tensor of the reinforcement in the referential configuration. The constitutive tensor transported to the updated configuration is affected by the fiber length, the cross section and the separation among the fibers that form the reinforcement. It can be obtained by pushing forward the constitutive tensor of the reference configuration as shown in Equation (2.10).

$$\widetilde{\mathbf{c}}_f^{\,\tau} = \vec{\phi}(\widetilde{\mathbf{C}}_f^S) \tag{2.10}$$

Thus the present formulation allows taking into account the loss of effectiveness of reinforcement in the response due to the short length effects which prevents a total transfer of forces from the matrix to the reinforcement. The stresses in the referential and in the updated configurations are given by Equations (2.11) and (2.12) respectively.

$$\begin{aligned} \mathbf{S} &= \underbrace{\left[1 - \frac{tanh(\beta \frac{l}{2})}{(\beta \frac{l}{2})}\right]}_{\varsigma} \mathbf{C}_f^S : \mathbf{E}^e \\ &= (\widetilde{\mathbf{C}}_f^S) : \mathbf{E}^e \end{aligned} \tag{2.11}$$

$$\boldsymbol{\tau} = \widetilde{\mathbf{c}}\,{}^{\tau}_{f} : \mathbf{e}^{e} \tag{2.12}$$

The factor ς represents the correction factor due to the presence of short length reinforcement in the composite.

2.1.2 Latest developments on the theory of mixtures

Among the latest developments in the engineering field that have been attempted to analyze composite materials using the theory of mixtures there is the serial-parallel (SP) continuum approach proposed by Rastellini et al. [99] and a later work based on the SP mixing theory proposed by Martinez et al. [71], among others.

The serial-parallel (SP) continuum approach

The SP continuum approach was developed assuming that the components of the composite behave as parallel materials in the fibers alignment direction and as serial materials in the orthogonal direction. The aim of the SP model is to make the composite behavior dependent on the constitutive laws of the component materials according to their volume fraction and to their morphological distribution inside the composite.

The proposed composite model is based on the appropriate management of the constitutive models of component phases within a continuum framework by making use of suitable 'closure equations' that characterize the composite micro-mechanics.

Two versions of the model were formulated, which basically differ in the closure equations taken into account: a) the basic serial parallel (BSP) model, which inherits the closure equations that considers an iso-strain hypothesis in the fiber direction and an iso-stress hypothesis in the transversal direction and; b) the enriched serial parallel (ESP) model, which is formulated to improve the transverse and shear stiffness underestimated by the BSP model.

The formulation asserts that the constitutive laws of each phase still apply to their corresponding volume-averaged state variables. However, this definition by itself is not sufficient for the characterization of a material model, since the definition of a material model for the composite needs the introduction of additional equations that specify somehow the interaction between the component phases. These additional sets of equations are referred to as closure equations. Therefore the resulting material model depends crucially on the adopted specific closure equation that characterizes the mechanical interaction at the micro-scale.

The equations governing the BSP model problem are:

(1) the constitutive laws of both materials:

$$\begin{aligned} {}^{c}\dot{\boldsymbol{\sigma}} &= {}^{c}\boldsymbol{g}\left({}^{c}\boldsymbol{\varepsilon},\ {}^{c}\boldsymbol{\beta},\ {}^{c}\dot{\boldsymbol{\varepsilon}}\right) \\ {}^{c}\dot{\boldsymbol{\beta}} &= {}^{c}\boldsymbol{h}\left({}^{c}\boldsymbol{\varepsilon},\ {}^{c}\boldsymbol{\beta},\ {}^{c}\dot{\boldsymbol{\varepsilon}}\right) \end{aligned} \tag{2.13}$$

where ${}^{c}\dot{\boldsymbol{\sigma}}$ and ${}^{c}\dot{\boldsymbol{\beta}}$ are the evolution of stress and of the internal variables. With $c = f, m$, where the superscripts f and m denote the quantities related to each of the two phases of the composite, the fiber and matrix respectively.

(2) the equation relating average strains and stresses:

$$\begin{aligned} \boldsymbol{\varepsilon} &= {}^{f}k\,{}^{f}\boldsymbol{\varepsilon} + {}^{m}k\,{}^{m}\boldsymbol{\varepsilon} \\ \boldsymbol{\sigma} &= {}^{f}k\,{}^{f}\boldsymbol{\sigma} + {}^{m}k\,{}^{m}\boldsymbol{\sigma} \end{aligned} \tag{2.14}$$

where $\boldsymbol{\varepsilon}$ and $\boldsymbol{\sigma}$ are the composite total strain and the stress, respectively. The volumetric fraction of each phase is denoted by ${}^{f}k$ and ${}^{m}k$.

(3) the BSP closure equations:

$$\begin{aligned} {}^{m}\boldsymbol{\varepsilon}_{\mathbf{P}} &= {}^{f}\boldsymbol{\varepsilon}_{\mathbf{P}} \\ {}^{m}\boldsymbol{\sigma}_{\mathbf{S}} &= {}^{f}\boldsymbol{\sigma}_{\mathbf{S}} \end{aligned} \tag{2.15}$$

where the subscripts **S** and **P** correspond to the serial and parallel behavior of each component of the composite.

To solve the system of nonlinear equations that defines the BSP problem a specifically devised Newton-Raphson iterative strategy was developed. The proposed algorithm is a general solver for composites that uses the constitutive models of component materials as 'black boxes'. The composite algorithm makes use of the following serial-parallel decomposition tangent operators.

$${}^{c}\mathbf{C} = \begin{bmatrix} \dfrac{\partial^{c}\boldsymbol{\sigma}_{\mathbf{P}}}{\partial^{c}\boldsymbol{\varepsilon}_{\mathbf{P}}} & \dfrac{\partial^{c}\boldsymbol{\sigma}_{\mathbf{P}}}{\partial^{c}\boldsymbol{\varepsilon}_{\mathbf{S}}} \\ \\ \dfrac{\partial^{c}\boldsymbol{\sigma}_{\mathbf{S}}}{\partial^{c}\boldsymbol{\varepsilon}_{\mathbf{P}}} & \dfrac{\partial^{c}\boldsymbol{\sigma}_{\mathbf{S}}}{\partial^{c}\boldsymbol{\varepsilon}_{\mathbf{S}}} \end{bmatrix} = \begin{bmatrix} {}^{c}\mathbf{C}_{\mathbf{PP}} & {}^{c}\mathbf{C}_{\mathbf{PS}} \\ \\ {}^{c}\mathbf{C}_{\mathbf{SP}} & {}^{c}\mathbf{C}_{\mathbf{SS}} \end{bmatrix} \tag{2.16}$$

with

$$\begin{aligned} {}^{c}\mathbf{C}_{\mathbf{PP}} &= \mathbf{P}_{\mathbf{P}} : {}^{c}\mathbf{C} : \mathbf{P}_{\mathbf{P}} \\ {}^{c}\mathbf{C}_{\mathbf{PS}} &= \mathbf{P}_{\mathbf{P}} : {}^{c}\mathbf{C} : \mathbf{P}_{\mathbf{S}} \\ {}^{c}\mathbf{C}_{\mathbf{SP}} &= \mathbf{P}_{\mathbf{S}} : {}^{c}\mathbf{C} : \mathbf{P}_{\mathbf{P}} \\ {}^{c}\mathbf{C}_{\mathbf{SS}} &= \mathbf{P}_{\mathbf{S}} : {}^{c}\mathbf{C} : \mathbf{P}_{\mathbf{S}} \end{aligned} \tag{2.17}$$

with $c = m, f$. Where ${}^{c}\mathbf{C}$ is the consistent tangent operator for each component, $\mathbf{P_P}$ is the fourth order tensor that recovers the parallel components of stress and strain and $\mathbf{P_S} = \mathbf{I} - \mathbf{P_P}$ recovers the complementary serial component.

The serial part of matrix strain ${}^{m}\boldsymbol{\varepsilon}_{\mathbf{S}}$ is selected as the independent variable of the Newton–Raphson scheme to be adopted for the composite algorithm. Then for the initial approximation of the unknown it may be stated that the strain increment maintains the tangent evolution of the previous step. The constitutive model of each material are evaluated to determine their constitutive tangent tensors corresponding to the previous step (time t). The increment of the unknown is determined assuming that the total strain increment is distributed among the constituent materials according to their previous step tangent stiffness as show in Equation (2.18).

$$[{}^{m}\boldsymbol{\Delta\varepsilon}_{\mathbf{S}}]_0 = \mathbf{A} : \left[{}^{f}\mathbf{C}_{\mathbf{SS}} : [\boldsymbol{\Delta\varepsilon}_{\mathbf{S}}] + {}^{f}k \left({}^{f}\mathbf{C}_{\mathbf{SP}} - {}^{m}\mathbf{C}_{\mathbf{SP}} \right) : [\boldsymbol{\Delta\varepsilon}_{\mathbf{P}}] \right] \tag{2.18}$$

with

$$\begin{aligned} [\boldsymbol{\Delta\varepsilon}_{\mathbf{S}}] &= {}^{t+\Delta t}[\boldsymbol{\varepsilon}_{\mathbf{S}}] - {}^{t}[\boldsymbol{\varepsilon}_{\mathbf{S}}] \\ [\boldsymbol{\Delta\varepsilon}_{\mathbf{P}}] &= {}^{t+\Delta t}[\boldsymbol{\varepsilon}_{\mathbf{S}}] - {}^{t}[{}^{m}\boldsymbol{\varepsilon}_{\mathbf{S}}] \end{aligned} \tag{2.19}$$

and

$$\mathbf{A} = \left({}^{m}k^{f}\mathbf{C}_{\mathbf{SS}} + {}^{f}k^{m}\mathbf{C}_{\mathbf{SS}} \right)^{-1} \tag{2.20}$$

The initial value of the unknown is given by Equation (2.21).

$$[{}^{m}\boldsymbol{\varepsilon}_{\mathbf{S}}]_k = {}^{t}[{}^{m}\boldsymbol{\varepsilon}_{\mathbf{S}}] + [{}^{m}\boldsymbol{\Delta\varepsilon}_{\mathbf{S}}]_0 \tag{2.21}$$

where the index k denotes the iteration number of the Newton-Rhapson method.

The total strain tensors of the components in serial and parallel are determined as a function of the updated value of $[{}^{m}\boldsymbol{\varepsilon}_{\mathbf{S}}]_k$.

$$[{}^m\boldsymbol{\varepsilon}]_k = [{}^m\boldsymbol{\varepsilon}_{\mathbf{P}}] + [{}^m\boldsymbol{\varepsilon}_{\mathbf{S}}]_k \tag{2.22}$$

$$\left[{}^f\boldsymbol{\varepsilon}\right]_k = \left[{}^f\boldsymbol{\varepsilon}_{\mathbf{P}}\right] + \left[{}^f\boldsymbol{\varepsilon}_{\mathbf{S}}\right]_k \tag{2.23}$$

with

$$\begin{aligned} [{}^m\boldsymbol{\varepsilon}_{\mathbf{P}}] &= \left[{}^f\boldsymbol{\varepsilon}_{\mathbf{P}}\right] = {}^{t+\Delta t}[\boldsymbol{\varepsilon}_{\mathbf{P}}] \\ \left[{}^f\boldsymbol{\varepsilon}_{\mathbf{S}}\right]_k &= \frac{1}{{}^f k}{}^{t+\Delta t}[\boldsymbol{\varepsilon}_{\mathbf{S}}] - \frac{{}^m k}{{}^f k}[{}^m\boldsymbol{\varepsilon}_{\mathbf{S}}]_k \end{aligned} \tag{2.24}$$

The residue is evaluated and its norm is compared against the tolerance to find out whether the stress equilibrium has been achieved as expressed in Equations (2.25) and (2.26).

$$[\boldsymbol{\Delta\sigma}_{\mathbf{S}}]_k = [{}^m\boldsymbol{\sigma}_{\mathbf{S}}]_k - \left[{}^f\boldsymbol{\sigma}_{\mathbf{S}}\right]_k \tag{2.25}$$

$$\|[\boldsymbol{\Delta\sigma}_{\mathbf{S}}]_k\| \leq Tolerance \tag{2.26}$$

with

$$\begin{aligned} [{}^m\boldsymbol{\sigma}_{\mathbf{S}}]_k &= \mathbf{P}_{\mathbf{S}} : [{}^m\boldsymbol{\sigma}]_k \\ \left[{}^f\boldsymbol{\sigma}_{\mathbf{S}}\right]_k &= \mathbf{P}_{\mathbf{S}} : \left[{}^f\boldsymbol{\sigma}\right]_k \end{aligned} \tag{2.27}$$

In case the equilibrium expressed in Equation (2.26) is not fulfilled, the initial prediction of the matrix strain tensor has to be corrected means of the Jacobian of the residual forces. The Jacobian is obtained deriving the residue function with respect to the unknown as expressed in Equation (2.28).

$$\mathbf{J} = [{}^m\mathbf{C}_{\mathbf{SS}}]_k + \frac{{}^m k}{{}^f k}\left[{}^f\mathbf{C}_{\mathbf{SS}}\right]_k \tag{2.28}$$

with

$$\begin{aligned} [{}^m\mathbf{C}_{\mathbf{SS}}]_k &= \mathbf{P}_{\mathbf{S}} : [{}^m\mathbf{C}]_k : \mathbf{P}_{\mathbf{S}} \\ \left[{}^f\mathbf{C}_{\mathbf{SS}}\right]_k &= \mathbf{P}_{\mathbf{S}} : \left[{}^f\mathbf{C}\right]_k : \mathbf{P}_{\mathbf{S}} \end{aligned} \tag{2.29}$$

And the update of the matrix of strains corresponding to the serial part of the composite is expressed as:

$$[{}^m\boldsymbol{\varepsilon}_{\mathbf{S}}]_k := [{}^m\boldsymbol{\varepsilon}_{\mathbf{S}}]_k - [\mathbf{J}]_k^{-1} : [\boldsymbol{\Delta\sigma}_{\mathbf{S}}]_k \tag{2.30}$$

where $k := k + 1$.

In addition to the iterative algorithm, for the solution of the global problem, the computation of the tangent operator is also required. If the global problem is solved via the finite element method, for example, this operation must be accomplished when assembling the elemental stiffness matrix. The derivation of the tangent matrix for the composite is performed by linearizing the equations governing the BSP model.

In the BSP model and other formulations, the iso-strain in parallel direction and iso-stress in serial directions are the usual and simpler assumptions when obtaining the properties of composite material. However the iso-stress assumption in orthogonal directions to the fiber (pure serial behavior in transverse directions) constitutes a lower bound for the transverse/shear stiffness of the composite and for this reason the BSP model needs to be enriched in order to predict the transversal/shear behavior more accurately, therefore an evolved version of the method is proposed in the enriched serial/parallel (ESP) model.

The governing equations for the ESP model maintain the structure of the governing equations for the BSP model (Equations (2.13-(2.15)). The only difference is the use different close equations to provide a better account for the internal morphology of the composite and for the stress/strain concentration in the matrix as expressed as follows:

$$({}^m\boldsymbol{\varepsilon})^* = [{}^m\mathbf{K}]^{-1} :^m \boldsymbol{\varepsilon} \tag{2.31}$$

$$({}^m\boldsymbol{\sigma})^* = {}^m\mathbf{K} : {}^m\boldsymbol{\sigma} \tag{2.32}$$

$$({}^m\mathbf{C})^* = {}^m\mathbf{K} : {}^m\mathbf{C} : {}^m\mathbf{K} \tag{2.33}$$

with

$${}^m\mathbf{K} = \mathbf{P_P} : \mathbf{I} : \mathbf{P_P} +^m \gamma \mathbf{P_S} : \mathbf{I} : \mathbf{P_S} \tag{2.34}$$

It is worth noting here that ${}^f\gamma = 1$, since the fiber stress remains uniform, and consequently it is not necessary to perform a change of variables for fiber material. The gamma parameter ${}^m\gamma$ may be obtained through experimental calibration with lamina tests data, or through analytical analysis. By means of micro-mechanical considerations it is possible to adopt values of the gamma parameter ${}^m\gamma$ in terms of the fiber volume fraction ${}^fk$ and the ratio between fiber and matrix Young modules $R = {}^fE/{}^mE$. The following analytical expression for the parameter ${}^m\gamma$ is proposed:

$${}^m\gamma = \frac{\sqrt{\eta + \omega^2 (1 - \eta)}}{\eta + \omega (1 - \eta)} \tag{2.35}$$

where $\omega = 1 + (R-1)\sqrt{f^k}$ and $\eta = \frac{\sqrt{f^k}}{1+f^k}$

Among the findings obtained in this study, it was concluded that the basic SP model, as well as the inverse rule of mixtures method, underestimates the experimental values, while the enriched SP model obtains an approximation to experimental data as good as the one given by the Halpin-Tsai equation. Nevertheless, the Halpin-Tsai equation is restricted to the linear elastic region, while the ESP model also provides answers for the non-linear behavior of the composite material.

In a more recent work, Martinez et al. [71], implemented the serial-parallel mixing theory developed by [99] in a tri-dimensional framework and applied it for the numerical simulation of structures of reinforced concrete (RC) retrofitted with carbon fiber reinforced polymers (CFRP). In this study a different way to compute the tangent constitutive tensor of the composite is proposed. The tensor of each constitutive material of the composite is obtained by means of a perturbation method. The perturbation method consists in defining n small perturbations of the strain vector, to obtain n stress vectors that will be used to obtain the numerical expression of the tangent constitutive tensor.

In order to simulate the effect of performing a structural retrofitting in a damaged structure, it is necessary to add the CFRP reinforcement once the structure is already damaged. With the purpose to simulate this process in a more realistic manner, a construction-stages algorithm is implemented in a finite element code, so that it is possible to add or remove structural elements during the calculation process.

The algorithm proposed enables to run the numerical simulation for the desired load cases, with only some structural elements active in the structure. Being possible to add new elements at a given load case, without interrupting the calculation process. These elements must be free from strains and stresses when they are activated. All this process if performed within the serial-parallel mixing theory framework.

From the results achieved in this research it was proved that the serial-parallel rule of mixtures can obtain the composite performance by combining the mechanical behavior of its different constituents, each one computed with its own specific constitutive equation. The theory takes into account the directional behavior of the fiber constituents and it is capable of reproducing with great accuracy the effect that CFRP have for retrofitting RC structures.

2.2 The effective medium approximation and the self-consistent method

The multi-scale homogenization theory as it is known nowadays is the result of numerous research studies, most of them based on the mean field model approach originally proposed

by Eshelby [26]. The method consisted in finding the stresses present in an elastic solid when a region of the solid called 'inclusion' suffered a change of shape and size which is represented by a uniform homogeneous deformation as if the surrounding material were absent. This study demonstrated that the results for the inclusion can be used to find how a uniform stress is disturbed by the presence of an ellipsoidal cavity, or more generally an ellipsoidal region whose elastic constants differ from those of the remaining material. The Eshelby problem is posed as follows:

- Consider an infinite, isotropic, linear elastic solid, with (homogeneous) Young's modulus E and Poisson's ratio ν.
- The solid is initially stress free, with displacements, strains and stresses u_{ij}=ε_{ij}=σ_{ij}=0.
- Some unspecified external agency then induces a uniform 'transformation strain' ε^T_{ij} inside an ellipsoidal region, with semi-axes a_1, a_2, a_3 centered at the origin as shown in Figure 2.1. The 'transformation strain' can be visualized as an anisotropic thermal expansion if the ellipsoidal region were separated from the surrounding elastic solid, it would be stress free, and would change its shape according to the strain tensor ε^T_{ij}.

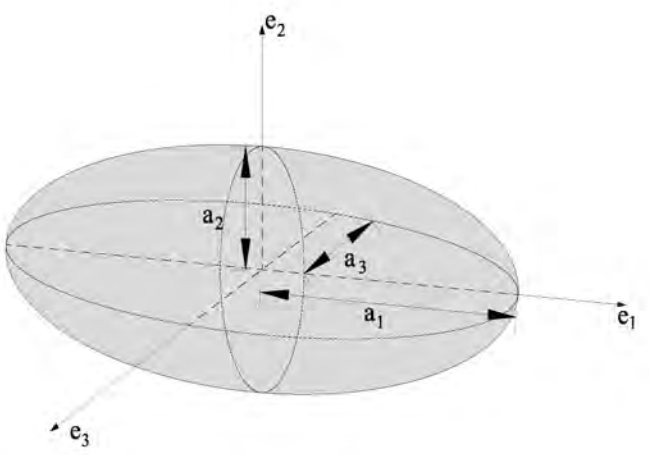

Figure 2.1: Ellipsoidal region of the Eshelby inclusion

- Because the ellipsoid is encapsulated within the surrounding elastic solid, the stress, strains and displacement fields are induced throughout the elastic solid. These fields must be defined carefully because the initial configuration for the solid could be chosen in a number of different ways. From now on, u_i will denote the displacement of a material particle from the initial, unstressed configuration, as the transformation strain is introduced. The total strain is defined as:

$$\varepsilon_{ij} = \frac{1}{2}\left[\frac{\partial u_i}{\partial x_j} + \frac{\partial u_j}{\partial x_i}\right] \tag{2.36}$$

- Inside the ellipsoid, the total strain consists of the transformation strain together with an additional elastic strain $\varepsilon_{ij} = \varepsilon^T_{ij} + \varepsilon^e_{ij}$. Outside the ellipsoid, $\varepsilon_{ij} = \varepsilon^e_{ij}$. The stress in the solid is related to the elastic part of the strain by the usual linear elastic equations:

$$\sigma_{ij} = \frac{E}{1+\nu}\left[\varepsilon^e_{ij} + \frac{\nu}{1-2\nu}\varepsilon^e_{kk}\delta_{ij}\right] \tag{2.37}$$

The Eshelby solution gives full expressions for these fields. It has proved to be one of the most important solutions in all of linear elasticity: it is of some interest in its own right, because it provides some insight into the mechanics of phase transformations in crystals. More importantly, a number of very important boundary value problems can be solved by manipulating the Eshelby solution. These include (i) the solution for an ellipsoidal inclusion embedded within an elastically mismatched matrix; (ii) the solution for an ellipsoidal cavity in an elastic solid; (iii) solutions for circular and elliptical cracks in an elastic solid. In addition, the Eshelby solution is used extensively in theories that provide estimates of elastic properties of composite materials.

Several authors directly further developed the work of Eshelby. Among those, Hashin [49], obtained bounds and expressions for the elastic moduli of two- or many-phase non-homogeneous materials by an approximate method based on the variational theorems of the theory of elasticity and on a concentric-spheres model. On another study, Budiansky [12] performed a heuristic analysis for the determination of the elastic moduli of a composite material in which the several constituents are isotropic and elastic. The results are applied to heterogeneous materials composed of contiguous, more-or-less spherical grains of each of the phases. Mori and Tanaka [77], developed a method of calculating the average internal stress in the matrix of a material containing inclusions with transformation strain. In this work it was shown that the average stress in the matrix is uniform throughout the material and independent of the position of the domain where the average treatment is carried out.

The self-consistent method may be considered as an extension of the effective medium approach. It was initially proposed by Kröner [60] for determining the macroscopic properties of polycrystalline solids. This model is particularly suitable for multiphase materials where the different phases are arranged to form an interpenetrating network as it happens with the different grains of a polycrystalline material. Hill [51] estimates the macroscopic elastic moduli of two-phase composites by a method that takes account of the inhomogeneity of stress and strain in a way similar to the Hershey-Krner theory of crystalline

aggregates. The phases may be arbitrarily aeolotropic and may have any concentration, but are required to have the character of a matrix and effectively ellipsoidal inclusions.

A more elaborate version of the classic self-consistent approach is the model of three phases or generalized self-consistent model due to Christensen and Lo [18], which is resolved when the inclusions are spheres or undefined cylindrical fibers. This method which is not strictly a mean-field model embeds the spherical inclusions (or fibers) in a spherical (or cylindrical) cap which represents the elastic properties of the matrix. The set formed by the inclusion and the matrix in turn is embedded in a medium infinity with the effective properties of multiphase materials to be determined. The values of the effective elastic constants of the material are obtained integrating the differential equations governing the behavior of the three-phase boundary conditions and of the applied loads. This model is particularly suitable for multiphase materials whose microstructure is formed for spherical inclusions of different sizes that are scattered in an array.

Gonzalez and Llorca [40] developed a model to compute the mechanical behavior of two-phase materials including the effects of damage or changes in the volume fraction of each phase. The material is represented by an interpenetrating network of randomly distributed spheres, which are assumed to behave as isotropic elasto-plastic solids. The incremental self-consistent method is used to compute the effective response of the material as well as the elastic stress redistribution due to damage or phase change. As an example, the model predictions are compared with experimental results previously reported for a particle-reinforced metal-matrix composite, which presented damage by reinforcement fracture during deformation. The model predictions, in terms of the tensile stress-strain curve, the onset of plastic instability and the fraction of broken particles at failure were in reasonable agreement with the experimental results, showing the ability of the model to simulate the mechanical behavior of two-phase materials including the effect of damage.

In more recent works, Molinari [76] proposed average models for heterogeneous viscoplastic and elastic-viscoplastic materials, which in turn formed the basis of the work of Mercier et al. [72], in the validation of an interaction law for the Eshelby inclusion problem in elasto-viscoplasticity. Based on these two studies described previously, Mercier and Molinari [73] proposed two self-consistent schemes for perfectly disordered materials and a Mori-Tanaka model for composite materials. The first self-consistent scheme is valid for any non-linear behavior. The second one is dedicated to aggregates with phases having the same strain rate sensitivity. It is observed that predictions based on the second self-consistent model are accurate as compared to exact solutions obtained previously for a two-phase linear viscoelastic aggregate. Both schemes provide similar results when non-linear behavior is considered. Meanwhile the proposed Mori-Tanaka scheme predicts accurately overall response of the composite material and the scheme is able to capture the strain and stress histories in the phases, crucial when dealing for example with residual stresses after metal forming operation.

2.3 Bounding methods

The bounding methods are based on providing lower and upper limits to the total stiffness of the system. These methods generally try to obtain simpler expressions for the effective thermo-elastic properties looking for the minimum potential and complementary energies.

2.3.1 The classical bounds of Voigt and Reuss

The idea of the Voigt approach was to determine elastic moduli by averaging stresses, expressed in terms of strains, over all possible pattern orientations. The method assumes strain uniformity throughout the composite material as in case of the specimen presented in Figure 2.2, in which a n-phase composite of domain Ω is being loaded axially causing a uniform field of strains.

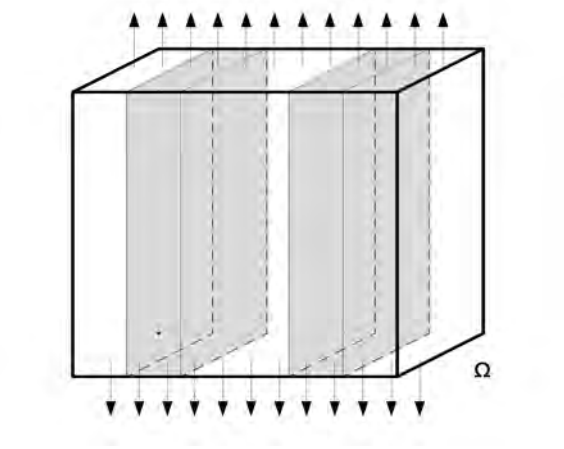

Figure 2.2: Specimen with strain uniformity in all the phases of the composite

Taking into account that the average strain of each phase is equal to the applied strain, then a rule-of-mixture-type assumption as expressed in Equation (2.38) can be made.

$$\boldsymbol{\varepsilon}_{(\Omega)} = \boldsymbol{\varepsilon}_{(\Omega_1)} = \boldsymbol{\varepsilon}_{(\Omega_2)} = \cdots = \boldsymbol{\varepsilon}_{(\Omega_n)} \tag{2.38}$$

where $\boldsymbol{\varepsilon}_{(\Omega)}$ and $\boldsymbol{\varepsilon}_{(\Omega_n)}$ represent the deformation of the composite and of the $n-th$ component of the composite material, respectively. Considering that each component is linear-elastic, the stresses can be obtained for each phase as:

$$\boldsymbol{\sigma}_{(\Omega_1)} = \mathbf{C}_1 \cdot \boldsymbol{\varepsilon}_{(\Omega)},\ \boldsymbol{\sigma}_{(\Omega_2)} = \mathbf{C}_2 \cdot \boldsymbol{\varepsilon}_{(\Omega)},\ \cdots, \boldsymbol{\sigma}_{(\Omega_n)} = \mathbf{C}_n \cdot \boldsymbol{\varepsilon}_{(\Omega)} \tag{2.39}$$

$\mathbf{C}_n$ represents the elasticity tensor of the $n-th$ component of the composite material. The force balance in the load direction can be written as:

$$\boldsymbol{F}_{(\Omega)} = \boldsymbol{\sigma}_{(\Omega)} \cdot A_{(\Omega)} = \boldsymbol{F}_{(\Omega_1)} + \boldsymbol{F}_{(\Omega_2)} \ldots + \boldsymbol{F}_{(\Omega_n)} \tag{2.40}$$

where

$$\boldsymbol{F}_{(\Omega_1)} = \boldsymbol{\sigma}_{(\Omega_1)} \cdot A_{(\Omega_1)},\ \boldsymbol{F}_{(\Omega_2)} = \boldsymbol{\sigma}_{(\Omega_2)} \cdot A_{(\Omega_2)},\ \cdots, \boldsymbol{F}_{(\Omega_n)} = \boldsymbol{\sigma}_{(\Omega_n)} \cdot A_{(\Omega_n)} \tag{2.41}$$

$A_{(\Omega_n)}$, $\boldsymbol{F}_{(\Omega_n)}$ and $\boldsymbol{\sigma}_{(\Omega_n)}$ are the cross-sectional areas, the acting forces and the stresses in each of the n-th phase components, meanwhile $A_{(\Omega)}$, $\boldsymbol{F}_{(\Omega)}$ and $\boldsymbol{\sigma}_{(\Omega)}$ are the corresponding averaged values over the composite. Taking Equations (2.38) and (2.40) into account, the following relationship can be obtained:

$$\mathbf{C}_{(\Omega)} = \sum_{i=1}^{n} \mathbf{C}_i \cdot \phi_i \tag{2.42}$$

where $\mathbf{C}_{(\Omega)}$ is the effective elastic tensor of the composite, ϕ_i and $\mathbf{C}_i$ are the volume fraction and the elasticity tensor corresponding to the i phase, respectively.

On the other hand, Reuss [101] proposed to determine the elastic moduli by averaging strains, expressed in terms of stresses assuming stress uniformity as in the case shown in Figure 2.3, when all constituents are assumed to have the same stress.

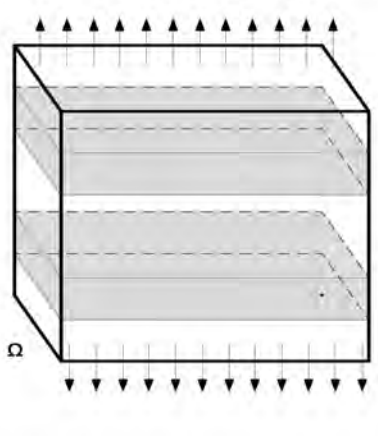

Figure 2.3: Specimen with stress uniformity in all the phases of the composite

The Reuss estimates gives the following estimation of the effective elastic tensor of the composite.

$$\mathbf{C}_{(\Omega)} = \left[\sum_{i=1}^{n} \frac{\phi_i}{\mathbf{C}_i} \right]^{-1} \tag{2.43}$$

The Voigt and Reuss estimates tried to provide exact estimations of the elastic moduli of materials with random microgeometries. However, these estimations give only upper and lower bounds for the elastic moduli of a composite with an arbitrary random geometry. The Reuss estimation gives the lower bound of the elastic moduli for the composite, and the Voigt estimation gives the upper bound. The Voigt-Reuss bounds depend exclusively on the phase volume fractions and do not require any further information or assumption concerning the microstructure. The bounds for the effective moduli of composites are valid form arbitrary microstructures, isotropic and anisotropic.

2.3.2 Variational bounding methods

Hashin and Shtrikman [50] used this variational formulation for the derivation of upper and lower bounds for the effective elastic moduli of quasi-isotropic and quasi-homogeneous multiphase materials of arbitrary phase geometry. In the formulation is demonstrated that when the ratios between the different phase moduli are not too large the bounds derived are close enough to provide a good estimate for the effective moduli. The variational principle derived analytical expressions which provide bounds for the elastic constants of a heterogeneous material with a random isotropic distribution of phases.

Walpole [122] generalized the bounds of Hashin and Shtrikman for materials with several phases, while Beran and Molyneux [8] used the variational method to obtain the limits of two-phase materials based on the probability function of three points where the effective elastic properties depend on the elastic constants of each phase and two parameters that provide information about the microstructure of the material.

In more recent works the nonlinear problem using the variational bounding method is addressed by Ponte Castañeda [96] where two dual versions of a variational principle are presented and applied to determine bounds and estimates for the effective energy functions of nonlinear composites with prescribed volume fractions in the context of the deformation theory of plasticity. The classical bounds of Voigt and Reuss for completely anisotropic composites are recovered for the new variational principles and are given as alternative simpler forms. Also, the use of a novel identity allows the determination of simpler forms for nonlinear Hashin-Shtrikman bounds, and estimates, for isotropic, particle-reinforced composites, as well as for transversely isotropic, fiber-reinforced composites. Additionally, third-order bounds of the Beran type are determined for the first time for nonlinear composites. Meanwhile Talbot and Willis [115] developed bounds of third order for the overall response of nonlinear composites whose response can be described in terms of a convex potential function. Bounds are constructed for the overall, or effective, potential of the composite, given the individual potentials of its constituents. Steady-state creep is considered explicitly but the results apply equally well to physically nonlinear elasticity, or deformation-theory plasticity, if strain-rate is reinterpreted as infinitesimal strain. The fields used in this study have the property of bounded mean oscillation. The use of a theorem that applies to such fields permits the construction of the bounds that were

previously inaccessible. Results for three-point correlations are presented for an isotropic two-phase composite, each component of which is isotropic and incompressible. The generalized Hashin-Shtrikman-type bounds were also investigated by allowing the parameter corresponding to the three-point correlations to take its extreme values.

Lahellec and Suquet [66] developed a method for determining the overall behavior of composite materials comprised of nonlinear inelastic constituents using incremental variational principles in which the evolution equations describing the constitutive behavior of the phases are reduced to the minimization of an incremental energy function. The paper is devoted to the effective response of heterogeneous materials, whose individual constituents exhibit both reversible and irreversible effects in their mechanical behavior. Upon time-discretization of the constitutive differential equations, an incremental variational principle has been derived, by means of which the problem can be reduced to the minimization of a single non-quadratic incremental potential. A strategy, inspired by the variational procedure of Ponte Castañeda [96], has been used to linearize the non-quadratic condensed potential and also to define an 'effective internal variable' per phase at each time-step. Comparisons with full-field simulations show that the present model is good as long as the variational procedure is accurate in the purely dissipative setting, when elastic deformations are neglected. If this is the case, the present model accounts in a very satisfactory manner for the coupling between reversible and irreversible effects and is therefore an accurate model for treating nonlinear viscoelastic and elasto-viscoplastic materials. However in certain situations, the variational procedure is not accurate in the purely dissipative limit and examples of such situations are given. In order to enhance this study a more refined scheme, still based on the condensed variational potential with a different linearization strategy based on an anisotropic linear viscoelastic composite, is proposed by Lahellec and Suquet [67]. In this second part of the study, a proper modification of the second order procedure of Ponte Castañeda is proposed and leads to replacing, at each time-step, the actual non-linear viscoelastic composite by a linear viscoelastic one. The linearized problem is even further simplified by using an 'effective internal variable' in each individual phase. The resulting predictions are in good agreement with exact results and improve on the predictions of the secant model proposed in the first part of this research.

Though most of the analytical models presented in the sections above are reasonably effective in predicting equivalent material properties for relatively simple geometries and low volume fraction of second phase inclusions, they are often incapable of depicting the evolution of stresses and strains in the microstructure. On the other hand, arbitrary microstructural morphology, which is frequently encountered in actual heterogeneous materials, cannot be treated with these models. Moreover, the constitutive response of the constituent phases is also somewhat restricted and predictions with large property mismatches are not very reliable.

2.4 Asymptotic homogenization theory

The asymptotic homogenization theory laid the foundation for the study of composite materials in media with periodic structures using a multi-scale approach. This theory has proven to be a powerful technique for the analysis of structural arrangements in which two or more length scales naturally exist. These two scales are the microscopic scale of inter-second phase spacing and the macroscopic scale characterizing overall dimensions of the structure. Through the use of asymptotic expansions of displacement and stress fields and appropriate variational principles, the homogenization methods can provide not only the effective (homogenized) material parameters, but also distributions of stresses and strains at the two levels. There are two main monographic books on the subject which laid the mathematical basis for the method and emphasized its application in the solution of mechanical problems by Bensoussan et. al. [7] and by Sanchez-Palencia [103].

Bensoussan et al. [7] developed an asymptotic expansion of the solution in terms of a parameter ϵ which is the ratio of the period of the structure to a typical length in the region. If the period of the structure is small compared to the size of the region in which the system is to be studied, then an asymptotic analysis is called to obtain an asymptotic expansion the link from a microscopic description to a macroscopic description of the behavior of the system. The asymptotic problem is formulated in mathematical terms as a family of partial differential operators, depending on the small parameter ϵ. The partial differential operators may be time independent or time dependent, steady or of evolution type, linear or nonlinear, etc. These operators have coefficients which are periodic (or in many cases almost periodic) functions in all or in some variables with periods proportional to ϵ. Since ϵ is assumed to be small, we have a family of operators with rapidly oscillating coefficients. The link from the microscopic to the macroscopic description of the behavior of the system is given by solving the problem in two scales defined by the spatial variables x and y, where x is a macroscopic quantity and $y = x/\epsilon$ is a microscopic one ; y is associated with the small length scale of the inclusions or heterogeneities.

The two-scale process introduced in the partial differential equations of the problem produces equations in x, in y and in both variables. Generally speaking, equations in y are 'solvable' if the microscopic structure is periodic, and this leads to a 'rigorous' deduction of the macroscopic equations (in x) for the global behavior. 'Rigorous' is here understood in the sense of 'straight-forward if the two-scale scheme is postulated' and, moreover, in most problems, a mathematical proof of the convergence of solutions to the 'homogenized solutions'. It is emphasized that the 'homogenized coefficients' depend on the local structure of the medium, which may be obtained by numerical solution of boundary value problems in a period of the structure which has boundary conditions mostly of the periodic type. In the following paragraphs the standard classical formulation of this theory is given following the notation as expressed by Sanchez-Palencia in a later work [104].

2.4.1 Two-scale asymptotic expansions and local periodicity

In mathematics an asymptotic expansion is defined as the formal series of functions which has the property that when the series is truncated after a finite number of terms, it provides an approximation to a given function, as the argument of the function tends towards a particular, often infinite, point. This method has been applied in several scientific areas in pure and applied mathematics to represent the behavior of several physical phenomena. For example, in classical mechanics of vibrations, the asymptotic expansion method is applied to describe the motion of an oscillating pendulum when a small factor (in this case a small damping factor) modifies the motion, which should be otherwise, periodic in time. Due to the damping effect, the response of the system is such that each 'period' is almost analogous to the preceding one, however the cumulative effect of the damping causes important differences (of the amplitude, for instance) of the motion of two 'far in time' located periods as shown in Figure 2.4.

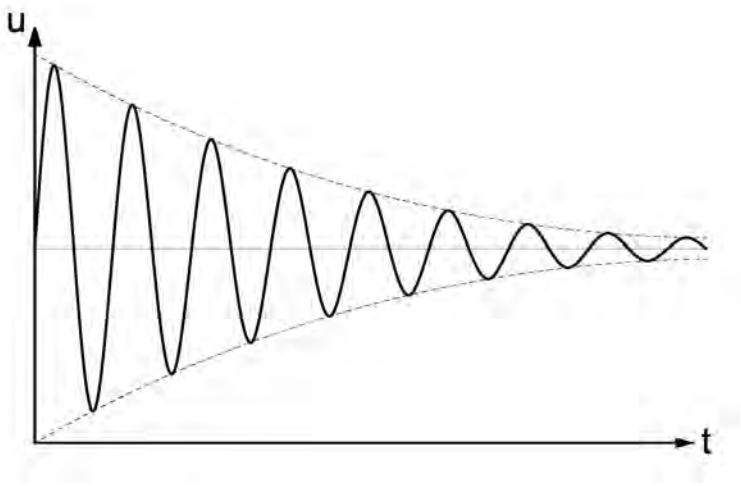

Figure 2.4: Response of a damped harmonic oscillator

Besides the time factor t, another two variables are needed to mathematically describe this type of phenomena: the variable $t^* = t$ and $\tau = \epsilon t$, corresponding to the so-called fast and slow times respectively. The variable ϵ is the small parameter related to the damping of the system. The asymptotic expansion to find the solution for $u^\epsilon(t)$ is given by the expression of the form:

$$u^\epsilon(t) = u^0(t^*(t), \tau(t)) + \epsilon u^1(t^*(t), \tau(t)) + \cdots \tag{2.44}$$

Where the local periodic phenomena is described by the dependence on t through t^*, and

the slow modulation by the dependence on t through τ, then derivative of the function with respect to the two parameters is given by Equation (2.45).

$$\frac{d}{dt} = \frac{\partial}{\partial t^*} + \epsilon \frac{\partial}{\partial \tau} \tag{2.45}$$

Making analogous considerations, the later formulation can be applied to mathematically describe the behavior of solids when subjected to small or large perturbations. Let Ω be a body made of a composite material in the R^3 space of the standard coordinates (x_1, x_2, x_3). Moreover, we assume that its mechanical properties are periodic described by the small parameter ϵ. In the auxiliary space of the variables (y_1, y_2, y_3), a parallelepipedic period denoted by Y (with edges Y_1, Y_2, Y_3) is considered as illustrated in Figure 2.5 as well as the parallelepipeds obtained by translations of an integer number of periods in the directions of the axes.

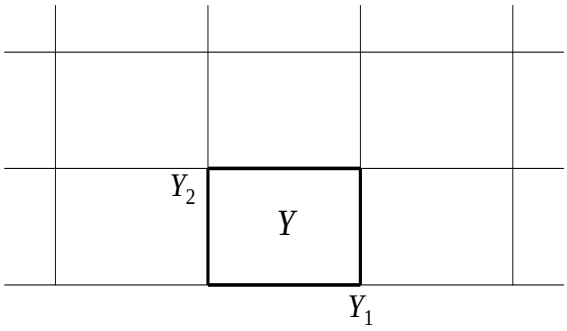

Figure 2.5: Periodical space Y

Now, if it is considered that ϵY is the homothetic of Y with ratio ϵ and that the body Ω has a ϵY-periodic structure, then a property $u^\epsilon(x)$ that represents some property of the mechanical process is searched under the form of an asymptotic expansion. The variable u may denote displacement, stress or some other property. The asymptotic expansion has the following form:

$$u^\epsilon(x) = u^0(z(x), y(x)) + u^1(z(x), y(x)) + \cdots \tag{2.46}$$

with

$$z(x) = x \;\; ; \;\; y(x) = \frac{x}{\epsilon} \tag{2.47}$$

In order to reduce the expression, for the sake of simplicity Equation (2.46) can be expressed as:

$$u^\epsilon(x) = u^0(x, y) + u^1(x, y) + \cdots \tag{2.48}$$

and the derivative of the function with respect to the two scales is given by:

$$\frac{d}{dx_i} = \frac{\partial}{\partial x_i} + \frac{1}{\epsilon}\frac{\partial}{\partial y_i} \tag{2.49}$$

With the purpose to study the influence of external effects on the macroscopic scale response of a composite, an expansion of the type presented in Equation(2.48) with functions u^i Y-periodic with respect to the variable y and smooth with respect to x is studied. Each function $u^i(x, y)$ is defined on Ω x Y (or on Ω x R^3, since the function is Y-periodic).

Let's consider a periodic medium domain Ω which is divided in periodic unit-cells as presented in Figure 2.6. If the values of the function $u^i(x, y)$ at two points P^1,P^2 homologous by periodicity corresponding to two contiguous periods are compared then it can be stated that by periodicity the dependence on y is the same and the dependence on x is 'almost the same' because the distance P^1-P^2 is small and therefore u^i is a smooth function of x. On the other hand, let P^3 be a point homologous to P^1 by periodicity, but located far from P^1. The dependence of u^i on y is the same, but the dependence on x is very different because P^1 and P^3 are not near to each other. Finally we compare the values of u^i at two different points P^1 and P^4 of the same period. The dependence on x is almost the same, but dependence on y is very different because P^1 and P^4 are not homologous by periodicity, since in fact, the distance P^1-P^4 is 'large' when measured with the variable y. The concepts expressed in the preceding paragraphs are known as the *local periodicity hypothesis*.

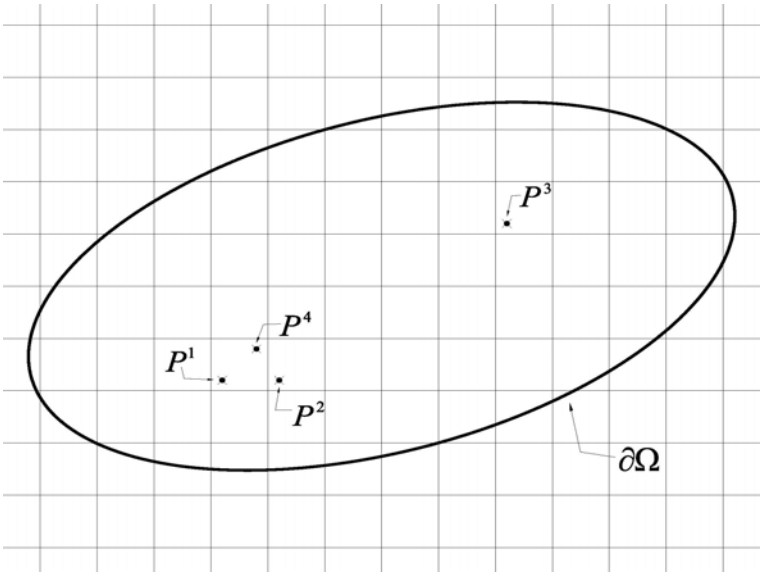

Figure 2.6: Periodic domain Ω

It is evident that this locally periodic expansion is fit to describe the solution in regions of Ω far from its boundary, or from regions where the local effects are not ϵY-periodic, such as discontinuities of the microscopic structure, consequently in such regions the asymptotic expansion may be of different nature. Therefore it can be stated that the solution using asymptotic expansions is mainly affected by two factors:

1. The first is the scale of Ω and arises from the forces applied and the conditions at the boundaries.

2. The second is due to the periodic structure, which is given by the arrangement of the components.

2.4.2 Model equations for composite structures

To express the model equations using asymptotic expansions, the formulation expressed by Devries et al. [22] and later extended by Ghosh et al. [34] is followed in the next paragraphs. This formulation considers an elastic body which occupies a region Ω related to a system of orthonormal axes $(0,x_1,x_2,x_3)$. The body is subjected to a system of body forces $\boldsymbol{f}$ and of surface forces $\boldsymbol{F}$ on a portion Γ_F of the boundary $\partial\Omega$. The other portion of the boundary is Γ_0, on which a zero displacement condition is imposed. The material is covered by a set of identical periods with the same geometrical configuration.

A period characteristic of the material similar to that presented in Figure 2.5 denoted by Y has been designated and enlarged by homothetics. The small parameter ϵ designates the homothetic ratio which relates Y to a period in the elastic material. Therefore, it can be stated that the elastic structure of the material is fully described if it is given over a single period Y related to the orthonormal axis system $(0,y_1,y_2,y_3)$. Let $C_{ijkl}(y)$ be the coefficients of elasticity on Y, which generally change very quickly with respect to y, but satisfy rigorously the symmetry relations as expressed by Equation (2.50).

$$C_{ijkl}(y) = C_{jikl}(y) = C_{klij}(y) \tag{2.50}$$

The functions $y \rightarrow C_{ijkl}(y)$ defined on Y are extended by Y-periodicity to the entire space $(0y_1y_2y_3)$, assumed to be covered by contiguous periods identical to Y. Then, the coefficients of elasticity C^{ϵ}_{ijkl} in the material Ω are defined by:

$$C^{\epsilon}_{ijkl} = C_{ijkl}(y), \quad y = \frac{x}{\epsilon} \tag{2.51}$$

The terms presented in Equation (2.51) can also be expressed as:

$$\mathbf{C}(y) = \{C_{ijkl}(y)\}, \quad \mathbf{C}^{\epsilon}(x) = \mathbf{C}\left(\frac{x}{\epsilon}\right), \quad \boldsymbol{\sigma} = \{\sigma_{ij}\} \tag{2.52}$$

Therefore, the stresses and displacements fields of the heterogeneous material should satisfy the following boundary value problem.

$$\begin{aligned}
\frac{\partial \sigma_{ij}^{\epsilon}}{\partial x_j} &= -f_i, && in\ \Omega && (2.53)\\
\sigma_{ij}^{\epsilon} &= C_{ijkl}^{\epsilon}\varepsilon_{kl}^{\epsilon}, && \varepsilon_{kl}^{\epsilon} = \frac{1}{2}\left(\frac{\partial u_k^{\epsilon}}{\partial x_l^{\epsilon}} + \frac{\partial u_l^{\epsilon}}{\partial x_k^{\epsilon}}\right) && (2.54)\\
\sigma_{ij}^{\epsilon}\cdot \boldsymbol{n} &= \boldsymbol{F}, && on\ \Gamma_F && (2.55)\\
u_i^{\epsilon} &= 0, && on\ \Gamma_0 && (2.56)
\end{aligned}$$

Where $\boldsymbol{n}$ is the unit normal to the boundary. Since small deformation is assumed, the normal vector does not change significantly with load. In homogenization theory, the Y-periodic displacement rate or increment field is approximated by an asymptotic expansion with respect to parameter ϵ.

$$\boldsymbol{u}^{\epsilon}(x) = \boldsymbol{u}^0(x,y) + \epsilon \boldsymbol{u}^1(x,y) + \epsilon^2 \boldsymbol{u}^2(x,y) + \ldots,\ y = \frac{x}{\epsilon} \tag{2.57}$$

Since it is known that the spatial x^{ϵ} derivative of any function Φ depends on the two length scales, it can be expressed as:

$$\frac{\partial}{\partial x_i^{\epsilon}}\left[\Phi\left(x, y = \frac{x}{\epsilon}\right)\right] = \frac{\partial \Phi}{\partial x_i} + \frac{1}{\epsilon}\frac{\partial \Phi}{\partial y_i} \tag{2.58}$$

Therefore the strain field tensor may be expressed as follows:

$$\varepsilon_{kl}^{\epsilon} = \frac{\partial u_k^{\epsilon}}{\partial x_l^{\epsilon}} = \frac{1}{\epsilon}\frac{\partial u_k^0}{\partial y_l} + \left(\frac{\partial u_k^0}{\partial x_l} + \frac{\partial u_k^1}{\partial y_l}\right) + \epsilon\left(\frac{\partial u_k^1}{\partial x_l} + \frac{\partial u_k^2}{\partial y_l}\right) + \cdots \tag{2.59}$$

The stress field is given by:

$$\sigma_{ij}^{\epsilon} = \frac{1}{\epsilon}\sigma_{ij}^0 + \sigma_{ij}^1 + \epsilon\sigma_{ij}^2 + \ldots \tag{2.60}$$

with

$$\begin{aligned}
\sigma_{ij}^0 &= C_{ijkl}(y)\frac{\partial u_k^0}{\partial y_l}\\
\sigma_{ij}^1 &= C_{ijkl}(y)\left(\frac{\partial u_k^0}{\partial x_l} + \frac{\partial u_k^1}{\partial y_l}\right) && (2.61)\\
\sigma_{ij}^2 &= C_{ijkl}(y)\left(\frac{\partial u_k^1}{\partial x_l} + \frac{\partial u_k^2}{\partial y_l}\right)
\end{aligned}$$

Putting the expansion set in Equation (2.60) in the form of equilibrium Equation (2.53), and setting each coefficient of ϵ^i (i = -1, 0, 1,2, . ..) to zero, results in the following set of equations.

$$\begin{aligned} \frac{\partial \sigma_{ij}^0}{\partial y_j} &= 0 \\ \frac{\partial \sigma_{ij}^1}{\partial y_j} + \frac{\partial \sigma_{ij}^0}{\partial x_j} &= 0 \\ \frac{\partial \sigma_{ij}^2}{\partial y_j} + \frac{\partial \sigma_{ij}^1}{\partial x_j} + f_i &= 0 \end{aligned} \tag{2.62}$$

If the two scales represented by the variables x and y are considered independent, the set of Equations (2.62) form a recursive system of differential equations for the functions $u_i^0, u_i^1, u_i^2, \ldots$ parameterized by x, which has a solution of the form:

$$-\frac{\partial}{\partial y_i}\left(a_{ij}(y)\frac{\partial \Phi}{\partial y_j}\right) = F \qquad in\ Y \tag{2.63}$$

for a Y-periodic function $\Phi = \Phi(x, y)$ has a unique solution defined by:

$$\langle F \rangle = \frac{1}{|Y|}\int_Y F\ dy = 0 \tag{2.64}$$

where the $\langle \cdot \rangle$ operator denotes mean value and $|Y|$ denotes the volume of the representative volume of the element (RVE). Equations (2.61) and (2.62) together with (2.64) leads to the trivial solution for $\sigma_{ij}^0 = 0$ and therefore it may be established that u^0 is only a function of x, this is:

$$\sigma_{ij}^0 = 0, \quad and \quad u_i^0 = u_i^0(x) \tag{2.65}$$

- *Microscopic equilibrium equation and homogenized constitutive relation*

Substituting Equation (2.65) into the second Equation of set (2.62), it leads to the Y-domain (RVE domain) equilibrium equation:

$$\frac{\partial \sigma_{ij}^1}{\partial y_j} = 0 \qquad in\ Y \tag{2.66}$$

Neglecting the terms associated with ϵ in Equations (2.59) and (2.60) the constitutive relation in Y of Equation (2.56) is expressed as:

$$\sigma_{ij}^{\epsilon} = \sigma_{ij}^{1} = C_{ijkl}^{\epsilon}\varepsilon_{kl}^{\epsilon} \tag{2.67}$$

with

$$\varepsilon_{kl}^{\epsilon} = \bar{\varepsilon}_{kl} + \varepsilon_{kl}^{*} = \left(\frac{\partial u_k^0}{\partial x_l} + \frac{\partial u_k^1}{\partial y_l}\right) \tag{2.68}$$

where $\varepsilon_{kl}^{\epsilon}$ is the local or microstructural strain tensor, for which $\bar{\varepsilon}_{kl} = \partial u_k^0/\partial x_l$ is an averaged macroscopic part, and $\varepsilon_{kl}^{*} = \partial u_k^1/\partial y_l$, is denoted as a fluctuating strain tensor.

Due to the linearity of σ^1 and u^1, these variables can be expressed as follows:

$$\sigma_{ij}^{1} = s_{ij}^{kl}(y)\frac{\partial u_k^0}{\partial x_l}, \qquad u_i^1 = \chi^{kl}(y)_i\frac{\partial u_k^0}{\partial x_l} \tag{2.69}$$

where s_{ij}^{kl} is a Y-antiperiodic function and χ^{kl} is a Y-periodic function representing characteristic modes of the RVE and with Equation (2.70) representing the equilibrium at the microscopic scale.

$$\frac{\partial s_{ij}^{kl}(y)}{\partial y_j} = 0 \tag{2.70}$$

Substituting Equations (2.69) in Equation (2.61) yields the microscopic constitutive relations as:

$$s_{ij}^{kl}(y) = C_{ijkl}^{\epsilon}\left[I_{ij}^{kl} + \frac{\partial \chi^{kl}}{\partial y}\right] \tag{2.71}$$

where I_{ij}^{kl} is a fourth-order identity tensor expressed as:

$$I_{ij}^{kl} = \frac{1}{2}\left(\delta_{ik}\delta_{jl} + \delta_{il}\delta_{jk}\right) \tag{2.72}$$

Substituting Equation (2.71) in the solution of σ_{ij}^{1}, the expression stays as follows:

$$\sigma_{ij}^{1} = C_{ijkl}^{\epsilon}\left[I_{ij}^{kl} + \frac{\partial \chi^{kl}}{\partial y}\right]\frac{\partial u_k^0}{\partial x_l} \tag{2.73}$$

and by taking the mean value in the domain Y as the homogenized tension

$$\left\langle \sigma_{ij}^{1} \right\rangle = C_{ijkl}^{x}\frac{\partial u_k^0}{\partial x_l} \tag{2.74}$$

where

$$C^x_{ijkl} = \langle C_{ijkl}(y) \rangle - \left\langle C_{ijpq}(y) \frac{\partial \chi^{kl}(y)_p}{\partial y_q} \right\rangle \tag{2.75}$$

These coefficients are independent of the macroscopic scale $\mathbf{x}$ and they define the equivalent homogeneous material. These vales are known as the homogenized coefficients.

- *Macroscopic equilibrium equation*

The equation of equilibrium in the macroscopic domain is obtained by taking the mean of the third equation presented in (2.62) on Y and applying the condition (2.64) to the first term $\partial \sigma^2_{ij}/\partial y_j$ leads to an averaged form of the global equilibrium equation as:

$$\frac{\partial \left\langle \sigma^1_{ij} \right\rangle}{\partial x_j} + f_i = 0 \qquad in\ \Omega \tag{2.76}$$

Therefore, the averaged stress $\mathbf{\Sigma} = \left\langle \sigma^{\mathbf{1}} \right\rangle$ and the displacement field u^0 are the solution to the elastic problem defined by the following set of equations:

$$\begin{aligned}
\frac{\partial \Sigma_{ij}}{\partial x_j} &= -f_i && in\ \Omega && (2.77)\\
\Sigma_{ij} &= C^x_{ijkl} \bar{\varepsilon}_{kl} && && (2.78)\\
\Sigma_{ij} \cdot \boldsymbol{n} &= \boldsymbol{F}, && on\ \Gamma_F && (2.79)\\
u^0_i &= 0, && on\ \Gamma_0 && (2.80)
\end{aligned}$$

The averaged stress field $\mathbf{\Sigma}$ is also known as the macroscopic stress field, meanwhile the strain field $\boldsymbol{E}$ expressed in Equation (2.81) is referred as the macroscopic strain field.

$$\boldsymbol{E} = \bar{\varepsilon}_{kl} \tag{2.81}$$

Equation (2.81) satisfies the following condition:

$$\boldsymbol{E} = \langle \bar{\varepsilon}_{kl} + \varepsilon^*_{kl} \rangle \tag{2.82}$$

- *Application procedure*

To use the formulation presented above, a process called localization procedure is presented. In this process it is remarked that the stress field σ^1_{ij} is the first term of the asymptotic expansion of the stress field $\sigma^\epsilon(x)$ solution of the initial physical problem. This field it is known as the microscopic stress field. Then for each point $x \in \Omega$ there is a small ϵY period which gives a stress field σ^1_{ij}.

It can be demonstrated that:

$$\sigma^{\epsilon}(x) - \sigma^{1}_{ij}\left(x, \frac{x}{\epsilon}\right) \to 0, \qquad \textit{in the } L^1(\Omega) \textit{ norm} \tag{2.83}$$

when ϵ tends to zero.

Equation (2.83) proves that $\sigma^{1}_{ij}\left(x, x/\epsilon\right)$ is an approximation of $\sigma^{\epsilon}(x)$ when ϵ is small.

The microscopic stress field $\sigma^{1}_{ij}, y = x/\epsilon$ can be computed as follows:

1. Determine the six vector fields χ^{kl} on Y associated with the tensor I^{kl} solution of problem (2.71), which is an elastic-type problem on the non-homogeneous domain Y.

2. Obtain the homogenized coefficients C^{x}_{ijkl} from the vector fields $\chi^{kh}(y)$, as in determined in (2.75).

3. By solving the homogenized elastic problem presented in Equations (2.77)-(2.80) on Ω, the macroscopic stress field $\boldsymbol{\Sigma}$ and the macroscopic deformation field $\boldsymbol{E} = \bar{\varepsilon}_{kl}$ are obtained for $x \in \Omega$.

4. For any point x fixed in Ω, the stress field σ^{1}_{ij} field on Y shows how the macroscopic stress $\boldsymbol{\Sigma} = \left\langle \sigma^{\mathbf{1}} \right\rangle$ is located within in a ϵY period at $x \in \Omega$.

The asymptotic homogenization theory has been applied in conjunction with several numerical methods in order to perform multiple scale analysis, such as the finite element method, the Voronoi cell finite element model, the stochastic analysis, etc. to solve linear elastic and non-linear problems. The combination of the asymptotic homogenization with these methods it is what gives origin to what later was denominated as multi-scale homogenization. In the next section a thorough description of the most notables existing multi-scale homogenization techniques is presented.

2.5 Multi-scale homogenization

The multi-scale homogenization has emerged as one of the most promising methods to compute the response of composite structures. In the last years a variety of direct micro-macro methods, also known as global-local analysis have been developed as the evolving result of the application of the asymptotic homogenization theory. These approaches estimate the relevant stress-strain relationship at a macroscopic point by performing calculations on a separated scale determined by a macroscopic point using different methods to compute the structural response at the different scales.

Suquet [110] laid down the basic principles of homogenization with the purpose of finding the constitutive equations for the averaged effective or macroscopic properties of a

heterogeneous material. The multi-scale homogenization of composite materials can be established following the next three-step scheme. The scheme is illustrated as well in Figure 2.7:

- Definition of a volume element, which is statistically representative for the whole material microstructure under consideration. The size of the representative volume element (RVE) should be large enough to contain a sufficient number of micro-heterogeneities of which the constitutive behavior of these individual constituents is assumed to be known. The RVE should permit micromechanical analysis in the framework of available computational resources.

- Localization (macro-micro transition): microscopic boundary conditions are obtained based on the macroscopic input variables (e.g. strain tensor), taking into account the geometry, constitutive laws, etc.

- Homogenization (micro-macro transition): macroscopic output variables are obtained based on the computation of the microscopic behavior of the RVE. Macroscopic properties of the equivalent homogeneous medium are evaluated.

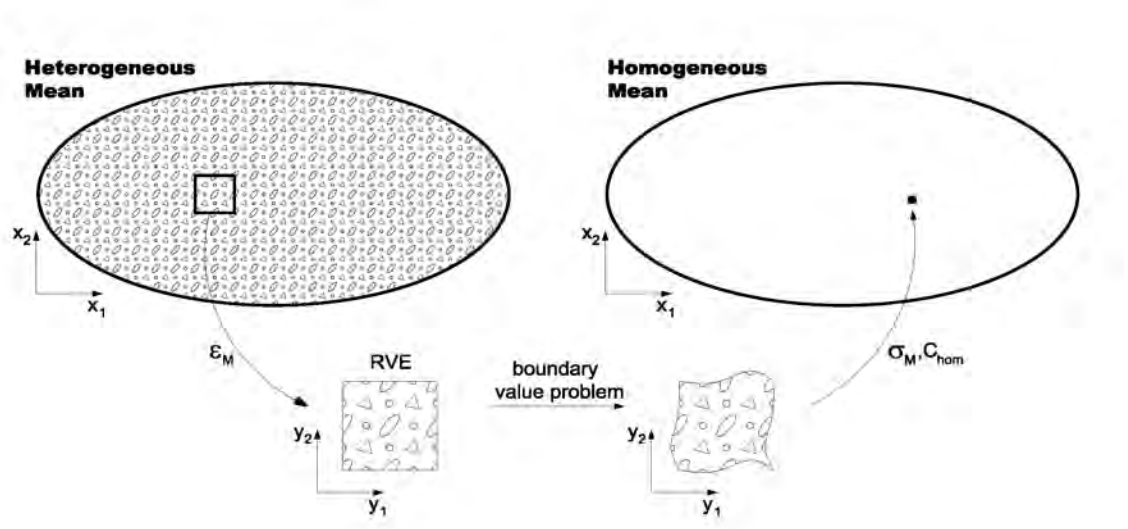

Figure 2.7: Homogenization scheme in two scales

It must be highlighted however, that the concept of homogenization is applicable only if at least two length scales in the problem can be defined. Several features that result very convenient for the analysis of composites are offered by the multi-scale computational homogenization techniques, as mentioned by Koutnetzova et al. [58]. Among the most remarkable features there are:

- No explicit assumptions on the format of the macroscopic local constitutive equations are required, since the macroscopic constitutive behavior is obtained from the solution of the associated microscale boundary value problem.
- The techniques are suitable for arbitrary material behavior, including physically nonlinear and time dependent.
- Permit the incorporation of large deformations and rotations on both micro and macrolevel.
- Possibility to introduce detailed microstructural information, including the physical and geometrical evolution of the microstructure, into the macroscopic analysis.
- Consent to use of almost any modeling method to compute the numerical response on the microlevel, e.g. the finite element method, the boundary element method, the Voronoi cell method, or numerical methods based on fast Fourier transforms, etc.

Regardless of the apparent fact that the multi-scale homogenization requires a computationally expensive coupled nested solution, it may be considered as a valuable tool to analyze composite structures due to the ability to establish non-linear micro-macro structure property relations with relatively easiness. This feature is particularly useful in the cases where the complexity of the mechanical and geometrical microstructural properties prohibits the use of other modeling techniques. The seemingly high computational cost of the method can be solved by using parallel computation. By doing this the main drawback of the homogenization method is diminished.

2.5.1 Determination of the representative volume element

As pointed out in the preceding section, the multi-scale homogenization is based on the use of a representative volume element (RVE). The RVE is a representative domain that is employed to determine the corresponding effective properties for the homogenized macroscopic model. The RVE definition corresponds to a microstructural subregion that is representative of the entire microstructure in an average sense. For the case of composites, it is assumed that it must contain a sufficient number of inclusions, which makes the effective moduli independent of assumed homogeneous tractions or displacements on the RVE boundary.

Among the different ways to characterize the representative volume element there are two significantly different approaches to define it as pointed out by Drugan and Willis [23]. The first approach arises from the perspective that in order to characterize macroscopic composite constitutive response, the statistical nature of the microstructure of the composites must be recognized. This point of view leads to the conclusion that the smallest RVE for which a macroscopic effective constitutive theory could apply is one that is sufficiently large to be statistically representative of the composite, so it can include effectively a sampling of all possible microstructural configurations that occur in the composite.

This approach implies that the RVE must include a very large number of the composites microheterogeneities (such as grains, inclusions, voids, cracks, fibers, etc.). Such statements are invariably qualitative; therefore studies that focus on the overall composite response generally state that the RVE must be chosen 'sufficiently large' compared to the microstructural size for the approach to be valid. The second approach defines the RVE as the smallest material volume element of the composite for which the usual spatially constant overall modulus macroscopic constitutive representation is a sufficiently accurate model to represent mean constitutive response. A thorough examination of the several RVE definitions found in the literature can be consulted in the review made by Gitman et al. [39].

There is consensus in the literature review that the RVE is clearly defined for two situations as Ostoja-Starzewski [94] pointed out: (i) when there is a unit cell in a periodic microstructure (i.e. the volume element is chosen so as to contain a single inclusion in a matrix phase) as seen in Figure 2.8a and (ii) when there is a volume containing a very large set of micro-scale elements, possessing statistically homogeneous and ergodic properties as presented in Figure2.8b.

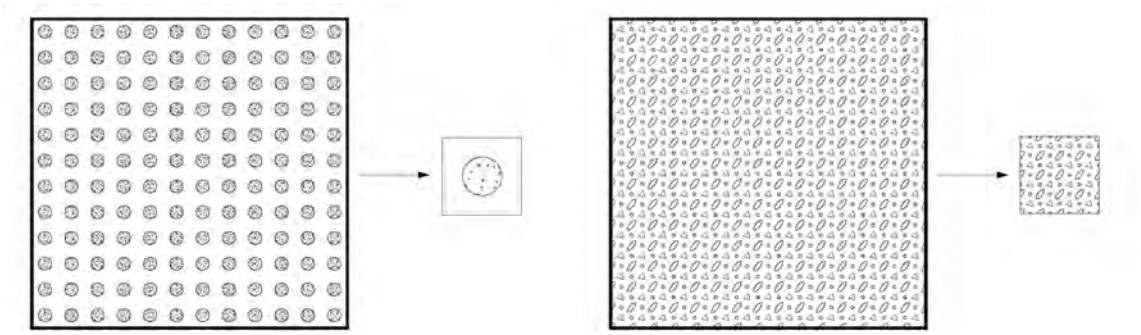

(a) (b)

Figure 2.8: Modeling of representative volume element: (a) unit cell approach; (b) statistical and ergodic approach.

2.6 Computational techniques to obtain the numerical response of composite materials

Several computational methods have been developed to addressed the problem that multiscale homogenization poses in a rather straightforward manner. Different procedures have been implemented to assess the macroscopic influence of the micro-structural parameters by addressing the large computationally effort that this method requires in the best possible way. In the following sections an overview of the most outstanding works found in the literature using different computational techniques to solve the multi-scale homogenization problem is presented.

2.6.1 Multi-scale homogenization using the FE method

The idea of using a finite element discretization to model the multi-scale approach was first addressed by Renard and Marmonier [100]. The method consists in solving two finite element problems, one for each scale. In the micro scale the geometry of the RVE is meshed and homogenization rules are used to link these microfinite element computations to the macroscopic scale. Guedes and Kikuchi [43] implemented the homogenization method to model the mechanical behavior of linear elastic composite materials. A finite element-based computational tool to perform the homogenization was developed by means of two separated blocks. The first generates the material properties for a general structure meanwhile, the second, computes localized information (displacements, stresses and strains).

Swan and collaborators [112, 111], developed a framework within the context of the displacement finite element method for applying periodic boundary conditions to period basic cells under the influence of applied macroscopically homogeneous stresses and strains. The performance of both the stress and strain driven methods are demonstrated and assessed on a complete set of homogenization computations for an elasto-plastic composite.

In 1988, Smith et al. [108] presented a homogenization method that accounts for large deformations and viscoelastic material behavior. This method is based on . A multi-level finite element program was implemented based on the classical homogenization theory assuming local spatial periodicity of the microstructure as depicted in the schematic representation presented in Figure 2.9.

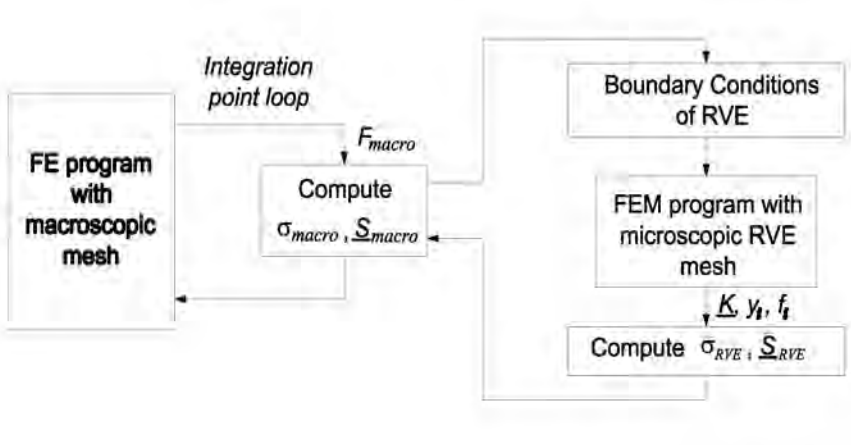

Figure 2.9: Schematic representation of the multi-level finite element program (Smith et al. [108]).

The microstructure is identified by a representative volume element (RVE) with conformity

of opposite boundaries at any stage of the deformation process. The local macroscopic stress is obtained by applying the local macroscopic deformation, represented by the deformation tensor imposing appropriate boundary conditions and averaging the resulting. On each iteration cycle of the macroscopic finite element procedure the integration point stress σ_{macro} and stiffness $\underline{S}_{macro}$ are obtained by a separate finite element analysis on the RVE that is assigned to that macroscopic integration point. RVE averaged stress $\overline{\sigma}_{RVE}$ and stiffness $\overline{\underline{S}}_{RVE}$ are computed from the actual RVE vertex positions y_i, forces f_i, and stiffness matrix $\underline{K}$ and subsequently returned to the macroscopic integration point as σ_{macro} and $\underline{S}_{macro}$ In this study it was demonstrated that the method successfully predicted the mechanical response of a perforated plane strain sheet.

The generalization of the mathematical homogenization method based on double-scale asymptotic expansion to account for damage effects in heterogeneous media was presented by Fish et al. [30]. This generalization consisted in deriving a closed-form expression relating local fields to overall strains and damage. Non-local damage theory was introduced by establishing the concept of non-local phase fields (stress, strain, free energy density, damage release rate, etc.) in a manner analogous to that currently practiced in concrete. The numerical results presented demonstrated the applicability and the potential of the method.

Terada et al. [116] presented a study in which the convergence of the homogenization method is examined. Among the main findings of this study it was demonstrated numerically that the periodic boundary conditions provide the most reasonable estimates among the class of possible choices for statistical homogeneous media. Numerical simulation also justified that the asymptotic homogenization can be applied to the analysis of general heterogeneous media by taking the unit cell size as large as possible. Moreover, it was concluded that the periodicity of RVE geometry when evaluating the effective properties is not strictly required.

Feyel and Chaboche [27] discussed the behavior of periodic or quasi-periodic structures reinforced by long fiber SiC/Ti as that presented in Figure 2.10. These authors demonstrated that it was possible to consider realistic composite structural computations that yields a detailed geometric description and constitutive equations giving access to microstructural data, instead of only obtaining phenomenological macroscopic data difficult to correlate with the local mechanical state. The essential role of the fiber/matrix interface strength at the microscopic scale was highlighted, since it conditions the macroscopic behavior, especially the damage and failure phases.

Zalamea [126] developed a two-scale numerical method within the context of homogenization theory assuming the periodicity of the internal structure of the material. Oller et al. [90] extended this work by addressing the problem of the steep gradient that appears in the macroscopic field variables. This gradient is produced by the local boundary effects and was solved by performing a refinement of the finite element mesh on the mi-

croscale. By doing this, the periodic condition on the boundaries of the cells near to the perturbation is maintained

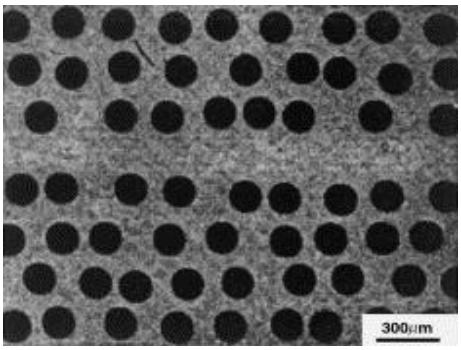

Figure 2.10: Quasi-Periodic microstructure of a SiC/Ti composite (taken from Feyel and Chaboche [27]).

Ladevèze and coworkers [62, 64] proposed a mixed, multilevel domain decomposition method or, more precisely as a 'structure decomposition' method in which the structure is partitioned into substructures and 'material' interfaces which, themselves, are particular substructures. Each of these entities has its own variables and equations. The two-scale description takes place only at the interfaces, where forces and displacements are split into 'macro' contributions and 'micro' complements. The macro quantities are some mean values over space and time of the forces and displacements, such that the macroforces verify the macroequilibrium at the interfaces a priori.

Many more studies have been conducted using multi-scale homogenization in conjunction with the FE method, however these jobs are not discussed in this section as they are modified or extended versions that follow specific approaches when applying the homogenization method, so they need to be treated separately, as may be the case of homogenization in 3D (Section 2.6.6), multi-scale homogenization studies using a high-order formulation (Section 2.6.7) or the hierarchical multi-scale approach (Section 2.6.8).

2.6.2 Multi-scale homogenization using the Voronoi cell method

The Voronoi cell finite element method (VCFEM) was proposed as an alternative to the traditional method of finite elements to solve nonlinear problems of composite materials. The Voronoi cell finite element model originates from Dirichlet tessellation of a representative material element (RME). The Tessellation of a RME is a process of subdivision of space, determined by a set of points, such that each point has associated with it a region that is closest to it than to any other. The method discretizes the domain into a network of multisided convex 'Voronoi' polygons containing one second phase inclusion at most. Taking by example the composite material depicted in Figure 2.11a, the corresponding discretization using Dirichlet tessellation results in a network of Voronoi polygons, as shown

in Figure 2.11b. Each Voronoi cell is a basic structural finite element containing an inclusion embedded in the matrix with independent formulation stresses and displacements which can be identified with the basic structural elements as depicted in Figure 2.11c and can be directly treated as elements in the FE method.

The Voronoi cell finite element method has the potential for establishing a direct correlation between techniques of quantitative metallography for actual heterogeneous materials microstructures and their stress/deformation analysis. The numerical implementation technique drastically reduces the number of degrees of freedom of analysis using finite elements which reproduce the complex stress and strain fields that appear near the inclusions.

Formulations have been developed for directly treating multiple phase Voronoi polygons as elements in a finite element model by Ghosh and Mukhopadhyay [37, 38] for linear elasticity and by Ghosh and Liu [35] for micropolar thermo-elasticity. Tessellation methods have been used by Spitzig et al. [109] and by Brockenbrough et al. [11] for quantitative

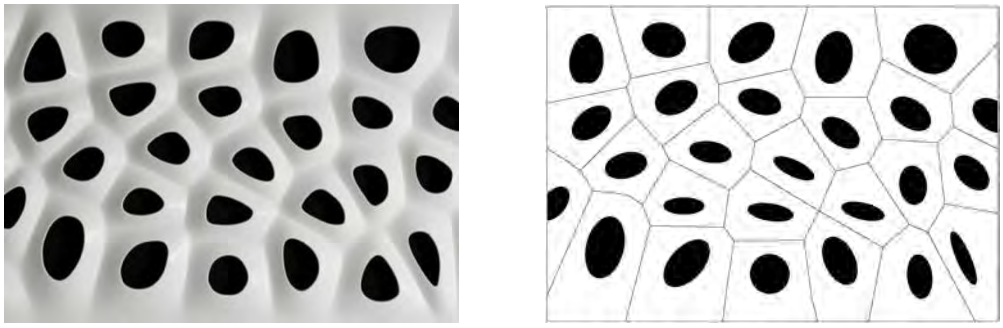

(a) (b)

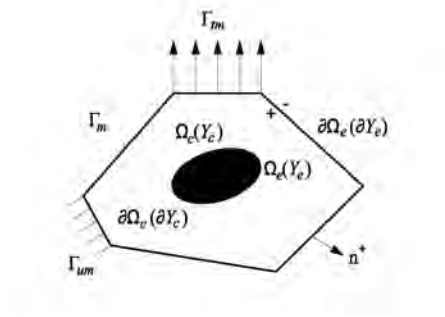

(c)

Figure 2.11: Representation of a heterogeneous structure with the VCFEM. (a) Composite material formed by two composites randomly distributed; (b) heterogeneous structure discretized by Dirichlet tessellation; (c) basic structural element represented by a Voronoi cell.

characterization of micrographs obtained from automatic image analysis systems. This method has also been coupled with asymptotic homogenization theory for simultaneous prediction of global and local responses of elastic structures by Ghosh et al. [33]. Ghosh and Moorthy [36] applied the method to solve small deformation elastic-plasticity problems for arbitrary heterogeneous materials.

Ghosh and coworkers [34] presented a multiple-scale computational tool for performing elasto-plastic analysis of heterogeneous materials with inclusions and voids in the microstructure. The microscopic analysis is conducted with the Voronoi Cell finite element model while a conventional displacement based FEM code executes the macroscopic analysis. The introduction of micromechanics consideration tremendously enhances VCFEM accuracy for various microstructures at very moderate computational efforts. However a shortcoming of the homogenization method in its present form is the incorporation of boundary condition at regions of material discontinuity. Boundary conditions should be applied in the microstructure and not at the macroscopic level as is presently done. The boundary effect can become pronounced in some cases, and then homogenization results become less accurate near the boundary.

Lee et al. [69] proposed a hierarchical multiple scale computational model to concurrently predict evolution of variables at the structural and microstructural scales, as well as to track the incidence and propagation of microstructural damage. The microscopic analysis is conducted with VCFEM while a conventional displacement based FEM code executes the macroscopic analysis. Adaptive schemes and mesh refinement strategies are developed to create a hierarchy of computational sub-domains with varying resolution. Such hierarchy allow for differentiation between non-critical and critical regions, and help in increasing the efficiency of computations through preferential 'zoom in' regions. Coupling between the scales for regions with periodic microstructure is accomplished through asymptotic homogenization, while other regions of nonuniformity and non-periodicity are modeled by true microstructural VCFEM analysis.

This method results effective for the study of composites with random distribution and also it can represent a unit cell of periodic continuum even in some cases with a single Voronoi finite element; this represents an advantage in terms of computational time. However, even when the overall average value of these fields is very approximated to the results obtained by a unit cell, it may affect the response of the microscopic fields, since the assumptions that this formulation is supported on are based on the results of a single Voronoi element resulting in poor accuracy in comparison to the unit cell results (obtained by various finite elements). Moreover, the formulation may present some difficulties when pursuing the solution to problems of periodic continuum with complicated forms of heterogeneities and with composites with more than two phases.

2.6.3 Multi-scale homogenization using FFT-based methods

Among the numerical methods developed as an alternative to the Finite Element Method to solve the problem of homogenization of composite materials there is a method introduced by Moulinec and Suquet [78, 79] to determine the local and overall responses of nonlinear composites based on the Fast Fourier Transform (FFT) to solve the unit cell problem, even when the constituents have a nonlinear behavior.

The initial idea of the method proposed was to make direct use of these digital images of the real microstructure in the numerical simulation. The method avoids the difficulty that represents using a model mesh since the algorithm requires data sampled in a grid of regular spacing in order to directly use the digital images of the microstructure. The method makes use of an iterative process which not requires the formation of a stiffness matrix reducing the number of degrees of freedom and therefore reducing the size of the problem.

Nevertheless, the method has some limitations due to a lack of convergence for materials containing voids or rigid inclusions as Moulinec and Suquet [80] and Michel et al. [74] pointed out in later papers. Several developments have been proposed in the last decade in this research field, among the latter [10, 127], however major improvements have not been found and the initial problem that poses the use of the FFT method to solve composite materials remains without being fully answered.

2.6.4 Multi-scale homogenization using stochastic analysis

Several procedures have been developed using stochastic homogenization to compute the local and global properties of multi-phase periodic composites. Most of these methods consist on obtaining effective properties derived from the homogenization method in order to transform a heterogeneous medium into a homogeneous one with the purpose of reducing the number of the degrees of freedom; however, the vast majority of the schemes based on the stochastic homogenization have been formulated for the elastic range only, limiting the application and the relevance of these type of methods by this restriction. Among the studies that make use of this methodology there are the publications presented by [57, 53, 124, 102, 118].

2.6.5 Analysis of composite materials using ANN

Artificial neural networks (ANN) have emerged as one of the most useful concepts in the field of artificial intelligence used in different applications, such as in medical applications, image and speech recognition, classification and control of dynamic systems, and in several engineering applications and in recent years have been started to be used in modeling the mechanical behavior of composite materials. The ANN architecture generally used consist of a number of layers following the scheme presented in Figure 2.12, in which the layer where the input patterns are applied is called the input layer, the layer where the output

is obtained is the output layer, and the layers between the input and output layers are hidden layers. Neurons in each layer are fully or partially interconnected to preceding and subsequent layer neurons with each interconnection having associated connection strength.

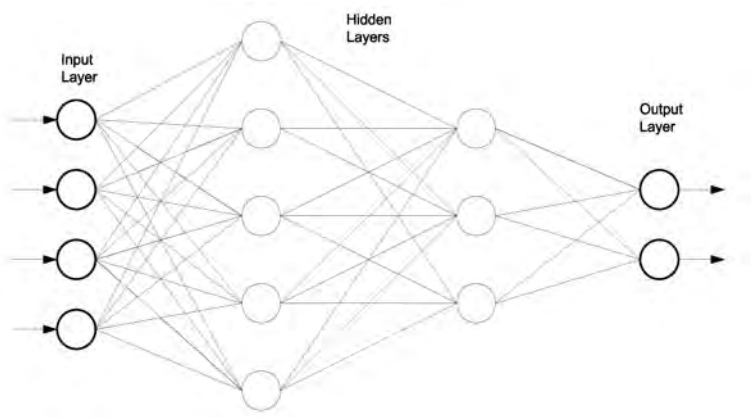

Figure 2.12: General configuration of an artificial neural network

In the field of composite materials analysis plenty of research has been done to predict the response with the help of the ANN techniques. Among some of the most relevant studies found, Zhang and Friedrich [128] looked at the various applications of ANN to obtain the numerical response of polymeric composites, polymers, metals as well as other materials. Pidaparti and Palakal [95] proposed a back-propagation neural network for predicting the non-linear stress-strain behavior of graphite-epoxy laminates. The process involved specifying fiber-angles, initial and incremental stresses for which the trained network will predict the corresponding total strain. The study showed that ANN analysis can be effectively used to represent the cyclic stress-strain behavior in composites.

Aymerich and Serra [3] used a back-propagation ANN to predict the fatigue strength of APC2, an AS4-graphite in a thermoplastic peek matrix with fibers. The sequences examined assured a wide range of failure modes ranging from matrix-dominated to fiber-dominated behavior. Among the main findings of this study were that although the use of ANN resulted in some good fatigue life prediction in fiber- reinforced composites, a larger set of experimental data representative of the failure modes and the laminate sequences was necessary. Lee et al. [68] used the fatigue data for five carbon reinforced plastics and one glass-reinforced plastic laminate to evaluate the performance of ANN in fatigue life prediction of composites. This study raised very interesting conclusions, highlighting that ANN can be trained to model constant-stress fatigue behavior at least as well as other prediction methods and can provide accurate results from quite small experimental databases; however, they noticed that there seems little prospect of transferring the predictive capability of a network with any degree of accuracy from one family of composites to another.

Todoroki [117] studied the monitorization of the delamination of composite laminates by means of using ANN. Changes in electrical resistance were used to identify delamination cracks in carbon/ epoxy laminates. The authors concluded that although the results obtained showed that the ANN estimated the exact location and size of the delamination for the specimens tested, it was not the most convenient tool of diagnosis to identify delamination in composites. Chandrashekhara et al. [17] developed a method of determining the contact force on laminated composite plates subjected to low velocity impact by using FEM and ANN. A finite element model based on a higher-order shear deformation theory is used to calculate the strain pattern and contact force for low-velocity impact. The ANN is trained using the results from the FEA. In this study is concluded that the network can be used for on-line estimation of contact force if the impact-induced strain pattern can be obtained experimentally or numerically.

Haj-Ali and Kim [45] presented an approach to generate nonlinear and multi-axial constitutive models for fiber reinforced polymeric composites using ANNs. The ANN constitutive models were integrated with displacement-based FE software for the nonlinear analysis of composite structures. The ANN constitutive models were trained with experimental data obtained from off-axis tension/compression and pure shear tests. The ability of the ANN models to predict material response was tested directly and through FE analysis of a notched composite plate. Notched composite plates were also tested to verify the FE, with ANN material models, to predict general nonhomogeneous responses at the structural level. It was demonstrated that the proposed FE-ANN simulation code can be used for the analysis of layered composite plate and shell structures.

By using ANN in the computation of composites, which are executed usually in the frame of FE2 approach in multilevel homogenization, costly constitutive calculi in many points of integration are replaced by using a suitably trained ANN to recall the effective constitutive relationships for the homogenization process at the higher structural level. The training of the ANN can be done during regular computation, usually executed in multiscale analysis. However, the main drawback of this approach is that since the computational process in the non-linear range is an evolving process (i.e. the homogenized nonlinear tensor of the composite changes for every load increment) requiring a new training cycle for the ANN for every load increment, making the method to lose its main advantage, since this training may result time consuming.

Several other studies have been performed involving composite materials; however they were more focused on the validation of the ANN than on the analysis of composites or in the usage of ANN in manufacturing process optimization of composites, which lie out of the scope of this research. Another methods using ANN's were developed in other computational contexts such as the works presented by Unger and Könke [121] and Lefik et al. [70] developed under a hierarchical multi-scale approach presented in Section 2.6.8. For a thorough review of the use of ANN in the analysis of composite materials the reader

is referred to [56].

2.6.6 Multi-scale homogenization in 3D

The expansion of two-dimensional multi-scale homogenization to a three-dimensional formulation is a non-trivial endeavor due to different characteristic micromechanical solutions and differences in geometric considerations that may affect the homogenization process (i.e. boundary and periodicity conditions). Among the different formulations found, one of the first studies that deal with homogenization in three dimensions was performed by Guedes and Kikuchi [43]. This homogenization method obtained the effective average constants of linear elastic 2D and 3D composite materials by considering their microstructure. The homogenized elastic constants for macroscopic stress analysis were obtained for typical composite materials to show the capability of the method.

Haj-Ali and Muliana [46] introduced a three-dimensional micromechanical modeling approach for the nonlinear viscoelastic behavior of pultruded composites. Simplified 3D micromechanical models were proposed to compute the effective response of the different layers used in the pultruded cross sections. These models recognize the in situ response of the fiber and matrix constituents. Another micro-model for a sub-laminated model is proposed for the nonlinear effective continuum response of a periodic layered medium. The last part of the study is concerned with the calibration of the in situ fiber and matrix properties to use the calibrated modeling framework to predict the effective viscoelastic response under different multi-axial stress states. Experimental creep tests with off-axis coupons are used to assess these predictions. In an extension of this work the same authors [47] addressed the modeling of nonlinear viscoelastic behavior in laminated composites. The multi-scale 3D structural framework proposed uses both 3D and shell based FE models. In the case of 3D elements, the sublaminate model represents the nonlinear effective response at each material point (Gauss point). In the case of shell elements, each layer is explicitly modeled with one or more integration points under plane stress condition and the sublaminate model is reduced to the classical lamination theory in this case. Constant transverse-shear cross-sectional stiffness is assumed for the shell elements. This assumption is valid in the cases where the transverse stresses in the different layers are very small compared to the in-plane stresses. The 3D micromechanical models provide for the effective nonlinear constitutive behavior for each Gauss point. The shell element's effective through-thickness response is generated at select integration points on its reference surface by integrating the effective micromechanical response over all Gaussian points. The proposed formulation is depicted in Figure 2.13.

Following the same framework, in a latter work Haj-Ali et al. [44] addressed the modeling and analysis of thick-section fiber reinforced plastic (FRP) composite materials. The proposed modeling framework is applied to a pultruded composite system. It consists of two alternating layers with unidirectional fiber (roving) and continuous filaments mat (CFM) reinforcements. Nonlinear 3D micromechanical models representing the different

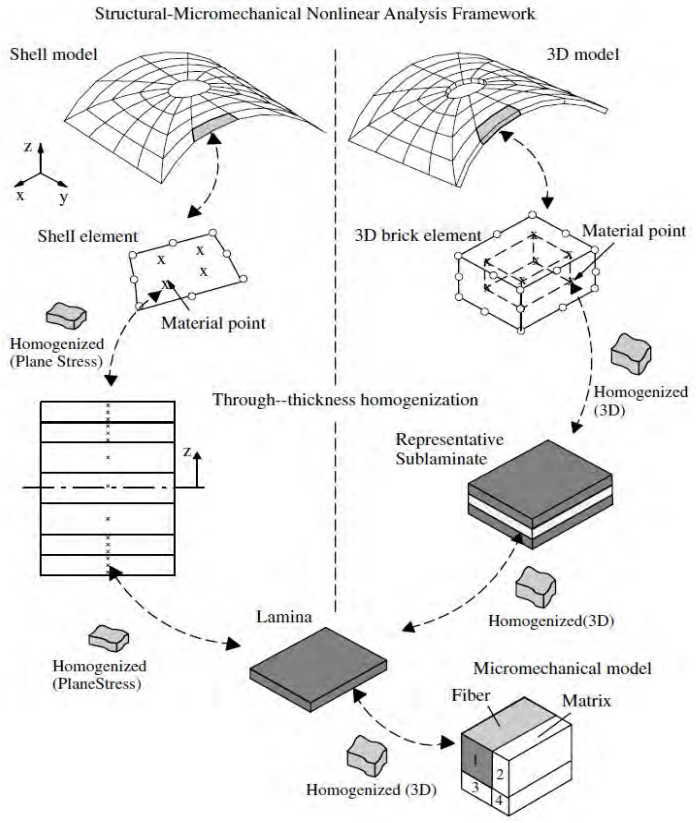

Figure 2.13: multi-scale micromechanicalstructural framework for nonlinear viscoelastic analysis of laminated composite structures (taken from Haj-Ali and Muliana [47]).

composite layers were used to generate through-thickness composite's effective responses. Experimental data was used to verify the predictions of the CFM micromodel predictions for the effective elastic and nonlinear uniaxial compression response. The results obtained demonstrated good prediction capabilities for effective properties and for multi-axial nonlinear behavior of pultruded composites.

Cartraud and Messager [15] developed a formulation to compute the effective elastic properties of periodic beam-like structures. The homogenization theory is used and leads to an equivalent anisotropic Navier-Bernoulli-Saint-Venant beam. The overall behavior is obtained from the solution of basic cell problems posed on the three-dimensional period of the structure and solved using three-dimensional finite element implementation. The procedure is first applied to two corrugated zigzag and sinus beams subjected to in-plane loading. The axial elastic properties of a stranded wire-cable are computed as well.

Galli et al. [32] developed an elastoplastic three-dimensional homogenization model for

particle reinforced composites. The microstructure is expressed generating particles in a pre-existent constrained Delaunay tetrahedralization of a cubic volume by means of a modified random absorption algorithm. This technique allows generating models with different amounts of reinforcement by using the same FE mesh. Homogenization is carried out for a typical particle reinforced metal matrix composite with different reinforcement volume fractions with the RVE size evaluated for both elastic and elastoplastic behaviours. In this latter case the RVE size depends on the amount of plastic strain which develops in the matrix material and a criterion to evaluate the model representativeness is proposed based on the amount of elastic energy stored in the composite. In another work that uses Delaunay decomposition of a cubic volume, Wellmann et al. [123] proposed a homogenization method for granular material modeled by a three-dimensional discrete element method that uses superellipsoids as particles. Macroscopic quantities are derived from the microscopic quantities resulting from a DEM simulation by averaging over a RVE. The resulting expression for the stress tensor consists of a summation over the inter-particle contact forces on the RVE boundary. The corresponding strain tensor is obtained by integration over the displacement field defined by the mass centers of the particles on the RVE boundary. This boundary is defined as the convex hull of the particle centers. The determination of the convex hull by a Delaunay triangulation yields a discretization of the boundary and the enclosed volume right away. The homogenization strategy is validated by DEM simulations of compression and shear tests of cohesionless granular assemblies.

2.6.7 Multi-scale homogenization using higher-order deformation formulations

The multi-scale methods mentioned in the previous sections are commonly denominated as first-order approaches, since in the mathematical formulation considers only the first gradient of the macroscopic displacement field. The first-order computational homogenization technique has been proved to be a very versatile strategy to retrieve the macroscopic mechanical response of non-linear multi-phase materials. However, there are some limitations in the application of the first-order homogenization schemes that derive from the assumption that the microstructural length scale is significantly smaller than its macrostructural counterpart. To overcome the problems that may be derived from the fundamental assumption of the first-order formulations, several authors have suggested using higher-order approximations, e.g. Cosserat, couple-stress, strain-gradient, or non-local continua to describe the behavior of either the microstructural constituents or the homogenized macrostructure or both, or to employ generalized continuum models at both levels simultaneously.

Forest et al. [31] applied the asymptotic homogenization method to analyze linearly elastic Cosserat microstructural constituents. It was shown that depending on the ratio of the micro structural intrinsic Cosserat length and the macrostructural size, the homogenized material should be treated either as a classical (Cauchy) continuum with volume couples or as a Cosserat medium. More recently, De Bellis [21] presented a Cosserat multi-

scale technique for masonry structures based on an adaptation of a Cosserat medium at the macro-level and a Cauchy medium at the micro-level. The formulation consisted on adding to the traditional Cauchy continuum formulation additional strain and stress variables in order to reproduce an independent rotational degree of freedom assigned to every material point.

Ponte-Castañeda [97] proposed a procedure to compute the effective behavior of nonlinear composite materials that consisted in replacing the nonlinear potentials for each phase by their quadratic Taylor approximations, evaluated at appropriate estimates for the average strains in their respective phases. The procedure was applied to composites with two isotropic phases and with statistically isotropic particulate microstructures, by taking advantage of the Hashin-Shtrikman estimates for linear and non-linear plastic composites. Estimates were obtained also for transverse and longitudinal shear loading of a fiber-reinforced composite with a statistically isotropic distribution of fibers in the transverse plane. The approach was found to be useful in the context of the classical secant modulus method. In particular, the use of second moments was found to be helpful in incorporating compressibility effects on the effective behavior of a porous material with an incompressible matrix phase.

Kouznetsova et al. [59] developed a gradient-enhanced computational homogenization procedure that allows modeling of microstructural size effects. The macroscopic deformation gradient tensor and its gradient are imposed on a RVE to incorporate the microstructural size and to account for non-uniform macroscopic deformation fields within the microstructural cell. The second-order computational homogenization scheme is obtained through the generalization of the first-order case. The coupling between the kinematics of both scales relies on a Taylor series expansion of the classical nonlinear deformation map, $\vec{x} = \phi(\vec{X})$, applied to a finite material vector $\Delta\vec{x}$ in the deformed state:

$$\Delta\vec{x} = \mathbf{F}_{\mathrm{M}} \cdot \Delta\vec{X} + \frac{1}{2}\Delta\vec{X} \cdot {}^{3}\mathbf{G}_{\mathrm{M}} \cdot \Delta\vec{X} + \emptyset\left(\Delta\vec{X}^{3}\right) \tag{2.84}$$

Hence, the macroscopic (coarse scale) kinematics is determined through the deformation gradient tensor $\mathbf{F}_{\mathrm{M}} = \left(\vec{\nabla}_{0\mathrm{M}}\vec{x}\right)^{\mathrm{c}}$ and its Lagrangian gradient ${}^{3}\mathbf{G}_{\mathrm{M}} = \vec{\nabla}_{0\mathrm{M}}\mathbf{F}_{\mathrm{M}}$. From the solution of the microstructural BVP the macroscopic stress tensor and the higher-order stress tensor are derived based on an extension of the Hill-Mandel condition. This condition requires the microscopic volume average of the variation of work performed on the RVE to equal the local variation of the work on the macro-scale.

Taking into account that on the macro level the modeling deals with a full gradient higher-order continuum the relations for the macroscopic first PiolaKirchhoff stress tensor $\mathbf{P}_{\mathrm{M}}$ and the macroscopic higher-order stress tensor ${}^{3}\mathbf{Q}_{\mathrm{M}}$ are obtained. Expressed in terms of

volume averages of the microstructural quantities, the macroscopic stress tensor $\mathbf{P}_{\mathrm{M}}$ again equals the volume average of the microscopic stress tensor $\mathbf{P}_{\mathrm{m}}$.

$$\mathbf{P}_{\mathrm{M}} = \frac{1}{V_0} \int_{V_0} \mathbf{P}_{\mathrm{m}} \mathrm{d}V_0 \tag{2.85}$$

However, as for the kinematical quantities, the macroscopic higher-order stress tensor ${}^3\mathbf{Q}_{\mathrm{M}}$ does not equal the volume average of the gradient of the microscopic stress tensor $\nabla_{0\mathrm{m}}\mathbf{P}_{\mathrm{m}}$. The following relation holds instead:

$${}^3\mathbf{Q}_{\mathrm{M}} = \frac{1}{2V_0} \int_{V_0} \left(\mathbf{P}^{\mathrm{c}}_{\mathrm{m}} \vec{X} + \vec{X} \mathbf{P}_{\mathrm{m}} \right) \mathrm{d}V_0 \tag{2.86}$$

From the computational point of view, the method proposed gives a solution of the microstructural problem as fast as the classical approach, since it remains as a classical BVP. The only difference that it presents is in the solution of the higher-order equilibrium problem on the macro level representing an additional computational effort due to the gradient-enhancement procedure. The method presented can be used as a versatile tool to numerically obtain a higher order constitutive response with direct account for the collective behaviour and evolution of the microstructural features or to construct and verify micromechanically based closed-form higher-order constitutive models.

Kaczmarczyk et al. [54] extended Kouznetsova's second-order scheme to encompass not only periodic-type boundary conditions for the RVE but also traction and displacement boundary conditions in a generalized unified manner. The BC's construction was decoupled from the method by which they are numerically enforced. The numerical enforcement was undertaken using projection matrices for multiple constraints in a simple and efficient manner. In an extension of the previous work Kaczmarczyk et al. [55], presented a study of the microstructural size effect and higher-order deformation using second-order computational homogenization. The response of the RVE subjected to different boundary conditions confirmed that the commonly held assumption that the displacement boundary conditions provide an upper bound solution while the traction boundary conditions provide a lower bound when using second-order computational homogenization. Another important conclusion was that the result was dependent on the intrinsic length of the RVE and that for problems in which there is a poor separation of scales, size effect is an important consideration.

Coenen et al. [20] proposed a computational homogenization technique for thin-structured sheets based on the computational homogenization concepts for first- and second-order continua in three-dimensions. The 3D heterogeneous sheet is represented by a homogenized shell continuum for which the constitutive response is obtained from the nested

analysis of a RVE on the microstructural scale, incorporating the full thickness of the sheet and an in-plane representative cell of the macroscopic structure. At an in-plane integration point of the macroscopic shell, the generalized strains, i.e. the membrane deformation and the curvature, are used to formulate the boundary conditions for the microscale RVE problem. At the RVE scale, all microstructural constituents are modeled as an ordinary 3D continuum, described by the standard equilibrium and the constitutive equations. Upon proper averaging of the RVE response, the macroscopic generalized stress and the moment resultants are obtained. In this way, an in-plane homogenization is directly combined with a through thickness stress integration. From a macroscopic point of view, a numerical generalized stressstrain constitutive response at every macroscopic in-plane integration point is obtained. A scheme of the computational homogenization for structured thin sheets proposed by Coenen et al. is presented in Figure 2.14.

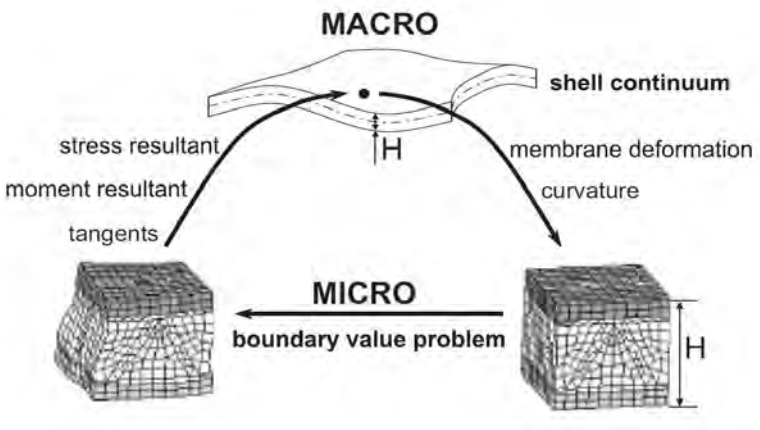

Figure 2.14: General scheme of the computational homogenization for heterogeneous thin sheets (taken from Coenen et al. [20]).

2.6.8 Hierarchical multi-scale approaches

In multi-scale homogenization of composite materials in some cases the gap that exists between the different scales (i.e. the local scale, in a two-scale homogenization scheme, and the component phases) is significantly large, causing in many cases a high gradient of the macroscopic stress/strain fields, making the commonly used two-scale homogenization unsuitable for the analysis of composites. To solve this problem a hierarchical multi-scale approach was developed.

The idea of hierarchical modeling originated as an approach to overcome the difficulties that are present in multi-scale modeling when analyzing highly heterogeneous materials. Hierarchical modeling can be portrayed as a methodology with a tree-like structure which

links the adaptive selection of mathematical models from a structural level that lies beneath the actual scale. This assumption leads to the suggestion that, at a chosen scale, a representative volume element (RVE) exists and can be formed to contain entities of lower scales such that a property of interest at the RVE scale can be derived by appropriate averaging over the RVE volume.

A schematic representation of a hierarchical modeling is presented in Figure 2.15 where a three-scale hierarchical multi-scale approach is depicted. The three-scale hierarchical structure consists of a macroscale, a mesoscale and a microscale. The macroscale constitutive model is obtained by homogenizing the mesoscale response. The mesoscale corresponds to a RVE of the macrostructure and it is response is obtained in turn through periodic assembly of microstructural arrangements.

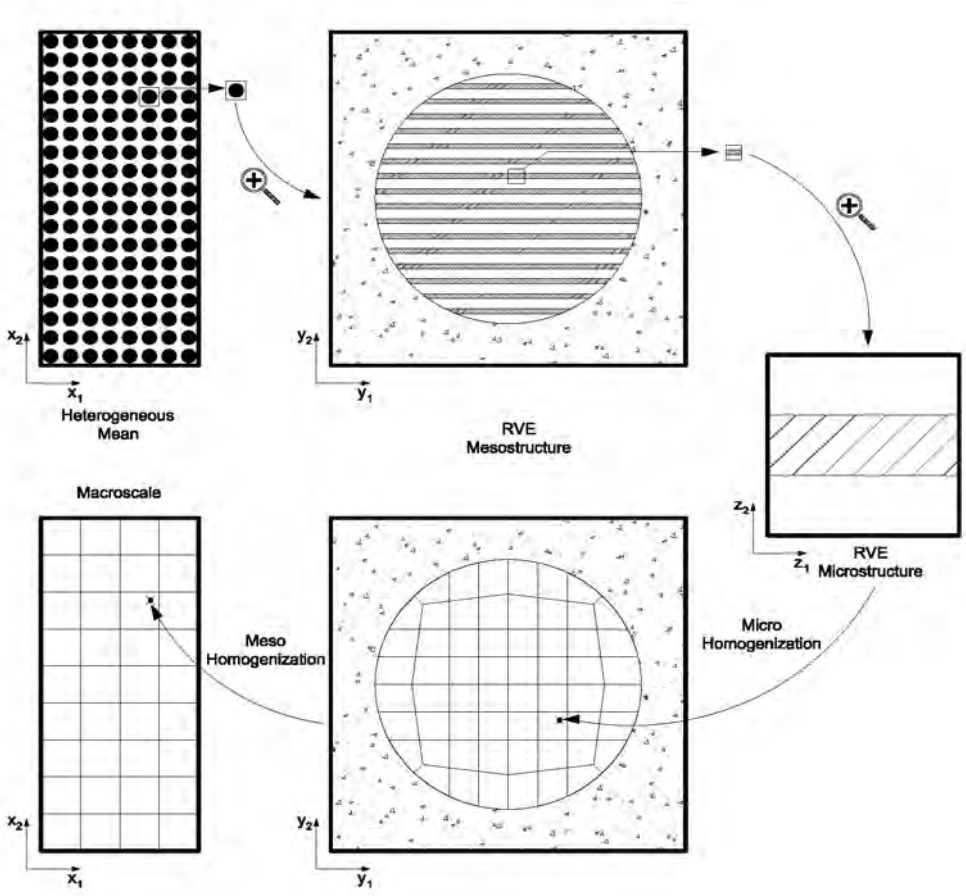

Figure 2.15: General scheme of a three-scale hierarchical analysis applied to composite materials and structures.

The hierarchical multi-scale approach has been addressed by several authors implying the

use of more than 2 scales in the analysis process. Among those authors, Takano et al. [114] proposed a four-level hierarchy modeling for the analysis of textile composites such as woven and knitted fabric. The four scales consisted in: global, local, mesostructural and microscopical level. The stresses at the mesostructure, which is a periodic unit cell of textile composite materials consisting of fiber bundles and matrix, can be evaluated accurately by the homogenization method and finite-element mesh superposition technique. The latter technique makes it possible to overlay arbitrary local fine mesh on the global rough mesh. Anisotropic damage mechanics is also utilized for strength evaluation at the mesoscale. Three-dimensional modeling of the mesostructure of woven and knitted fabric composite materials is shown.

Takano and Okuno [113] proposed a three-scale computational method to analyze fracture in composites that simultaneously considers the microstructure of the heterogeneous materials, the macroscopic component, and the fracture origin such as interface or crack. The synergetic application of the asymptotic homogenization and mesh superposition methods to problems with strong scale mixing is emphasized. The scale gap between the microstructure and the component is very large and the fracture origin is at the middle scale between them. The overall behavior is analyzed by means of the homogenization of the heterogeneity expressed by the unit cell model, while the fracture origin is modeled directly with the microscopic heterogeneity by another microscopic mesh. The microscopic mesh is superposed onto the macroscopic mesh. This mesh superposition method can analyze the non-periodic microscopic stress at the crack tip under a non-uniform macroscopic strain field with high gradient.

Unger and Könke [121]proposed a multiscale approach on different spatial scales using neural networks. Based on a set of mesoscale simulations a system of neural networks is trained to approximate the response of simple concrete-like structures. A macroscale constitutive model is obtained by homogenizing the mesoscale response. Special focus is put on the mesh sensitivity, since the mesoscale model includes softening and consequently the width of the localization zone compared to the dimension of the mesoscale model will influence the model response. Lefik et al. [70] proposed different concepts for the use of Artificial Neural Networks in modeling of composites and hierarchical structures. Starting from a relatively small set of suitable numerical experiments performed on a unit cell, a proper set of corresponding input-output data is created to train the network to identify the effective properties. Furthermore, ANN based procedures can be exploited in a multiscale analysis as a tool for the stress-strain recovery at lower levels of the hierarchical structure and/or to estimate the state of yielding of the materials. These procedures are good enough to be iterated across the various levels of a hierarchical structure to compute effective characteristics and predict some properties of stress and strains fields defined on the micro-cell, reducing thus the time of computations in homogenization of hierarchical composite.

Zheng and Fish [125] presented a hierarchical model reduction approach aimed at reducing

computational complexity of non-linear homogenization at multiple scales is developed. The method consists of the following salient features: (1) formulation of non-linear unit cell problems at multiple scales in terms of eigendeformation modes that a priori satisfy equilibrium equations at multiple scales and thus eliminating the need for costly solution of discretized non-linear equilibrium, (2) the ability to control the discretization of the eigendeformation modes at multiple scales to maintain desired accuracy, and (3) hierarchical solution strategy that requires sequential solution of single-scale problems. A two-scale formulation is verified against a one-dimensional model problem for which an analytical solution can be obtained and a three-scale formulation is validated against tube crash experiments.

Hierarchical multi-scale approaches involving more than two scales represents a promising approach towards the research and development of various advanced materials such as advanced composite materials, polycrystalline materials, and porous materials. Yet, while computational homogenization approaches can drastically reduce the computational cost of the direct numerical simulation (let's say a FE simulation) they remain computationally prohibitive, in many cases, for non-linear problems involving more than two scales. For example, in a two-scale non-linear problem, the unit cell (or RVE) has to be solved a number of times equal to the product of number of quadrature points at a coarse-scale times the number of load increments and iterations at the coarse scale. With each additional scale the number of times the finest-scale unit cell problem has to be solved is increased by a factor equal to the product of the number of quadrature points, load increments and iterations at the previous scale, thus the method becomes very expensive computationally and depending on the case, unachievable.

This page is intentionally left blank.

Chapter 3

Homogenization theory using a multi-domain decomposition method

In this chapter the concepts that serve as basis to the homogenization theory using a multi-domain decomposition approach are presented within a two-scale framework following a mathematical formulation of first-order. The problem formulation based on the relationship between the strains at a macro scale, by means of the transformation experienced by the periodicity vectors that are contained on a micro scale, is thoroughly explained in this section. The application of the periodic boundary conditions in the micro scale is carefully examined as well as the determination of the average strains, stresses and internal variables measures. The computation of the homogenized linear-elastic and non-linear constitutive tensors of the composite obtained by means of perturbations methods are explained in detail. The problems that originate the local effects in the global response of the composite when applying the multi-domain decomposition method are discussed in detail and its solution is addressed following a practical approach.

3.1 Introduction

Numerous efforts have been made to mathematically model composite materials and structures using the homogenization method by using suitable multi-scale techniques with relatively good approximation to the real global response of the composite and in some cases even providing information about the deformation mechanisms that occur in the microstructure of the composite, as it was shown in Chapter 2. Nevertheless, the vast majority of the existing homogenization techniques present a limitation, since most of them are suitable for arrangements that present only one periodic or quasi-periodic distribution over the entire domain of the composite. This limitation restricts the potential of the homogenization method since a large number of composites and structures are set by two or more periodic distributions.

Hence, it may be very helpful if the classical multi-scale homogenization method of analysis could be expanded to analyze this type of structural arrangements when they require to be considered as a single structure at once. Therefore, the main objective of this investigation is to develop a method that is capable of analyzing composite structures with several periodic distributions by partitioning the entire domain of the composite into substructures making use of the classical homogenization theory.

On the other hand, in the literature review presented in the previous chapter it was inferred that homogenization methods that make use of higher order methods appear to have a better ability to establish micro-macro relationships which are reflected in the capacity of consider size effects and macroscopic localization. However, despite these apparent advantages, formulations that make use of higher order formulations present some drawbacks that from a practical point of view they may be considered of high importance.

Among the main disadvantages present in the high-order formulation methods it was found that they generally involve elements that make use of a larger number of nodes and degrees of freedom in a finite element mesh which may result in an increment of the computational effort of the multi-scale scheme. Another limitation is that these methods need additional boundary conditions with respect to first-order formulations. Furthermore, the selection of higher-order boundary conditions is rather an arbitrary task which makes that the solution obtained by this type of methods is not fully standardized so far, since this selection is a matter of choice. Because of the aforementioned reasons, in this research the decision of following a first-order computational scheme was adopted to formulate the multi-domain homogenization method.

The micro-macro coupling procedure that follows the first-order homogenization procedure can be identified as a 'deformation driven' procedure. This procedure consist in that given a deformation at the macro scale (or global) level, expressed by the strain gradient tensor $\bar{\boldsymbol{\varepsilon}}$, the homogenized stress $\bar{\boldsymbol{\sigma}}$ and the homogenized constitutive tensor $\bar{\mathbf{C}}$ can be determined at the micro scale (or local) level based on the interaction among the constituents at the RVE or unit cell.

The first-order homogenization framework presented here takes knowledge from the formulation proposed by Zalamea [126] and that later was extended by Oller et al. [90] and by Badillo and Oller [4]. The formulation is based on classical homogenization approaches originated from the asymptotic homogenization theory. The basic features of the theory were highlighted in Sections 2.4 and 2.5, meanwhile that the mathematical formulation of the classical homogenization theory and the main difficulties found on its implementation are described and discussed in detail in the following sections of this chapter.

3.2 General concepts and basic hypothesis

The homogenization theory formulates the problem of analyzing composite materials using a multi-level approach in which two or more length scales of different order of magnitude naturally exist. In this study all the formulation will be expressed following a two-scale approach. The first scale is identified as the macro scale (or global level), in which the overall behavior of the structure is taken into account as if it were a homogeneous material. The second scale is referred to as the micro scale (or local level), which is characterized by a representative elementary volume or unit cell, in which the microstructural fields are defined. The division of the problem in two scales is justified when the difference in magnitude between these scales is large. That is, if L is the dimension of the global mean or the characteristic wavelength of the macroscopic problem and if l is the dimension of the cell or the period of the characteristic wavelength in the microstructure, the relationship between the two scales, $\epsilon = l/L$ tends to zero.

This formulation, seeks to take advantage of the local periodicity hypothesis arising from the periodicity of the internal structure of the composite. This hypothesis shows that the symmetries of the field variables naturally take place as a consequence of the principle of minimization of energy. This principle ensures that each of the RVEs or unit cell domains that represent the microstructure seeks the inner balance with the minimum energy consumption. Since by definition these domains are considered equal and are placed next to each other then the field of forces and displacements generated in these domains results the same.

3.2.1 Base vectors and local periodicity

According to the definition of periodic continuum, the internal structure of the composite should be generated by repetition of the components. This phenomenon causes some symmetry in the solid, which allows dividing the composite into unit cells or RVEs in a way that each particle that conforms the continuum is related to other particles that are distributed recurrently following a periodicity ratio. This means that by periodicity any point inside a cell or RVE has an equivalent point in each of neighboring cells. These points are known as periodic points. According to this characterization, the link that connects each periodic point is known as a base vector of periodicity (or periodicity vector). Therefore each RVE or unit cell is associated to a specific base vector of periodicity.

Now, let's take for example the cell represented in Figure 3.1. If the contour of the cell is taken as reference, the periodic faces ∂ of the neighboring cells remain 'parallel' by means of the periodicity vectors $\boldsymbol{D}$; this happens even when the cells suffer a change on their form. This fact guarantees the compatibility of displacements at the global scale, otherwise it would produce an overlap in the configuration of the composite or form voids or gaps. Note that this particular field displacement has the characteristic of maintaining the local periodicity of the continuum. Something similar occurs with the forces generated

on the boundary of the cell, since the forces acting on the face of a cell, by the principle of action and reaction are transmitted with the same magnitude and in opposite direction to the neighbor cell. Hence, in these cells, the forces produced are of the same magnitude and in opposite directions to their periodic faces. This principle has been called in homogenization as a field of anti-periodic force (see Figure 3.3).

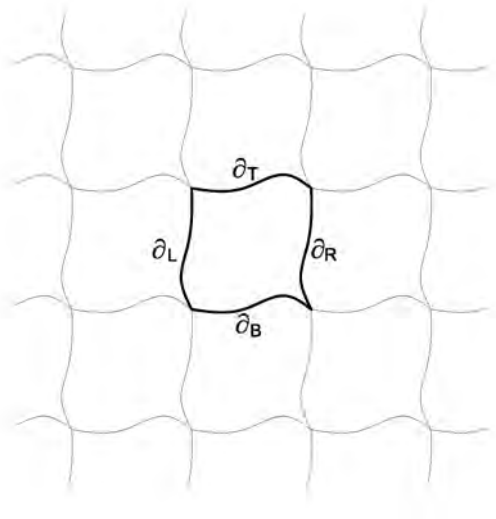

Figure 3.1: Schematic representation of the local periodicity hypothesis on a RVE

An analysis of the displacement fields that are generated in a periodic domain reveals that these displacements produce two effects simultaneously. The first is a differential displacement of the particles within the cell, which causes deformation of the faces. If this shift does not alter the periodicity vectors, the displacement can be understood as a disturbance since it only happens at the microstructural level. The second consequence of the periodic displacement field is that it changes the base of the periodic vectors. These two effects, which occur simultaneously, are very important since the first, which can be considered as a differential displacement of the particles, is required for the cells to reach their internal balance, meanwhile that the second, which alters the periodicity vectors, is directly associated to the deformation of the continuum. It must be remarked that the macro scale deformation is linked to the transformation that the periodicity vectors experience, in other words, to the relative displacement between periodic points.

3.3 Formulation of the problem using homogenized variables

The problem of homogenization is based on the relationship between the strains that arise on the macro scale with the transformation suffered by the periodicity vectors that are

contained on the microscale. The strain deformation at the macroscale can be related to the relative displacement between the periodic points that take place at the microstructural level by means of the homogenization of the strain and stress tensors; once this relationship is completed then it can be formulated and solved the equation that dictates the balance of the composite structure.

In classical homogenization approaches it has been found that there are three different types of boundary conditions: i) prescribed displacements, ii) prescribed tractions, and iii) prescribed periodicity. From these three boundary conditions, it has been pointed out by different authors that periodic boundary conditions provide a better estimation of the homogenized properties than the other two, since periodic conditions preserve the periodicity of the RVE or unit cell in the deformed state (see for example Terada et al. [116]).

3.3.1 Homogenized strain tensor

Consider a point P inside a composite material body Ω in two dimensions, formed by a periodic distribution of the component materials, which at the macro scale level is associated to a reference coordinate system $\boldsymbol{X}$. Assuming that an amplification of the point P at the macroscopic domain could be represented by the cell domain Ω_c located on a system of coordinates in the referential space $\boldsymbol{Y}$ in a way that the material components of the composite can be perfectly identified. In the space $\boldsymbol{Y}$ the referential (or also known as material) space configuration, the cell domain Ω_c is associated with the periodicity vectors $\boldsymbol{D}$ as shown in the left in Figure 3.2, meanwhile at the updated configuration the same space is associated to the vectors $\boldsymbol{d}$ as shown in the right of the same figure.

In this figure, the points P_0, P_1, P_2, represent the periodic points of a cell in the reference coordinate system. Therefore, the periodicity vectors in this case, are defined by the distance between these points, as follows:

$$D^i = Y_{P_i} - Y_{P_0} \quad ; \quad i = 1, 2 \tag{3.1}$$

Moreover, consider also that the continuum Ω undergoes a displacement $\boldsymbol{u}(x, y)$, which generates a new position at the updated configuration of the particles at the macro scale as follows: $\boldsymbol{x} = \boldsymbol{X} + \boldsymbol{u}$. At the micro scale level meanwhile, the cell is represented at the updated configuration by $\boldsymbol{y}$, as presented in Figure 3.2. The updated displacement field $\boldsymbol{u}$ translate the position of the points P_0, P_1, P_2, of the material space coordinates to the position p_0, p_1, p_2 in the updated configuration. According to the hypothesis of local periodicity, the continuum is deformed but its variables maintain the local periodicity. Consequently, the cell is associated with a new base of frequency vectors $\boldsymbol{d}$, defined by the position of the periodic points in the updated configuration as:

$$d^i = y_{p_i} - y_{p_0} = D^i + u_{P_i} - u_{P_0} \quad ; \quad i = 1, 2 \tag{3.2}$$

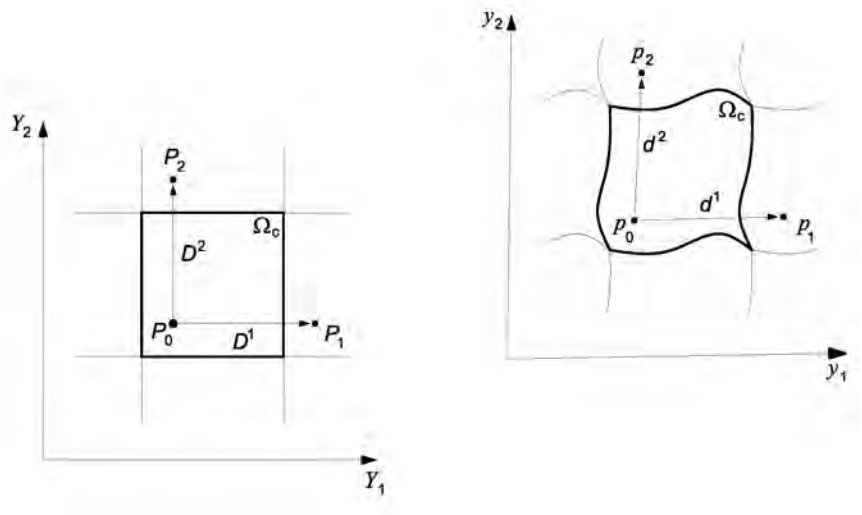

Figure 3.2: Schematic representation of the relation of the periodicity vectors in the referential and updated configurations.

where $\boldsymbol{d}$ is called the updated periodicity vector and $u_{P_i} - u_{P_0}$ is the relative displacement between periodic points.

The transformation of the cell space is associated with the change at the periodicity vectors. The partial derivative of these vectors is defined as follows:

$$\frac{\partial d^i}{\partial D^j} = \frac{\partial \left(y_{p_i} - y_{p_0}\right)}{\partial \left(Y_{P_i} - Y_{P_0}\right)} \tag{3.3}$$

From the macroscopic point of view the periodicity vectors represent some infinitesimal vectors, therefore under the global scale the change over these vectors can be expressed as:

$$\frac{\partial d^i}{\partial D^j} = \lim_{D \to 0} \left[\frac{\partial \left(y_{p_i} - y_{p_0}\right)}{\partial \left(Y_{P_i} - Y_{P_0}\right)} \right] \simeq \frac{\partial x^i}{\partial X^j} = \bar{\boldsymbol{F}} \tag{3.4}$$

Hence,

$$\boldsymbol{d} = \bar{\boldsymbol{F}} \cdot \boldsymbol{D} \tag{3.5}$$

where $\bar{\boldsymbol{F}}$ is the homogenized deformation gradient tensor. This simple change of scale allows determining the macro scale strain field through to concepts that are commonly applied in classical continuum mechanics. Now, in order to obtain the homogenized strain tensor, first we compute the square of the length of the updated periodical vector.

$$\begin{aligned} |\boldsymbol{d}|^2 &= \boldsymbol{d}^T \cdot \boldsymbol{d} \\ &= \boldsymbol{D}^T \cdot \bar{\boldsymbol{F}}^T \cdot \bar{\boldsymbol{F}} \cdot \boldsymbol{D} \end{aligned} \tag{3.6}$$

Afterwards, the difference between the square of the length of the periodicity vectors in the updated and those in the reference configuration is computed as:

$$\begin{aligned} |\boldsymbol{d}|^2 - |\boldsymbol{D}|^2 &= \left[\boldsymbol{D}^T \cdot \bar{\boldsymbol{F}}^T\right] \cdot \left[\bar{\boldsymbol{F}} \cdot \boldsymbol{D}\right] - \boldsymbol{D}^T \cdot \boldsymbol{D} \\ &= \boldsymbol{D}^T \cdot \left[\bar{\boldsymbol{F}}^T \cdot \bar{\boldsymbol{F}} - \mathbf{I}\right] \cdot \boldsymbol{D} \end{aligned} \tag{3.7}$$

Since by definition the Green Lagrange tensor for an homogeneous material is given by $\boldsymbol{\varepsilon} = \frac{1}{2}\left[\boldsymbol{F}^T \cdot \boldsymbol{F} - \mathbf{I}\right]$, by making the analogy to the two-scale formulation presented here, Equation (3.7) can be expressed as a measure of the strain at the macoscopic scale $\bar{\boldsymbol{\varepsilon}}$ as:

$$|\boldsymbol{d}|^2 - |\boldsymbol{D}|^2 = 2\boldsymbol{D}^T \cdot \bar{\boldsymbol{\varepsilon}} \cdot \boldsymbol{D} \tag{3.8}$$

Therefore, the Green Lagrange tensor obtained as a measure of the strain at the macro scale can be called the homogenized strain tensor. This tensor is fully associated with the change of the periodicity vectors.

$$\bar{\boldsymbol{\varepsilon}} = \frac{1}{2}\left[\bar{\boldsymbol{F}}^T \cdot \bar{\boldsymbol{F}} - \mathbf{F}\right] \tag{3.9}$$

This strain deformation quantifies the overall change of the cell's space under a periodic displacement field and is independent of the patterns generated in the contours of the cells. Moreover, since this homogenized strain deformation tensor measures the deformation that occurs between the domain boundary periodic faces or points of the cell, this value also corresponds to the average value of the strain deformation at the domain as shown in Equation (3.10).

$$\begin{aligned} \bar{\boldsymbol{\varepsilon}} &= \langle \boldsymbol{\varepsilon}(y) \rangle_{\Omega_c} \\ &= \frac{1}{V_c}\int_{V_c} \boldsymbol{\varepsilon}(y)\, dV_c \\ &= \frac{1}{V_c}\int_{V_c} \frac{1}{2}\left[\nabla_y \boldsymbol{u} + (\nabla_y \boldsymbol{u})^T\right] dV_c \end{aligned} \tag{3.10}$$

where $\langle \boldsymbol{\varepsilon}(y) \rangle_{\Omega_c}$ is the micro scale strain field, Ω_c is the domain of the cell, V_c is the volume contained in Ω_c, and $\nabla_y \boldsymbol{u}$ is the gradient of the displacement of a particle with respect to the updated configuration $\boldsymbol{y}$. Moreover, this definition coincides with the classic equation of the averaged solution and with the asymptotic homogenization theory presented in Chapter 2.

3.3.2 Homogenized stress tensor

The local stress field $\boldsymbol{\sigma}$ at the microscale in addition to being periodic, is in equilibrium throughout the entire periodic solid. Therefore, the local stress field must satisfy an equilibrium equation inside the entire volume of the cell V_c. Using the Cauchy equilibrium equation on the micro scale and neglecting the inertia forces, since the problem is formulated considering static equilibrium, the equilibrium equation that ensures balance in the microstructure can be expressed as:

$$\int_{S_c} \sigma_{ij} n_j \, dS_c - \int_{V_c} \rho b_i \, dV_c = 0 \tag{3.11}$$

where $\boldsymbol{n}$ is a unit normal vector of the surface element, ρ is the mass, $\boldsymbol{b}$ is the force associated with the mass, S_c is the boundary surface of the unit cell's domain Ω_c.

Considering that the cell's domain is very small from the macroscopic point of view ($\Omega_c \to 0$), then it can be assumed that the value of the forces of the volume are also small and tend to zero. Therefore Equation (3.11) may be reformulated as:

$$\lim_{\Omega_c \to 0} \left(\int_{S_c} \sigma_{ij} n_j \, dS_c \right) \approx 0 \quad ; \quad \lim_{\Omega_c \to 0} \left(\int_{V_c} \rho b_i \, dV_c \right) \approx 0 \tag{3.12}$$

The first integral of the expressions presented in Equation (3.12) indicates the concept of balance in the microstructure, i.e. the integral of the forces on the contour of the cell domain Ω_c is zero. In contrast, the second integral shows that at the microstructure level the effect of mass forces is not required to be taken into account, since the cell is relatively small, which makes that the integral over the mass forces is of an order of negligible magnitude.

Moreover, let's consider now two surface elements ∂S located at periodic points with unitary normal vectors (n_1 and n_2) in opposite directions as those presented in Figure 3.3. The tractions that emerge on opposite boundaries of the unit cell are deduced by translation along directions of invariance of the lattice and are opposite vectors. These vectors depends not only on the position, but also the orientation of the surface element addressed by n. By definition of periodic surfaces, the orientation vectors n_1 and n_2 outside the domain of the cell are equal but opposite. If the effects of mass and inertia forces are neglected, since the forces are relatively very small, the principle of action and reaction ensures that the surface force $\boldsymbol{f} = \boldsymbol{t}(\boldsymbol{n}) dS_c$ in the two periodic surface elements ∂S are of equal magnitude and of opposite direction. This principle is expressed as the antiperiodic stress field in the boundary of the cell in the homogenization formulation.
Now, if a second order tensor $\bar{\sigma}_{ij}$ is defined as the average of the forces at the boundaries of the cell as:

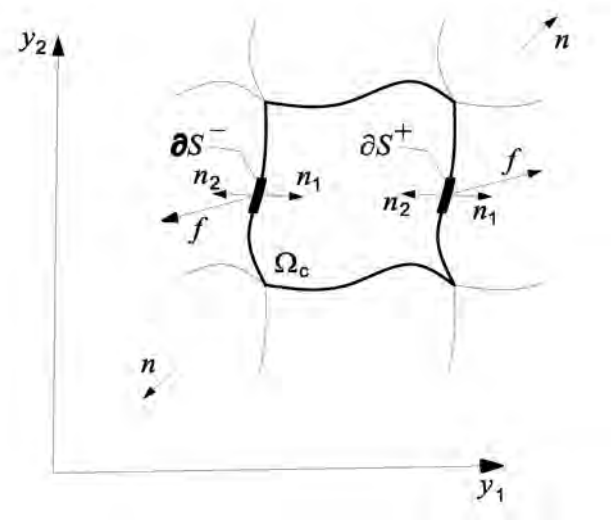

Figure 3.3: Schematic representation of the traction forces that appear on opposite boundaries of the unit cell or RVE.

$$\bar{\sigma}_{ij} = \frac{\int_{S_c} y_k \sigma_{ir} n_r \, dS_c}{\int_{S_c} y_k n_j \, dS_c} \tag{3.13}$$

where k and r = contracted indexes. Thus, if the effect of the volume forces is disregarded ($\sigma_{ij,j} = 0$), and using the divergence theorem gives the following average theory equation:

$$\begin{aligned} \bar{\sigma}_{ij} &= \frac{\int_{V_c} y_{k,r} \sigma_{ir} \, dV_c}{\int_{V_c} y_{k,j} \, dV_c} \\ &= \frac{\int_{V_c} \delta_{k,r} \sigma_{ir} \, dV_c}{\int_{V_c} y_{k,j} \, dV_c} \\ &= \frac{1}{V_c} \int_{V_c} \sigma_{ij} \, dV_c \end{aligned} \tag{3.14}$$

The overall surface force $\bar{\boldsymbol{t}}(\hat{\boldsymbol{n}})$ is defined as the average of the forces on the boundary of the cell S_c, that is determined by the direction of the macro scale unitary vector $\hat{\boldsymbol{n}}$. The force $\bar{\boldsymbol{t}}(\hat{\boldsymbol{n}})$ can be identified as the homogenized traction vector as follows:

$$\begin{aligned} \bar{t}_i\left(\hat{\boldsymbol{n}}\right) &= \frac{\int_{S_c} y_k \sigma_{ir} n_r \, dS_c}{\int_{S_c} y_k n_j \, dS_c} \cdot \hat{n}_k \\ &= \frac{1}{V_c} \int_{V_c} \sigma_{ij} \, dV_c \cdot \hat{n}_k \end{aligned} \tag{3.15}$$

The value of the right hand side of Equations (3.15) is a linear function that depends on the direction of $\hat{\boldsymbol{n}}$. Since by definition we have that:

$$\bar{t}_i\left(\hat{\boldsymbol{n}}\right) = \bar{\sigma}_{ij} \cdot \hat{n}_k \tag{3.16}$$

The tensor $\bar{\boldsymbol{\sigma}}$ satisfies at the macro scale level the same requirements as the stress tensor $\boldsymbol{\sigma}$ for the case of homogeneous materials. Consequently, the tensor $\bar{\boldsymbol{\sigma}}$ is hereinafter referred as the homogenized stress tensor. Consider now that the entire domain of the periodic continuum Ω can be represented as a homogeneous material composed of a large number of cells that are exactly alike. Therefore, it is possible to express the global balance equation as the integral of the balance equation on each of these cells as:

$$\int_{V_\Omega} \left(\frac{1}{V_c} \int_{V_c} \sigma_{ij,j}\, dV_c \right) dV_\Omega + \int_{V_\Omega} \left(\frac{1}{V_c} \int_{V_c} \rho\, b_i\, dV_c \right) dV_\Omega = 0 \tag{3.17}$$

On the macro scale, the body forces per unit volume have to be considered because at this level their magnitude can be significant. These forces may be computed as the average of the volume forces inside the cell as:

$$\bar{b}_i = \frac{1}{V_c} \int_{V_c} \rho\, b_i\, dV_c \tag{3.18}$$

Substituting Equations (3.14) and (3.18) in Equation (3.17) and using the divergence theorem, the global balance equation becomes:

$$\int_{V_\Omega} \bar{\sigma}_{ij,j}\, dV_\Omega + \int_{V_\Omega} \bar{b}_i\, dV_\Omega = 0 \tag{3.19}$$

Equation (3.19) is valid for any region Ω of the composite material, therefore it is also valid even when a very small domain is chosen, since the limit is the cell's domain. Consequently the homogenized local equation of static equilibrium is obtained based on this preceding equation and is expressed in the following way:

$$\bar{\sigma}_{ij,j} + \bar{b}_i = 0 \tag{3.20}$$

3.4 Linear-elastic homogenized formulation in two scales

In order to assemble the general formulation in the linear elastic range using a double scale method, the behavior of the composite is obtained by considering the cell as a structural unit and by considering the problem as a quasi-static problem expressed in small strains. The variables of the problem are established and the governing equations are formulated following this approach. For simplicity, we consider in this work that the component materials are perfectly bonded, however the method does not exclude the possibility of debonding among the component materials.

3.4.1 Linear formulation at the macro scale

To formulate the problem at the macrostructural level first, a boundary value problem (BVP) which consists of a composite material domain Ω is considered. The internal structure of this material is arranged periodically, such that with respect to a macro scale $\boldsymbol{x}$ the material is considered as an homogeneous material. The domain of the material is limited by the boundary $\partial\Omega$, with the following boundary conditions:

$$\begin{aligned} \partial\Omega_u \cap \partial\Omega_t &= 0 \\ \partial\Omega_u \cup \partial\Omega_t &= \partial\Omega \end{aligned} \tag{3.21}$$

where $\partial\Omega_u$ is the boundary in which the displacement is known (Dirichlet condition), and $\partial\Omega_t$ is the boundary where the forces are known (Neumann condition).

The kinematics of the problem is related to a displacement field $\boldsymbol{u}(x)$ on the macro scale, which expresses the displacement of each particle of the domain Ω. Furthermore, the internal structure of the composite is susceptible of being divided into very small structural units called cells or RVEs, whose domain is characterized by Ω_c, in a way that the entire domain Ω can be represented by an orderly repetition of these cells, which gives origin to the two-scale homogenized analysis. These two scales of different order of magnitude, are arranged in a such way that for each particle x_i at the domain Ω there is a cell domain Ω_c which consequently contains a local space y_i.

At the macro scale level, the problem of obtaining the response of composite materials becomes a BVP similar to those problems in which homogeneous materials are solved. Therefore, the displacement $\boldsymbol{u}(x)$ and stress $\bar{\boldsymbol{\sigma}}(x)$ fields at the BVP at the macro scale level must satisfy the following set of equations:

$$\frac{\partial\, \bar{\boldsymbol{\sigma}}(x)}{\partial x} + \bar{\boldsymbol{b}} = 0 \qquad \textit{equilibrium equation in } \ \Omega \tag{3.22}$$

$$\bar{\boldsymbol{\sigma}}(x) = \frac{1}{V_c}\int_{V_c} \boldsymbol{\sigma}(x,y)\, dV_c \qquad \textit{constitutive equation in } \ \Omega \tag{3.23}$$

$$\boldsymbol{u}(x) = \bar{\boldsymbol{u}}(x) \qquad \textit{displacements in } \ \partial\Omega_u \tag{3.24}$$

$$\bar{\boldsymbol{\sigma}}(x)\cdot\boldsymbol{n} = \bar{\boldsymbol{t}}\,(x) \qquad \textit{forces in } \ \partial\Omega_t \tag{3.25}$$

3.4.2 Linear formulation at the micro scale

To formulate the problem at the microstructural level it is necessary to establish the boundary conditions that attain the cell domain. In a standard homogeneous material problem, the boundary conditions present are similar to those presented above in Equations (3.21). However, for the case of the unit cell or RVE of the composite, special boundary conditions are required, such as to introduce the local periodicity of the displacement field and

forces at the microstructural level. By considering that the composite undergoes a macro scale deformation, the local periodicity hypothesis implies that the domain is associated with a periodicity vector in the space of reference, and to another periodicity vector at the updated configuration. The change or transformation of the periodicity vectors represents a relative displacement (shift) between periodic points, as pointed out before in Equation (3.2). However, under the global perspective (where $|\boldsymbol{D}| \to 0$) this relative displacement can be interpreted as:

$$\begin{aligned} \boldsymbol{d} - \boldsymbol{D} &= \lim_{|D|\to 0} (\boldsymbol{u}_{p+D} - \boldsymbol{u}_p) \\ &= \nabla \boldsymbol{u}(x) \cdot \boldsymbol{D} \end{aligned} \tag{3.26}$$

where $\nabla \boldsymbol{u}(x)$ is the displacement gradient at the macro scale. Following the approximation made by Zalamea [126] considering a small strain formulation, the relative displacement between the cell boundary's periodic points can be approximated by taking into account only the symmetric part of the velocity gradient tensor, called the deformation rate tensor; meanwhile the effect of the anti-symmetric part of the velocity gradient tensor, called the spin tensor is neglected. Then the relative displacement between the cell boundary's periodic points can be expressed as:

$$\boldsymbol{u}_{p+D} - \boldsymbol{u}_p \cong \bar{\boldsymbol{\varepsilon}} \cdot \boldsymbol{D} \tag{3.27}$$

where $\bar{\boldsymbol{\varepsilon}}$ is the homogenized strain tensor or strain tensor at the macro scale.

Furthermore, the external forces on the domain of the cell associated with two periodic boundary surface elements are equal in magnitude but in opposite directions. This condition ensures the periodicity of the field of forces and should be satisfied when the cell reaches the equilibrium under the minimum energy consumption. Under these considerations, the local microstructural problem of composite materials on the local scale y is reduced to solve the following boundary value problem in the domain of the cell Ω_c.

$$\frac{\partial\, \boldsymbol{\sigma}(y)}{\partial y} = 0 \qquad \textit{equilibrium equation in } \ \Omega_c \tag{3.28}$$

$$\boldsymbol{\sigma}(y) = \mathbf{C}(y) : \boldsymbol{\varepsilon}(y) \qquad \textit{constitutive equation in } \ \Omega_c \tag{3.29}$$

$$\boldsymbol{u}_{p+D} - \boldsymbol{u}_p = \bar{\boldsymbol{\varepsilon}}(x) \cdot \boldsymbol{D} \qquad \textit{periodic displacements in } \ \partial\Omega_{c_u} \tag{3.30}$$

$$\boldsymbol{t}_{p+D} = -\boldsymbol{t}_p \qquad \textit{periodic forces in } \ \partial\Omega_{c_t} \tag{3.31}$$

where the micro scale stress $\boldsymbol{\sigma}(y)$ and strain $\boldsymbol{\varepsilon}(y)$ fields are the unknowns of the problem, $\mathbf{C}(y)$ is the constitutive tensor corresponding to the respective component material at each point inside the domain which may represent any kind of mechanical behavior (elastic, plastic, etc.), $\bar{\boldsymbol{\varepsilon}}(x)$ is the homogenized strain tensor, $\boldsymbol{D}$ represents the periodicity vectors

which relate the periodic boundary points of the cell and the traction vector t. In the equations presented above it can be observed that the periodic displacement and forces in the boundary of the cell $\partial\Omega_{c_u}$ and $\partial\Omega_{c_t}$, are directly related to the homogenized (or global) strain tensor $\bar{\boldsymbol{\varepsilon}}(x)$ at the macro scale level. Consequently, due to this fact the two problems are coupled, and therefore, the solution of the problem on the macro scale is obtained following a classic procedure, using the equilibrium equation in a discrete solid which requires that the micro scale BVP conditions be satisfied in each point of the macro domain Ω.

Periodicity conditions on the cell's domain

Analytical problems frequently require specific constraints to be imposed on certain solution variables in order to achieve a desired solution. These constraints may consist of certain continuity requirements, the imposition of specified values for the solution variables, or conditions to be satisfied between certain variables. This is the case of the problem formulated in Equations (3.28-3.31) which poses a well conditioned BVP whose solution represents the equilibrium of the microstructure. This equilibrium is restated through the virtual work formulation to a balance of forces inside the domain with respect to the forces that act on the boundary of the same domain as:

$$\boldsymbol{R}(\boldsymbol{\sigma}) = \boldsymbol{F}(\boldsymbol{t}) \tag{3.32}$$

where $\boldsymbol{R}(\boldsymbol{\sigma})$ represent the forces inside the cell domain that are in function of the internal stresses (it can be represented simply as $\boldsymbol{R}$), meanwhile $\boldsymbol{F}(\boldsymbol{t})$ are the forces on the boundary of the cell originated by the external traction forces (which can be represented simply as $\boldsymbol{F}$). This problem can be expressed in a discrete way by using the Finite Element Method; in this case the latter equation can be rearranged in the following way:

$$\boldsymbol{K} \cdot \boldsymbol{u} = \boldsymbol{F} \tag{3.33}$$

where $\boldsymbol{K}$ is the global stiffness matrix of the structure, $\boldsymbol{u}$ is the displacements nodal vector and $\boldsymbol{F}$ the force vector on the boundary of the domain of the cell. However, the system of equations represented by Equation (3.33) must include restrictions of the periodic displacements and forces over the boundary of the domain as exposed in the preceding paragraphs of this chapter. In this case, a general formulation that permits the imposition of the boundary conditions to any kind of cell type is desired (i.e. in shape and space).

The implementation of the restrictions on the displacements and forces corresponding to the degrees of freedom of the domain's boundary, derived from the periodicity requirement, can be accounted for through several methods such as elimination of redundant unknowns, penalty methods, Lagrange multipliers, etc. as remarked by Michel et al. [74]. Each method has its advantages and disadvantages according to the nature of the problem;

in this study the technique that is considered as the most appropriate for the resolution of this problem is the method that employs the Lagrange multipliers. The Lagrange multiplier method can operate on the variational or weighted residual formulations as Bathe [5] points out.

Lagrange multipliers

Lagrange multipliers can be used to find the extrema of a function $\boldsymbol{f}(x_1, x_2, \cdots, x_n)$ ($\boldsymbol{f}$ is a multivariate function) subject to the constraint $\boldsymbol{g}(x_1, x_2, \cdots, x_n) = 0$, where $\boldsymbol{f}$ and $\boldsymbol{g}$ are functions with continuous first partial derivatives on the open set containing the curve $\boldsymbol{g}(x_1, x_2, \cdots, x_n) = 0$, with $\nabla \boldsymbol{g} \neq 0$ at any point on the curve, where ∇ is the gradient operator. The method of Lagrange multipliers is based on a simple observation concerning the perpendicularity of the gradient of the objective function to the constraint curve at an optimal point.

As a brief explanation to the Lagrange multipliers method, consider a problem, which calls for maximizing its objective function $\boldsymbol{f}(x, y)$, subjected to the constraint $\boldsymbol{g}(x, y) = k$ (where k is any constant). It is assumed that both functions $\boldsymbol{f}(x, y)$ and $\boldsymbol{g}(x, y)$ are continuously differentiable functions. To illustrate this explanation, consider Figure 3.4, in which as the levels of the curves of $\boldsymbol{f}(x, y)$ increase, short sections of the curves of $\boldsymbol{f}(x, y)$ form secant curves to $\boldsymbol{g}(x, y) = k$. It follows that the highest level curve of $\boldsymbol{f}(x, y)$ inter-

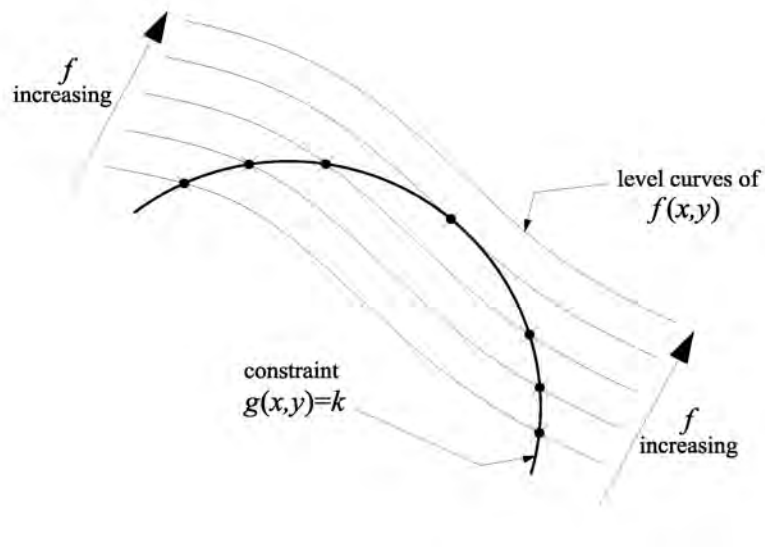

Figure 3.4: Representation of the variation of the function $\boldsymbol{f}(x, y)$

secting $\boldsymbol{g}(x, y) = k$ must be tangent to the curve $\boldsymbol{g}(x, y) = k$, which is possible only if their gradients ∇f is and $\nabla \boldsymbol{g}$ are parallel as presented in Figure 3.5.

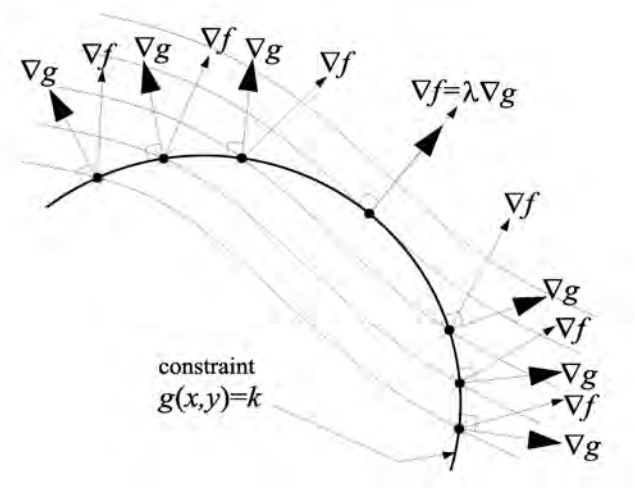

Figure 3.5: Representation of the variation of the function $\boldsymbol{f}(x, y)$ as function of the gradients $\nabla \boldsymbol{g}$ and $\nabla \boldsymbol{g}$.

If $\nabla \boldsymbol{g}$ is parallel to $\nabla \boldsymbol{g}$, then there is a number $\boldsymbol{\lambda}$ for which:

$$\nabla f = \boldsymbol{\lambda} \nabla \boldsymbol{g} \tag{3.34}$$

Thus, the extrema of $\boldsymbol{f}(x, y)$ subject to $\boldsymbol{g}(x, y) = k$ must occur at the points which are the solution to the following system of equations:

$$\left\langle \boldsymbol{f}_x, \boldsymbol{f}_y \right\rangle = \boldsymbol{\lambda} \left\langle \boldsymbol{g}_x, \boldsymbol{g}_y \right\rangle, \qquad \left\langle \boldsymbol{g}_x, \boldsymbol{g}_y \right\rangle = k \tag{3.35}$$

Equation (3.35) is called a Lagrange multiplier problem meanwhile $\boldsymbol{\lambda}$ is referred as a Lagrange multiplier.

Implementation of the periodicity conditions

In many cases it is often that symmetry considerations can be invoked to reduce the periodicity conditions to usual boundary conditions, when both the geometry and the loading exhibit sufficient symmetry. For example, when the unit cell exhibits a plane of symmetry (both for its material properties and its geometry), the local problem can be reduced to a problem on half of the unit cell with standard boundary conditions on the plane of symmetry; following a two-dimensional approach, another example could be considered in the case that the unit cell has two orthogonal lines of symmetry, then the local problem can be reduced to a local problem on one fourth of the original unit cell where the boundary conditions on the plane of symmetries would be the standard ones. But even under a large number of geometric symmetry conditions, multiaxial overall stress states, such as off-axis tension, do not satisfy the required symmetries and the periodicity conditions

cannot be eliminated; therefore, in this formulation, only the full geometry of the cell will be considered for the representation of the RVE.

The numerical solution of the RVE domain requires that each node located on the boundary resulting from the discretization must take into account the conditions of periodicity of displacements and forces. Such conditions are introduced in the system of equations presented in Equation (3.33) by means of the Lagrange multipliers as mentioned earlier. This method however, also has its disadvantages, such as increasing the number of equations, increasing the bandwidth of the stiffness matrix and generating null terms in the stiffness matrix. Nevertheless, this technique is still considered as the most suitable for the resolution of the augmented system including the periodic conditions, since some improvements have been made afterwards in order to get rid of these disadvantages.

Among the improvements that were made to the this method, Anthoine [2] proposed dividing the Lagrange multipliers into two groups, $\boldsymbol{\lambda}_1$ and $\boldsymbol{\lambda}_2$. This two operators relate the boundary forces on the restricted nodes and the corresponding periodic magnitudes. By doing this, the problem where zeros appear on the diagonal of the stiffness matrix $\boldsymbol{K}$ is solved, therefore a more stable method is obtained. The steady state of the increased functional by the Lagrange multipliers is given by:

$$\begin{aligned}\prod = &\frac{1}{2}\boldsymbol{u}^T \cdot \boldsymbol{K} \cdot \boldsymbol{u} - \boldsymbol{u}^T \cdot \boldsymbol{F} + \boldsymbol{\lambda}_1^T \cdot (\boldsymbol{k}_p \cdot \boldsymbol{u} - \Delta \boldsymbol{D}) \\ &+\boldsymbol{\lambda}_2^T \cdot (\boldsymbol{k}_p \cdot \boldsymbol{u} - \Delta \boldsymbol{D}) + \frac{1}{2}\left(\boldsymbol{\lambda}_1 - \boldsymbol{\lambda}_2\right)^T \cdot (\boldsymbol{\lambda}_1 - \boldsymbol{\lambda}_2)\end{aligned} \tag{3.36}$$

The minimization of $\prod$ leads to a well-conditioned symmetric linear system provided that $\boldsymbol{K}$ is also a well-conditioned symmetric matrix. The minimization of the global system is done by minimizing the functional with respect to the three unknown vectors $\boldsymbol{u}$, $\boldsymbol{\lambda}_1$ and $\boldsymbol{\lambda}_2$ as:

$$\frac{\partial \prod^*}{\partial \boldsymbol{u}} = 0; \quad \frac{\partial \prod^*}{\partial \boldsymbol{\lambda}_1} = 0; \quad \frac{\partial \prod^*}{\partial \boldsymbol{\lambda}_2} = 0 \tag{3.37}$$

Expressed in matrix terms stays as:

$$\begin{bmatrix} \boldsymbol{K} & \boldsymbol{k}_p^T & \boldsymbol{k}_p^T \\ \boldsymbol{k}_p & \mathbf{I} & -\mathbf{I} \\ \boldsymbol{k}_p & -\mathbf{I} & \mathbf{I} \end{bmatrix} \cdot \begin{bmatrix} \boldsymbol{u} \\ \boldsymbol{\lambda}_1 \\ \boldsymbol{\lambda}_2 \end{bmatrix} = \begin{bmatrix} \boldsymbol{F} \\ \Delta \boldsymbol{D} \\ \Delta \boldsymbol{D} \end{bmatrix} \tag{3.38}$$

where $\boldsymbol{K}$ is the stiffness matrix of the RVE; $\boldsymbol{k}_p$ is an arrangement matrix that relates the degrees of freedom of the nodes of the boundary. Each row of this matrix contains the value -1 on each degree of freedom which is restricted and the value +1 corresponding periodic node to the restricted one, meanwhile that the rest of the other values are equal

to zero; $\mathbf{I}$ is the identity matrix; $\boldsymbol{u}$ is the displacement vector; $\boldsymbol{F}$ is the force vector; $\Delta \boldsymbol{D}$ is the relative nodal displacement vector for the periodic degrees of freedom of the nodes of the boundary. The two vectors $\boldsymbol{\lambda}_1$ and $\boldsymbol{\lambda}_2$ are obviously equal and correspond to the reaction forces associated with the Dirichlet boundary conditions.

In order to illustrate the assembly of the aforementioned system let's take for example the schematic representation of the RVEs presented in Figures 3.6a and 3.6b.

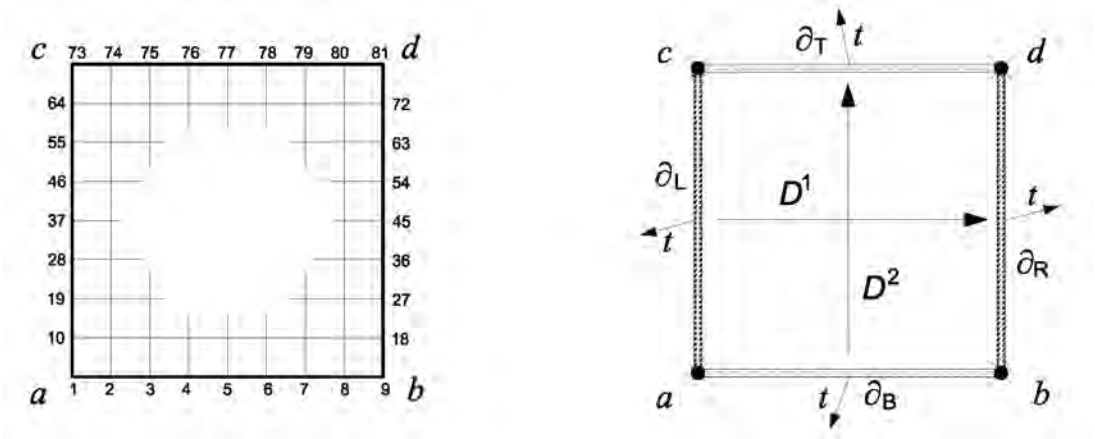

(a) Squared cell array

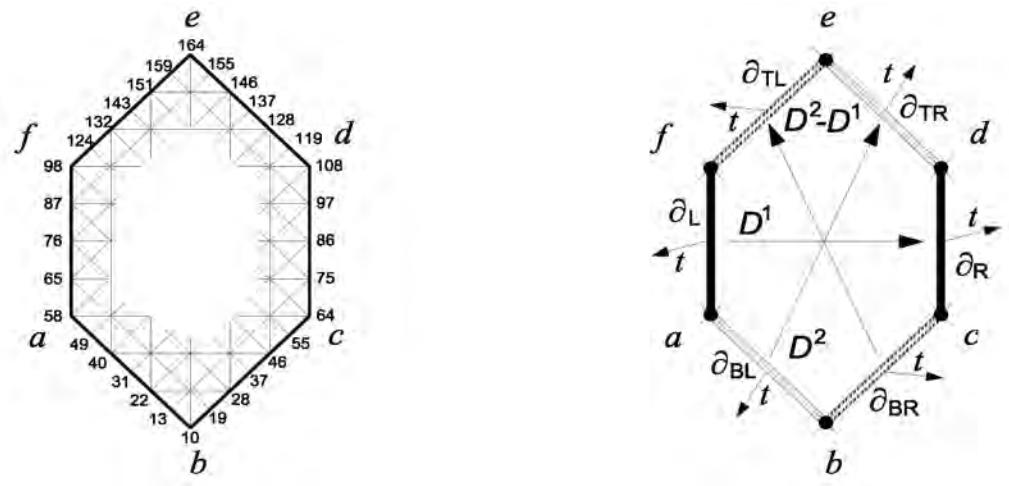

(b) Hexagonal cell array

Figure 3.6: Discretization of the unit cell or RVE into FE and relationship of the periodic faces of the boundaries for different geometric arrays.

In the left side of the figure the discretization of the RVEs into finite elements is presented,

meanwhile on the right side the boundaries of the RVEs divided into pairs of periodic faces are presented. In the case of the squared cell presented in Figure 3.6a, the boundary of the RVE is divided into two pairs of periodic faces related by the vectors $\boldsymbol{D}^1$ and $\boldsymbol{D}^2$, meanwhile that for the hexagonal cell in Figure 3.6b, the boundary is divided into three pairs of periodic faces, which are related by the vectors $\boldsymbol{D}^1$, $\boldsymbol{D}^2$, and $\boldsymbol{D}^2 - \boldsymbol{D}^1$ (in other words, by means of a linear combination of the vector $\boldsymbol{D}^2 - \boldsymbol{D}^1$).

The periodicity relationships of the boundary of the RVE, needs to be translated for its implementation in a Finite Element code by expressing the periodic vertices and nodes that relate the periodic points of the faces in terms of nodal points. This information is presented in Table 3.1, where the number of periodic vertices, the number of pairs of periodic nodes, the node numbers of periodic vertices and the node numbers of periodic pair of nodes is presented for the two RVEs depicted above in Figures 3.6a and 3.6b.

Geometry of the cell	*Squared*	*Hexagonal*
Number of periodic vertices	4	3
Number of pairs of periodic nodes	14	13
Node numbers of periodic vertices	1,9,73,81	58,64,84
Node numbers of periodic pair of nodes	*2-74*	*13-119*
	3-75	*22-128*
	4-76	*31-137*
	5-77	*40-146*
	6-78	*49-155*
	7-79	*19-124*
	8-80	*28-132*
	10-18	*37-143*
	19-27	*46-151*
	28-36	*55-159*
	37-45	*65-75*
	46-54	*76-86*
	55-63	*87-97*
	64-72	- -

Table 3.1: Periodicity relationships of the boundary for two RVE geometry configurations.

The information presented in Table 3.1 for the case of the squared cell seems to be very straightforward, therefore no explanation of this will be made. However for the case of the hexagonal cell, some clarifications will be made since in this case this cell has 6 vertices (a, b, c, d, e, f), however due to the definition of periodicity, the vertices of a hexagonal cell are divided into two groups of periodic vertices, so only one node needs to be

fixed. Therefore the number of periodic vertices for the hexagonal RVE is three (vertices a,c,e or b,d,f). The nodes associated to these vertices determine the periodicity vectors $\boldsymbol{D}$.

The position or the cell space is set through the periodicity vertices. Suppose that vertex number 58 of the hexagonal cell is set in its initial position, then the position of the nodes 64 and 164, at different load increments, is set by the relative displacement $\bar{\boldsymbol{\varepsilon}} \cdot \boldsymbol{D}$ respect to node 58. The position of the other nodes of the boundary is it unknown, but what is known is that the relative displacement between each pair of periodic nodes (for example, the node 13 to node 119, 55 to 159, etc.) is defined at the $\boldsymbol{k}_p$ matrix, meeting the condition imposed $\bar{\boldsymbol{\varepsilon}} \cdot \boldsymbol{D}$ within the vector $\Delta \boldsymbol{D}$. In these nodes, the forces outside the domain have the same magnitude (which is unknown) but on opposite direction to each other. These forces are represented by the Lagrange multipliers $\boldsymbol{\lambda}_1$ and $\boldsymbol{\lambda}_2$.

Note that since the cell definition is a purely geometric concept, therefore any cell configuration can be used to represent the periodic internal structure of the continuum. Therefore, the proposed method should provide the same result from any geometric cell arrangement. In other words, the formulation must be objective.

Although this method may appear quite heavy in computational terms, since two more unknowns are needed for each periodic boundary condition, its general character is a strong advantage when implementing the homogenization method, making it feasible to characterize any type of geometrical shape of RVE.

3.4.3 Determination of the homogenized elastic constitutive tensor

The determination of the elastic constants of the composite structure is formulated following the basis presented in the theory of averages and in the asymptotic expansion theory [7, 22, 34, 103, 110]. Considering that all the constituents of the composite materials are elastic and without admitting the possibility of debonding between the component materials, the elastic constitutive law for the composite which relates the global variables, in a similar way as in the classical expression for homogeneous materials can be expressed as:

$$\bar{\boldsymbol{\sigma}}(x) = \bar{\mathbf{C}}(x) : \bar{\boldsymbol{\varepsilon}}(x) \tag{3.39}$$

where $\bar{\mathbf{C}}(x)$ is the tensor formed by the elastic constants of the homogenized composite, called homogenized elastic constitutive tensor, meanwhile $\bar{\boldsymbol{\sigma}}(x)$ and $\bar{\boldsymbol{\varepsilon}}(x)$ are the homogenized stress and strain tensors.

From Equation (3.39) it can be obviously established that the response of the composite can be determined through the homogenized material constitutive tensor when a strain deformation is applied on the composite; however, on the case of composites, obtaining the homogenized material constitutive tensor is not a straightforward task when two or more material components with different volumetric participations are part of the composite.

One way to obtain this constitutive tensor is by applying a homogenized $\bar{\boldsymbol{\varepsilon}}(x)$ deformation on the cell domain in order to compute the homogenized stress tensor $\bar{\boldsymbol{\sigma}}(x)$. The strain deformation can be applied in terms of small perturbations to the cell, in order to activate the elastic properties of the composite. Then, the homogenized stresses in the cell is computed for each strain deformation applied according to Equation (3.23). Once this operation is performed, it may be possible to obtain the composite elastic constants according to the following expression:

$$\bar{\mathbf{C}}(x) = [\bar{\boldsymbol{\sigma}}(x)] : [\bar{\boldsymbol{\varepsilon}}(x)]^{-1} \tag{3.40}$$

However, since the homogenized elastic constitutive tensor $\bar{\mathbf{C}}(x)$ is of fourth order tensor and the homogenized stress and strain tensors $\bar{\boldsymbol{\sigma}}(x)$ and $\bar{\boldsymbol{\varepsilon}}(x)$ are tensors of second order, the above equation has an infinite number of solutions. Nevertheless, if the condition of orthotropy is considered and a system of equations with different perturbations is applied in each of the principal directions, the homogeneous constitutive tensor can be obtained component by component, making the problem to have a unique solution.

Perturbation method at the linear-elastic range

The method applied to obtain the elastic constants of the composite is associated to the procedure followed by the theory of averages and by the asymptotic expansion theory. It consist in applying small perturbations (small displacements) to the cell in each of the principal directions separately in order to activate the different elastic constants of the composite. For the case of bi-dimensional problems which are idealized as a plane stress or plain strain problem, the homogenized elastic constitutive tensor can be expressed in matrix for as:

$$\bar{\mathbf{C}}(x) = \begin{bmatrix} \bar{C}_{xxxx} & \bar{C}_{xxyy} & 0 \\ \bar{C}_{yyxx} & \bar{C}_{yyyy} & 0 \\ 0 & 0 & \bar{C}_{xyxy} \end{bmatrix} \tag{3.41}$$

If the perturbations are applied by means of the set of independent strains of Equations (3.42-3.44) in each of the principle directions as:

$$\bar{\boldsymbol{\varepsilon}}_1(x) = [\bar{\varepsilon}_{xx}, 0, 0] \tag{3.42}$$

$$\bar{\boldsymbol{\varepsilon}}_2(x) = [0, \bar{\varepsilon}_{yy}, 0] \tag{3.43}$$

$$\bar{\boldsymbol{\varepsilon}}_3(x) = [0, 0, 2\bar{\varepsilon}_{xy}] \tag{3.44}$$

A set of field stresses is obtained correlated to the strains applied independently for each direction as expressed in Equations (3.45).

$$\bar{\boldsymbol{\sigma}}[\bar{\boldsymbol{\varepsilon}}_1(x)] \quad ; \quad \bar{\boldsymbol{\sigma}}[\bar{\boldsymbol{\varepsilon}}_2(x)] \quad ; \quad \bar{\boldsymbol{\sigma}}[\bar{\boldsymbol{\varepsilon}}_3(x)] \tag{3.45}$$

The coefficients of the homogenized tensor of Equation (3.41) are given by the following set of equations:

$$\bar{C}_{xxxx} = \frac{\bar{\sigma}_{xx}\bar{\boldsymbol{\varepsilon}}_1(x)}{\bar{\varepsilon}_{xx}} \tag{3.46}$$

$$\bar{C}_{xxyy} = \frac{\bar{\sigma}_{xx}\bar{\boldsymbol{\varepsilon}}_2(x)}{\bar{\varepsilon}_{yy}} \tag{3.47}$$

$$\bar{C}_{yyyy} = \frac{\bar{\sigma}_{yy}\bar{\boldsymbol{\varepsilon}}_2(x)}{\bar{\varepsilon}_{yy}} \tag{3.48}$$

$$\bar{C}_{yyxx} = \frac{\bar{\sigma}_{yy}\bar{\boldsymbol{\varepsilon}}_1(x)}{\bar{\varepsilon}_{xx}} \tag{3.49}$$

$$\bar{C}_{xyxy} = \frac{\bar{\sigma}_{xy}\bar{\boldsymbol{\varepsilon}}_3(x)}{2\bar{\varepsilon}_{xy}} \tag{3.50}$$

The technique used to obtain the coefficients of the homogenized constitutive tensor is independent of the shape and type of strain that is applied to the cell. This means that the homogenized constitutive tensor it will always be the same, even if another set of distortions it is applied to the cell, as long as the cell properties remain within the elastic range. The hypothesis of symmetry of the constitutive tensor has been expressed by Suquet [110] assuming that the elastic homogenized constitutive tensor shows the classic symmetries if the components of the composite have a periodic distribution. Therefore if the condition to ensure the periodicity of the continuum is met, it can be stated that the hypothesis of symmetry of the homogenized elastic constitutive tensor as expressed in Equation (3.51) is satisfied.

$$\bar{C}_{xxyy} = \bar{C}_{yyxx} \tag{3.51}$$

It must be noted that, as long as all the constituents of the composite remain at the linear range of behavior, the constitutive tensor $\bar{\mathbf{C}}(x)$ will remain without any modification. Nevertheless, it must be taken into account that this factor changes when any of the components of the composite enters into the nonlinear range; therefore the homogenized constitutive tensor must be computed according to the state of charge endured by the composite structure for every and each load step after any of the constituents that form part of the composite goes beyond the linear range.

3.5 Non-linear homogenized formulation in two scales

In the linear-elastic formulation presented in Section 3.4, the assumption of a linear-elastic material is implied in the use of a constant stress-strain matrix for both scales and in the assumption that the boundary conditions remain unchanged, since constant constraint relations are considered in the computation of the global response. However, in the analysis of solid and structural mechanics, when any of these assumptions is not meet, a non-linear analysis must be performed instead.

The non-linearity of a problem is defined by several factors, since it may be caused by material or kinematic effects. In a materially-nonlinear analysis, the non-linear effects lie only on the stress-strain relation. However, there are other types of nonlinearities, such as those in which the boundary conditions change during the motion of the body under consideration. In the case of composite materials, the non-linear behavior can be originated due to several causes: matrix and fiber non-linear constitutive behavior, microfailure effects (matrix microcracking, fiber-matrix debonding), and fiber failure (fiber buckling), etc. In either case, the composite material behaves as a non-linear one, depending on the local history of the constituent materials. In this research the non-linearity of the problem is defined by the non-linear effects given by the stress-strain relation. Other types of nonlinearities lie out of the scope of this research and should be subject of further research.

In the nonlinear problem the geometric and kinematic expressions that were established for the elastic problem remain valid. The local equilibrium equations, both at the macro and micro scale presented in Sections 3.4.1 and 3.4.2, also remain valid; however, the elastic behavior material laws, represented at Equations (3.23) and (3.29) have to be replaced by their non-linear counterparts in order to reproduce the inelastic behavior of each component material on the micro-structure and of the entire composite at the global scale.

3.5.1 Basic concepts for the formulation of the non-linear equation

In classical Continuum Mechanics formulations, the linear and non-linear behavior of materials is established by using constitutive equations. These equations relate two physical quantities that is specific to a material or substance, and approximate the response of that material to a set of external forces. In the linear case is common to approximate the constitutive equation by means of a simple proportionality parameter taken from the properties of the material. This stress-strain constitutive relation is commonly known as Hooke's law. Nevertheless, in the non-linear case a much more elaborated formulation is needed to account for the tensorial properties and the rate of response of the materials expressed in Equation (3.52).

$$\dot{\boldsymbol{\sigma}} = \mathbf{C}^{T_{nl}} : \dot{\boldsymbol{\varepsilon}} \tag{3.52}$$

where $\mathbf{C}^{T_{nl}}$ represents the non-linear constitutive tangent tensor of a constituent material.

Different mathematical equations have been established to represent the ideal phenomenological behavior of many homogeneous and isotropic materials. Several constitutive equations have been developed and are available at the literature on the topic reproducing the behavior of different materials (elastic, plastic, viscous, with stiffness degradation, with strength degradation etc.).

The deduction of the constitutive equations is usually performed starting from a potential energy Φ and expressed in function of different variables (free variables, internal variables and dependent variables). A generalization of this procedure can be expressed by the following expressions:

a) Free energy of the material:

$$\boldsymbol{\Phi} = \boldsymbol{\Phi}(\boldsymbol{\varepsilon}, \boldsymbol{\alpha}) \tag{3.53}$$

b) Free variable. Strain tensor:

$$\boldsymbol{\varepsilon} = \frac{1}{2}\left(\frac{\partial u}{\partial y} + \frac{\partial u^T}{\partial y}\right) \tag{3.54}$$

c) Internal variables:

$$\boldsymbol{\alpha} = \{\alpha_k\} \qquad k = 1, ..., n \tag{3.55}$$

d) Dependent variable. Stress tensor:

$$\dot{\boldsymbol{\sigma}} = \dot{\boldsymbol{\sigma}}\left(\Phi, \dot{\boldsymbol{\varepsilon}}, \alpha\right) \tag{3.56}$$

The scheme presented in Equations (3.53-3.56) to obtain a constitutive equation is valid only for the case of a component material. However, when dealing with composite materials or structures composed of two or more materials, each material that is part of the composite will behave in a characteristic manner according to the physical and chemical properties that govern their behavior. Several attempts have been made to obtain constitutive equations of composite materials by considering the composite material as a homogeneous one; nevertheless this is a complicated process that not only depends on the material properties of the components but also on the volumetric participation within the composite and on the spatial configuration with respect to the whole specimen.

In this formulation, the homogenization method is applied in order to avoid this complicated process, but above all to make it possible to analyze almost any composite material configuration independently of the material behavior of its components and of the geometric pattern in which they are arranged.

The non-linear formulation in this study is derived based on the field variables for each

component at the micro-structural level. However, as Suquet [110] pointed it out, performing a task such as this will depend on an infinite number of variables. In order to avoid this inconvenient it is decided that the most appropriate way to obtain the non-linear constitutive equation should be done through a formulation based on a numerical algorithm implementation.

The numerical algorithm implementation is carried out through a reproduction of the field variables of stress and strain at the micro-structural level, which are function of the behavior and of the geometric form of the component materials. Therefore, the entire field of internal variables of the components within the cell domain represents the internal variables of the constitutive equation of the composite. Thus, in order to formulate a constitutive equation for the composite (at the global level), there is no need to operate directly with the constitutive equations of the components (at the local level), nor with its geometry. Following a formulation like this, results in obtaining a method of general character which can be applied in the solution of almost any type of composite material or structural configuration.

3.5.2 Non-linear formulation at the macro scale

The non-linear formulation at the macro scale follows the same postulations as in the linear-elastic case. The formulation considers the BVP of a domain Ω which represents a composite material and which is delimited by a boundary $\partial\Omega$ where $\partial\Omega_u$ is the part of the boundary where the displacements are known (Dirichlet condition) and $\partial\Omega_t$ is the part of the boundary where the forces are known (Newman condition). Again, the internal structure of the composite is considered as prone of being divided into very small structural units called cells or RVEs, whose domain is characterized by Ω_c, in a way that the entire domain Ω can be represented by an orderly repetition of these cells.

As in the linear case, the BVP at the macro scale level must satisfy the following set of equations:

$$\frac{\partial\, \bar{\boldsymbol{\sigma}}(x)}{\partial x} + \bar{\boldsymbol{b}} = 0 \qquad \textit{equilibrium equation in } \ \Omega \tag{3.57}$$

$$\bar{\boldsymbol{\sigma}}(x) = \frac{1}{V_c}\int_{V_c} \boldsymbol{\sigma}(x,y)\, dV_c \qquad \textit{constitutive equation in } \ \Omega \tag{3.58}$$

$$\boldsymbol{u}(x) = \bar{\boldsymbol{u}}(x) \qquad \textit{displacements in } \ \partial\Omega_u \tag{3.59}$$

$$\bar{\boldsymbol{\sigma}}(x)\cdot\boldsymbol{n} = \bar{\boldsymbol{t}}\,(x) \qquad \textit{forces in } \ \partial\Omega_t \tag{3.60}$$

However, according to Equation (3.52) a constitutive relation of the composite at the non-linear range needs to be established in an incremental way in order to satisfy Equation (3.58) on the BVP expressed above, such as:

$$\dot{\bar{\boldsymbol{\sigma}}}\,(x) = \bar{\mathbf{C}}^{T_{nl}}\,(x) : \dot{\bar{\boldsymbol{\varepsilon}}}\,(x) \tag{3.61}$$

where $\bar{\mathbf{C}}^{T_{nl}}(x)$ represents the non-linear homogenized constitutive tangent tensor of the composite structure.

3.5.3 Non-linear formulation at the micro scale

At the micro scale the non-linear problem considers a domain Ω_c that represents the unit cell or RVE of the composite, which is repeated periodically. At the microstructural scale the problem consists in obtaining the displacement $\boldsymbol{u}(y)$ and stress $\boldsymbol{\sigma}(y)$ fields satisfying the following set of equations on the BVP.

$$\frac{\partial\, \boldsymbol{\sigma}(y)}{\partial y} = 0 \qquad \textit{equilibrium equation in } \ \Omega_c \tag{3.62}$$

$$\dot{\boldsymbol{\sigma}}(y) = \mathbf{C}(y) : \dot{\boldsymbol{\varepsilon}}(y) \qquad \textit{constitutive equation in } \ \Omega_c \tag{3.63}$$

$$\boldsymbol{u}_{p+D} - \boldsymbol{u}_p = \bar{\boldsymbol{\varepsilon}}(x) \cdot D \qquad \textit{periodic displacements in } \ \partial\Omega_{c_u} \tag{3.64}$$

$$\boldsymbol{t}_{p+D} = -\boldsymbol{t}_p \qquad \textit{periodic forces in } \ \partial\Omega_{c_t} \tag{3.65}$$

where $\mathbf{C}(y)$ is the constitutive tensor corresponding to the respective component material at each point inside the domain which may represent any kind of mechanical behavior (plasticity, damage, etc.). The problem at the micro scale is associated to the macro scale through the strain tensor $\bar{\boldsymbol{\varepsilon}}(x)$.

3.5.4 Formulation of the equilibrium equation of the composite in two scales

The constitutive equation for the composite is formulated as an incremental algorithm which controls the global strain deformation of the composite through an increment $\dot{\bar{\boldsymbol{\varepsilon}}}(x)$ on the instant of time Δt. The response of the composite at the current time $t + \Delta t$ is given by the homogenized stress tensor according to the following expression:

$$\bar{\boldsymbol{\sigma}}(x)^{t+\Delta t} = \bar{\boldsymbol{\sigma}}(x)^{t} + \bar{\mathbf{C}}^{T_{nl}}(x)^{\Delta t} : \dot{\bar{\boldsymbol{\varepsilon}}}(x)^{\Delta t} \tag{3.66}$$

Expression (3.66) strictly agrees with Equation (3.14); therefore it can be expressed in terms of the microscopic variables over the RVE or unit cell as:

$$\begin{aligned} \bar{\boldsymbol{\sigma}}(x)^{t+\Delta t} &= \frac{1}{V_{\Omega_c}} \int_{V_{\Omega_c}} \left[\boldsymbol{\sigma}^{t}(\boldsymbol{\Phi}(y), \bar{\boldsymbol{\varepsilon}}(x)^{t}, \boldsymbol{\alpha}(y)^{t}) + \dot{\boldsymbol{\sigma}}^{\Delta t}(\boldsymbol{\Phi}(y), \dot{\bar{\boldsymbol{\varepsilon}}}(x)^{\Delta t}, \dot{\boldsymbol{\alpha}}(y)^{\Delta t}) \right] dV_{\Omega_c} \\ &= \frac{1}{V_{\Omega_c}} \int_{V_{\Omega_c}} \boldsymbol{\sigma}^{t+\Delta t}(\boldsymbol{\Phi}(y), \bar{\boldsymbol{\varepsilon}}(x)^{t+\Delta t}, \boldsymbol{\alpha}(y)^{t+\Delta t}) dV_{\Omega_c} \end{aligned} \tag{3.67}$$

where $\boldsymbol{\Phi}(y)$ represents the potential energy and $\boldsymbol{\alpha}(y)$ represents the internal variables within the cell's domain. The solution of Equation (3.67) represents the mechanical response of the composite using the homogenization method in two scales.

Now, assume a quasi-static behavior of a given composite material, where the geometric data of the microstructure it is known (domain Ω_c). Suppose that the variables problem in a given time t are known, i.e. the stress $\bar{\boldsymbol{\sigma}}(x)^t$ and strain $\bar{\boldsymbol{\varepsilon}}(x)^t$ homogenized tensors and the internal variables $\boldsymbol{\alpha}(y)^t$ at the composite domain Ω throughout the cell or RVE domain. Consequently, since the composite is assumed in equilibrium, the residue r^t is approximately equal to zero. This is expressed as in a general form as:

$$r^t = \left| R(\bar{\boldsymbol{\sigma}})^t - F(\bar{\boldsymbol{t}}^{\,n})^t \right| \simeq 0 \tag{3.68}$$

where $R(\bar{\boldsymbol{\sigma}})$ represent the forces inside the composite domain that are in function of the internal homogenized stresses, meanwhile $F(\bar{\boldsymbol{t}}^{\,n})$ are the forces on the boundary of the composite domain originated by the external traction forces. According to Equation (3.66) the increment in the response of the composite for the time $t + \Delta t$, depends on the homogenized strain rate increment $\dot{\bar{\boldsymbol{\varepsilon}}}(x)^{\Delta t}$.

$$\begin{aligned} \dot{\bar{\boldsymbol{\sigma}}}(x)^{\Delta t} &= \bar{\mathbf{C}}^{T_{nl}}(x)^{\Delta t} : \dot{\bar{\boldsymbol{\varepsilon}}}(x)^{\Delta t} \\ &= \bar{\boldsymbol{\sigma}}(x)^{t+\Delta t} - \bar{\boldsymbol{\sigma}}(x)^t \end{aligned} \tag{3.69}$$

with:

$$\bar{\boldsymbol{\varepsilon}}(x)^{t+\Delta t} = \bar{\boldsymbol{\varepsilon}}(x)^t + \dot{\bar{\boldsymbol{\varepsilon}}}(x)^{\Delta t} \tag{3.70}$$

The systems of equations presented in the expressions (3.57-3.60) and (3.62-3.65) represent the balance of the BVP in each of the scales. The solution to this two BVP's must be performed as a coupled system as established in Equation (3.67). This implies an infinite number of boundary value problems, one at the macro scale and the rest in the micro scale (one for each integration point of the macro scale). Hence the difficulty of solving non-linear problems by using the homogenization theory. A pivotal role on the coupled solution is played by the non-linear homogenized constitutive tensor, since the rate of convergence depends on it. Therefore, an appropriate strategy to obtain it is desired.

3.5.5 Formulation of the homogenized non-linear constitutive tensor

The homogenized constitutive tensor was successfully obtained in the linear range by computing the homogenized stress tensor $\bar{\boldsymbol{\sigma}}(x)$ when a small strain deformation $\bar{\boldsymbol{\varepsilon}}(x)$ was applied into the cell to activate the elastic properties of the composite as expressed in Section 3.4.3. Nevertheless, if the same formulation is used to compute the homogenized constitutive tensor on the non-linear range it may result in a rough approximation of the composite response, since the stresses on the unit cell or RVE may vary considerably from one element to another depending on the material and geometric configuration of the cell. This may lead to numerical problems, especially in high stages of non-linear behavior.

Obtaining the non-linear response of a composite material is a difficult task since the homogenized non-linear constitutive tensor changes according to the applied load. This process involves a huge computational cost. Several procedures have been developed in order to obtain the non-linear homogenized constitutive tensor with the minimum computational effort possible. These include, for example, the construction of a database with the homogenized properties, performing sensitivity analysis, applying Fast Fourier Transforms, using a characteristic deformation mode superposition method, etc. For a thorough review of many of the methods developed so far, see Chapter 2. However in all the procedures available so far, the only constant, is the enormous computational effort required to compute the tensor when the composite structure lies within the nonlinear range. Among the several methods found, the perturbation based methods appear to be the most efficient procedures developed so far to compute the homogenized non-linear tensor as suggested by Miehe [75]. In this formulation the perturbation-based method presented by Badillo and Oller [4] is adopted to compute the non-linear tangent tensor of the composite materials and structures presented in this study.

The method consists in applying a perturbation to obtain the non-linear tangent constitutive tensor $\mathbf{C}^{T_{nl}}$ of each element of the unit cell that represents the composite. The non-linear performance at the RVE or unit cell is implemented through the constitutive models (developed a priori). The implementation of the periodicity conditions on the cell domain also remain the same as in the linear range, thus at first glance no further assumptions have to be made to solve the problem at the local or microstructural level when the RVE enters into the non-linear range.

Once that the tangent tensor is computed for each and every element of the unit cell or RVE, it must be stored in order to calculate the homogenized non-linear tangent constitutive tensor $\bar{\mathbf{C}}^{T_{nl}}$ over the entire volume of the cell, in a way that will allow us to solve the constitutive problem of the composite material expressed by Equation (3.61). The homogenized tangent non-linear constitutive tensor is computed over the entire volume of the unit cell or RVE following the classical definition given by the average method as expressed in Equation (3.71).

$$\bar{\mathbf{C}}^{T_{nl}}(x) = \frac{1}{V_{\Omega_c}} \int_{V_{\Omega_c}} C_{ij}^{T_{nl}} dV_{\Omega_c} \tag{3.71}$$

The expression presented in Equation (3.71) is analogous to the one presented in Equation (3.41) for the linear elastic case since both expressions would yield the same linear elastic constitutive tensor. The difference among these two expressions is that in the Equation (3.41) the homogenized constitutive tensor is computed directly from the homogenized elastic stress and strains tensors of the cell, meanwhile that in Equation (3.71) the constitutive tensor it is obtained from the integration over the volume of the cell's domain of the tangent constitutive tensors from each integration point. The perturbation method is numerically explained in Section 4.4.2 in the Chapter 4.

3.6 Formulation of the homogenization method following a multi-domain decomposition approach

In this section, the concepts that were exposed in the paragraphs above, that form part of the classical homogenization method, are further applied following a multi-domain decomposition scheme. The objective of the micro-macro approach developed in this research is to set the mathematical framework to take into account the decomposition of the structure into an assembly of substructures following a more practical approach than the ones present in the few multi-domain decomposition schemes existing to date.

3.6.1 Previous studies on multi-domain decomposition

Several micro-macro approaches have been developed to obtain mathematically the response of composite materials and structures using the classical homogenization method of periodic or quasi-periodic arrangements. However very few attempts have been made in order to fulfill the need to analyze multi-domain periodic arrangements when they are required to be considered as a single structure at once by using the homogenization method.

Among the first works on this subject, Fish and Wagiman [29] presented a generalization of the mathematical homogenization theory to account for locally non-periodic solutions. The authors proposed dividing the problem in different sections. In the portion of the problem domain where the material is formed by a spatial repetition of the base cell and the macro scale solution is smooth, a double scale asymptotic expansion and solution periodicity are assumed, and consequently, mathematical homogenization theory is employed to uncouple the micro scale problem from the global solution. Meanwhile that for the rest of the problem domain it is assumed that the periodic solution does not exist (cutouts, cracks, free edges in composites, etc.) and the approximation space is decomposed into global and local scale fields. The compatibility between the two regions is explicitly enforced throughout the solution process.

Later on, Fish and Belsky [28] proposed a multi-grid method for a periodic heterogeneous medium in multi-dimensions. Special intergrid transfer operators were developed to simulate a low frequency response of the boundary value problem with oscillatory coefficients based on the classical homogenization method. An adaptive strategy was developed to form a nearly optimal two-scale computational model consisting of the finite element mesh entirely constructed on the microscale in the regions identified by the idealization error indicators, while elsewhere, the modeling level is only sufficient to capture the response of the homogenized medium.

On another work on the subject, Hami and Radi [48], developed two decomposition methods based on the partition of the structure in some substructures called the iterative substructure method and the method based on the symmetry groups. The composite is divided in certain number of identical subdomains or repetitive patterns having a repetitive

geometry. Furthermore the structure is defined as mechanically repetitive if it possesses incidental mechanical characteristics for each subdomain, where the operator of the structure is 'equivariant' under the action of the symmetry group.

Ladevèze and coworkers [63, 65, 81, 64] implemented a micro-macro computational strategy for the analysis of structures which are described up to the micro level, such as composite structures. The description of micro and macro quantities is performed on the interface arising from the decomposition of the structure. The first step of the method consists in the decomposition of the structure into an assembly of simple constituents: substructures and interfaces as presented in Figure 3.7.

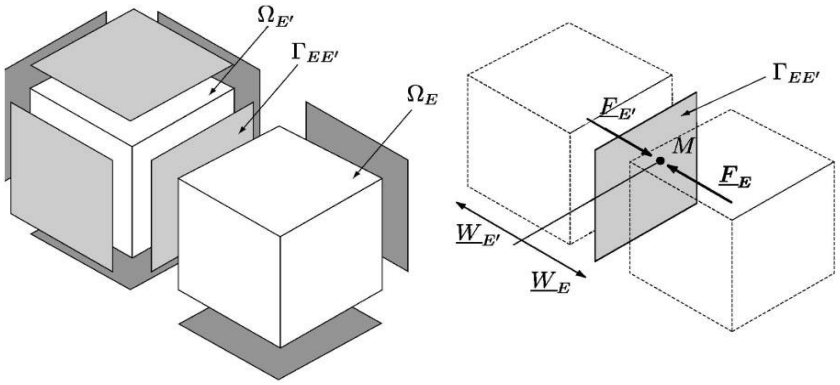

Figure 3.7: Decomposition of a structure into substructures and interfaces (taken from Ladevèze et al. [63]).

For instance, a substructure may contain one or several cells of a composite structure. Each of these components possesses its own variables and equations. An interface transfers both a distribution of displacements and a distribution of forces. The unknowns (displacements, forces, stresses and strains) are split into a set of macro scale quantities and a corresponding micro scale complement.

The second step of this micro-macro strategy is the use of the so-called LATIN (large time increment, Ladevèze [61]) method on the problem expressed as an assembly of substructures and interfaces to be solved. The LATIN method is conceived as a non-incremental iterative computational strategy applied over the entire studied time interval. For every computational iteration, a 'macro' problem, defined on the entire structure, has to be solved, along with a family of problems associated to a substructure, called 'micro' problems, whereas the 'macro' problem is related to the entire homogenized structure. This strategy involves numerical parameters that can be interpreted as interface stiffness. A study of the influence of these numerical parameters on both the displacement- and traction-based micro-macro computational strategies was presented. The resultant

micro-macro strategy displays convergence for stable materials under standard assumptions. In [65] Ladevèze and Nouy introduced a third scale and use an approximation technique for the macro-problem. This approximation is based on an analogy between the macro-homogenized structure and a Cosserat-like solid. Furthermore a radial loading approximation to solve the micro-problems was introduced. These improvements are noticeably when one has to deal with a large number of composite cells and needs to calculate a detailed solution in the time domain.

The multi-domain homogenization techniques described above, in some cases, offer improvements in the effectiveness and the robustness on the solution of multi-domain homogenization problems. However, despite this fact, the vast majority present some drawbacks since most of them are formulated and validated for the linear elastic range only. Furthermore, the level of complexity of the solutions proposed, make them impractical to carry out since, in order to apply such solutions, the number of degrees of freedom, and consequently the computational cost, is increased drastically. If it is taken into account that the homogenization method is already an expensive computational method itself, the application of such methods in the solution of large structures (composed by many unit cells or RVE) render them unfeasible to apply in most of the cases.

Due to the aforementioned reasons, in this research a multi-domain homogenization approach based on the principles of the classical homogenization theory is proposed with the purpose of avoid some of the limitations on the techniques existing on the subject that take into account the decomposition of the structure into an assembly of substructures. The method is valid on the linear on non-linear range of behavior taking into account classic non-linear material behavior such as damage and plasticity.

3.6.2 General framework and hypothesis of the multi-domain formulation

In order to establish the framework and hypothesis of the multi-domain formulation, let's consider a two-dimensional highly heterogeneous medium material body Ω, which is composed by two periodic domains Ω_1 and Ω_2, with different composite arrangements in each one of them, as presented in Figure 3.8.
The two subdomains in which the composite structure is divided are considered as two non-overlapping subdomains, such that:

$$\Omega = \Omega_1 \cup \Omega_2 \tag{3.72}$$

The curve which dissects the region over the two subdomains in Figure 3.8 can be considered as a boundary interface which can be defined as:

$$\Gamma_I - \Gamma_I^{'} = \Omega_1 \cap \Omega_2 \tag{3.73}$$

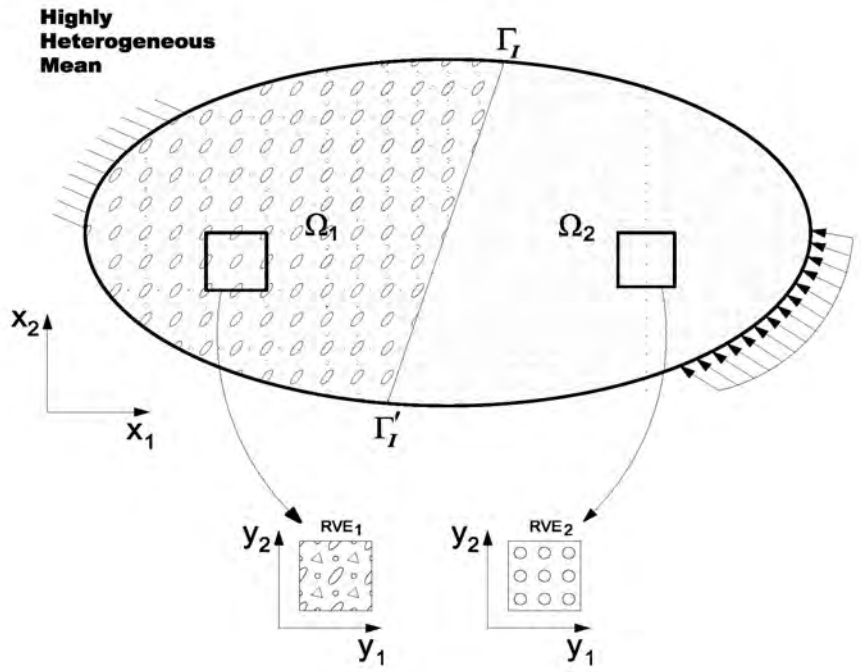

Figure 3.8: Schematic representation of a composite domain Ω assembled by two different periodic domains.

It is implied that the curve $\Gamma_I - \Gamma_I^{'}$ follows the element boundaries in which each of the subdomains is divided according to the element type selected at the numerical formulation (for example, a finite element formulation).

Now, let's assume that the boundary interface $\Gamma_I - \Gamma_I^{'}$ acts like a new boundary condition for each of the subdomains. By doing this then it can be considered that each of the subdomains behaves independently from each other. The boundary condition that represents the interface is expressed in terms of the forces and displacements on each side of the interface. The forces and displacements act as a 'virtual' boundary condition since they are equal on each side of the interface in order to preserve the equilibrium.

By applying the assumption mentioned above then the homogenization theory concepts exposed in Sections 3.4 and 3.5 can be applied separately on each of the periodic subdomains in which the structure is divided, since each one of them can be represented by a RVE or unit cell that perfectly characterizes the domain to which it is associated, as represented in Figure 3.9. The mathematical formulation is expressed on the following section.

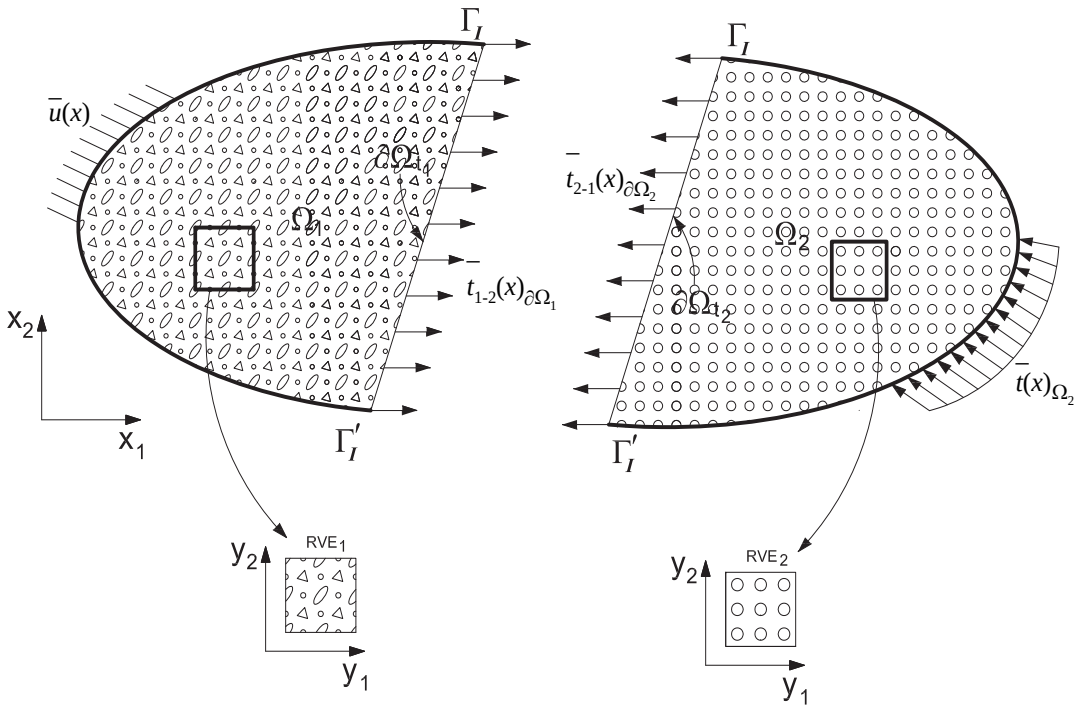

Figure 3.9: Schematic representation of the two different periodic domains divided by a Neumann-like boundary condition.

3.6.3 Multi-domain homogenization formulation in two scales

On the general formulation of the problem using homogenized variables, the problem was based on the relationship between the strains that arise on the macro scale with the transformation suffered by the periodicity vectors that are contained on the microscale as previously mentioned. Once this relationship was completed then the equation that dictates the balance of the composite structure could be formulated and solved. In the case of multi-domain homogenization, the balance equation must include all the subdomains that form part of the composite.

Taking as an example the composite domain Ω presented in Figure 3.8 assembled by two different periodic domains, the linear problem at the global scale can be characterized by a boundary value problem which consists of a highly heterogeneous composite material domain Ω which can be represented by a set of non-overlapping subdomains Ω_i (in this case i=1,2) joined at an interface called $\Gamma_I - \Gamma_I^{'}$. The internal structure of each subdomain is arranged periodically, such that with respect to a macro scale x the material corresponding to that that specific subdomain is considered as an homogeneous material.

If the composite domain Ω is characterized according to the different existing periodic

configurations, represented by the subdomains Ω_i, as depicted in Figure 3.9 then it can be assumed that the boundary conditions can be expressed in terms of the subdomain in which they are positioned or with respect to the whole domain Ω.

According to the aforementioned description, the composite is subjected to the following boundary conditions: (a) a prescribed displacement (in terms of a fixed boundary condition) on the left of the subdomain Ω_1; (b) a prescribed traction force on the right of the subdomain Ω_2; and (c) a prescribed body force $\boldsymbol{b}$ over the entire composite domain Ω. The boundary value problem at the global scale stays as follows:

$$\frac{\partial\, \bar{\boldsymbol{\sigma}}(x)}{\partial x} + \bar{\boldsymbol{b}} = 0 \qquad \textit{equilibrium equation in } \ \Omega \tag{3.74}$$

$$\bar{\boldsymbol{\sigma}}(x)_{\Omega_1} = \frac{1}{V_{\Omega_1}} \int_{V_{\Omega_1}} \boldsymbol{\sigma}(x,y)\, dV_{\Omega_1} \qquad \textit{constitutive equation in } \ \Omega_1 \tag{3.75}$$

$$\bar{\boldsymbol{\sigma}}(x)_{\Omega_2} = \frac{1}{V_{\Omega_2}} \int_{V_{\Omega_2}} \boldsymbol{\sigma}(x,y)\, dV_{\Omega_2} \qquad \textit{constitutive equation in } \ \Omega_2 \tag{3.76}$$

$$\boldsymbol{u}(x) = \bar{\boldsymbol{u}}(x)_{\Omega_1} \qquad \textit{displacements in } \ \partial\Omega_{1(u)} \tag{3.77}$$

$$\bar{\boldsymbol{\sigma}}(x) \cdot \boldsymbol{n} = \bar{\boldsymbol{t}}(x)_{\Omega_2} \qquad forces \textit{ in } \ \partial\Omega_{2(t)} \tag{3.78}$$

Additionally two 'virtual' boundary conditions are taken into account, since the displacements and forces must be equal on both sides of the interface, this is expressed as:

$$\boldsymbol{u}(x)_{\partial\Omega_1} = -\boldsymbol{u}(x)_{\partial\Omega_2} \qquad \textit{displacements at interface } \Gamma_I - \Gamma_I^{'} \tag{3.79}$$

$$\bar{\boldsymbol{t}}_{1-2}(x)_{\partial\Omega_1} = -\bar{\boldsymbol{t}}_{1-2}(x)_{\partial\Omega_2} \qquad forces \textit{ at interface } \Gamma_I - \Gamma_I^{'} \tag{3.80}$$

It is considered that the equilibrium of forces and displacements on each side of the interface is enforced by the periodic conditions at the local scale. By expressing the multi-domain homogenization formulation at the global scale as in Equations (3.74-3.80), the problem can be solved in a similar manner as in the case of a single periodic domain.

This assumption however, may raise some uncertainties about the principles on which the theory of homogenization is based upon, since in order to provide a rigorous deduction of global and local behavior, the composite structure has to obey two mainly hypothesis: (i) The microstructure has to be periodic, i.e., the composite material is locally formed by the spatial repetition of very small microstructures (RVE's or unit cells); and (ii) There is uniformity of the macro scale fields within the unit cell domain, i.e., the global terms are periodic with the same period as that of the microstructure. In the case of the region defines boundary interface $\Gamma_I - \Gamma_I^{'}$ the coupled global-local effects of the two heterogeneous

means Ω_1 and Ω_2 are not necessarily periodic in the sense of assumptions (i) and (ii). Therefore, although both materials are periodic, the solution in the vicinity of $\Gamma_I - \Gamma_I^{'}$ is not periodic, since there will exist a high presence of local effects. Consequently, according to the exact mathematical definition, the use of asymptotic expansion for the purpose of obtaining local distribution of stresses and strains at the micro scale level, will generally yield poor approximations of the local fields.

Local fields effects

The influence of the local fields on the global response in the vicinity of the boundary interface $\Gamma_I - \Gamma_I^{'}$ between two periodic arrangements expressed on the paragraphs above presents a lot of similarities with the case of periodic media in the vicinity of free edges, where only assumption (i) holds. Some solutions have been proposed to address the problem in the vicinity of free edges, such as that proposed by Sanchez-Palencia [105], in which an asymptotic expansion of the solution of $\boldsymbol{u}^{\epsilon}(x)$ of different nature in the boundary layer region is investigated by introducing the complementary term $\boldsymbol{u}^{1c}$ under the form:

$$\boldsymbol{u}^{\epsilon}(x) = \boldsymbol{u}^{0}(x) + \epsilon \left[\boldsymbol{u}^{1}(x,y) + \boldsymbol{u}^{1c}(x,y)\right] + \boldsymbol{O}(\epsilon^{2}) \tag{3.81}$$

The numerical solution of this problem showed that the effect of adding this complementary term is significant on points located near the boundary edge. Conversely, the gradient in some generalized sense tends to zero, as the point where the solution is computed moves away from the boundary edge.

The result obtained in [105] agrees with that obtained by Dumontet [24], in which an approximation of the local stresses near a Neumann boundary for an elastic material with a periodic structure is performed by means of a higher order formulation. This formulation consists in adding boundary layers terms, which are supposed periodic parallel to the boundary, to the classical terms of the expansion of the displacement and stresses of the homogenization theory. The numerical results obtained proved that the boundary stresses decrease exponentially according to the orthogonal variable to the free boundary.

Oller et al. [90] take this discussion further, pointing out that high gradients of the macro scale variable fields at a certain structural point involves a perturbation of these fields in the neighboring cells, which apparently contradicts the basic periodicity hypothesis. However, the authors consider this hypothesis as an idealization of the variational field problem, which in fact should be translated into a slow change on the macro scale variables. The authors put as an example two points (A and B) on the macro scale on which there is a high stress or strain gradient between them as presented in Figure 3.10.

Since the homogenization theory considers that the dimensions of the cell tend to zero from a general scale point of view (assumption (i) on the paragraphs above), therefore it is supposed that, the gradient (or rate change) between the cell represented by point

A and the neighboring cell is very small. This pattern is repeated over a period d until the cell represented by point B is reached. However, the real problem differs from this idealization, since, due to the finite dimension of the cell, a finite number of them may exist between both points. On the right-hand side of the same figure, the variation of the micro scale fields is indicated. This variation is understood as the field variable error made over the period d that in turn represents the length of the cell. The authors suggest that by diminishing the size of the cell (understood as a reduction of the finite element at the global scale) and assuming that the amplitude of the field variable stays constant a reduction on the error on the computed results is obtained. These assumptions are extrapolated to the boundaries of the cell, since by diminishing the dimensions at the macrostructure, the cell dimensions also diminish, making the periodicity error on the border of the macro scale domain to tend to zero.

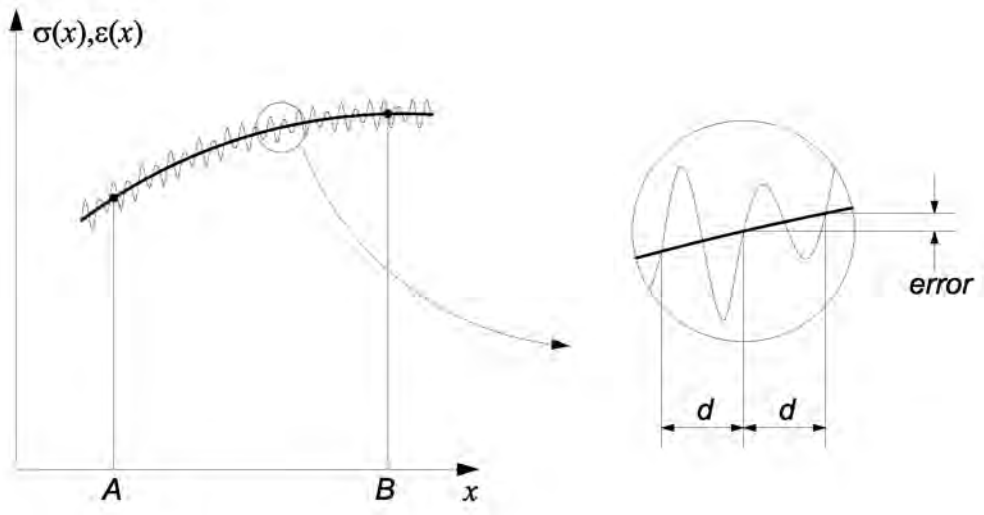

Figure 3.10: Schematic representation of the variational field problem of a quasi-periodic function.

In this study, the same assumptions and considerations made in [90] are applied to analyze the problem presented in Figures 3.8 and 3.9, for the case of a highly heterogeneous composite domain assembled by several different periodic domains. Thus, the problem at the local scale at the vicinity of the interface remains exactly the same as in the case of the formulation presented in Sections 3.4 and 3.5 for the linear and non-linear homogenized formulations in two scales for a single periodic domain.

It must be remarked that the convergence on the solution, in cases where high strain gradients are present, greatly depends on the size of the finite element at the global scale. Large finite elements at the global scale may render the local periodicity hypothesis to be inappropriate or unsuitable to reach convergence in cases like when Dirichlet boundary

conditions exist. By reducing the element size at critical areas, the concept of periodicity (or cuasi-periodicty) is preserved, since the jump in the gradients decreases along with the size of the elements. This concept is in total agreement to the ideas exposed in those studies made by Sanchez-Palencia [105], Dumontet [24] and Oller et al. [90]. This method is presented as an alternative to some of the existing solutions which make use of penalty methods, error minimization algorithms or high order formulations, by following a more practical approach.

Chapter 4

Numerical implementation

In this chapter the numerical formulation of the multi-domain homogenization approach is implemented by means of a finite element code following the two scale approach developed in Chapter 3. The weak formulation at the macroscopic or global level is expressed based on considering different periodic subdomains within the composite structure. Meanwhile that the solution at the local level is expressed through the mathematical formulation on the cell or RVE domain taking into account the periodic boundary conditions. The nested solution scheme of the finite element implementation is thoroughly described, including the numerical implementation of the procedure to obtain the homogenized non-linear constitutive tensor by means of a perturbation method and the description of the approach used for the parallelization routine of the computational tool.

4.1 Introduction

In the state of the art presented in Chapter 2, several methods of analysis that make use of the homogenization method were presented. In this study the multi-domain homogenization method in two scales is developed under a finite element (FE) method formulation. Although other methods may offer better advantages in the analysis of composites under certain conditions, the FE method was selected over the rest of the methods analyzed since it presents more advantages than drawbacks with respect to the others.

One of the most outstanding alternative methods found on the state of the art was the formulation that employs the Voronoi cell method. This method appears to be highly effective for the study of composites with random distribution. The method is even capable to represent a unit cell of a periodic continuum in some cases with a single Voronoi finite element. This feature gives a great advantage since the method results computationally relatively economical. However, the method presents some drawbacks in the sense that the fields at the micro scale are given by a single Voronoi element, therefore the accuracy is less than that obtained in a FE formulation by a unit cell with various elements (although the overall average value of these fields is rough as well). Nevertheless, the main difficulty

found in this method is that since this technique discretizes the domain into a network of multisided convex Voronoi polygons formed by a matrix-like component and a second phase inclusion at most.

On the other hand, the finite element formulation has the advantage that it can be implemented over existing finite element codes may serve as starting platform for the numerical implementation of the homogenization formulation. This FE codes generally have been previously tested, meanwhile that if other formulations are selected they will have to be built from scratch.

4.2 General concepts for the numerical implementation of the finite element formulation

The numerical implementation of the multi-domain homogenization method is carried out through of a nested solution scheme in two scales by means of two finite element programs, one for each on the scales. The general framework of the solution consists in that for each Gauss point of each finite element at the global scale, a finite element problem defined by the RVE or unit cell has to be solved in order to obtain the response at the microstructure that will give the averaged solution at the macroscale.

For the global scale the problem is expressed at the linear range by means of the boundary value problem given by Equations (3.22)-(3.25), meanwhile that for the local scale the BVP is expressed by Equations (3.28)-(3.31). For the case of the non-linear problem, the local equilibrium equations of the linear range, both at the macro and micro scales have to be represented by their non-linear counterparts, in order to reproduce the inelastic behavior of each component material on the micro-structure and of the entire composite at the global scale as expressed in Section 3.5.

The BVP at the local scale has to take into account the correct application of the boundary conditions represented by the prescribed positions of the anchor nodes (i.e. the four corner nodes on a rectangular cell or RVE) and the kinematic constraints on the opposite boundaries in order to apply the periodicity conditions on the cell domain. On the other hand, the BVP problem at the global scale has to carry out the particular task of implementing a proper strategy to achieve convergence of the whole structure.

4.3 Linear-elastic finite element method formulation

In the differential formulation of the homogenized method presented in Section 3.4, the equilibrium and constitutive requirements were established in terms of small displacements following a linear-elastic formulation. In the resulting system of differential equations all the compatibility requirements were already contained since the solution is a continuous one. The system of equations was complemented by additional differential equations that

impose the appropriate conditions on the state variables in order that all compatibility requirements were satisfied. Furthermore, all boundary conditions were established to fully complete the formulation of the problem. With all these assumptions, the finite element equilibrium equations derived satisfy the following linear static formulation:

$$\boldsymbol{K} \cdot \boldsymbol{u} = \boldsymbol{F} \tag{4.1}$$

Equation (4.1) correspond to a linear analysis of a structural problem because the displacement response $\boldsymbol{u}$ is a linear functions of the applied load vector $\boldsymbol{F}$. The fact that the displacements are small is reflected into the evaluation of the matrix $\boldsymbol{K}$ and load vector $\boldsymbol{F}$ because all integrations should be performed over the original volume of the finite elements, and the strain-displacement matrix $\boldsymbol{B}$ of each element is assumed to be constant and should be independent of the element displacements. The assumption of a linear-elastic material is implied in the use of a constant stress-strain matrix for both scales ($\mathbf{C}$ for the local and $\bar{\mathbf{C}}$ for the global scale).

Form the mathematical point of view, the differential formulation or 'strong form' solution of the partial differential equations (PDEs) that represent the problems expressed at the paragraphs above in both scales represent the analytical exact solution; therefore this problems require that the relationships that are described at the PDEs must be satisfied at every mathematical point in the domain. From the numerical point of view, however, finding a solution that is fully satisfied is a difficult task or even in some cases impossible to accomplish. Nevertheless, an alternative solution to the BVPs can be achieved from a numerical point of view by setting the PDEs following a 'weak form'. The formulation of finite element method can be considered as an extension of the weak formulation, since it is based on the discretization over the domain of the BVP.

4.3.1 Weak formulation

The term 'weak form' is sometimes referred as variational form, or weighted residuals form because the solution of the PDEs is approximated with the use of trial functions. The weak formulation for the global and local scales that form part of the homogenization method are described following the general formulation in the linear elastic range presented in Section 3.4.

Weak formulation at the macro scale or global level

The differential Equation (3.22), which establishes the local equilibrium at the macroscopic scale, can be rewritten as:

$$\nabla \bar{\boldsymbol{\sigma}}\left(x\right) + \rho\left(x\right) \boldsymbol{b}\left(x\right) = 0 \tag{4.2}$$

where $\nabla \bar{\boldsymbol{\sigma}}\left(x\right)$ is the divergence of the homogenized stress tensor and $\rho\left(x\right) \boldsymbol{b}\left(x\right)$ is the value of the mass forces of the composite. Equation (4.2) must be zero at all points of the

domain Ω and also must satisfy the boundary conditions imposed in Equation (3.25) in the case that the composite is defined by one periodic domain only. In the case that more than one periodic configuration exist in the composite domain, Equation (4.2) must satisfy the boundary conditions imposed in all the subdomains Ω_i of the structure. Following the formulation presented in Section 3.6, in a multi-domain homogenization environment with two subdomains the BVP represented by Equations (3.74-3.78) must be satisfied altogether with the two additional 'virtual' BCs represented by Equations (3.79) and (3.80). For the case that more subdomains existed a similar formulation should be followed depending on the number of periodic subdomains Ω_i existing on the composite domain.

Applying the weighted residual method on the described expression (for a detailed explanation of the method, see [129]), we have that:

$$\int_{\Omega_i} \boldsymbol{w} \cdot [\nabla \bar{\boldsymbol{\sigma}}\,(x)] d\Omega_i + \int_{\Omega_i} \boldsymbol{w} \cdot [\rho\,(x)\,\boldsymbol{b}\,(x)] d\Omega_i + \int_{\partial\Omega_i} \boldsymbol{w} \cdot [\bar{\boldsymbol{t}}\,(x) - \bar{\boldsymbol{\sigma}}\,(x) \cdot \boldsymbol{n}] d\partial\Omega_i = 0 \quad (4.3)$$

where i denotes the different periodic subdomains of the structure, $\boldsymbol{w}$ is an arbitrary set of test functions associated with the displacement field, which satisfies the Dirichlet boundary conditions on $\partial\Omega_i$, meanwhile $\bar{\boldsymbol{t}}\,(x)$ represents the forces, known also as traction vector, imposed on the boundary $\partial\Omega_i$ which satisfies the Neumann boundary conditions. In this case $\bar{\boldsymbol{t}}\,(x)$ also includes the additional BC that represents the set of 'virtual' forces at each of the interfaces $\Gamma_I - \Gamma_I^{'}$ present in the structure domain. Applying the divergence theorem, the first term of Equation (4.3) can be expressed as:

$$\int_{\Omega_i} \boldsymbol{w} \cdot [\Delta \bar{\boldsymbol{\sigma}}\,(x)] d\Omega_i \equiv - \int_{\Omega_i} \nabla \boldsymbol{w} : \bar{\boldsymbol{\sigma}}\,(x)\, d\Omega_i + \int_{\partial\Omega_i} \boldsymbol{w} \cdot [\bar{\boldsymbol{\sigma}}\,(x) \cdot \boldsymbol{n}] d\partial\Omega_i \quad (4.4)$$

Now, the weak form of the static balance equation at the macro scale can be rearranged as follows:

$$- \int_{\Omega_i} \nabla \boldsymbol{w} : \bar{\boldsymbol{\sigma}}\,(x)\, d\Omega_i + \int_{\Omega_i} \boldsymbol{w} \cdot [\rho\,(x)\,\boldsymbol{b}\,(x)] d\Omega_i + \int_{\partial\Omega_i} \boldsymbol{w} \cdot \bar{\boldsymbol{t}}\,(x) d\partial\Omega_i = 0 \quad (4.5)$$

To choose the weighting vector $\boldsymbol{w}$ the Galerking method is applied. This method makes use if the principle of virtual displacements by choosing as weight vector a hypothetical displacement field $\delta\boldsymbol{u}(x)$, which is not associated with any current system of external loads and that also satisfies the geometric conditions of the boundaries $\partial\Omega$. In this way, the weak form of the equilibrium equation at the macroscopic scale can be written as an expression of the principle of virtual work as:

$$\int_{\Omega_i} \delta\boldsymbol{\varepsilon}(x) : \bar{\boldsymbol{\sigma}}(x) d\Omega_i = \int_{\Omega_i} \delta\,\boldsymbol{u}(x) \cdot [\rho(x)\boldsymbol{b}(x)]\, d\Omega_i + \int_{\partial\Omega_i} \delta\,\boldsymbol{u}(x) \cdot \bar{\boldsymbol{t}}(x) d\partial\Omega_i \quad (4.6)$$

where $\delta\boldsymbol{\varepsilon}(x)$ is the virtual strain field obtained from the virtual displacement field $\delta\boldsymbol{u}(x)$ at the macroscopic scale x. The homogenized stress tensor is obtained from the material elastic constants $\bar{\boldsymbol{\sigma}}(x) = \bar{\mathbf{C}}(x) : \bar{\boldsymbol{\varepsilon}}(x)$ as expressed previously in Equation (3.39).

From Equation (4.6) it is inferred that the two scales that are involved in the homogenization method have been decoupled since this expression is described in terms that involve only the macroscopic scale x. However, the homogenized elastic constitutive tensor $\bar{\mathbf{C}}(x)$ and the homogenized stress tensor $\bar{\boldsymbol{\sigma}}(x)$ have to be determined by the interaction of the constituents at the local scale.

The virtual work statement that expresses Equation (4.6) is precisely the weak form of the equilibrium equations at the macroscopic scale, and it is valid for linear and non-linear stress-strain relations as pointed out by Zienkiewicz and Taylor [129].

Weak formulation at the micro scale or local level

The solution of the boundary value problem at the macroscopic or local level is achieved through the mathematical formulation on the cell or RVE domain presented in Section 3.4.2, where the local equilibrium equations at each point and the microstructure altogether with the special boundary conditions are presented following a differential formulation.

Using the method of weighted residuals as in the case of the macroscopic level and recalling that since the cell is relatively small the effect of mass forces is negligible then the weak formulation at the micro scale level leads to the following expression:

$$-\int_{\Omega_c} \nabla \boldsymbol{w} : \boldsymbol{\sigma}(y) d\Omega_c + \int_{\partial\Omega_c} \boldsymbol{w} \cdot \boldsymbol{t}(y) d\partial\Omega_c = 0 \tag{4.7}$$

And the weak form of the equilibrium equation at the micro scale written as an expression of the principle of virtual work stays as:

$$\int_{\Omega_c} \delta\boldsymbol{\varepsilon}(y) : \boldsymbol{\sigma}(y) d\Omega_c = \int_{\partial\Omega_c} \delta\boldsymbol{u}(y) \cdot \boldsymbol{t}(y) d\partial\Omega_c \tag{4.8}$$

where $\delta\boldsymbol{\varepsilon}(y)$ is the virtual strain field obtained from the virtual displacement field $\delta\boldsymbol{u}(y)$ at the micro scale y. The virtual displacement field is an admissible field that satisfies the condition of displacements in the boundary of the cell, i.e. $\boldsymbol{u}_{p+D} - \boldsymbol{u}_p = \bar{\boldsymbol{\varepsilon}}(x) \cdot D$, while the traction vector $\boldsymbol{t}(y)$ is generated on the boundary of the cell by periodicity of the force field, i.e. $\boldsymbol{t}_{p+D} = -\boldsymbol{t}_p$. The periodicity of the continuum is implemented by applying the Lagrange multipliers as presented in Equation (3.38).

Once the problem on the cell or RVE is solved, the elastic constants are easily obtained and the homogenized stress $\bar{\boldsymbol{\sigma}}(x)$ according to the process explained in Section 3.4.3.

4.3.2 Finite element implementation

As it was explained on the preceding paragraphs, the numerical implementation of the multi-domain homogenization method is carried out through of a nested solution scheme of two finite element programs. A finite element problem represented by a RVE or unit cell has to be solved to obtain the homogenized response for each Gauss point that forms part of a finite element discretization at the global scale.

FE implementation at the macro scale or global level

The equilibrium formulation is discretized now into finite elements in which the body of interest is subdivided into N_{elem} elements. In this case, since the macroscopic domain Ω can be composed by several subdomains, then the discretization of the overall domain is made by means of a set of χ non-overlapping subdomains, according to the multi-domain formulation presented in Section 3.6, which are in turn discretized in a sequence of non-overlapping elements $\Omega_{(e)}$, such that:

$$\Omega = \left[\bigcup_{e=1}^{N_{elem}} \Omega_{1(e)}\right] \cup \left[\bigcup_{e=1}^{N_{elem}} \Omega_{2(e)}\right] \cup \cdots \cup \left[\bigcup_{e=1}^{N_{elem}} \Omega_{\chi(e)}\right] \tag{4.9}$$

The global displacement field can be obtained through conventional spatial interpolation as:

$$\bar{\boldsymbol{u}}(x) = \sum_{i=1}^{n_{node}} N_{(e)}^{u_i}\, \bar{\boldsymbol{u}}(x)_{(e)}^{i} = \boldsymbol{N}_{(e)}^{u}\, \bar{\boldsymbol{u}}(x)_{(e)} \tag{4.10}$$

where $\boldsymbol{N}_{(e)}^{u} = \left[N_{(e)}^{u_1}, N_{(e)}^{u_2}, \cdots, N_{(e)}^{u_n}\right]$ are the interpolation functions of displacement of the element (e) and $\bar{\boldsymbol{u}}(x)_{(e)}$ are the nodal displacements at the global label.

Following a small strain formulation, the strain deformation as a function of the displacement for each element is given by:

$$\begin{aligned} \bar{\boldsymbol{\varepsilon}}(x)_{(e)} &= \frac{1}{2}\left[\left(\nabla \boldsymbol{N}_{(e)}^{u}\, \bar{\boldsymbol{u}}(x)_{(e)}\right) + \left(\nabla \boldsymbol{N}_{(e)}^{u}\, \bar{\boldsymbol{u}}(x)_{(e)}\right)^{T}\right] \\ &= \frac{1}{2}\left[\left(\nabla \boldsymbol{N}_{(e)}^{u}\right) + \left(\nabla \boldsymbol{N}_{(e)}^{u}\right)^{T}\right] \bar{\boldsymbol{u}}(x)_{(e)} \\ &= \boldsymbol{B}_{(e)} \bar{\boldsymbol{u}}(x)_{(e)} \end{aligned} \tag{4.11}$$

where the matrix $\boldsymbol{B}_{(e)}$ is known as the matrix of derivatives of the shape functions and ∇ is the divergence operator. Applying the method of weighted residuals, through the principle

of virtual work following Equation (4.6), to any element (e) of the macrostructure, then the equilibrium equation stays as:

$$\int_{\Omega_{(e)}} \boldsymbol{B}_{(e)}^{T} \bar{\mathbf{C}}(x) \boldsymbol{B}_{(e)} \bar{\boldsymbol{u}}(x)_{(e)} d\Omega = \int_{\Omega_{(e)}} \boldsymbol{N}_{(e)}^{u} \left[\rho(x) \boldsymbol{b}(x)\right] d\Omega + \int_{\partial\Omega_{(e)}} \boldsymbol{N}_{(e)}^{u} \bar{\boldsymbol{t}}(x)_{(e)} d\partial\Omega \quad (4.12)$$

where the member on the left side of Equation (4.12) represents the internal forces for each element meanwhile that the expressions on the right side of the equation correspond to the external forces applied to the same, as specified in the following equations.

$$\boldsymbol{f}_{int_{(e)}} = \left[\int_{\Omega_{(e)}} \boldsymbol{B}_{(e)}^{T} \bar{\mathbf{C}}(x) \boldsymbol{B}_{(e)} \bar{\boldsymbol{u}}(x)_{(e)} d\Omega\right] \bar{\boldsymbol{u}}(x)_{(e)} = \boldsymbol{k}_{(e)} \bar{\boldsymbol{u}}(x)_{(e)} \quad (4.13)$$

$$\boldsymbol{f}_{ext_{(e)}} = \int_{\Omega_{(e)}} \boldsymbol{N}_{(e)}^{u} \left[\rho(x) \boldsymbol{b}(x)\right] d\Omega + \int_{\partial\Omega_{(e)}} \boldsymbol{N}_{(e)}^{u} \bar{\boldsymbol{t}}(x)_{(e)} d\partial\Omega \quad (4.14)$$

The total values of the internal ($R\left[\boldsymbol{\sigma}(x)\right]$) and external ($F\left[\boldsymbol{t}(x)\right]$) forces at the macrostructure result from the assemblage of the contributions of each element as:

$$\begin{aligned} R\left[\boldsymbol{\sigma}(x)\right] &= \mathrm{A}_{e=1}^{n_{elem}} \boldsymbol{f}_{int_{(e)}} \\ &= \mathrm{A}_{e=1}^{n_{elem}} \boldsymbol{k}_{(e)} \bar{\boldsymbol{u}}(x)_{(e)} = \boldsymbol{K}\, \bar{\boldsymbol{u}}(x) \end{aligned} \quad (4.15)$$

$$F\left[\boldsymbol{t}(x)\right] = \mathrm{A}_{e=1}^{n_{elem}} \boldsymbol{f}_{ext_{(e)}} = \boldsymbol{F}(x) \quad (4.16)$$

where A is the standard assembly operator of the finite element method (see e.g. [52]). Naturally, the system must satisfy the equilibrium Equation (4.1), i.e. $R\left[\boldsymbol{\sigma}(x)\right] = F\left[\boldsymbol{t}(x)\right]$.

Numerical integration at the macro scale

The numerical integration at the macro scale it is implemented by applying the finite element method isoparametric formulation. The principal idea of this formulation is to achieve the relationship between the element displacements at any point and the element nodal point displacements directly through the use of interpolations functions. The spatial area of the element it is transformed into an isoparametric space by using isoparametric elements. For example the vector of internal forces expressed in Equation (4.13) is evaluated by numerical integration (also known as numerical quadrature) as:

$$\boldsymbol{f}_{int_{(e)}} = \sum_{l=1}^{n_{\mathrm{int}}} \boldsymbol{B}_{(e)}^{T} \bar{\mathbf{C}}(x) \boldsymbol{B}_{(e)} \bar{\boldsymbol{u}}(x)_{(e)} \Big|_{x=x_{(e)}^{l}} w^{l} j_{(e)} \quad (4.17)$$

where $\bar{\mathbf{C}}(x)$ is the homogenized elastic constitutive tensor, which is obtained at the micro or local scale, $x_{(e)}^{l}$ represents each integration point of the macrostructure ($x_{(e)}^{l} \in \Omega_{(e)}$), w^{l} is the corresponding weight, $j_{(e)}$ is the Jacobian of the element, and n_{int} is the number of integration points for the element $\Omega_{(e)}$.

FE implementation at the micro scale or local level

In this case, the domain at the micro scale represented by the unit cell or RVE Ω_c is conformed by means of a sequence of non-overlapping elements $\Omega_{c_{(e)}}$, such that:

$$\Omega_c = \left[\bigcup_{e=1}^{N_{elem}} \Omega_{c_{(e)}} \right] \tag{4.18}$$

By using the conventional spatial interpolation, the displacement field is determined for each of the nodes that are part of the cell domain $\Omega_{c_{(e)}}$ as for the case of the global scale.

$$\boldsymbol{u}(y) = \sum_{i=1}^{n_{node}} N^{u_i}_{(e)}\, \boldsymbol{u}(y)^i_{(e)} = \boldsymbol{N}^u_{(e)}\, \boldsymbol{u}(y)_{(e)} \tag{4.19}$$

where $\boldsymbol{N}^u_{(e)} = \left[N^{u_1}_{(e)}, N^{u_2}_{(e)}, \cdots, N^{u_n}_{(e)} \right]$ are the interpolation functions of displacement of the element (e) and $\boldsymbol{u}(y)_{(e)}$ are the nodal displacements of the unit cell or RVE at the local label.

The strain deformation as a function of the displacement for each element is given by:

$$\begin{aligned} \boldsymbol{\varepsilon}(y)_{(e)} &= \frac{1}{2}\left[\left(\nabla \boldsymbol{N}^u_{(e)}\, \boldsymbol{u}(y)_{(e)} \right) + \left(\nabla \boldsymbol{N}^u_{(e)}\, \boldsymbol{u}(y)_{(e)} \right)^T \right] \\ &= \frac{1}{2}\left[\left(\nabla \boldsymbol{N}^u_{(e)} \right) + \left(\nabla \boldsymbol{N}^u_{(e)} \right)^T \right] \boldsymbol{u}(y)_{(e)} \\ &= \boldsymbol{B}_{(e)} \boldsymbol{u}(y)_{(e)} \end{aligned} \tag{4.20}$$

where the matrix $\boldsymbol{B}_{(e)}$ is the matrix of derivatives of the shape functions and ∇ is the divergence operator. The equilibrium equation presented at the weak formulation (Equation 4.7) applying the method of weighted residuals stays as:

$$\int_{\Omega_{c_{(e)}}} \boldsymbol{B}^T_{(e)} \mathbf{C}(y) \boldsymbol{B}_{(e)} \boldsymbol{u}(y)_{(e)} d\Omega_c = \int_{\partial\Omega_{c_{(e)}}} \boldsymbol{N}^u_{(e)} \boldsymbol{t}(y)_{(e)} d\partial\Omega_c \tag{4.21}$$

where the member on the left side of Equation (4.21) represents the internal forces for each element meanwhile that the expression on the right side corresponds to the external forces applied to the same, as specified in the following equations.

$$\boldsymbol{f}_{int_{(e)}} = \left[\int_{\Omega_{c_{(e)}}} \boldsymbol{B}^T_{(e)} \mathbf{C}(y) \boldsymbol{B}_{(e)} \boldsymbol{u}(y)_{(e)} d\Omega_c \right] \boldsymbol{u}(y)_{(e)} = \boldsymbol{k}_{(e)} \boldsymbol{u}(y)_{(e)} \tag{4.22}$$

$$\boldsymbol{f}_{ext_{(e)}} = \int_{\partial\Omega_{c(e)}} \boldsymbol{N}^u_{(e)} \boldsymbol{t}(y)_{(e)} d\partial\Omega_c \tag{4.23}$$

The total values of the internal ($R[\boldsymbol{\sigma}(y)]$) and external ($F[\boldsymbol{t}(y)]$) forces at the microstructure result from the assemblage of the contributions of each element as in the case of the macrostructure presented in Equation (4.1). The system must satisfy the equilibrium Equation (4.1) of the internal and external forces $R[\boldsymbol{\sigma}(y)] = F[\boldsymbol{t}(y)]$.

However, the system of equations that fully describe the equilibrium equation at the local level following the homogenization method procedure described in Section 3.4, is augmented by the Lagrange multipliers in order to ensure the displacement periodic field according to Equation (3.38). The total size of the augmented system (size of the cell stiffness matrix) that results from the application of the periodicity conditions is given in Equation (4.24).

$$[(N_{Fnodes} \cdot N_{Dof}) + (2 \cdot N_{Ppairs} \cdot N_{Dof})]^2 \tag{4.24}$$

where N_{Fnodes} is the number of free nodes (i.e. nodes with no restrictions but that can be periodic nodes as well) on the RVE or unit cell, N_{Dof} is the number of degrees of freedom and N_{Ppairs} is the number of periodic nodes that are related on each of the periodic faces of the RVE or unit cell.

Numerical integration at the micro scale

In the case of the micro scale or local level, the stiffness matrix K of the RVE evaluated by numerical integration stays as:

$$\boldsymbol{K} = \mathrm{A}_{e=1}^{n_{elem}} \left[\sum_{l=1}^{n_{\mathrm{int}}} \boldsymbol{B}_{(e)}^T \mathbf{C}(y) \boldsymbol{B}_{(e)} \Big|_{y=y_{(e)}^l} w^l j_{(e)} \right] \tag{4.25}$$

where $\mathbf{C}(y)$ is the elastic constitutive tensor associated to a material component, $y_{(e)}^l$ represents each integration point of the microstructure ($y_{(e)}^l \in \Omega_{c_{(e)}}$), w^l is the corresponding weight, $j_{(e)}$ is the Jacobian of the element, and n_{int} is the number of integration points for the element $\Omega_{c(e)}$ and A is the standard assembly operator of the finite element method. The strain and stress field of the RVE are obtained under the framework of the system of equations following the periodicity restrictions as presented in Equation (3.38).

The homogenized macroscopic stress field $\bar{\boldsymbol{\sigma}}(x)$ is obtained by computing the average of the stress fields of each integration point of each element that forms part of the cell or RVE as expressed in Equation (3.14). The numerical integration of the homogenized stress field $\bar{\boldsymbol{\sigma}}(x)$ stays as follows:

$$\bar{\sigma}_{ij}(x) = \frac{1}{\sum_{i=1}^{n_{elem}} \left(\sum_{i=1}^{n_{\mathrm{int}}} w^l j_{(e)} \right)} \sum_{i=1}^{n_{elem}} \left(\sum_{i=1}^{n_{\mathrm{int}}} \sigma_{ij}(y_{(e)}^l) w^l j_{(e)} \right) \tag{4.26}$$

The independent field stresses ($\bar{\boldsymbol{\sigma}}[\bar{\varepsilon}_1(x)], \bar{\boldsymbol{\sigma}}[\bar{\varepsilon}_2(x)], \bar{\boldsymbol{\sigma}}[\bar{\varepsilon}_3(x)]$) needed to compute the linear-elastic homogenized constitutive tensor as expressed in Equations (3.45)-(3.50) on Section 3.4.3 are obtained using the numerical integration form expressed above in Equation (4.26).

4.4 Non-linear finite element method formulation

It is a widespread practice in engineering analysis that a non-linear analysis is always preceded by a linear one, since the non-linear analysis is considered as a natural extension of the complete analysis process beyond the assumptions made at the linear analysis. For this reason, the weak formulation and the finite element implementation presented in Sections 4.3.1 and 4.3.2 for the case of the linear formulation are taken as the starting point of the non-linear formulation presented in this section.

The expressions presented in the weak and the finite element formulations remain valid to characterize the non-linear behavior of the composite at both, the global and local scales. However, in the case of the non-linear analysis the constant relation among the stress and strain variables is not constant anymore as in the linear case. The new relation among these two variables is set by the non-linear constitutive tensor, which at the micro or local scale is given by the constitutive law of each material component meanwhile that for the whole composite is given by the homogenized non-linear constitutive tensor as described in Section 3.5.5.

The basic problem in a general non-linear analysis is to find the state of equilibrium of a body in function of the applied loads by using an incremental solution approach. The solution of the equilibrium equation of the composite in terms of homogenized variables is described in the following paragraphs.

4.4.1 Incremental solution of the equilibrium equation in two scales

Considering the solution of the non-linear response, it is recognized that the equilibrium relation of the composite, defined in Equation (3.68), must be satisfied throughout the complete history of load application. In the case of a static analysis, in which the time effect does not affect the equilibrium equations, the factor time is only a convenient variable which denotes different intensities of load application and their corresponding response configurations of the system for each load increment. In the case of a dynamic analysis though, the time variable must be included for the proper modeling of the actual physical situation of the system subject of analysis.

The non-linear response in the classical FE method is effectively carried out using a step-by-step incremental solution in which the total applied load is divided into several number of load steps. In the case of homogenization in two scales, to achieve the equilibrium of the composite, two different problems have to be solved, one at the macro scale or global level and another at the micro scale or local level. The response on each of the scales is obtained following an approach similar to the incremental solution implemented in classical FE (using a single scale) with slight variations. Both procedures are described below.

Incremental solution at the macro scale

The basic approach of the incremental step-by-step solution is to assume that the solution of the discrete time t is known and that the solution for the time $t+\Delta t$ is required, where $t+\Delta t$ is a suitable chosen time increment. Rearranging the equilibrium equation of the composite expressed in (3.68) for the case of the time $t+\Delta t$, it stays as:

$$R(\bar{\boldsymbol{\sigma}})^{t+\Delta t} - F(\bar{\boldsymbol{t}}^{\,n})^{t+\Delta t} = 0 \tag{4.27}$$

where $R(\bar{\boldsymbol{\sigma}})$ represent the forces inside the composite domain that are in function of the internal homogenized stresses $\bar{\boldsymbol{\sigma}}(x)$, meanwhile $F(\bar{\boldsymbol{t}}^{\,n})$ are the forces on the boundary of the composite domain originated by the external traction forces $\bar{\boldsymbol{t}}^{\,n}(x)$.

Since the solution it is known at time t and assuming that $F(\bar{\boldsymbol{t}}^{\,n})^{t+\Delta t}$ is independent of the strain deformations, then:

$$R(\bar{\boldsymbol{\sigma}})^{t+\Delta t} = R(\bar{\boldsymbol{\sigma}})^{t} + R(\bar{\boldsymbol{\sigma}}) \tag{4.28}$$

where $R(\bar{\boldsymbol{\sigma}})$ is the increment in nodal point forces corresponding to the increment in element displacements and stresses from time t to time $t+\Delta t$. This vector can be approximated using a tangent stiffness matrix $\bar{\boldsymbol{K}}^{t}$ which corresponds to the geometric and material conditions at time t.

$$R(\bar{\boldsymbol{\sigma}}) \doteq \bar{\boldsymbol{K}}^{t}\bar{\boldsymbol{u}}(x) \tag{4.29}$$

where $\bar{\boldsymbol{u}}(x)$ is a vector of incremental nodal point displacements. Now the tangent stiffness matrix can be expressed as:

$$\bar{\boldsymbol{K}}^{t} = \frac{\partial R(\bar{\boldsymbol{\sigma}})^{t}}{\partial \bar{\boldsymbol{u}}(x)^{t}} \tag{4.30}$$

The tangent stiffness matrix as expressed in Equation (4.30) corresponds to the derivative of the internal element nodal point forces $R(\bar{\boldsymbol{\sigma}})^{t}$ with respect to the nodal point displacements $\bar{\boldsymbol{u}}(x)^{t}$. Substituting Equations (4.28) and (4.29) into (4.27) it is obtained:

$$\bar{\boldsymbol{K}}^{t}\bar{\boldsymbol{u}}(x) = F(\bar{\boldsymbol{t}}^{\,n})^{t+\Delta t} - R(\bar{\boldsymbol{\sigma}})^{t} \tag{4.31}$$

Solving for $\bar{\boldsymbol{u}}(x)$, an approximation of the displacements at time $t+\Delta t$ can be computed as:

$$\bar{\boldsymbol{u}}(x)^{t+\Delta t} \doteq \bar{\boldsymbol{u}}(x)^{t} + \bar{\boldsymbol{u}}(x) \tag{4.32}$$

The exact displacements at time $t+\Delta t$ would be those that correspond to the applied loads $F(\bar{\boldsymbol{K}}^{\,n})^{t+\Delta t}$. Having evaluated an approximation to the displacements corresponding to time $t+\Delta t$, an approximation of the stresses and the corresponding nodal point forces can be evaluated for the same instant in order to compute the solution at the next time step. However, because of the assumption made in Equation (4.29), the solution obtained may have significant errors or in some cases would be unstable. It is then that an iterative process must be performed until the solution proposed in Equation (4.27) is achieved.

The widely used iteration methods in finite element analysis are based on the classical Newton-Rhapson technique. The method basically is an extension of the expressions presented in Equation (4.31) and (4.32). That is, having calculated an increment in the nodal point displacements, which defines a new total displacement vector, the incremental solution presented above can be repeated using the currently known total displacements instead of the displacements at time t. The equations used in the Newton-Rhapson procedure stay as follows:

$$ {}^{(i-1)}\bar{\boldsymbol{K}}^{t+\Delta t}\ {}^{(i)}\Delta\bar{\boldsymbol{u}}(x) \;=\; F(\bar{\boldsymbol{t}}^{\,n})^{t+\Delta t} - {}^{(i-1)}\,R(\bar{\boldsymbol{\sigma}})^{t+\Delta t} \tag{4.33} $$

$$ {}^{(i)}\bar{\boldsymbol{u}}(x)^{t+\Delta t} \;=\; {}^{(i-1)}\bar{\boldsymbol{u}}(x)^{t+\Delta t} + {}^{(i)}\,\Delta\bar{\boldsymbol{u}}(x) \tag{4.34} $$

where the subscript i denotes the iteration number.

The out-of-balance load vector $F(\bar{\boldsymbol{t}}^{\,n})^{t+\Delta t} - {}^{(i-1)}\,R(\bar{\boldsymbol{\sigma}})^{t+\Delta t}$ in Equation (4.33) corresponds to a load vector that is not yet balanced by element stresses, and therefore an increment in the nodal point displacements is required. This updating of the nodal point displacements in the iteration is continued until the out-of-balance loads and increments are small.

An important point on the iterative solution is that the correct calculation of ${}^{(i-1)}R(\bar{\boldsymbol{\sigma}})^{t+\Delta t}$ from ${}^{(i-1)}\bar{\boldsymbol{u}}(x)^{t+\Delta t}$ is crucial. Any errors in this computation will, in general, result in an incorrect response prediction. The correct evaluation of the tangent stiffness matrix ${}^{(i-1)}\bar{\boldsymbol{K}}^{t+\Delta t}\ {}^{(i)}$ is also important. However, it must be noted that in the assemblage of the homogenized stiffness matrix, the homogenized constitutive tensor $\bar{\mathbf{C}}(x)$ plays a direct role. Therefore, in the non-linear case the proper computation of the non-linear homogenized constitutive tensor $\bar{\mathbf{C}}^{Tnl}(x)$ is desired for an appropriate rate of convergence.

The importance of the non-linear homogenized constitutive tensor $\bar{\mathbf{C}}^{Tnl}(x)$ is highlighted in Table 4.1, since it shows that it is used at two points of the solution process: the evaluation of the stresses and the evaluation of the tangent stress-strain matrices. The stresses are used in the computation of the nodal point force vectors and in the non-linear strain stiffness matrices, meanwhile that the tangent stress-strain matrix is used to compute the linear strain stiffness matrices. A full description of the numerical determination of

the homogenized non-linear constitutive tensor is given in Section 4.4.2. The complete non-linear incremental solution process at the macro scale is summarized in Table 4.1.

Accepted and known solution at time t:	∘ stresses $\bar{\boldsymbol{\sigma}}(x)^t$ ∘ strains $\bar{\boldsymbol{\varepsilon}}(x)^t$ ∘ internal material parameters $\boldsymbol{\alpha}(x)_1, \boldsymbol{\alpha}(x)_2, ...$
1. *Known*:	• nodal point variables ${}^{(i-1)}\bar{\boldsymbol{u}}(x)^{t+\Delta t}$ and element strains ${}^{(i-1)}\bar{\boldsymbol{\varepsilon}}(x)^{t+\Delta t}$
2. *Compute*:	• stresses ${}^{(i-1)}\bar{\boldsymbol{\sigma}}(x)^{t+\Delta t}$ • tangent stress-strain matrix , denoted as ${}^{(i-1)}\bar{\mathbf{C}}(x)$, corresponding to ${}^{(i-1)}\bar{\boldsymbol{\sigma}}(x)^{t+\Delta t}$ • internal material parameters ${}^{(i-1)}\bar{\boldsymbol{\alpha}}(x)_1{}^{t+\Delta t}, {}^{(i-1)}\,\bar{\boldsymbol{\alpha}}(x)_2{}^{t+\Delta t}, ...$
a.	*In elastic analysis:* the strains ${}^{(i-1)}\bar{\boldsymbol{\varepsilon}}(x)^{t+\Delta t}$ directly give the stresses ${}^{(i-1)}\bar{\boldsymbol{\sigma}}(x)^{t+\Delta t}$ and the stress-strain matrix ${}^{(i-1)}\bar{\mathbf{C}}(x)$ with: $\bar{\mathbf{C}}(x) = [\bar{\boldsymbol{\sigma}}(x)] : [\bar{\boldsymbol{\varepsilon}}(x)]^{-1}$
b.	*In inelastic analysis:* an integration process is performed for the stresses according to: $${}^{(i-1)}\bar{\boldsymbol{\sigma}}(x)^{t+\Delta t} = \bar{\boldsymbol{\sigma}}(x)^t + \int_t^{(i-1)t+\Delta t} d\bar{\boldsymbol{\sigma}}(x)$$ and the tangent stress-strain matrix ${}^{(i-1)}\bar{\mathbf{C}}(x)^{Tnl}$ corresponding to the state $t+\Delta t$, end of iteration $(i-1)$, is evaluated consistent with this integration process. with: $\bar{\mathbf{C}}^{T_{nl}}(x) = \frac{1}{V_{\Omega_c}} \int_{V_{\Omega_c}} C_{ij}^{T_{nl}} dV_{\Omega_c}$
3. *Compute*:	• nodal point variables ${}^{(i)}\Delta\bar{\boldsymbol{u}}(x)$ using: ${}^{(i-1)}\bar{K}^{t+\Delta t}\ {}^{(i)}\Delta\bar{\boldsymbol{u}}(x) = F(\bar{\boldsymbol{t}}(x)^n)^{t+\Delta t} - {}^{(i-1)}\ R(\bar{\boldsymbol{\sigma}}(x))^{t+\Delta t}$, [Equation(4.33)] ${}^{(i)}\bar{\boldsymbol{u}}(x)^{t+\Delta t} = {}^{(i-1)}\ \bar{\boldsymbol{u}}(x)^{t+\Delta t} + {}^{(i)}\ \Delta\bar{\boldsymbol{u}}(x)$, [Equation(4.34)].
Repeat steps	*1 and 3 until convergence*

Table 4.1: Incremental solution process at the macro scale.

Incremental solution at the micro scale

At the micro scale the solution of the problem is formulated following a similar procedure than the one implemented at the macro scale with slight changes in the formulation with respect to the procedure described in Table 4.1.

One of the main differences in the local scale formulation is that in this case the problem is computed, iteratively until reaching convergence, for only one load increment corresponding to the load state obtained from the homogenized strains. This approach may lead to think that the solution at the micro scale is not an incremental solution as in the case exposed at the macro scale. However, although the solution is computed only once for each load increment, the solution it is an iterative procedure, since in order to compute the response at the time $t + \Delta t$, the values of the stresses $\boldsymbol{\sigma}(y)^t$, strains $\boldsymbol{\varepsilon}(y)^t$ and internal material parameters $\boldsymbol{\alpha}(y)^t$ at the last converged step of the micro structure at time t must be known. This fact makes the solution at the micro scale to be a fully iterative solution.

Nevertheless, storing and retrieving all this information is not an easy task, since the values of $\boldsymbol{\sigma}(y)^t$, $\boldsymbol{\varepsilon}(y)^t$ and $\boldsymbol{\alpha}(y)^t$ must be stored for each unit cell or RVE that represent each integration point at the macro scale. Therefore, special attention must be given to this fact on the implementation of the computational tool.

The other major difference with respect to the macro scale formulation is the use of the linear and non-linear constitutive tensors $\mathbf{C}(y)$ and $\mathbf{C}^{Tnl}(y)$ obtained directly from the constitutive models that reflect the actual behavior (plasticity, damage, etc.) of the different material components instead of the homogenized ones $\bar{\mathbf{C}}(x)$ and $\bar{\mathbf{C}}(x)^{Tnl}$.

Another procedure that is implemented at the micro scale is the computation of the homogenized non-linear constitutive tensor. The procedure is thoroughly explained in the following section.

4.4.2 Numerical determination of the homogenized non-linear constitutive tensor

The numerical determination of the homogenized non-linear constitutive tensor is based on a perturbation method presented by Badillo and Oller [4]. The formulation takes knowledge from a methodology proposed by Martinez et al. [71] in which the non-linear tangent tensor of a homogeneous material is obtained by means of a perturbation method. This formulation was adapted here to compute the non-linear tangent tensor for a composite unit cell or RVE conformed by two or more material components. The idea is to compute the homogenized non-linear constitutive tensor $\bar{\mathbf{C}}(x)^{Tnl}$ through the non-linear tangent constitutive tensor $\mathbf{C}^{T_{nl}}$ of each element of the unit cell as explained in Section 3.5.5.

The perturbation method applied at the non-linear range is implemented as an exten-

sion of the method at the linear range presented at Section 3.4.3. However, in this case the homogenized nonlinear tensor is computed using a slightly different approach from the one used to compute the linear tensor, as it is explained in the following paragraphs.

Perturbation method at the non-linear range

The method is implemented based on a finite element formulation framework. It consists in identifying first if any Gauss (integration) point of any element of the unit cell has entered in the non-linear range. If this is the case, the tangent constitutive tensor for the element where that Gauss point lies has to be calculated. The procedure to obtain the tangent constitutive tensor is based in performing a numerical derivation applying a perturbation technique in way that it can be useful to compute the non-linear response of any constitutive law.

The method is applied to obtain the non-linear tangent constitutive tensor $\mathbf{C}^{T_{nl}}$ of each element of the unit cell that represents the composite. The non-linear tangent constitutive tensor is obtained by solving numerically Equation (3.52). Using a matrix notation this equation can be expressed as:

$$\begin{bmatrix} \dot{\sigma}_1 \\ \vdots \\ \dot{\sigma}_n \end{bmatrix} = \begin{bmatrix} C_{11}^{T_{nl}} & \cdots & C_{1n}^{T_{nl}} \\ \vdots & \ddots & \vdots \\ C_{n1}^{T_{nl}} & \cdots & C_{nn}^{T_{nl}} \end{bmatrix} \begin{bmatrix} \dot{\varepsilon}_1 \\ \vdots \\ \dot{\varepsilon}_n \end{bmatrix} \tag{4.35}$$

The stress vector rate of Equation (4.35) can be obtained as the sum of k stress vectors, which are the product of the j component of the strain vector rate and the j column of the tangent stiffness tensor. This can be expressed as follows:

$$\dot{\boldsymbol{\sigma}} \equiv \sum_{j=1}^{k} \delta^{\,j}\boldsymbol{\sigma} = \sum_{j=1}^{k} \mathbf{C}_j^{T_{nl}} \cdot \dot{\boldsymbol{\varepsilon}}_j \tag{4.36}$$

where:

$$\mathbf{C}_j^{T_{nl}} = \begin{bmatrix} C_{1j}^{T_{nl}} & C_{2j}^{T_{nl}} & \cdots C_{k\,j}^{T_{nl}} \end{bmatrix}^T \tag{4.37}$$

Equation (4.37) is used to obtain the j column of the tangent constitutive tensor, which is unknown:

$$\mathbf{C}_j^{T_{nl}} = \frac{^{j}\dot{\boldsymbol{\sigma}}}{\dot{\boldsymbol{\varepsilon}}_j} \equiv \frac{\delta^{\,j}\boldsymbol{\sigma}}{\delta\boldsymbol{\varepsilon}_j} \tag{4.38}$$

The perturbation method consists in defining k small variations, or perturbations, of the strain vector $\delta\boldsymbol{\varepsilon}_j$, to obtain k stress vectors $\delta^{\,j}\boldsymbol{\sigma}$ that will be used in Equation (4.38) to obtain the numerical expression of the tangent constitutive tensor. It must be noted that in the numerical implementation of this procedure, the smaller the perturbation value that is used the better the computation of the tangent tensor will be. However if perturbation values close to zero are used in the computation of the tangent tensor, they may lead to an indeterminate solution. Therefore a restriction in the lower value of the perturbation condition must be given in order to avoid this problem.

The perturbation value defined for each component of the strain tensor is obtained taking into account that the smaller the perturbation value the better the approximation of the tangent constitutive tensor will be. Following this premise the strain perturbation is obtained according to the following rule:

$$\begin{aligned} &if \quad \boldsymbol{\varepsilon}_j \neq 0 \quad \rightarrow \quad \delta\boldsymbol{\varepsilon}_j = \boldsymbol{\varepsilon}_j \cdot 10^{-5} \\ &if \quad \boldsymbol{\varepsilon}_j = 0 \quad \rightarrow \quad \delta\boldsymbol{\varepsilon}_j = \min\{\boldsymbol{\varepsilon}_k\} \cdot 10^{-5} \qquad \forall k = 1, n \end{aligned} \tag{4.39}$$

By choosing the value of the perturbation according to expression (4.39) it is ensured that the strain increment is always small enough to ensure that the stress variation is close to the stress value computed on the actual load step analysis. However, there is the case when the strain values are close to zero, for which the previous procedure will produce perturbation values close to zero. These values may cause an indetermination in the solution of Equation (4.38). To prevent this situation, in order to avoid values close to zero, an extra condition is implemented on the procedure to obtain the perturbation values. The extra condition stays as:

$$\delta\boldsymbol{\varepsilon}_j > \max\{\boldsymbol{\varepsilon}_k\} \cdot 10^{-10} \qquad \forall k = 1, n \tag{4.40}$$

Table 4.2 summarizes the complete perturbation process to compute the nonlinear tangent constitutive tensor. The procedure described is suitable for the computation of any constitutive law and for any yield surface used.

Numerical integration of the homogenized tangent constitutive tensor

Once that the tangent tensor is computed for each and every element of the unit cell or RVE following the procedure described on Table 4.2, then it must be stored in order to calculate the homogenized non-linear tangent constitutive tensor $\bar{\mathbf{C}}^{T_{nl}}$. This will allow us to solve the constitutive problem of the composite material expressed by Equation (3.61).

The homogenized tangent non-linear constitutive tensor $\bar{\mathbf{C}}^{T_{nl}}$ is computed over the entire volume of the unit cell or RVE following the classical definition given by the average

Accepted and known solution using constitutive laws for a continuum in equilibrium:	∘ stresses $\boldsymbol{\sigma}$ ∘ strains $\boldsymbol{\varepsilon}$ ∘ internal material parameters $\boldsymbol{\alpha}$
1. *Define*:	• strain perturbation $\delta\boldsymbol{\varepsilon}_j$ according to Equations (4.39) and (4.40)
2. *Compute*:	• perturbed strain state vector as function of j: $\boldsymbol{\varepsilon}^* = \boldsymbol{\varepsilon} + {}^j\boldsymbol{\varepsilon}$ where ${}^j\boldsymbol{\varepsilon} = [0 \dots \delta\boldsymbol{\varepsilon}_j \dots 0]^T$ • perturbed stress state vector: $\boldsymbol{\sigma}^* (\boldsymbol{\varepsilon}^*, \boldsymbol{\alpha}^*)$ using constitutive law • stress increment: $\delta\, {}^j\boldsymbol{\sigma} = \boldsymbol{\sigma}^* - \boldsymbol{\sigma}$
3. *Compute*:	• column j in tangent stiffness matrix: $\mathbf{C}_j^{T_{nl}} = \dfrac{\delta\, {}^j\boldsymbol{\sigma}}{\delta\boldsymbol{\varepsilon}_j}$
Repeat steps	*from $j = 1, n$, where n is the number of tensorial components*

Table 4.2: Numerical algorithm to obtain the tangent constitutive tensor by means of a perturbation method at the micro scale.

method as expressed in Equation (3.71). The numerical integration of the homogenized tangent constitutive tensor stays as follows:

$$\bar{\mathbf{C}}^{T_{nl}}(x) = \frac{1}{\sum_{i=1}^{n_{elem}} \left(\sum_{i=1}^{n_{\text{int}}} w^l j_{(e)} \right)} \sum_{i=1}^{n_{elem}} \left(\sum_{i=1}^{n_{\text{int}}} C_{ij}^{T_{nl}}(y_{(e)}^l) w^l j_{(e)} \right) \tag{4.41}$$

where $\mathbf{C}^{T_{nl}}$ is the tangent constitutive tensor associated to a material component, $y_{(e)}^l$ represents each integration point of the microstructure ($y_{(e)}^l \in \Omega_{c_{(e)}}$), w^l is the corresponding weight, $j_{(e)}$ is the Jacobian of the element, n_{elem} is the total number of elements in the cell domain Ω_c and n_{int} is the number of integration points for the element $\Omega_{c(e)}$.

Furthermore, this process is adapted in order to explore the application of the method at the macro scale following the same concepts presented above.

4.5 Implementation of the multi-domain decomposition homogenization method

In practical analysis and design the most important steps of an analysis process are the correct idealization of the real problem, the formulation and solution of the force balance equations and the computation of the internal element stress distributions which are complemented by the proper interpretation and representation of the obtained results.

In the case of the multi-domain homogenization method, other aspects should be considered besides of the steps mentioned above, in order to achieve suitable coupling and computational efficiency at the double-scale method. The solution requires an efficient computational approach in order to take into account the enormous demands that the method requires in terms of computing resources (memory and speed), which are naturally linked to the size and complexity of the problem to be analyzed.

4.5.1 Computational complexity of the problem

The implementation of the multi-domain decomposition homogenization method represents a very complex problem, especially in the non-linear case. At the linear case the problem could be approached using only one cell (one cell per each subdomain) for all the integration points at the macro scale since the stresses and the homogenized constitutive tensor can be directly evaluated for a given strain state without the need to store the history of any variable. At the non-linear case tough, the problem becomes much more difficult to compute, since the integration process is needed from the state at time t to the current strain state, therefore the history of the variables that determine the material behavior (stresses, strains and internal variables at time t) must be stored separately for each unit cell that represent each integration point at the macro scale.

Furthermore, the implementation of the perturbation method presented in Section 4.4.2 to compute the homogenized non-linear tangent tensor for each unit cell or RVE that enters into the non-linear range also requires to store the variables that determine the material behavior at the current strain state in order to compute the non-linear tensor following the perturbation method procedure explained previously.

Moreover, an appropriate assembly of the computing codes at each of the two scales is needed since constant information transferring is performed through the whole computational process. The assemblage process requires a substantial organization effort due to the voluminous amount of information that is generated. Therefore, in order to achieve computational efficiency in the implementation of the multi-domain homogenization approach a convenient parallelization strategy is needed.

All the aforementioned reasons make the multi-domain homogenization approach to be a very demanding problem that requires an efficient computational strategy.

4.5.2 Nested solution set-up

The organization of the nested solution scheme of the double-scale multi-domain program is summarized in the following paragraphs. In this formulation, the finite element code PLCd is used as starting platform to apply the numerical implementation of the homogenization technique. The PLCd program can solve classic constitutive equations, such as damage, plasticity, visco-elasticity, damage-plasticity, etc. and uses several yield surfaces such as Von-Misses, Mohr-Coulomb, etc. For a thorough description of the code see [19].

The multi-domain decomposition homogenization technique consists first in dividing the problem in two scales; therefore the numerical implementation has to be developed in two different programs, one that deals with the macroscopic or global scale (called global program) and another one that deals with the micro or local scale (local program) .

The program at the global scale deals with the geometry of the problem, the boundary conditions and with the forces applied in the structure. The macro-structure is discretized into finite elements. Each macroscopic element is linked to a representative periodic domain that will be solved at the local program. Consequently, each integration point of the macro-structure is linked to a unique microstructural RVE or unit cell. The program assembles the stiffness matrix with the homogenized constitutive tensor given by the local program and applies the load increments. Once the system of equations is assembled and solved, the global program sends a set of homogenized strains to the local program and in return the local program gives a set of homogenized stresses. The global program looks for convergence iteratively and the whole process is repeated for each load step of the analysis.

Meanwhile, the program at the local scale, deals with the properties of the constituents of the composite by taking into account the constitutive equations of each one of them. The local program assembles the stiffness matrix of the elements of the cell with the corresponding constitutive tensor of the constituent. It transforms the field of strains given by the global program into a field of displacements that take into account the periodic conditions that result in a set of applied forces into the cell domain. The program assembles and solves the system of equations and calculates the residual forces considering each constitutive model of the constituents. The local program sends one set of homogenized stresses for each cell corresponding to each Gauss point of the global program in return to the set of homogenized strains given. The program looks for convergence iteratively.

The local program computes the linear elastic homogenized tensor in a first instance by applying a perturbation in order to activate the elastic components of the constituents of the composite. It computes the inelastic (tangent) non-linear homogenized tensor when one of the Gauss points of any of the elements of the cell lie within the inelastic range, following the procedure explained previously in Section 4.4.2, and sends the tensor to the global scale. A schematic representation of the implementation of the code involving the two scales of the homogenization technique proposed is presented in Figure 4.1.

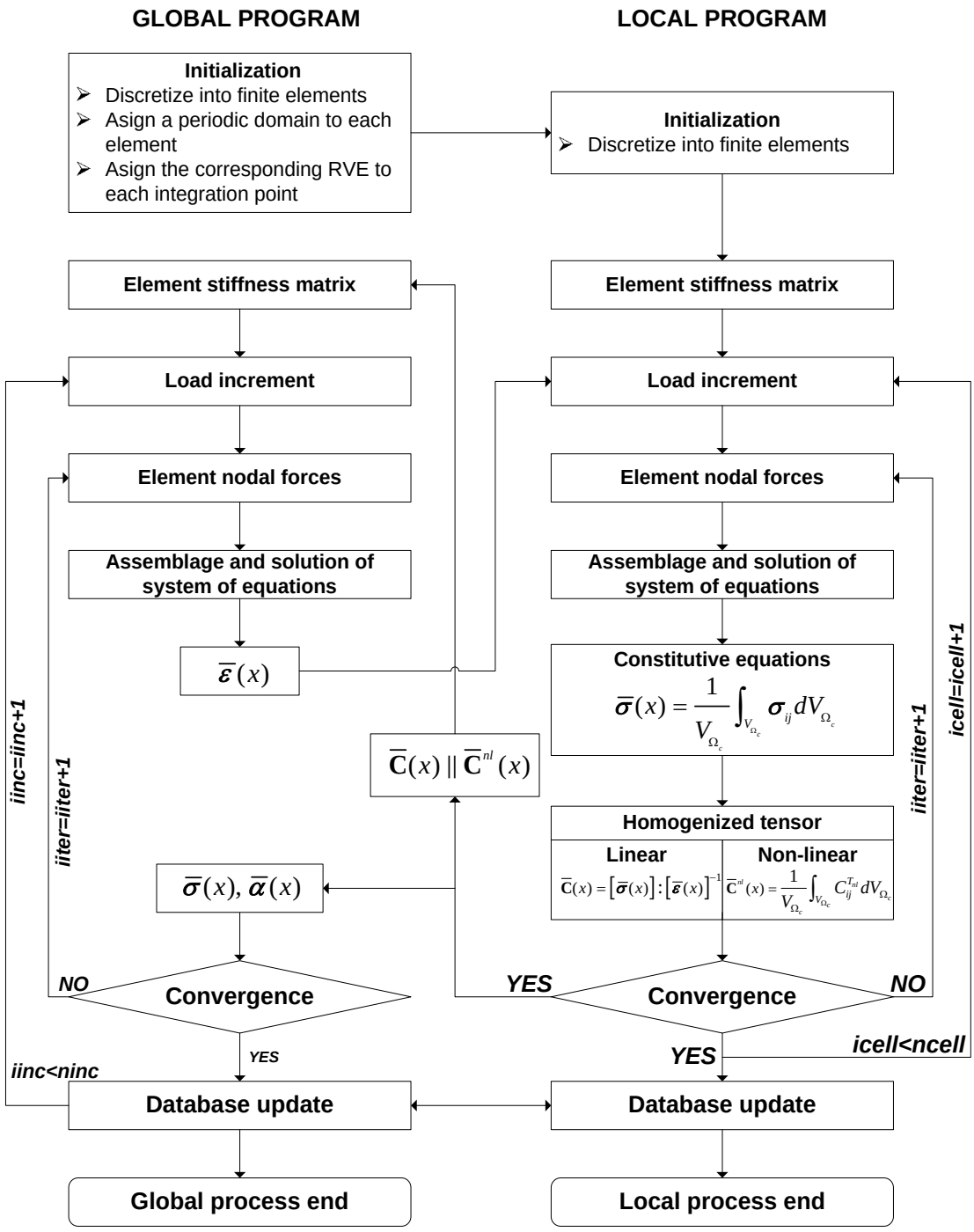

Figure 4.1: Schematic representation of the nested incremental-iterative solution for the multi-domain decomposition homogenization method.

4.5.3 Parallelization process

The nature of the nested incremental-iterative solution for the multi-domain decomposition homogenization method represents a huge computational effort, since as it was mentioned earlier each integration point at the macroscale becomes a finite element problem at the local scale, therefore a large amount of generated information and data exchange is expected during the whole computational process.

A significant aspect of the problem is that at the same macroscopic iteration, each of the problems represented at the local level by a RVE or a unit cell do not share any data among them, which makes them independent from each other. Due to this reason the computation of the problems at the local scale can be performed simultaneously or in parallel. Using a parallelized approach will reduce the computing time and will increase the capacity of the method to solve more complex problems with respect to those that can be solved with a single CPU processor.

Concurrent programming languages, libraries, application programming interfaces, and parallel programming models (such as algorithmic skeletons) have been created for programming parallel computers. These can generally be divided into classes based on the assumptions they make about the underlying memory architecture-shared memory, distributed memory, or shared distributed memory. In the implementation of the parallelization process in this research the application programming interface *OpenMP* (Open Multi-Processing) was employed. This application supports multi platform shared memory multiprocessing programming in C, C++, and Fortran on many architectures, including Unix and Microsoft Windows platforms. It consists of a set of compiler directives, library routines, and environment variables that influence run-time behavior. *OpenMP* is an implementation of multi-threading, a method of parallelization whereby the master 'thread' (a series of instructions executed consecutively) 'forks' a specified number of slave 'threads' and a task is divided among them. The threads then run concurrently, with the runtime environment allocating threads to different processors.

The section of code that is meant to run in parallel is marked accordingly, with a preprocessor directive that will cause the threads to form before the section is executed. Each thread has an 'id' attached to it which is an integer. The master thread has an id of '0'. After the execution of the parallelized code, the threads 'join' back into the master thread, which continues onward to the end of the program.

By default, each thread executes the parallelized section of code independently. 'Work-sharing constructs' can be used to divide a task among the threads so that each thread executes its allocated part of the code. The runtime environment allocates threads to processors depending on usage, machine load and other factors. The number of threads can be assigned by the runtime environment based on environment variables or in code using functions.

Load balancing

The equal division of work among threads in parallelization is known as load balancing. This issue is among the most important attributes for parallel application performance, because it ensures that the processors are fully operational most of the time. Without a correct balanced load, some threads may finish significantly before others, leaving processor resources idle reducing performance efficiency.

Poor load balancing is usually caused by variations in compute time among loop iterations. It is usually simple to determine the variability of loop iteration computing time by examining the source code. In most cases, you will see that loop iterations consume a uniform amount of time. *OpenMP*, by default, assumes that all loop iterations consume the same amount of time. This assumption leads *OpenMP* to distribute the iterations of the loop among the threads in roughly equal amounts and in such a way as to minimize the chances of memory conflicts due to false sharing. This is possible because loops generally touch memory sequentially, so splitting up the loop in large parts like the first half and second half when using two threads-will result in the least chance for overlapping memory. While this may be the best choice for memory issues, it may be bad for load balancing. However, the inverse situation is also true; what may be best for load balancing may be bad for memory performance. Therefore, a balance between optimal memory usage and optimal load balancing should be attempted by measuring the performance of the case in question.

In the case of the multi-domain decomposition method presented in this thesis, the scheme followed to obtain a proper load balance was made by treating each periodic subdomain that forms part of the whole structure separately. This is done following the premise that each subdomain may behave differently from each other since one specific subdomain may have more non-linear properties than another one. The total number of processors available for the problem computation are all used in solving one periodic subdomain at the time and once that all the unit cells or RVEs belonging to that subdomain are analyzed and their results are stored then the program starts the process again for the next subdomain.

The micro-macro program organization for the multi-domain decomposition method follows the classical master-slave program approach. At the global program, the different periodic subdomains Ω_{c_i} are identified first and then the master program starts the parallelization process for each subdomain sequentially. The master program obtains from the macrostructure analysis the strain gradients for each integration point $\bar{\boldsymbol{\varepsilon}}^i(x)$ and starts the RVE or unit cell computations on each available processor by means of the slave programs (local programs).

Each local program analyzes one set of RVEs or unit cells based of the number of integration points present on each subdomain Ω_{c_i} and the number of processors N available

for computation. Therefore the strain gradients are grouped according to this definition in a vector group of strain gradients $\bar{\boldsymbol{\varepsilon}}^i(x)_n$ (where $n = 1, \ldots, N$) and they are delivered to the corresponding local program. Once the local analysis have been completed, the global program collects data from the local programs spawned (averaged stress tensors $\bar{\boldsymbol{\sigma}}^i(x)$, non-linear constitutive tensors $\bar{\mathbf{C}}^i(x)$ and average internal variables $\bar{\alpha}^i(x)$) as illustrated in Figure 4.2 where the scheme of the parallelization approach is presented.

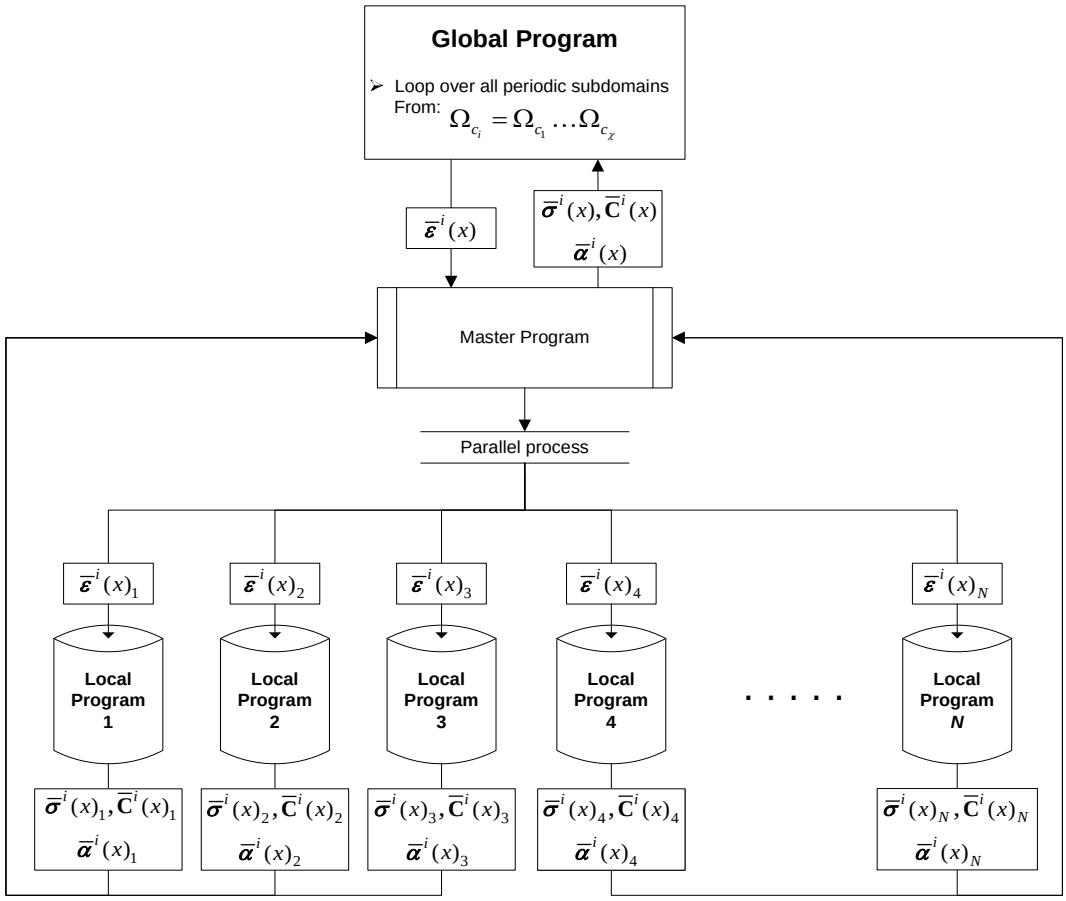

Figure 4.2: Schematic representation of the parallelization approach for the multi-domain decomposition homogenization method.

The algorithm to obtain the exact number of RVEs that each processor analyzes is presented in Figure 4.3. The algorithm starts by computing the nearest integer number N_{PGI} that results from dividing the number of integration points present N_{PGT} on each subdomain and the number of processors N available for computation (where $\|\|$ stands for

the function which returns the nearest integer number of a real number). Then the result R_{PGT} obtained from multiplying N_{PGI} by the number of processors N, is compared with the total number of integration points. If the result is equal, then the number of RVEs or unit cells per processor is equal to N_{PGI}. In the opposite case, this number is augmented or reduced according to D_{iff}, the absolute value of the difference between N_{PGT} and R_{PGT}, as depicted in Figure 4.3.

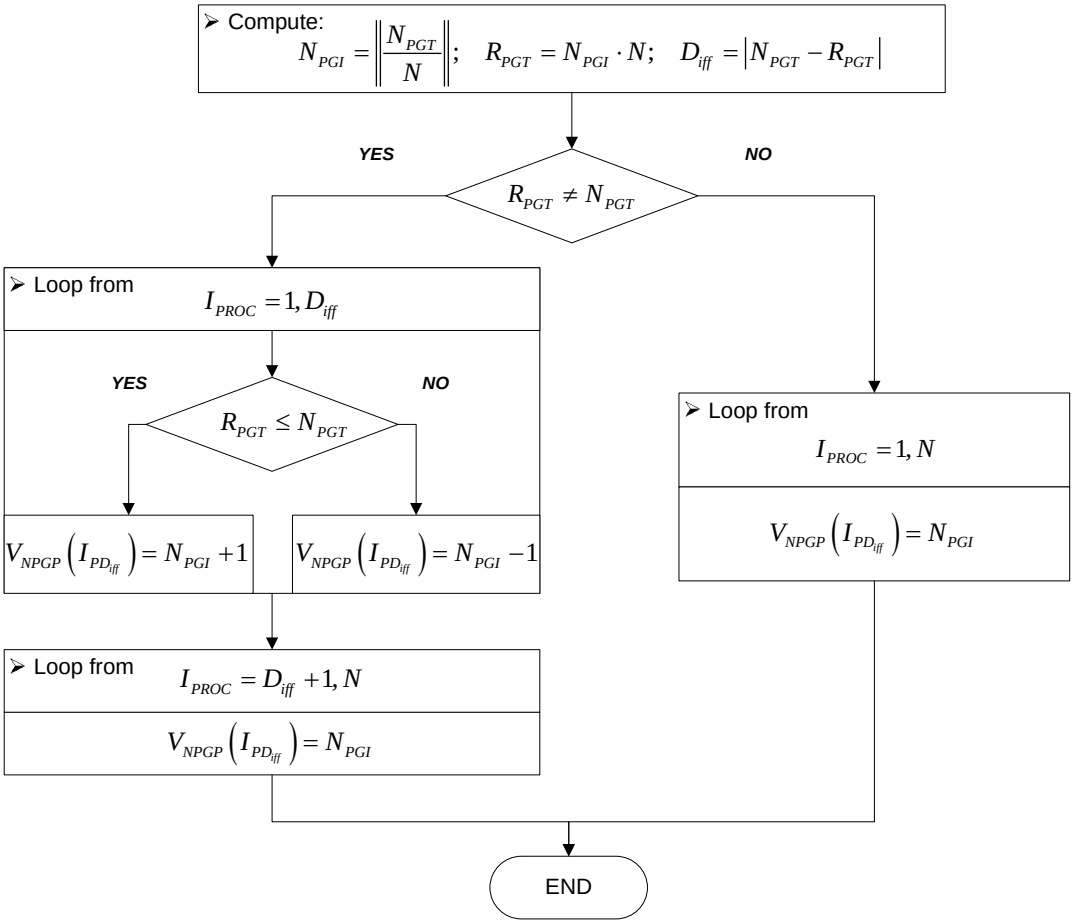

Figure 4.3: Algorithm for the load distribution of the parallelization scheme.

The parallelization scheme implemented in this study represents a very simple and straightforward process. If a thoroughly optimized parallelization process is desired, a more comprehensive algorithm should be implemented. Nevertheless, this task alone represents itself an extensive and complex topic which lies out of the scope and main objectives of this thesis and should be subject of further study. Despite this fact, the efficiency of the basic

parallelization process presented in the previous paragraphs is explored in one example presented in Section 6.1.3 with illustrative purposes.

This page is intentionally left blank.

Chapter 5

Effect of softening in homogenization analysis

In this chapter the effect of softening in two-scale homogenization is investigated following a smeared cracked approach (using plastic and damage models). Although this problem was not among the main objectives of this research it has been studied in order to solve the problem of objectivity in the non-linear response when using multiple-scale finite element when softening appears. Mesh objectivity is discussed first within the FE formulation and then the concepts exposed are extrapolated into the two-scale homogenization framework. The importance of the element characteristic length in a multi-scale analysis is highlighted in the computation of the specific dissipated energy when strain-softening occurs.

5.1 Introduction

Some materials that are subjected to inelastic processes caused by the action of imposed displacements exhibit, after a certain limit, a phenomenon called softening. During a process of uniaxial quasi-static loading, this softening appears physically as a reduction of the magnitude of the stresses accompanied by an increment of the strains. In continuum mechanics, it is known that the inclusion of strain-softening leads to the increment of strains in narrow strips. This phenomenon is known as strain-localization.

Several attempts have been made in order to properly model this phenomenon in different constitutive models that present strain softening, such as in the case of damage and plasticity. Within the context of the finite element method, the so-called 'local models' are implemented at the integration points of the model, since each point represents a finite space of the domain. Each integration point characterizes the behavior of the infinite number of material points that lie within its area of influence. At this scale, it is admitted by several authors that considering the softening behavior as a phenomenon dependent on the material and on the size of area of influence of the point on a discrete space is completely appropriate (see for example [6, 87]).

In this chapter the effect of softening in two-scale homogenization is investigated following a smeared cracked approach. The objective of this section is to find objectivity in the response when softening appears regardless of the mesh size in both scales. Mesh objectivity is discussed first within the FE formulation and then the concepts exposed are extrapolated into the two-scale homogenization framework.

5.2 Objectivity of the classical one-scale FE formulation response with strain-softening

An essential aspect in numerical modeling is objectivity, in particular the requirement that the results must be independent of the mesh choice. This aspect is especially noteworthy in the response of models which consider softening in the constitutive formulation. The problem that poses a continuum which exhibits strain-softening can be stated from assuming that the strain localization defines a nonlinear behavior zone, where energy is dissipated according to the size of this zone, while outside of it an elastic unloading process is developed.

The numerical implementation of the damage continuum formulation into the framework of the FE method requires a transformation of the involved variables into a discrete formulation. In order to better explain this transformation, let us consider a 2D beam of length l, which is fixed on the left side and is axially loaded outwards on the right side. Moreover, lets consider a strong discontinuity (for example a jump in the displacement field) takes place at a certain cross-section S of the beam as depicted in Figure 5.1.

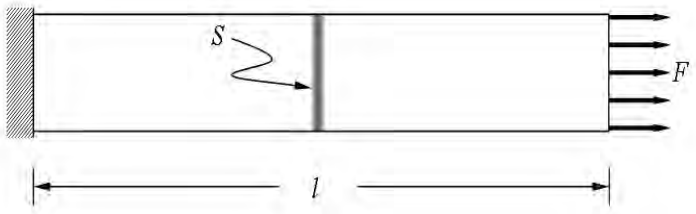

Figure 5.1: Schematic representation 2D beam with strong discontinuity.

The classical fracture mechanics classifies the fracture energy per unit area G_f as a material property which is defined as the amount of energy required to dissipate to open a crack of unit area. Following a simple formulation based on a uniaxial behavior, the fracture energy per unit area can be expressed as:

$$G_f = \frac{W_f}{A_f} \tag{5.1}$$

where W_f is the energy dissipated by the fracture at the end of quasi-static process, and A_f is the total area of the crack. The fracture energy is adopted as the binding parameter

between fracture mechanics and the constitutive model based on classical mechanics, which is formulated to represent the macroscopic behavior of a fissured solid material. The coupling of both theories is given by the following dissipation condition:

$$W_f = G_f A_f = \int_V g_f \, dV \tag{5.2}$$

where g_f is the maximum specific energy dissipated by a continuum model in pure traction. The schematic representation of the relation between fracture mechanics and classical mechanics is depicted in Figure 5.2.

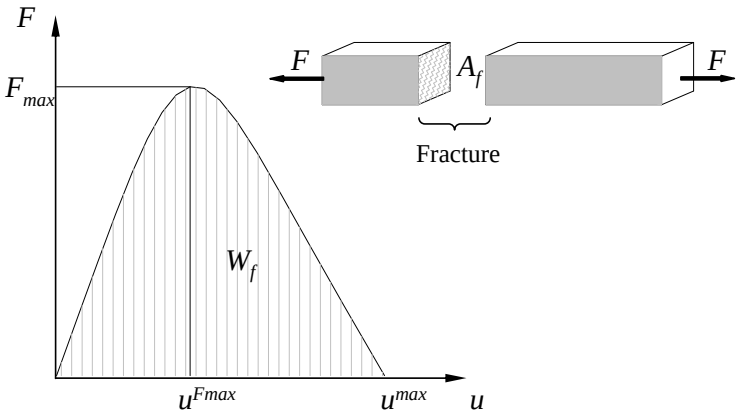

(a) fracture mechanics

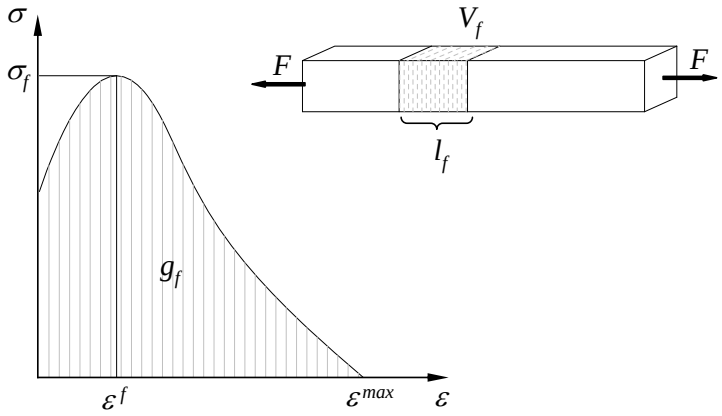

(b) continuum mechanics

Figure 5.2: Schematic representation of damage.

From Equation (5.2) the objective relationship that should exist between the fracture

energy per unit area G_f, which is a material parameter, and the total energy per unit volume g_f is obtained. This is expressed as:

$$G_f = \frac{W_f}{A_f} = \int_V \frac{g_f}{A_f}\, dV \tag{5.3}$$

Since the volume where the fracture process is allocated is defined as $V = l_p\ A_f$ then Equation (5.3) becomes:

$$G_f = \frac{W_f}{A_f} = l_f\ g_f \quad \Rightarrow \quad g_f = \frac{G_f}{l_f} = \frac{W_f}{l_f\ A_f} \tag{5.4}$$

where l_f is the length of the area where the non-linear behavior will occur.

In the context of the FEM the state variables are computed at the integration points in terms of local strain and stresses. Thus, the length of the area where the non-linear behavior occurs is related to the volume (or area) of each finite element. Under this premise and considering the uniaxial case of Figure 5.1, the area where the dissipation process occurs on the FE formulation corresponds to only one strip of finite elements across the model mesh. Since the dissipation of the total energy on the loading process is proportional to the size of the finite elements, the energy dissipated would diminish as the elements become smaller upon mesh refinement. This problem represents a lack of objectivity in the response since different responses would be obtained depending on the mesh size.

This problem can be addressed by modifying the softening law as proposed by Bazant and Oh [6]. The authors remark that in a finite element method framework, the concept of strain softening should not be considered as a characteristic of the material only, since this aspect is related to the fracture energy G_f and to the size of the finite element where the energy dissipation process occurs. In each element, the computational width of the fracture zone is computed depending on the geometric dimensions of the elements. This width is known as the element characteristic length l_{ch} [83]. The specific dissipated energy $\mathscr{D}$ is then scaled for each element as expressed in Equation (5.5).

$$\mathscr{D}\ l_{ch} = G_f \tag{5.5}$$

This equation is analogous to Equation (5.4) where the maximum specific energy dissipated by a continuum model is obtained ($g_f\ l_f = G_f$).

In Figure 5.3a the schematic representation of the displacement and strain fields of the mode I fracture phenomenon of the beam of Figure 5.1 is presented in the context of continuum mechanics, meanwhile Figure 5.3b presents the approximation of the phenomenon

following a fracture distribution in a finite dimension zone. In these figures it is observed that in order to make compatible the discrete model with the continuum one, the strain evolution of the discrete model has to be normalized with respect to the element length h. On Figure 5.3b, the normalization appears only at the zone where the strong discontinuity exist for illustration purposes, however this normalization must be implemented at the whole structure since the whole structure could present this kind of phenomenon. This is done in order to make the softening modulus H_S, which defines the softening response dependent on the element size.

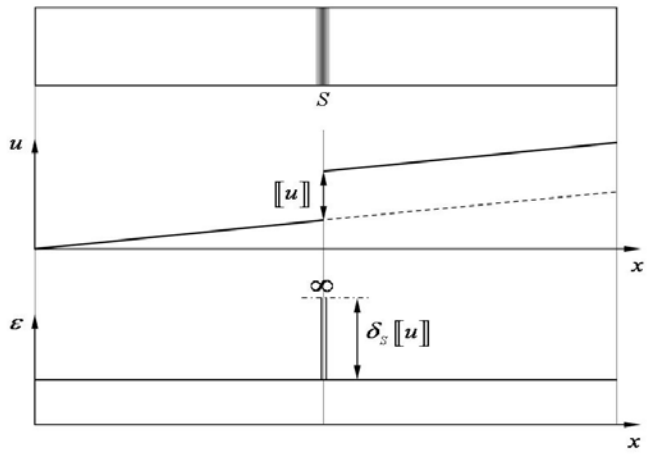

(a) continuum model

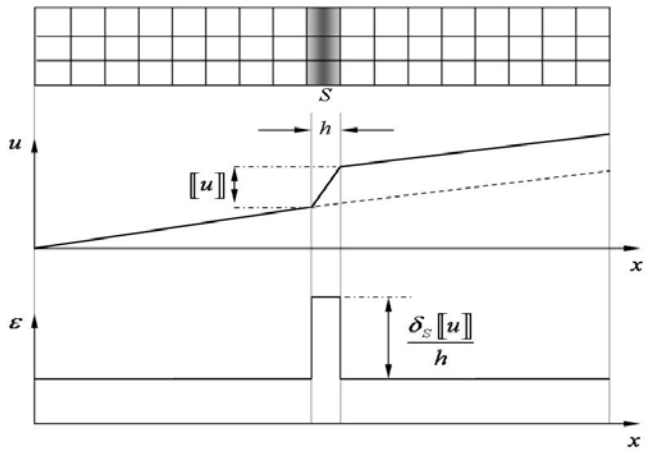

(b) discrete model

Figure 5.3: Schematic representation of the displacement and strain fields of the mode I fracture phenomenon.

Several studies have been done to provide objectivity on the results independently of the size of the finite element mesh (see Oliver [83], Oller [87] Oliver et al. [85], Cervera and Chiumenti [16], among others). Different values of the characteristic length have been proposed in some of those studies. For example, Bazant and Oh [6] associate the characteristic length to a crack band that has a zig-zag shape for the general case of a fracture that is not parallel to the mesh lines. This formulation restricts the use of 2D square elements and the characteristic length is given by:

$$l_{ch} = \frac{h}{\cos\ \alpha} \tag{5.6}$$

where h is the length of each of the sides of the element and α is the angle of the mesh along which the crack band advances with $|\alpha| < 45^o$. In the case where the crack propagation is parallel to the mesh lines, the characteristic length will be equal to the length of the element $l_{ch} = h$. Meanwhile, Cervera and Chiumenti [16] define the characteristic length as the representative size of the element, $l_{ch} = h$ for linear simplex elements and for 2D triangular elements, as:

$$l_{ch} = \sqrt{\frac{4}{\sqrt{3}} A_e} \tag{5.7}$$

being A_e the area of the element assuming that the triangular elements are equilateral.

5.2.1 Numerical example of damage constitutive model analysis using the classical one-scale FEM

To carry out the objectivity analysis in 2D with quadrilateral elements a test is performed of a plate fixed on the left side and loaded outwards on the opposite (right) side in order to simulate an ideal uniaxial tensile test as the one presented in Figure 5.4.

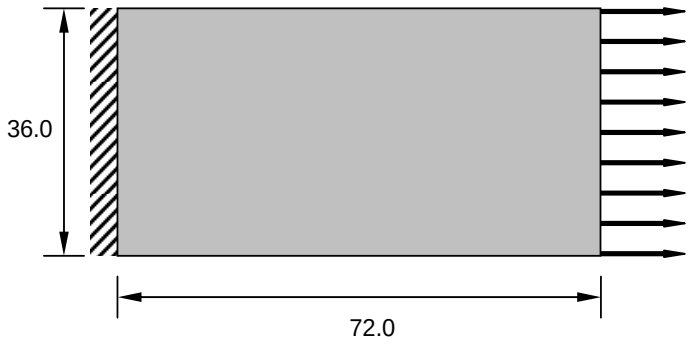

Figure 5.4: Schematic representation of axially loaded plate (units in cm).

The plate consists of a matrix-like material with a length and height equal to 0.72 m and 0.36 m respectively and with a thickness equal to 0.01 m. The behavior of the matrix-like material is expressed by the continuum damage model with exponential softening. The formulation of the constitutive model is fully described in Appendix A. The material parameters used to represent the behavior of the plate are: Young modulus E=3.5E4 MPa, Poisson modulus ν= 0.2, internal friction 30^o, compression strength σ_{y_c}=20 MPa, tensile strength σ_{y_t}=2.0 MPa, fracture energy G_f=0.25 kN/m and compression energy G_c=26.0 kN/m.

The specimen was modeled using different mesh arrangements in order to perform the objectivity analysis. The meshes are conformed by: a) square elements (P-2x4 and P-6x12); b) rectangular elements with the longest side of the element perpendicular to the loading direction (P-2x8 and P-4x16); and c) rectangular elements with the longest side of the element parallel to the loading direction (P-4x4 and P-8x8). The different mesh specimens are depicted in Figure 5.5.

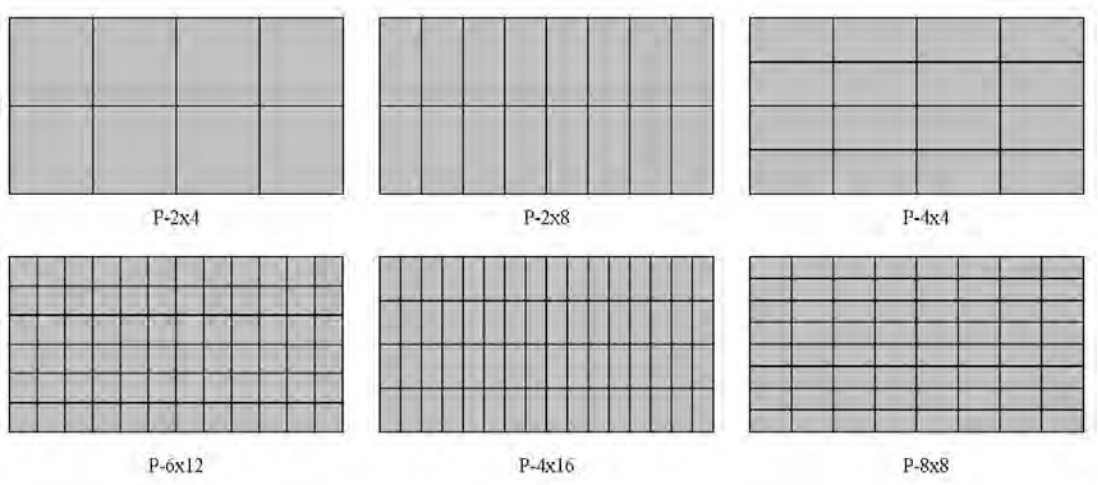

Figure 5.5: Mesh arrangements for the softening objectivity analysis using classical one-scale FEM.

Three different values of the characteristic length were assigned for each mesh element for comparative purposes: 1) equal to the square root of the area of the element $l_{ch} = \sqrt{A_e}$; 2) equal to the length of an integration point in the load direction $l_{ch} = h_{gp}$; and 3) equal to the full length of the element in the load direction $l_{ch} = h_e$.

The results obtained using the classical one-scale FEM in terms of capacity curves for the different mesh models and for the different values of the characteristic length assigned are presented in Figures 5.6-5.8. These values are compared with the response of the plate obtained by modeling it with one single finite element, which is considered as the reference solution.

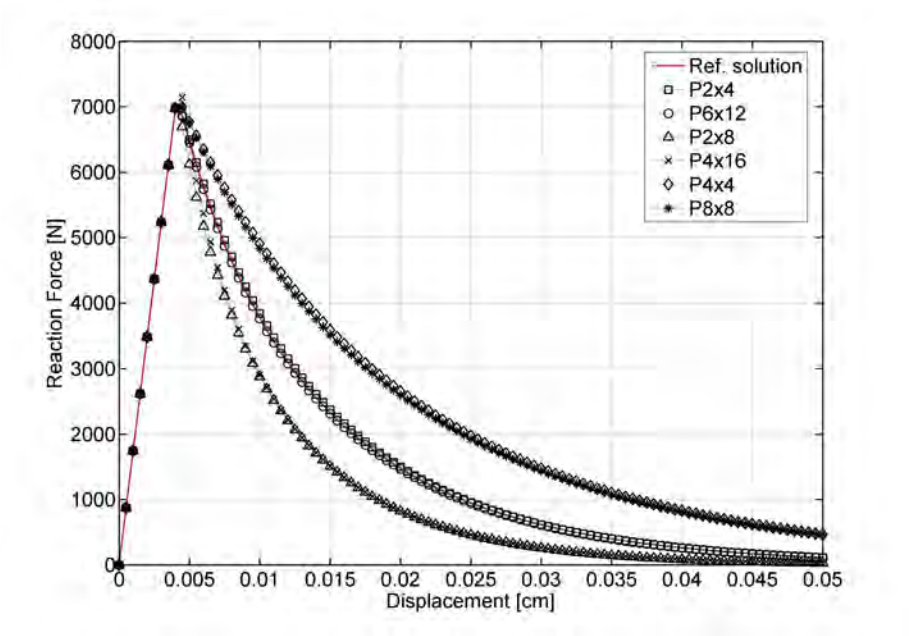

Figure 5.6: Classical one-scale FEM response with characteristic length equal to the square root of the area of the element $l_{ch} = \sqrt{A_e}$.

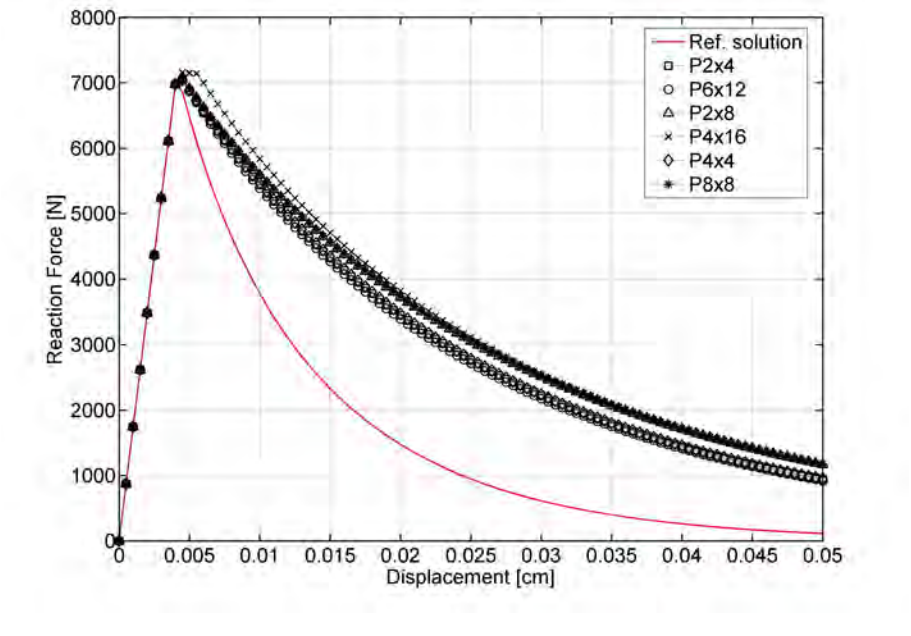

Figure 5.7: Classical one-scale FEM response with characteristic length equal to the length of an integration point in the load direction $l_{ch} = h_{gp}$.

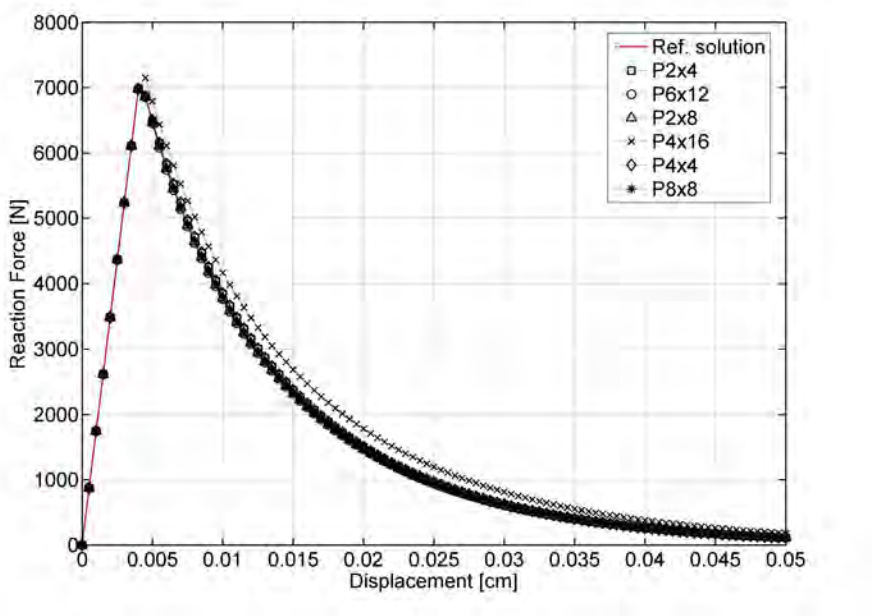

Figure 5.8: Classical one-scale FEM response with characteristic length equal to the length of the element in the load direction $l_{ch} = h_e$.

From the results presented in Figure 5.6, it is observed that for the FEM response with characteristic length equal to the square root of the area of the element $l_{ch} = \sqrt{A_e}$, the models with square elements compute the response of the plate well in agreement with the reference solution; on the other hand the rectangular elements with the longest side of the element perpendicular to the loading direction underestimate the response meanwhile that rectangular elements with the longest side of the element parallel to the loading direction overestimate the response.

For the case of the response with characteristic length equal to the length of an integration point in the load direction $l_{ch} = h_{gp}$ presented in Figure 5.7, there is uniformity on the responses obtained, however all of them overestimate the response with respect to the reference solution.

From the results presented in Figure 5.8 is demonstrated that the value of the characteristic length that gives objectivity in the response and that matches the reference solution is the value equal to the length of the element in the load direction $l_{ch} = h_e$ for the case of pure uniaxial testing. By using this characteristic length it is ensured that the global response of the structure will be always the same independently of the mesh size that is being used.

However it must be noted that the use of a fracture length dependent on the size of the mesh elements will give different evolution of stresses during the analysis process, since

the constitutive law in the inelastic range depends on the total energy per unit volume. For example, for large elements (hence with large fracture lengths) the fracture energy per unit of volume is lower, therefore the stress field will be lower in comparison than in the case with a mesh with smaller elements as it is exposed in Figure 5.9, where the stress-strain evolution for the different mesh sizes is plotted.

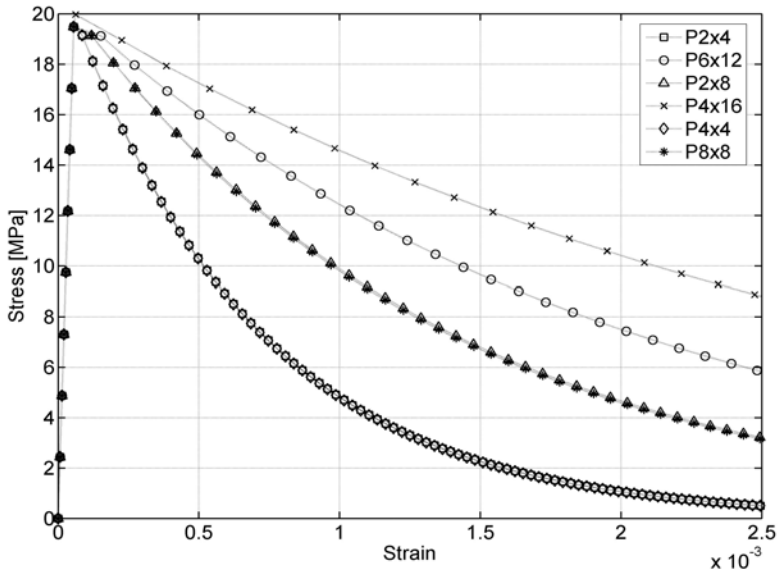

Figure 5.9: Stress-strain evolution for the different mesh arrangements using the classical one-scale FEM.

Some ambiguity existed regarding which characteristic length value should be used in order to obtain objectivity in the strain-softening response since the constitutive model is solved at each integration point of the structure. Therefore, it may be thought that the length to be used would be the corresponding to an integration point; however, the full solution is integrated over the volume of the finite element. Thus, in order to achieve objectivity and a proper structure response, the full length of the element should be used, as it was demonstrated in the previous example.

5.3 Objectivity in two-scale homogenization response with strain-softening

The objectivity aspect becomes more difficult to envision in the case of homogenization, since the estimation of the response is based on a two-scale formulation where each of the integration points of the global scale are associated in the local scale to a unit cell. In order to understand the problem using the homogenization method, let us consider the 2D beam with strong discontinuity as presented in Figure 5.1. Let us assume also that the beam is

composed by an homogeneous material which has damage behavior with strain-softening. The structure is represented by a macroscopic model and a microstructural unit cell as depicted in Figure 5.10.

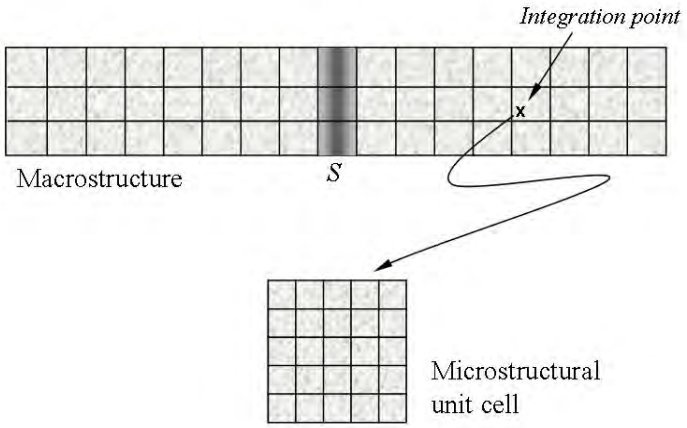

Figure 5.10: Schematic representation of the 2D beam with strong discontinuity. FE meshes at the macro scale and at the micro scale.

In the case of the classical one-scale FE formulation, the state variables are computed at the integration points in terms of local strain and stresses making the area where the non-linear behavior occurs to be related to the finite element volume, as it was demonstrated in the previous section. The problem of objectivity is addressed by modifying the softening law normalizing it with respect to the element length h, making the softening modulus H_S dependent on the element size as expressed in Equation (5.5).

For the case of the homogenization method in two scales, the non-linear behavior of the composite is defined by the constitutive model implemented at the micro scale; however the dissipation process occurs at the macro scale in the area defined by the size of the finite element (at the global level). Therefore, in order to ensure that the same energy is being dissipated at the macro structural point and at the corresponding unit cell, the energy dissipation process that occurs at the micro scale has to be 'normalized' with respect to the macroscopic zone where the dissipation process (i.e. the non-linear behavior) actually happens.

In first-order homogenization the size of the cell is commonly considered as irrelevant, since the state variables are obtained assuming uniformity of the macroscopic deformation over the entire microstructural cell. However, this assumption is completely valid only in the linear-elastic and in the perfectly plastic cases and partially valid in the case where strain-softening occurs.

When strain-softening occurs, the characteristic length of the element plays an impor-

tant role since to reproduce the energy dissipation process that occurs at the macroscale, the softening constitutive law implemented at the micro scale has to be normalized with respect to the fracture length corresponding to the finite element at the macroscale where the integration point lies within. Otherwise, the dissipation process would be biased depending on the size of the RVE.

The correlation among both scales is given by Equation (5.8), where the softening modulus $H_{S(micro)}$ implemented at the microstructure is dependent on the element size at the macrostructure $h_{(macro)}$.

$$H_{S_{(micro)}} = f\left(h_{(macro)}\right) \tag{5.8}$$

A numerical example similar to the one performed for the classical one-scale FEM response is presented to demonstrate the usefulness of the normalization process described above in order to achieve objectivity in the homogenized response when softening appears.

5.3.1 Numerical example of damage constitutive model analysis using the homogenization theory

The specimen analyzed in Section 5.2.1 using the classical one-scale FEM is analyzed here using the 2D two-scale homogenization method. In this case the response of the plate is given by the interaction among the macro structure at the global level and the micro structure at the local level. The plate dimensions and the boundary conditions are defined at the global level meanwhile that the constitutive law of the matrix-like material is defined at the local scale over a representative volume element (RVE) of the plate. An schematic representation of the 2D two-scale homogenization analysis is presented in Figure 5.11.

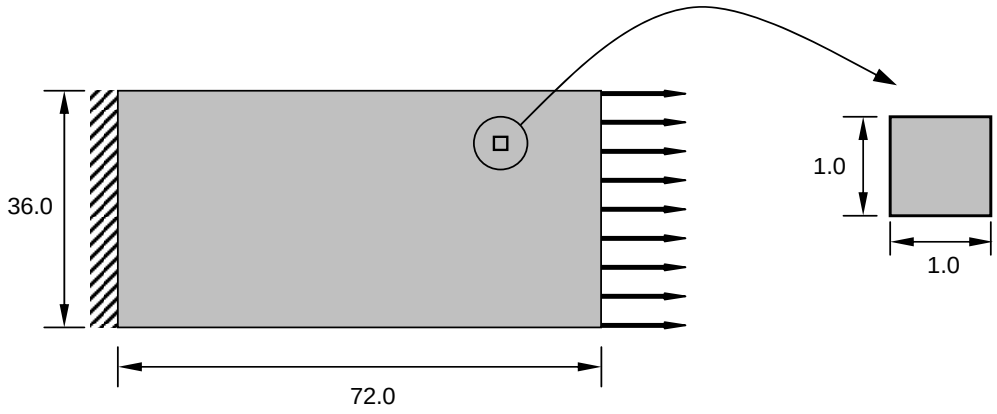

Figure 5.11: Schematic representation of axially loaded plate. Global and local scales (units in cm).

The plate dimensions and boundary conditions are the same than those described in the example analyzed in Section 5.2.1. Meanwhile at the micro scale, the unit cell was considered as a squared model with length and height equal to 0.01 m with a thickness equal to 0.01 m. The behavior of the matrix-like material by which the RVE is modeled is expressed by the continuum damage model with exponential softening using the same material parameters that in the aforementioned example.

The specimen at the macro scale was modeled using the same mesh arrangements depicted in Figure 5.5 used in the example modeled with the classical one-scale FEM. Meanwhile, the FE mesh model of the RVE consisted on 16 squared elements with 25 elements as depicted in Figure 5.12.

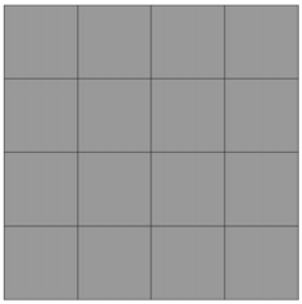

Figure 5.12: Mesh of the RVE model used on the homogenization analysis.

In the case of the classical one-scale FEM example presented in the previous section the mesh objectivity was reached for the case when the characteristic length of the element l_{ch} was equal to the length of the finite element in the load direction. Therefore in this case, this situation will be intended to be reproduced by using the two-scale homogenization method. In order to achieve this, the characteristic length of the finite elements of the unit cell mesh at the micro scale $l_{ch_{(micro)}}$ are normalized with respect to the size of the finite elements of the global scale mesh model $h_{(macro)}$. Furthermore the same analysis is performed on the different models for the case when no normalization is made (i.e. the characteristic length of the unit cell is obtained from the inner dimensions of the cell itself) for comparison purposes.

The homogenized response of the plates using square elements (P-2x4 and P-6x12), rectangular elements with the longest side of the element perpendicular to the loading direction (P-2x8 and P-4x16) and with rectangular elements with the longest side of the element parallel to the loading direction (P-4x4 and P-8x8) are presented in Figure 5.13 for the case when the characteristic length of the unit cell is obtained from the inner dimensions of the cell itself. In Figure 5.14 the same information is presented for the case when the normalization process is applied, i.e. when the characteristic length of the unit cell is normalized with respect to the full length of the macrostructural element where the integration point corresponding to that unit cell is located $l_{ch_{(micro)}} = h_{(macro)}$.

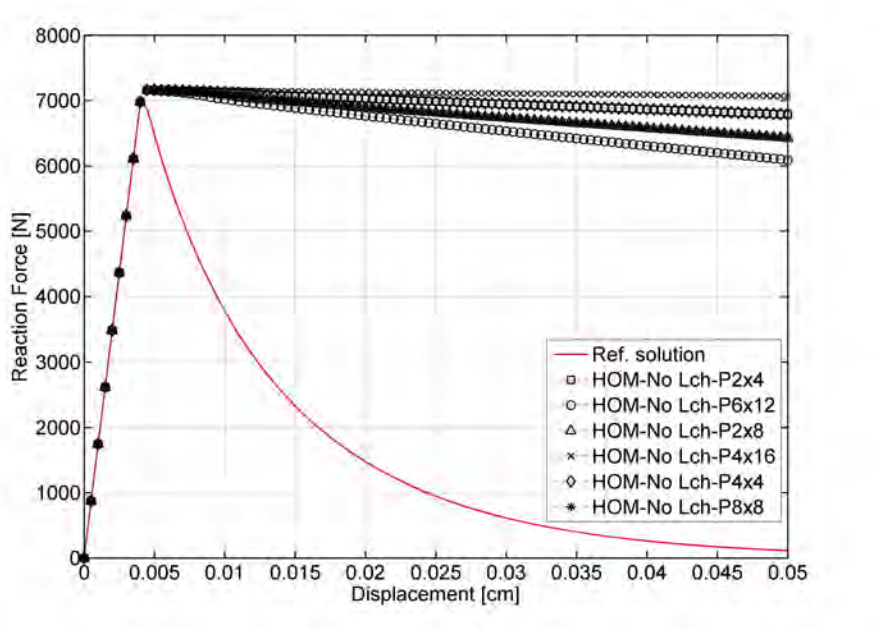

Figure 5.13: Homogenized response with characteristic length of the unit cell elements obtained from the inner dimensions of the cell.

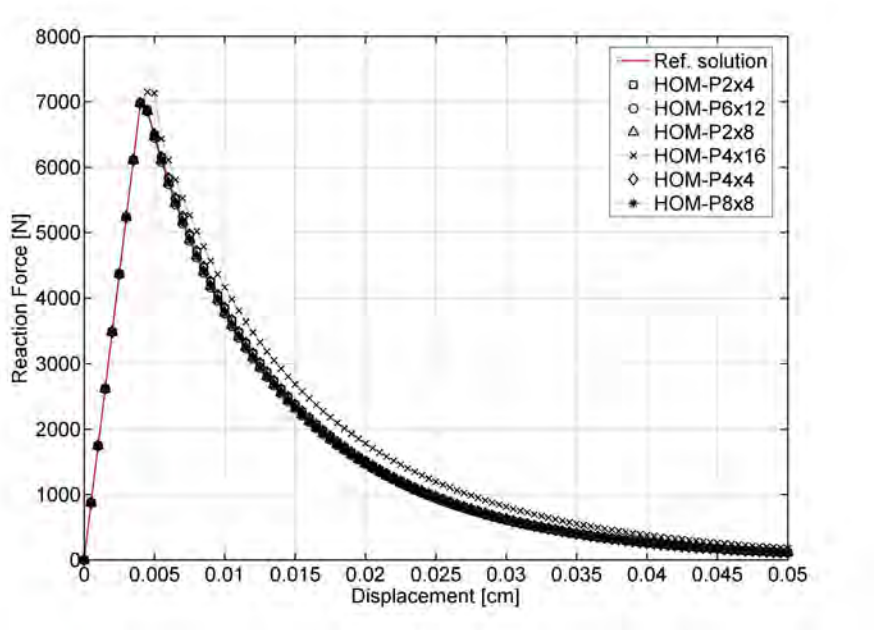

Figure 5.14: Homogenized response with characteristic length of the unit cell elements equal to the length of the element at the macrostructure $l_{ch_{(micro)}} = h_{(macro)}$.

In Figure 5.13 is observed that when the characteristic length of the unit cell is obtained from the inner dimensions of the unit cell, the response is completely overestimated with respect to the reference solution. According to the definition of given at Equation (5.4), the total energy per unit volume g_f is defined by the fracture energy per unit area G_f and by a plastic length l_f equal to the zone where the non-linear process occurs. Since in two-scale homogenization the constitutive behavior is implemented at the microscale, then the non-linear process occurs at a strip of finite elements corresponding to the unit cell. Since by definition the dimensions of the unit cell are much smaller with respect to those of the global scale, then this strip is much smaller than the one at the macroscale where the actual dissipation process occurs. Therefore, the total energy per unit volume g_f is completely overestimated since the plastic length is obtained directly from the inner dimensions of the unit cell without normalizing it with respect to the characteristic length of the global scale.

Meanwhile, in the case when the normalization with respect to the characteristic length of the global scale is made, the responses presented in Figure 5.14 are in well agreement with the reference solution and are equal for all the mesh arrangements, i.e. they present objectivity in the response. Figures 5.13 and 5.14 highlight the importance that the element characteristic length has in the energy dissipation process when using a first-order homogenization method as analysis tool when strain-softening occurs.

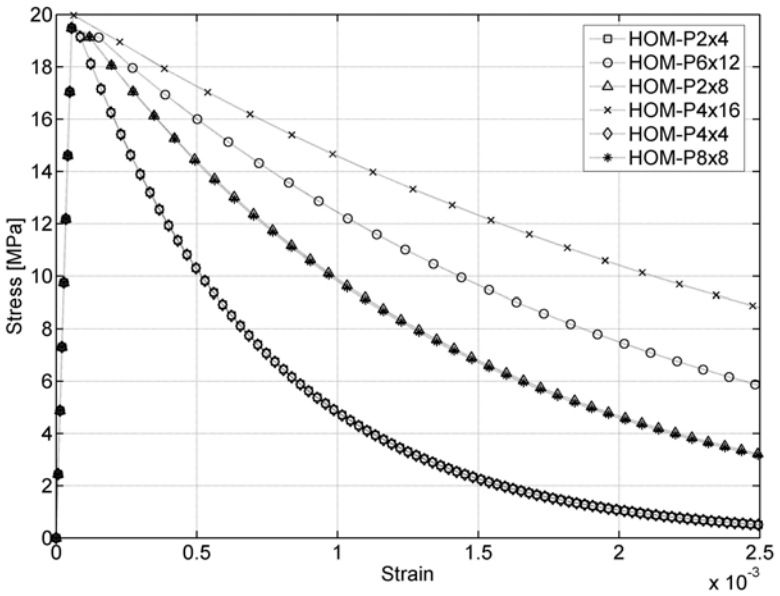

Figure 5.15: Stress-strain evolution for the different mesh arrangements with strain-softening using the FEM.

For the case of the stress-strain evolution presented in Figure 5.15 for the different mesh

sizes, the same behavior is obtained as in the case of the finite element method. Again, for large elements, the density fracture energy per unit of volume is lower, and the stress field is lower in comparison than in the case with a mesh with smaller elements due to the effect of using the fracture length of the macroscale on the constitutive law solved at the microscale.

It is important to highlight that this study was made based on uniaxial tension and the results obtained here are adequate for the 2D case when the case when the energy dissipation process occurs such that the fracture length corresponds to the element length in the load direction. However, in most of the structural analysis process, this condition is not met due the different existing boundary conditions and to the interaction among the different components of the structure. Therefore, the damage dissipation process may form along any of the element boundaries, which in the case of irregular elements may cause inadequate results. In order to avoid this inconvenient, it is recommended to the extent of the possibilities, to use square or equilateral triangular elements where all the sides of them are equal and where the fracture length will be equal, independently of the direction of the energy dissipation process. It can be said that by following the formulation presented in this section, the microscopic scale is related to the macroscopic scale in a simpler way than in the high order formulations for the case when strain-softening is present in one or more of the model constituents.

Chapter 6

Homogenization method applied to the analysis of composite materials and structures

The application of the homogenization method in the analysis of composite materials and structures is performed in this chapter in order to evaluate and explore the capabilities of the computational approach presented in this research. Comparative analysis between the two-scale homogenization method proposed and the classical one-scale FE method are carried out in various examples. Several aspects have been studied, such as analyzing different composite arrangements that include different types of materials, composites that present softening after the yield point is reached (e.g. damage and plasticity) in composites with one and with several periodic domains using different unit cell configurations. Furthermore, the effectiveness of the method proposed to compute the non-linear tangent tensor of the composite as well as the efficiency of the parallelization process are exposed in one of the examples presented.

6.1 Homogenization method applied to composites with one periodic domain

In this section the examples shown in the following paragraphs are presented to demonstrate the applicability of the homogenization method proposed when applied to the analysis of composite structures with one periodic domain. Various factors were taken into account to perform the analysis of the composite structures in order to verify the applicability of the proposed methodology such as modifying the mesh density, analyzing zones where high gradients may appear in critical regions and using different load conditions. The composites are analyzed first by means of the classical one-scale FE method by using the finite element program PLCd [19] and then by using the two-scale homogenized method proposed in this research in order to compare results.

6.1.1 Composite with long fibers subjected to tension and bending

The example consists of a rectangular plate composed by two materials, matrix and fibers, acting under plane stress conditions. The height and length of the plate are equal to 2.0 m and 1.0 m respectively, the thickness is equal to 0.01 m. The fibers have a width of 0.01 m and are placed vertically along the height of the plate (acting as long fibers). Fibers occupy 20% with respect to the total volume of the composite. The geometrical distribution of the fibers over the composite is presented in Figure 6.1.

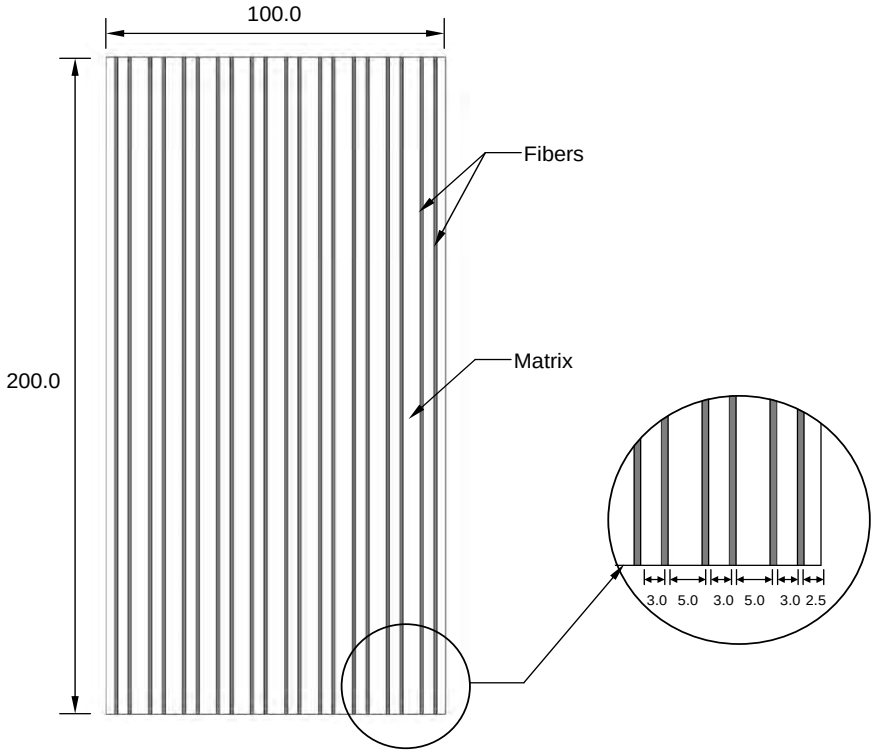

Figure 6.1: Schematic representation of the geometry of the composite plate (units in cm).

The plate is fixed at the bottom, meanwhile that at the top of the plate two types of prescribed boundary conditions are applied. The first consisted in pure axial (uniformly distributed) vertical load applied in terms of controlled displacements, meanwhile that the second consisted in axial load with a trapezoidal distribution. The load varies with a trapezoidal distribution with a scale factor from 1 at the right top corner to 10 at the left top corner. The boundary conditions and the two load conditions applied for the analysis of the composite plate are presented in Figure 6.2.

The matrix material is modeled assuming damage behavior meanwhile that for the fibers a perfect elasto-plastic model is used. Both constitutive models are described in Appendix

A and B, respectively. The constituent's material properties are specified in Table 6.1.

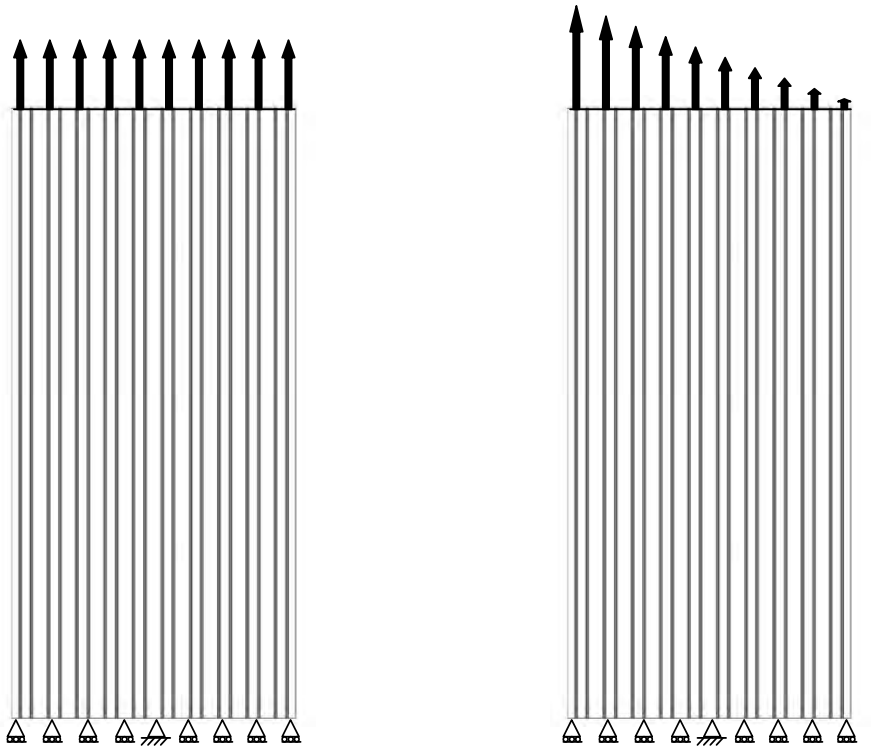

(a) Uniform load displacement

(b) Trapezoidal load distribution

Figure 6.2: Schematic representation of the boundary and load conditions applied for the analysis of the composite plate.

Material	*Matrix*	*Fiber*
Young Modulus	3.5E4 MPa	2.1E5 MPa
Poisson Modulus	0.2	0.3
Internal Friction	30^o	0.0^o
Compression Strength	20 MPa	200 MPa
Tensile Strength	2.0 MPa	200 MPa
Fracture Energy Gf/Gc	0.25 / 26.0 kN/m	- -

Table 6.1: Material properties of the plate components.

The composite plate is analyzed first by means of the classical one-scale FEM in order to use it as the reference solution and then by using the two-scale homogenized method implemented in this study.

Analytical models at the classical one-scale FEM and at the two-scale homogenization method

The classical one-scale FEM model of the composite plate was created using rectangular elements. The axial load was applied in terms of controlled displacements at the top nodes according with the two load distributions presented in Figure 6.2. The classical one-scale FEM model consisted on 8000 elements with 8181 nodes. Figure 6.3 presents the finite element mesh model for the composite plate.

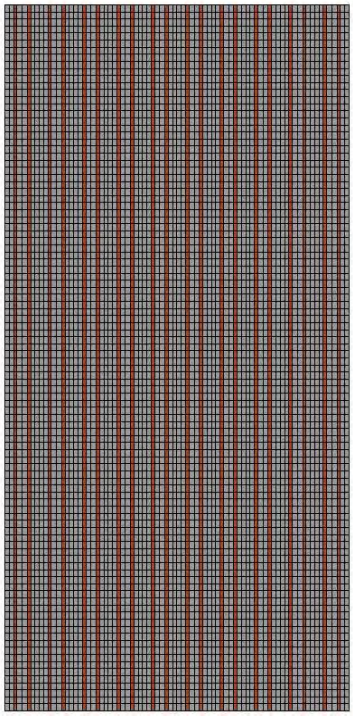

Figure 6.3: Classical one-scale finite element mesh of the composite plate.

For the case of the two-scale homogenized solution, two FE models are needed, one for macro structure and another for the micro structure. The first model represents the structure at the global scale level in which all the boundary conditions are applied. The second model represents the unit cell or RVE that characterizes the periodic internal structure of the composite and that takes into account the constitutive laws of each of the constituents.

At the macro structure or global level, two mesh densities were considered. Both macro models were created using quadrilateral elements. The first mesh model consisted on 200

elements with 231 nodes represented in Figure 6.4a referred as fine mesh, meanwhile that the second mesh model consisted on 72 elements with 91 nodes represented in Figure 6.4b referred as coarse mesh. The load was applied the same way as in the classical one-scale FE model in terms of controlled displacements of the nodes located on the top of the plate.

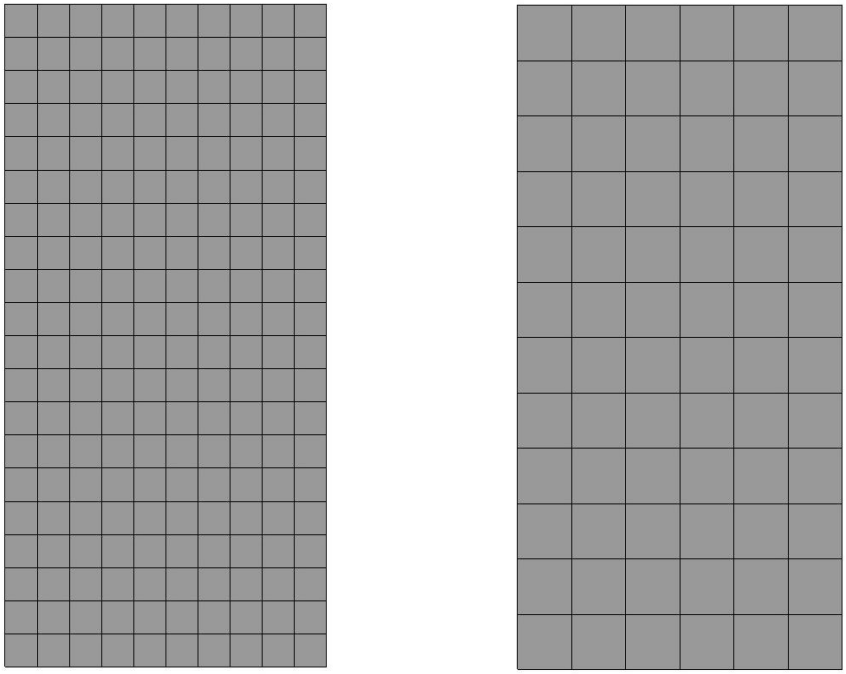

(a) Fine mesh (b) Coarse mesh

Figure 6.4: Meshes used at the global scale in the homogenization method.

The unit cell or RVE that represents the internal structure of the composite (from herein called local scale) it is defined as the smallest structure of a composite material whose properties are representative of the entire microstructure in an average sense with respect the whole structure, as it was mentioned in Section 2.5.1. The unit cell is assembled taking into account the geometric arrangement, the volumetric relationship of the materials and the constitutive behavior of the materials that form part of the composite.

A representation of the division of the internal structure of the composite plate through quadrilateral unit cells is presented in Figure 6.5. In this example, two different sizes of unit cells were considered in order to study the influence of the absolute size of the microstructure in the homogenization process. The large unit cell has a length and height equal to 0.1 m, meanwhile that for the small cell were equal to 0.02 m. In both cases the thickness was equal to 0.01 m. The unit cell FE models consisted on 40 elements with 54 nodes.

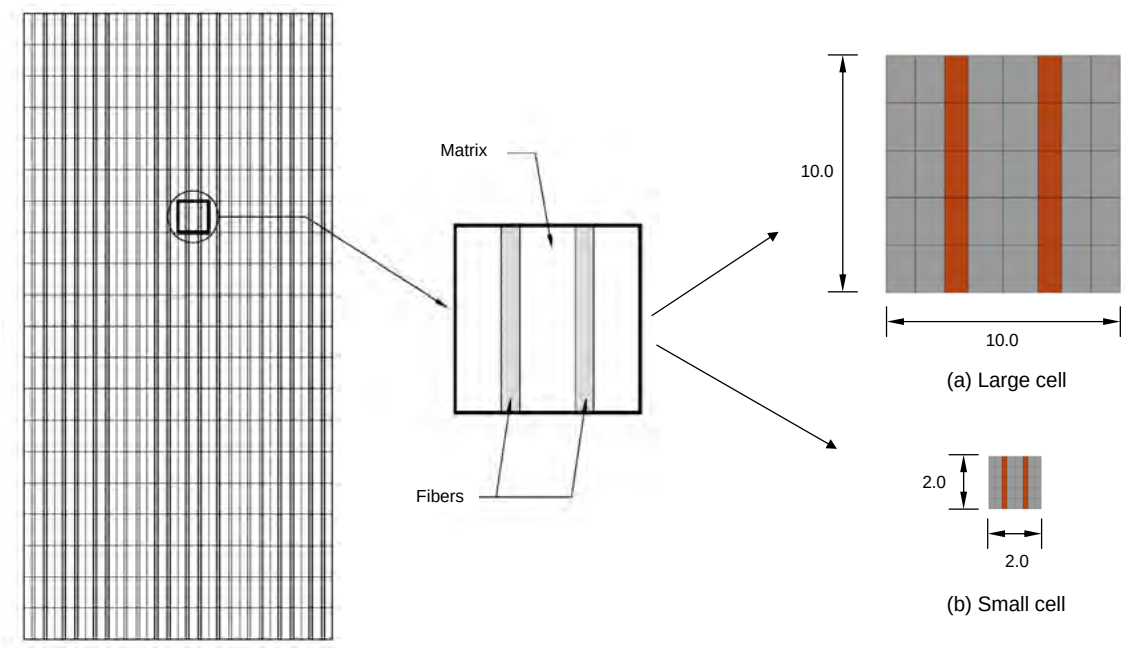

Figure 6.5: Representation of the division of the internal structure of the composite plate by means of quadrilateral unit cells and FE mesh discretization of the two unit cells used at the local level: (a) Large cell; and (b) Small cell (units in cm).

Results

Classical one-scale FE method and two-scale homogenization method computations were carried out for the two load cases, the uniformly distributed axial load and the trapezoidal load distribution. Figure 6.6 presents the capacity curve (force applied versus displacement) for the first load case for the classical one-scale FEM and the homogenized analysis for the two mesh densities used at the global scale (coarse and fine mesh) and for the two unit cell sizes considered (large and small cell). Figure 6.7 presents the same information for the second load case. Figures 6.8 and 6.9 present the same information than Figures 6.6 and 6.7 respectively in terms of displacement field distributions (at the two-scale homogenized solution only the global scale is depicted).

From the information presented in Figures 6.6-6.9, it can be stated that the global response of the composite computed with the homogenized models perfectly matches the solution computed obtained with the classical one-scale FEM for both load cases. The mesh refinement at the global scale in the homogenized model does not affect the solution since similar results are obtained for both mesh densities. Also the change of the size of the unit cell does not affect significantly the response in terms of the capacity curves or in the displacement field distribution. Figures 6.10-6.13 present the one-scale FE and the two-scale homogenized response in terms of stress and damage index distribution.

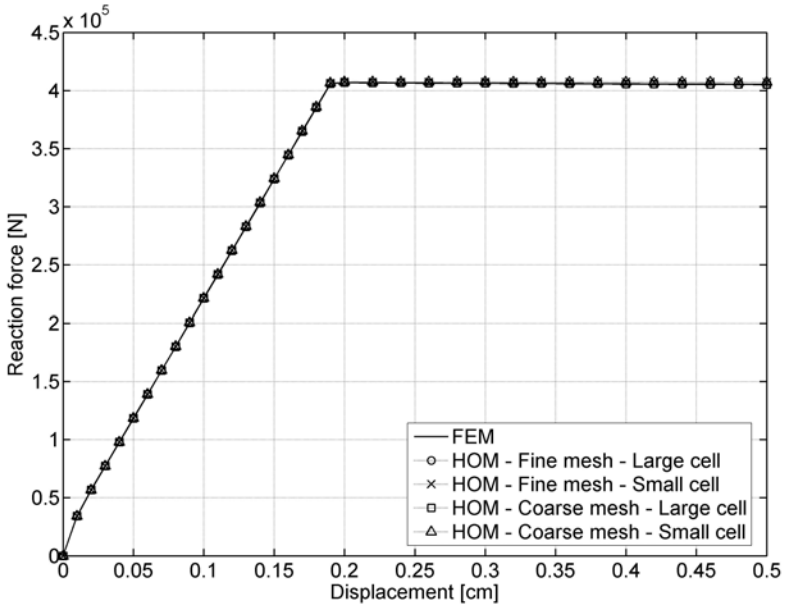

Figure 6.6: Capacity curves for the classical one-scale FE and the two-scale homogenized method. Pure axial traction load.

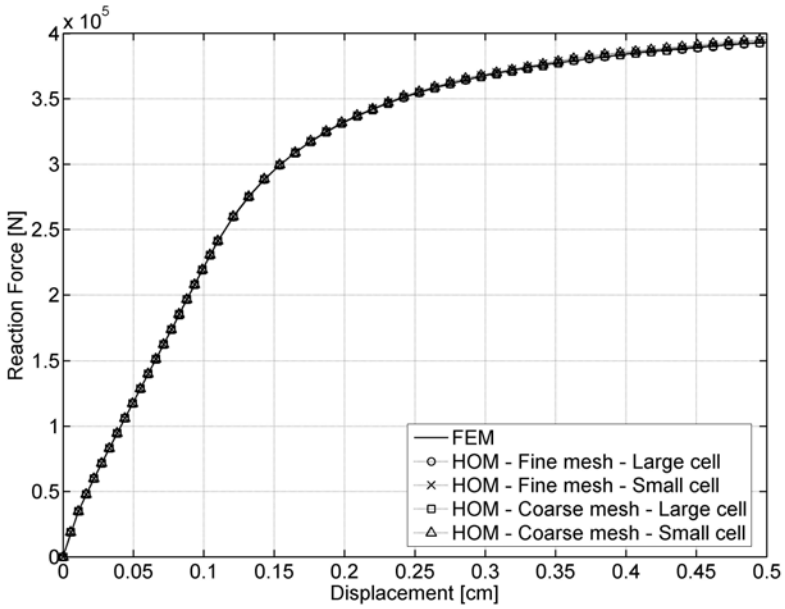

Figure 6.7: Capacity curves for the classical one-scale FE and the two-scale homogenized method. Trapezoidal traction load.

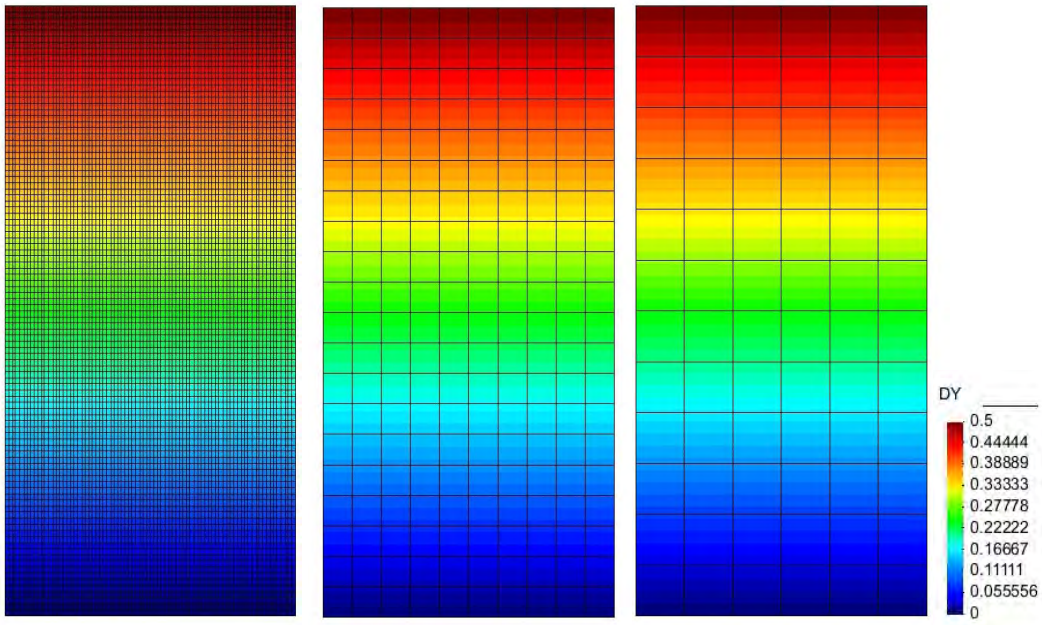

(a) one-scale FEM (b) HOM (fine mesh) (c) HOM (coarse mesh)

Figure 6.8: Displacement field distribution obtained with the classical one-scale FE method (FEM) and the two-scale homogenized method (HOM). Pure axial traction load (cm).

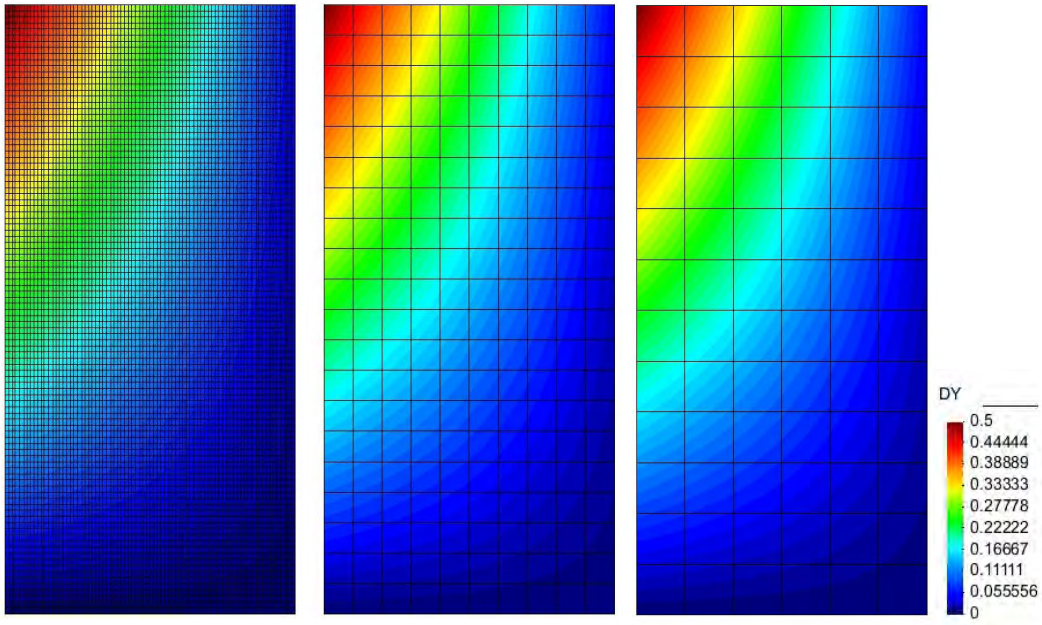

(a) one-scale FEM (b) HOM (fine mesh) (c) HOM (coarse mesh)

Figure 6.9: Displacement field distribution obtained with the classical one-scale FE method (FEM) and the two-scale homogenized method (HOM). Trapezoidal traction load (cm).

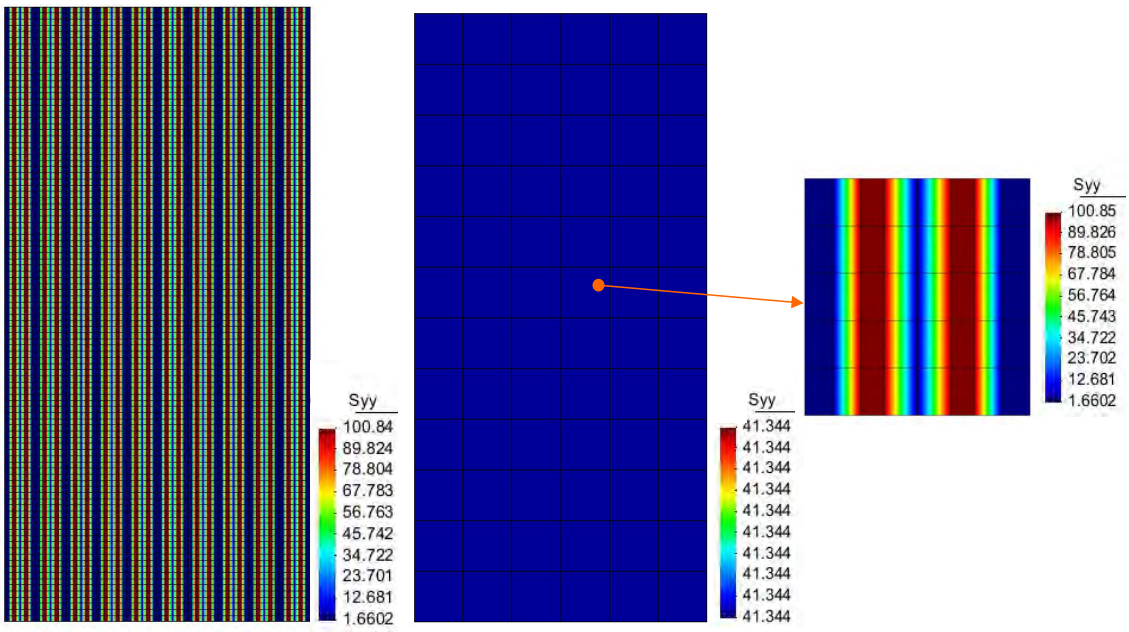

(a) one-scale FEM (b) global scale (c) local scale

Figure 6.10: Stress distribution obtained with the classical one-scale FE and the two-scale homogenized method (coarse mesh). Pure axial traction load (MPa).

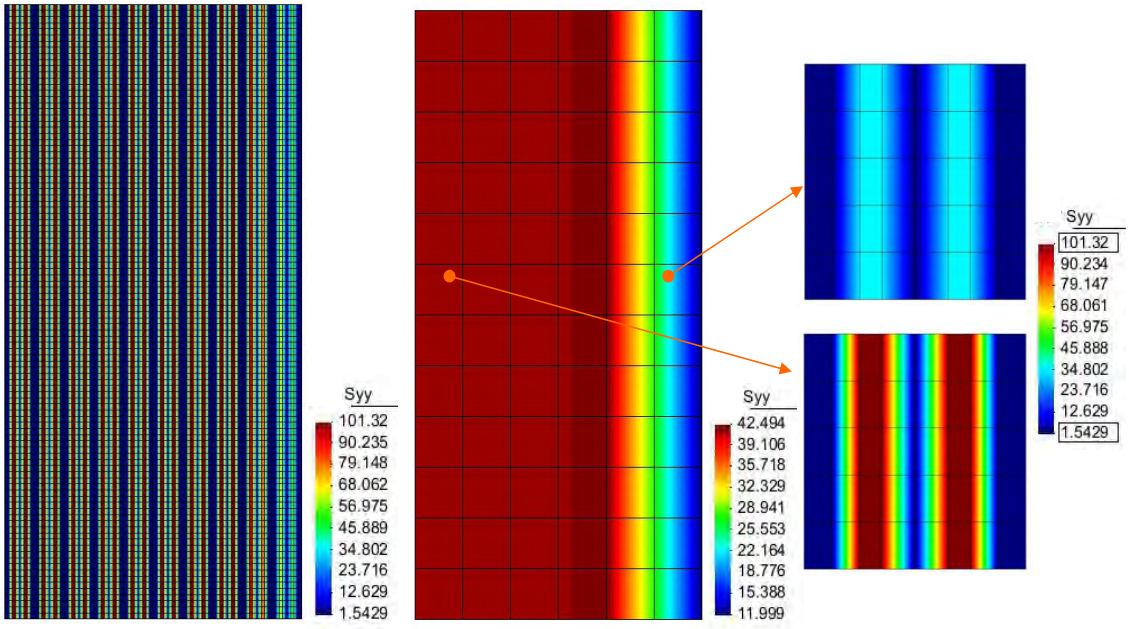

(a) one-scale FEM (b) global scale (c) local scale

Figure 6.11: Stress distribution obtained with the classical one-scale FE and the two-scale homogenized method (coarse mesh). Trapezoidal traction load (MPa).

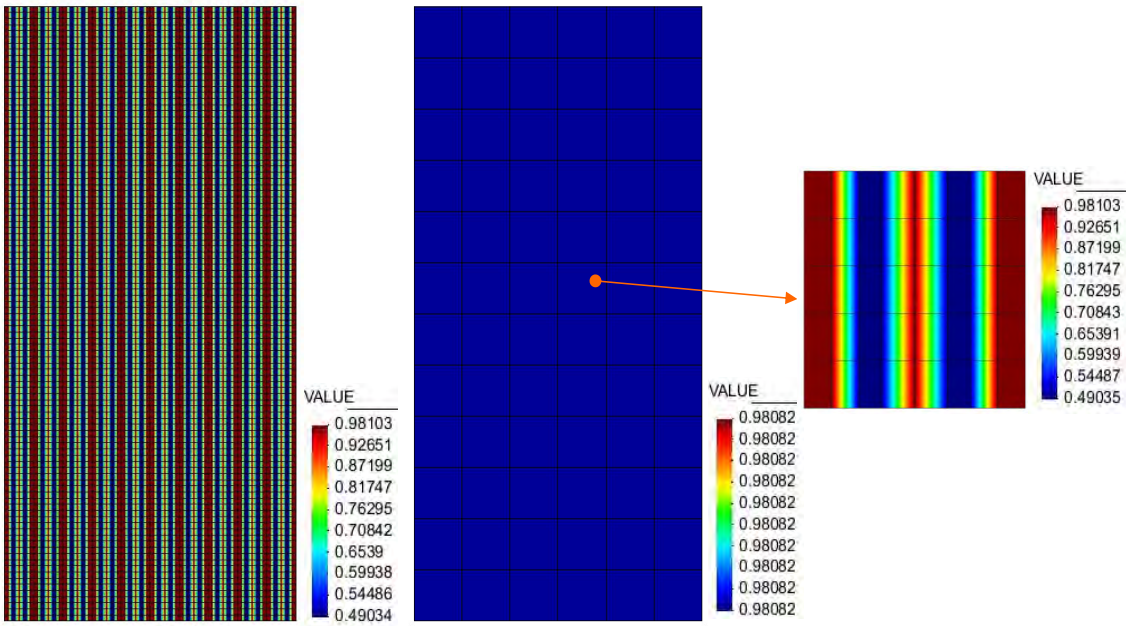

(a) one-scale FEM (b) global scale (c) local scale

Figure 6.12: Damage distribution obtained with the classical one-scale FE and the two-scale homogenized method (coarse mesh). Pure axial traction load.

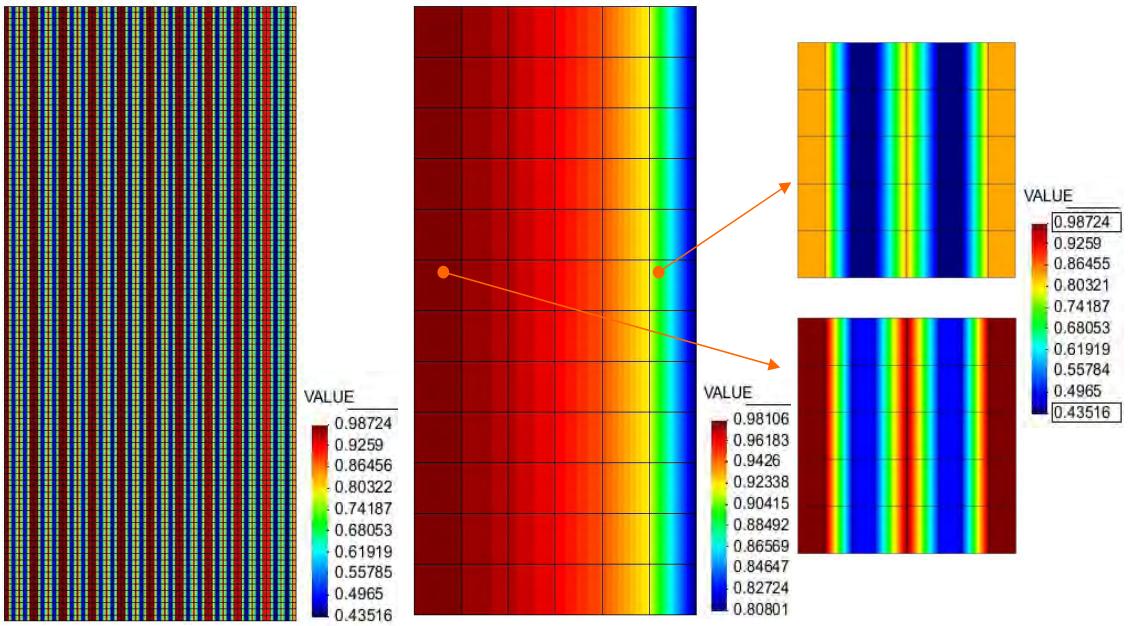

(a) one-scale FEM (b) global scale (c) local scale

Figure 6.13: Damage distribution obtained with the classical one-scale FE and the two-scale homogenized method (coarse mesh). Trapezoidal traction load.

In Figure 6.10, the stress distribution obtained with both methods is presented for the case of pure axial load. On the left of the figure the information is presented for the classical one-scale FE method in Figure 6.10a, meanwhile that for the case of the two-scale homogenization method this information is presented at both scales: the macro (global) and the micro (local) scale in Figure 6.10b and c respectively. On the homogenized response, this information is presented at the macro scale for the case of the coarse mesh only. On the other hand, at the micro scale the information is presented for the case of the large unit cell only. In both cases this decision was made for practical purposes, since similar results were found at the macro scale for the case of the fine mesh and at the micro scale for the case of the small unit cell. On the one-scale FE model, it is observed that the highest stress concentration is found at the fibers since they take most of the displacement load once the matrix material reached its yield threshold stress. At the macro scale, the stresses are obtained as the equivalent to the average of the volumetric participation of the constituents of the composite obtained at the local scale solution. Since the axial load distribution is uniform, the homogenized stresses are constant over the entire volume of the plate. These results agree well with respect to the classical definition of the average method implemented in the homogenization procedure of this study. Meanwhile, at the micro scale, the stress distribution at the unit cell perfectly matches the results obtained with the one-scale FE model for the entire load history.

Figure 6.11 presents the stress distribution obtained with the trapezoidal traction load. For the classical one-scale FE model presented in Figure 6.11a the maximum stress concentration is found on the fibers of the left side due to the trapezoidal loading conditions applied. At the macro scale on the homogenized model presented in 6.11b, the averaged stresses are higher on the elements of the left side of the plate, while a lower averaged stress concentration is found on the right side of the plate. At the micro scale, two unit cells are depicted on Figure 6.11c. On the lower part of the figure the stress distribution at a unit cell corresponding to an integration point at the left side of the plate is presented, meanwhile that at the upper part, the same information is presented for an integration point located on the right side of the plate, as illustrated on the figure. In this case the scale vector corresponding to unit cells was modified with respect to the classical one-scale FEM results in order to compare the response of both methods graphically. The depicted unit cells perfectly match the results obtained with the classical one-scale FE model for the entire load history.

Analogous results to those presented in Figures 6.10 and 6.11 for the case of distribution of stresses, are presented in Figures 6.12 and 6.13 for the case of damage index distribution. For the case of pure axial traction load presented in Figure 6.12, it is observed on the classical one-scale FE model that the damage concentration is found, naturally, at the matrix material strips of the plate. Meanwhile at the macro scale, the homogenized damage index is constant over the entire volume of the plate. On the other hand, at the micro scale, the damage index distribution at the unit cell perfectly matches the results obtained with the classical one-scale FE model for the entire load history.

For the case of the trapezoidal traction load presented in Figure 6.13, at the classical one-scale FE model the maximum damage index concentration is found at the matrix material located at the left side of the plate due to the trapezoidal loading conditions applied. At the macro scale, on the homogenized model, the averaged damage index is higher on the elements of the left side of the plate, while a lower averaged damage index concentration is found on the right side of the plate. At the micro scale, the damage index distribution perfectly matched the results obtained with the classical one-scale FE model for the entire load history. The scale of the cells was also modified with respect to the classical one-scale FE results for comparison purposes.

It is important to highlight that the homogenized damage index is computed as the average over the volume of the material that presents this type of behavior only (the volume of the material corresponding to the fibers is not contemplated). In the case that another type of material existed, where the parameter of an internal variable should be computed (such as viscoelastic or plastic strain index etc.) the same procedure should be applied (in this case the plastic model used, is considered as perfectly plastic, as a result no plastic strain index is computed). Therefore, in this study the homogenized value of this type of indexes are computed over the volume of the materials that contains them. This assumption is made in order to give a general assessment of the global state of the structure in terms of homogenized results.

Computational effort comparison among the classical one-scale FE method and the two-scale homogenization method of the composite with long fibers

Although it is well documented on the literature review that the computational procedure performed in multi-scale homogenization is a rather expensive process there are no explicit comparisons of the computational effort required at the multi-scale homogenization method with any other traditional method of analysis (such as the classical one-scale FE method). Such comparisons were rarely found in the existing literature or not found at all; however such comparisons give an idea of the enormous computational effort that a multi-scale homogenization analysis process requires.

In this example, a comparison of the computational effort among the classical one-scale FE method and the two-scale homogenization method is presented in Figure 6.14 for the case of the uniform axial load and in Figure 6.15 for the case of the trapezoidal load configuration. In both cases the two different meshes used at the global scale on the homogenization method are presented.

The results presented in Figures 6.14 and 6.15 were computed in the homogenized solution using a total of 6 processors in parallel. Also, in the solution process the homogenized non-linear tangent tensor was computed according to the method described in Sections 3.5.5 and 4.4.2. To represent the internal structure of the composite only the large cell was considered.

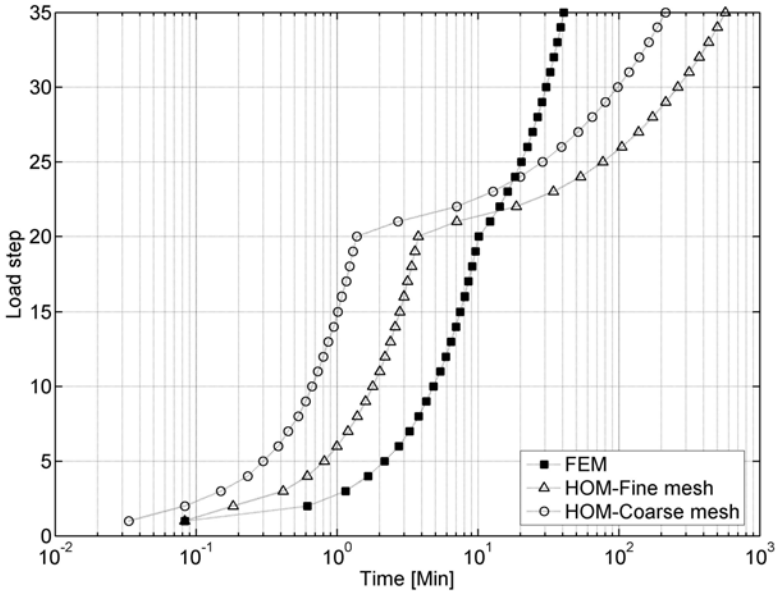

Figure 6.14: Convergence time for each load step for the classical one-scale FE method and the two-scale homogenization method. Pure axial traction load.

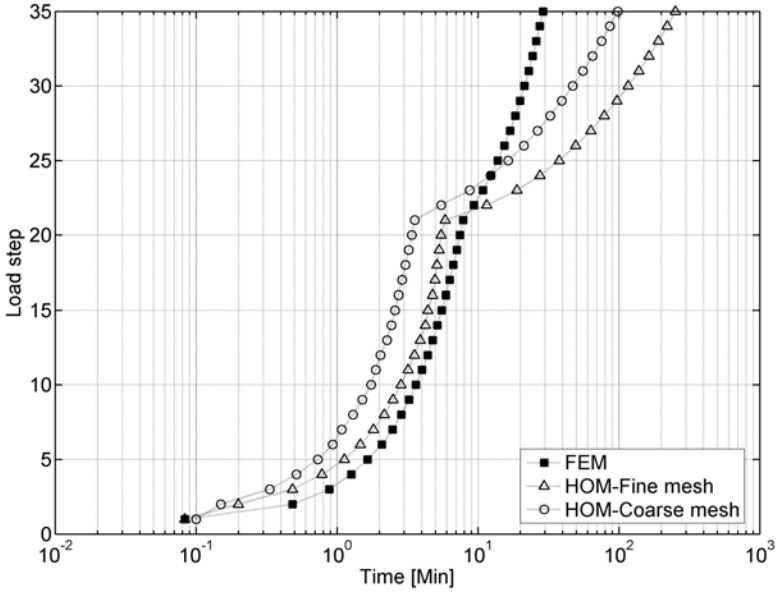

Figure 6.15: Convergence time for each load step for the classical one-scale FE method and the two-scale homogenization method. Trapezoidal traction load.

For the case of the uniform axial load presented in Figure 6.14 it was calculated that the total computing time (the accumulated time along the computing process) of the classical one-scale FE method (FEM) is faster 14 times than the two-scale homogenized solution with the fine mesh at the global scale (HOM-Fine mesh) and 5.3 times faster for the case of the coarse mesh (HOM-Coarse mesh).

On the other hand for the case of the trapezoidal traction load presented in Figure 6.15 it was calculated that the total computing time of the classical one-scale FE method (FEM is faster 8.7 times than the two-scale homogenized solution with the fine mesh at the global scale (HOM-Fine mesh) and 3.4 times faster for the case of the coarse mesh (HOM-Coarse mesh).

From the results presented for both load cases it is also observed that the homogenized results provide a much faster response when the structural response lays within the linear domain (up to step 21 of analysis); however this trend is reversed in the non-linear range and that such difference increases exponentially.

6.1.2 Validation of the method to obtain the homogenized tangent constitutive tensor

In this section, the method to obtain the homogenized tangent constitutive tensor presented in Sections 3.5.5 and 4.4.2 is presented for analysis and validation. This method was developed to compute the response for the next load increment at the time $t+\Delta t$ when the structure enters into the non-linear range. The method was originally implemented to obtain the non-linear tangent constitutive tensor $\mathbf{C}^{T_{nl}}$ of each element of the unit cell that represents the composite. Once the procedure is applied over each element on the unit cell that express some type of nonlinearity, the homogenized non-linear tangent tensor is obtained by computing the average solution over the entire volume of the unit cell or RVE as previously expressed Section 3.5.5. The homogenized non-linear constitutive tensor is computed as expressed in Equation (6.1).

$$\bar{\mathbf{C}}^{T_{nl}}(x) = \frac{1}{V_{\Omega_c}} \int_{V_{\Omega_c}} C_{ij}^{T_{nl}} dV_{\Omega_c} \tag{6.1}$$

where V_{Ω_c} is the RVE or unit cell's volume. Two other methods of computing the non-linear constitutive tensor of the composite were explored in the developing process to obtain a reliable and effective way to compute the homogenized tangent constitutive tensor: 1) a perturbation method at the global scale; and 2) a simple average method of the constitutive tensors at the actual time t. The perturbation method is explained in the section below and the average method is explained at the numerical example presented.

Perturbation method at the global scale

An analogous process to the one presented in Chapter 4 in Section 4.4.2 is implemented at the global scale in order to explore the application of the method by applying the perturbation process at the integration points of the macrostructure. The procedure is implemented following the same steps than when the perturbation is applied at the integration points of the microstructure. The general concepts presented in Table 4.2 remain identical, just with a significant change on the variables used. Instead of the variables commonly used at the level of the components (stresses $\boldsymbol{\sigma}$, strains $\boldsymbol{\varepsilon}$ and internal material parameters α), homogenized variables (homogenized stresses $\bar{\boldsymbol{\sigma}}$, homogenized strains $\bar{\boldsymbol{\varepsilon}}$ and homogenized internal material parameters $\bar{\alpha}$) are employed in this implementation process. Then, by following an analogous process to the one presented in Table 4.2 by employing homogenized variables, the j column of the non-linear homogenized tangent tensor computed at the global scale, stay as:

$$\bar{\mathbf{C}}_j^{T_{nl}}(x) = \frac{{}^j\dot{\bar{\boldsymbol{\sigma}}}(x)}{\dot{\bar{\boldsymbol{\varepsilon}}}_j(x)} \equiv \frac{\delta\, {}^j\bar{\boldsymbol{\sigma}}(x)}{\delta\bar{\boldsymbol{\varepsilon}}_j(x)} \tag{6.2}$$

where the homogenized stresses $\bar{\boldsymbol{\sigma}}(x)$ and the homogenized strains $\bar{\boldsymbol{\varepsilon}}(x)$ are computed according to the average theory definitions implemented at the RVEs or unit cells as described in Chapter 3.

Numerical comparison

The specimen used as example to demonstrate the viability of the numerical method to obtain the non-linear homogenized tangent constitutive tensor presented in this research corresponds to a numerical example presented in Section 6.1.1. The specimen corresponds to the coarse mesh configuration at the macroscale and represented by the large unit cell at the microscale. The results presented here are focused only on the validation and comparison of the method to obtain the homogenized tangent constitutive tensor.

The specimen is solved in three different ways: 1) by applying the perturbation method at the microscale (PMicro); 2) by applying the perturbation method at the macroscale (PMacro); and 3) by solving it with the homogenized tensor computed at the instant of time t (Nopert), obtained as the average of the constitutive tensors C_{ij} (linear or non-linear) over the volume of the cell at time t, as expressed in Equation (6.3).

$$\bar{\mathbf{C}}(x) = \frac{1}{V_{\Omega_c}} \int_{V_{\Omega_c}} C_{ij} dV_{\Omega_c} \tag{6.3}$$

where V_{Ω_c} is the RVE or unit cell's volume. Figures 6.16 and 6.17 present the capacity curves for the three different methods to obtain the response of the homogenized solutions under pure axial and trapezoidal traction load respectively. Figures 6.18 and 6.19 present the convergence time for each load step for both load cases. A total of 6 processors were used in the solution of the example.

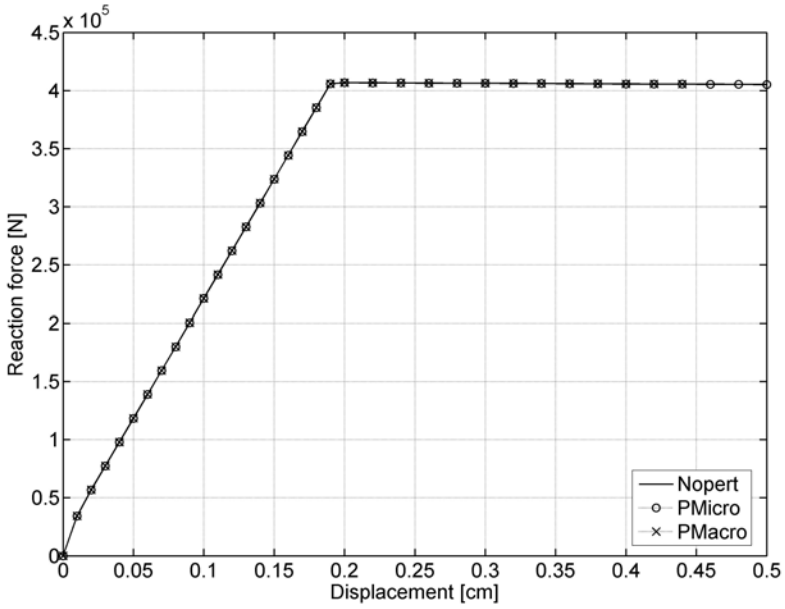

Figure 6.16: Capacity curves for the three different methods to obtain the response of the homogenized solutions. Pure axial traction load.

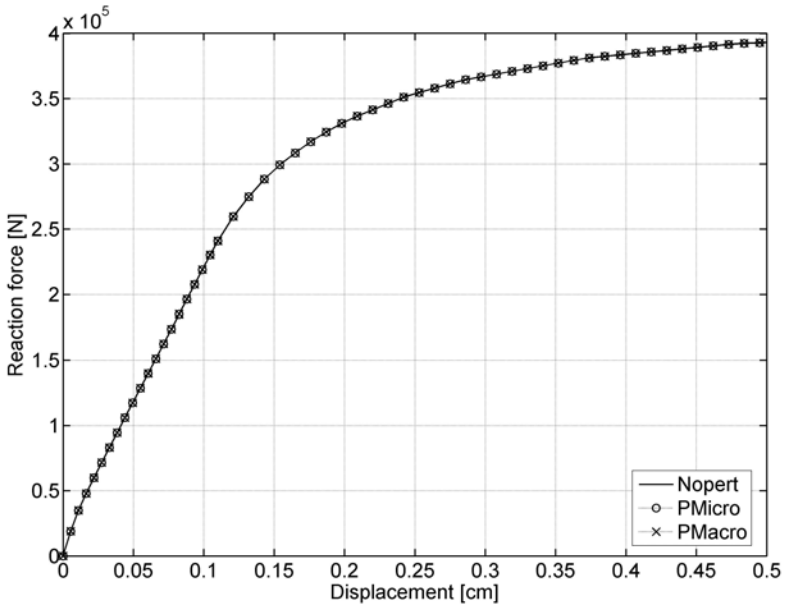

Figure 6.17: Capacity curves for the three different methods to obtain the response of the homogenized solutions. Trapezoidal traction load.

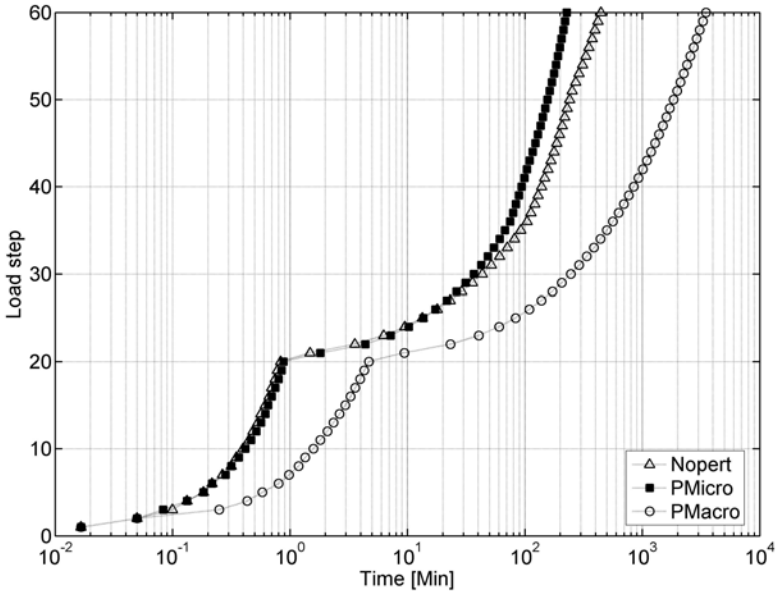

Figure 6.18: Convergence time for each load step for the three different methods to obtain the response of the homogenized solutions. Pure axial traction load.

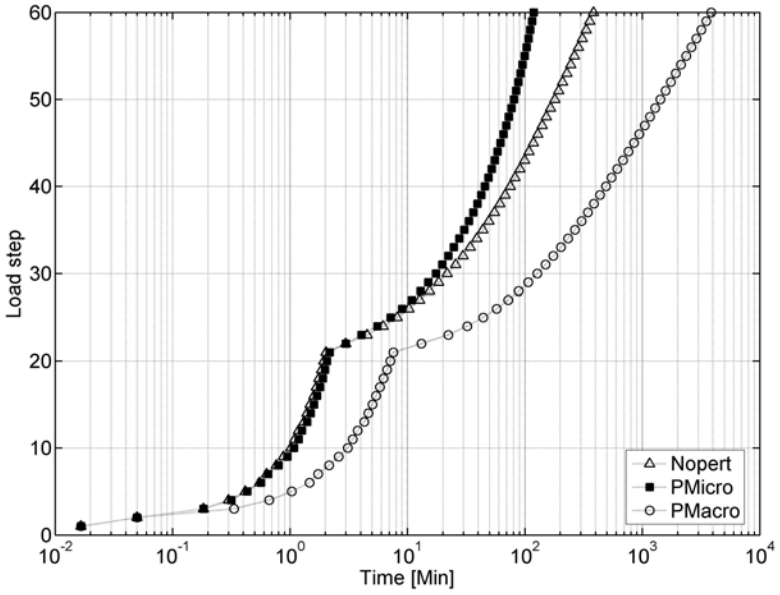

Figure 6.19: Convergence time for each load step for the three different methods to obtain the response of the homogenized solutions. Trapezoidal traction load.

From the Figures 6.16 and 6.17 presented above, it can be observed that the same response is obtained with the three methods in terms of the capacity curves. Meanwhile Figures 6.18 and 6.19 present the convergence time for each load step for both load cases. In these figures it can be observed that the method where no perturbation at all was used (Nopert) is slightly faster than the method where the perturbation is applied at the microstructure (PMicro) at the linear range and at the first stages of non-linear behavior. However, as the structure presents more nonlinearities, this trend is reversed. This effect is more evident on Figure 6.19 since in this case the structure presents a non-linear behavior much stronger than in the case when uniform traction load was applied. On the other hand, the method most expensive computationally in both, the linear and non-linear ranges, is where the perturbation is applied at the integration points of the macrostructure (PMacro).

For all the aforementioned reasons, the formulation where the perturbation is applied at the microstructure (PMicro), is the method that is used on all the analysis presented in this research.

6.1.3 Validation of the efficiency of the parallelization method

This section presents a performance evaluation of the parallelization method described previously in section 4.5.3. Although it is known that the performance of a parallel system remarkably varies for each application, the results shown here in this evaluation are presented with illustrative purposes.

In evaluating a parallel system, two performance measures of particular interest are speedup $S(p)$ and efficiency $E(p)$ [25]. Speedup is defined for each number of processors p as the ratio of the elapsed time when executing a program on a single processor (the single processor execution time) to the execution time when p processors are available. This is expressed as:

$$S(p) = \frac{T_1}{T_p} \tag{6.4}$$

Efficiency is defined as the average utilization of the p allocated processors. Ignoring I/O, the efficiency of a single processor system is 1. Speedup in this case is of course 1. In general, the relationship between efficiency and speedup is given by:

$$E(p) = \frac{S(p)}{p} = \frac{T_1}{p\,T_p} \tag{6.5}$$

where p is the number of processors, T_1 is the execution time of the sequential algorithm, T_p is the execution time of the parallel algorithm with p processors.

However, along with an increase in speedup comes a decrease in efficiency: as more processors are devoted to the execution of a software system, the total amount of processor

idle time can be expected to increase, due to factors such as contention, communication, and software structure. The efficiency is a value, typically between zero and one, which estimates how well-utilized the processors are in solving a problem compared to how much effort is wasted between communication and synchronization of the different algorithms used in the computation process. Therefore, in this research besides measuring the speedup, the efficiency of the basic parallelization scheme proposed, is explored in order to give a general assessment of the use of the computing resources by the method proposed.

A common mistake made, when measuring the efficiency of any parallelized algorithm, is the use of the execution time of a one-thread of the parallel implementation as the time of a sequential execution. The execution time of the one-thread parallel implementation is typically larger than that of the original sequential implementation. Therefore, in order to provide a proper estimation of the parallel efficiency, the performance of the original sequential code as a baseline should be used, otherwise the value of parallelization efficiency will be overestimated. The results presented in the following example were computed under this premise.

Numerical comparison

Again, the specimen presented in Section 6.1.1 on Chapter 6, corresponding to the coarse mesh configuration at the macroscale and represented by the large unit cell at the microscale, serves as example to demonstrate the efficiency of the parallelization method presented in this research. The specimen is solved using different number of processors for the two load cases used in the example as well as by using a sequential run of the program. Figures 6.20 and 6.21 present the speedup and efficiency profiles respectively for both load cases.

From the results presented in Figure 6.20 it is observed that the speedup scales adequately when adding more processors to the computing process. This trend is maintained even in for the trapezoidal load case in which most of the nonlinearities are concentrated on the left side of the plate. However, from the results presented in Figure 6.21, it is observed that the parallelization scheme has an efficiency of 50% approximately in both load cases. Also, it is observed that the efficiency decreases as the non-linear phase of the structure increases (starting around load step 21).

The efficiency values obtained seem reasonable according to the straightforwardness of the parallelization scheme implemented and to the several non-parallelizable (sequential) parts that the two-scale code has at the global scale. The efficiency obtained is considered adequate for the practical purposes of this investigation. Nevertheless, it is remarked again that if a thoroughly optimized parallelization process is desired, a more comprehensive algorithm should be investigated as the main subject of study in a different research project.

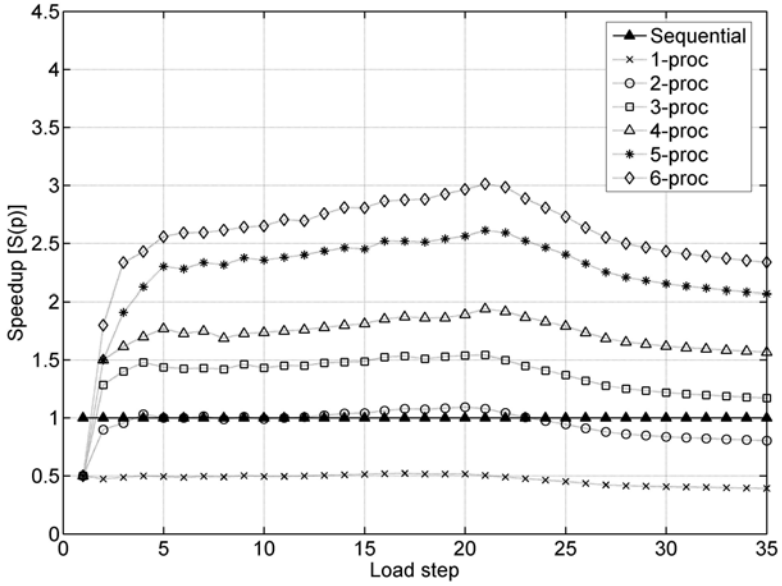

(a) Pure axial traction load

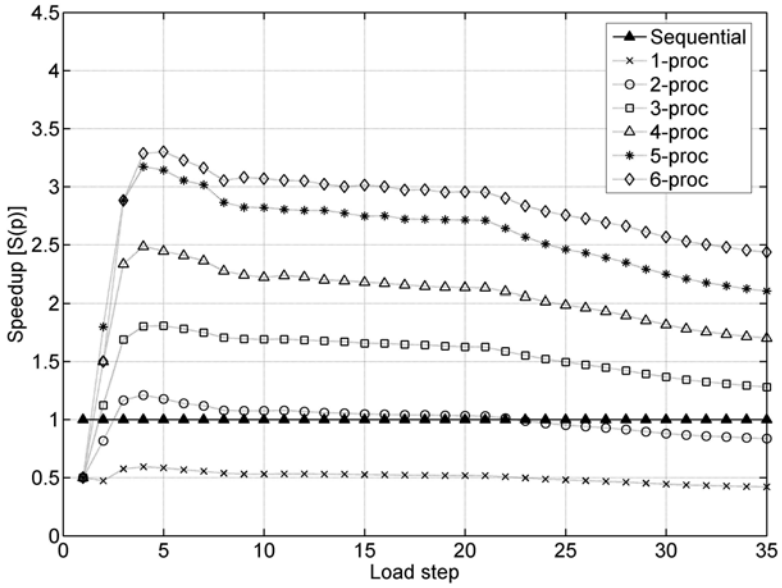

(b) Trapezoidal traction load

Figure 6.20: Speedup profiles for the two load cases used.

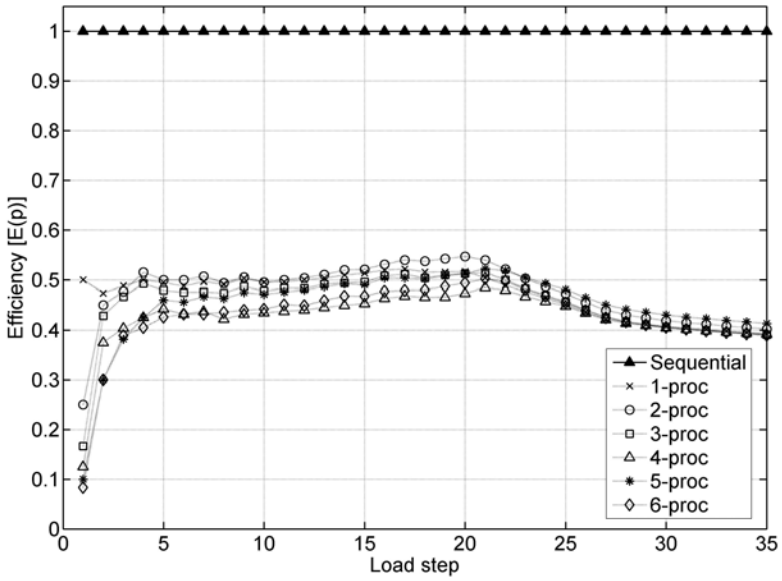

(a) Pure axial traction load

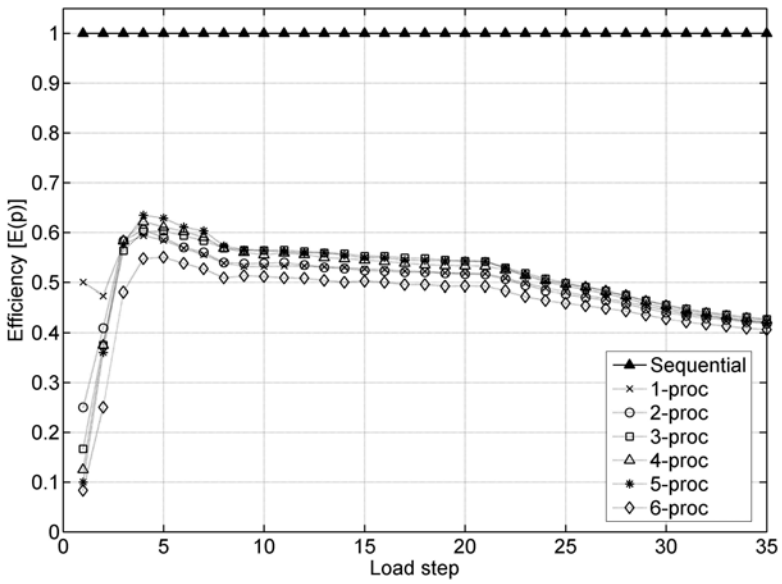

(b) Trapezoidal traction load

Figure 6.21: Efficiency profiles for the two load cases used.

6.1.4 Notched composite with long fibers subjected to tension

Several factors may affect the periodicity condition in which the homogenization method is based upon due to the appearance of high strain gradients. High strain gradients may be originated by several factors and usually are present in critical regions like free edges, interfaces, material discontinuities, in areas surrounding concentrated loads and in regions of evolving damage; therefore these critical conditions must be studied to verify the applicability of the method.

In this example, a rectangular notched composite with long fibers subjected to tension composed by two materials, matrix and fibers, acting under plane stress conditions is studied. This example is carried out in order to analyze the influence of including a zone where high strain gradients are present in the multi-scale homogenization analysis. The height and length of the plate are equal to 60 mm and 12 mm respectively with a notch in the middle of the plate of 0.5 mm of width and 3 mm of height. The thickness of the plate is equal to 1.0 mm. The fibers have a width of 0.25 mm and are placed horizontally along the length of the plate (acting as long fibers). Fibers occupy one third of the total volume of the composite. An schematic representation of the notched plate is depicted in Figure 6.22.

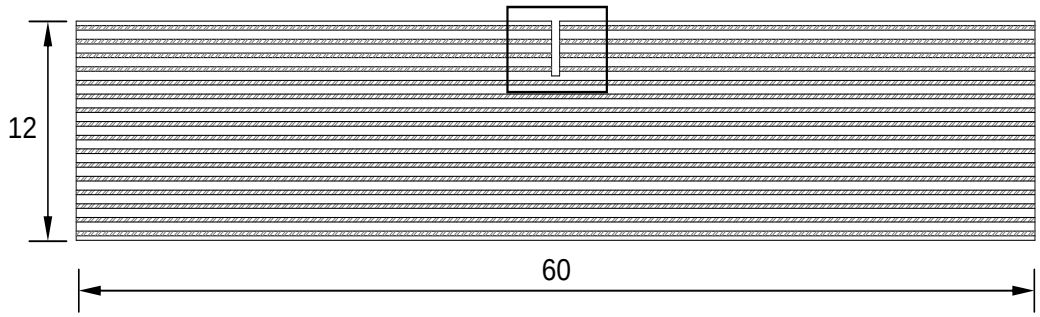

(a) Notched plate dimensions

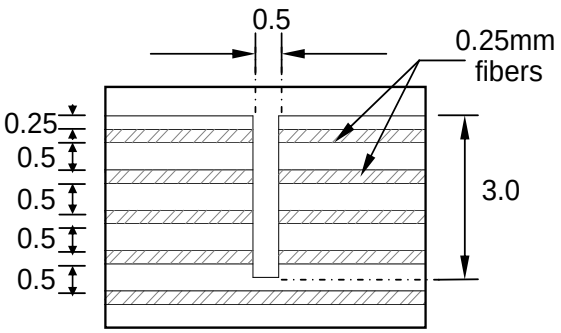

(b) Notch detail and matrix-fibers distribution

Figure 6.22: Schematic representation of the notched plate (dimensions in mm).

The matrix material is modeled assuming damage behavior meanwhile that the fibers are modeled using a perfect elasto-plastic model. The formulation of both constitutive models are fully described in Appendix A and B, respectively. The material properties of the constituents of the notched specimen are the same than those used in the example of Section 6.1.1 presented previously in Table 6.1. The plate is fixed at the left side and at the right side axially loaded with a tension force with uniform distribution. The boundary conditions applied for the analysis of the notched plate are presented in Figure 6.23.

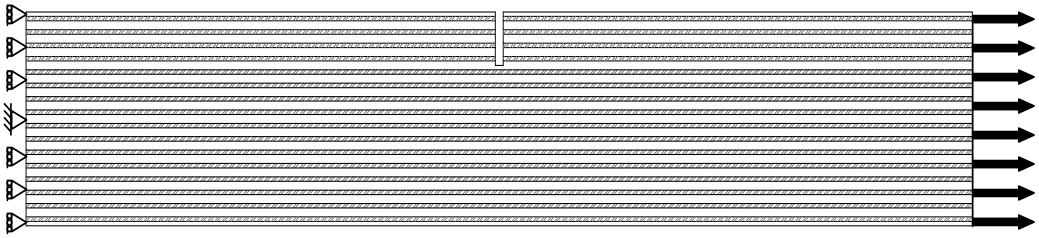

Figure 6.23: Schematic representation of the boundary and load conditions applied in the analysis of the notched plate.

The composite plate is analyzed first by means of the classical one-scale FEM and then by using the two-scale homogenized method implemented in this study.

Analytical models at the classical one-scale FEM and at the two-scale homogenization method

The classical one-scale FEM model of the composite plate was created using rectangular elements. The axial load was applied in terms of controlled displacements at the right nodes. The classical one-scale FEM model consisted on 11496 elements with 11797 nodes. Figure 6.24 presents the finite element mesh model for the composite plate.

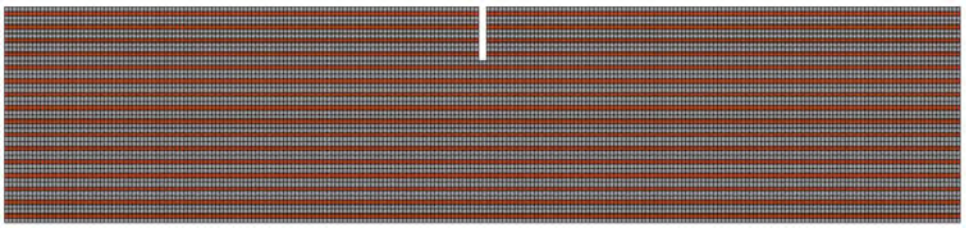

Figure 6.24: Classical one-scale finite element mesh of the notched plate.

For the case of the two-scale homogenized solution at the global level two mesh densities were considered. Both macro models were created using quadrilateral elements. The first mesh model consisted on 131 elements with 170 nodes represented in Figure 6.25a referred as coarse mesh, meanwhile that the second one consisted on 358 elements with 408 nodes represented in Figure 6.25b referred as fine mesh. The load was applied the same way as

in the finite element model, in terms of controlled displacements on the nodes located at the right side of the plate.

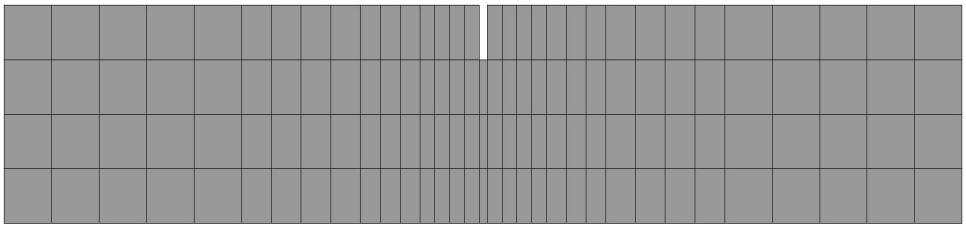

(a) Coarse mesh

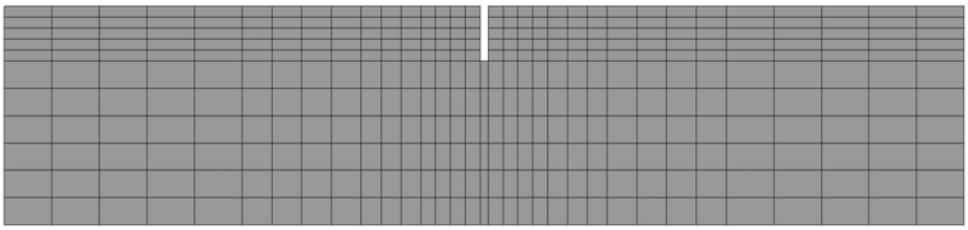

(b) Fine mesh

Figure 6.25: Meshes used at the global scale in the homogenization method.

On the other hand, for the case of the unit cell or RVE that represents the internal structure of the composite, two mesh densities were considered. The first mesh consisted on 36 elements with 49 nodes represented in Figure 6.26a referred as coarse mesh (or C1), meanwhile that the second one consisted on 144 elements with 169 nodes represented in Figure 6.26b referred as fine mesh (or C2). Both cells have the same length and height equal to 1.5 mm and a thickness equal to 1.0 mm. The fiber-matrix relationship on the unit cells follows the same ratio as in the one-scale FE model; thus fibers occupy one third of the total volume of the composite.

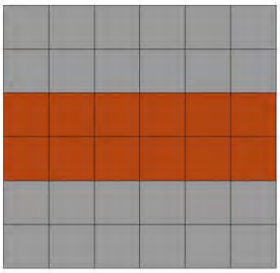

(a) Coarse mesh (C1)

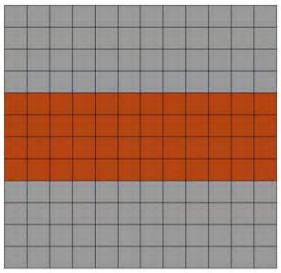

(b) Fine mesh (C2)

Figure 6.26: Meshes of the unit cells used at the local scale on the homogenized notched specimen.

Results

Figure 6.27 presents the capacity curve (force applied versus displacement) for the classical one-scale FE model used as reference solution and for the two-scale homogenized analysis for the two meshes at the global scale (coarse and fine mesh) and the two meshes used on the unit cells (coarse mesh-C1 and fine mesh-C2). Figure 6.28 presents the same information than Figure 6.27 in terms of displacement field distributions (at the two-scale homogenized solution only the global scale is depicted).

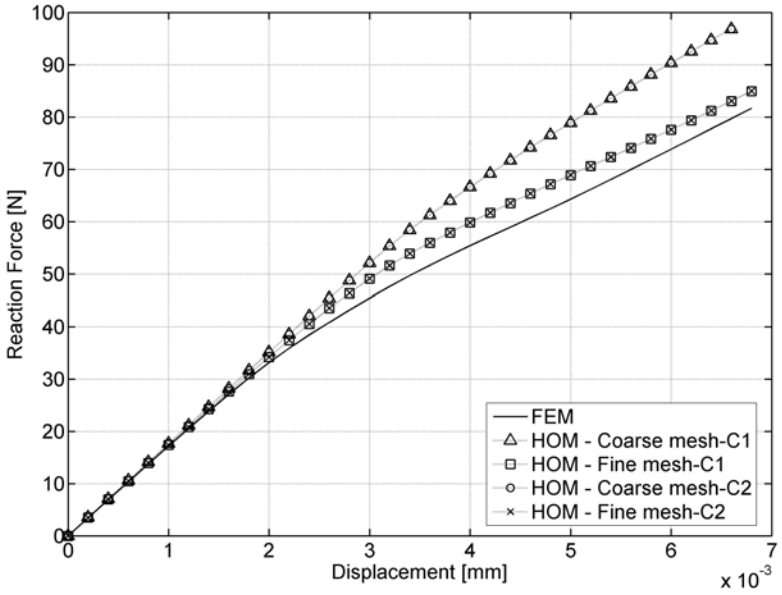

Figure 6.27: Capacity curves for the FE and homogenized methods of notched specimen.

From the information presented in Figures 6.27 and 6.28 it can be observed that the mesh refinement at the global scale affects the response in the two-scale homogenized model. A better approximation is obtained with the refined mesh than with the coarse mesh at the macro scale with respect to the reference one-scale FEM solution. This phenomenon may be overdue to the high strain gradients that are concentrated at the notched area, since as it has been discussed earlier, in Chapter 3, a significant gradient of the macroscopic variable fields at a certain structural point involves a perturbation of these fields in the neighboring cells. By making the refinement on the global mesh, the rapidly changing variational field is translated into a slower change of the macroscopic variables, diminishing the error with respect to the reference solution. Furthermore, the refinement on the global scale mesh reproduces better the kinematics of the deformation around the notch with respect to the one-scale FEM solution. On the other hand, the mesh refinement at the RVE (mesh C2) did not represent any major changes in the response with respect to those obtained with a coarser mesh at the RVE (mesh C1).

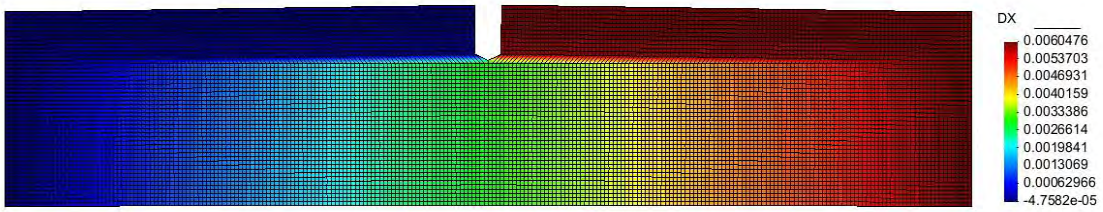

(a) One-scale FEM

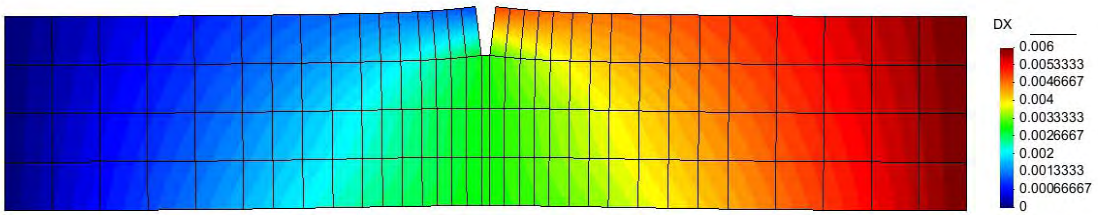

(b) Two-scale homogenization. Coarse mesh at global scale and coarse mesh at local scale (C1)

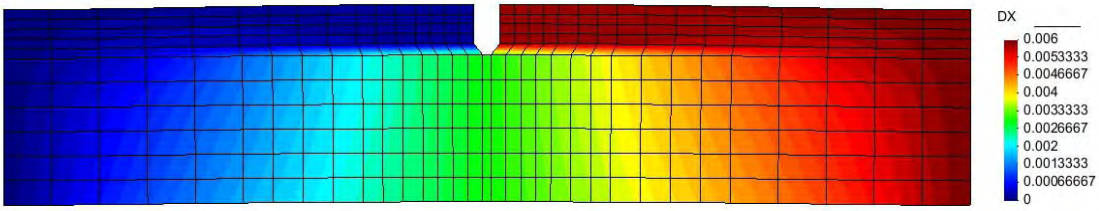

(c) Two-scale homogenization. Fine mesh at global scale and coarse mesh at local scale (C1)

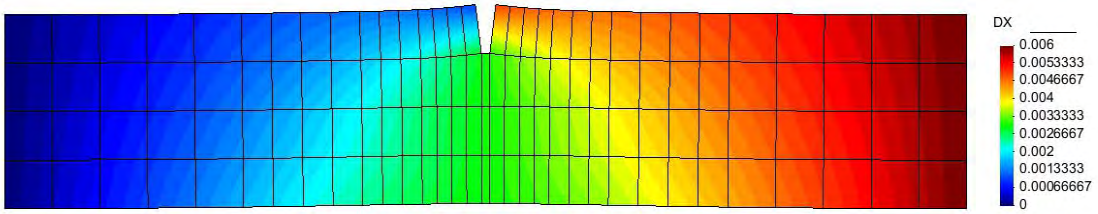

(d) Two-scale homogenization. Coarse mesh at global scale and fine mesh at local scale (C2)

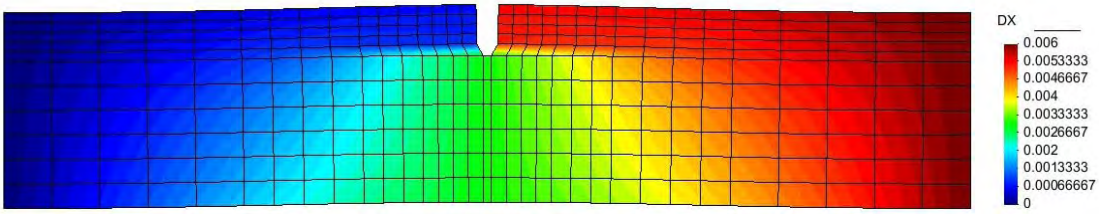

(e) Two-scale homogenization. Fine mesh at global scale and fine mesh at local scale (C2)

Figure 6.28: Displacement field distribution obtained with the classical one-scale FEM and the two-scale homogenization method (cm). Deformed geometry (x200).

Figure 6.29 presents the stress distribution obtained with the classical one-scale FEM and the two-scale homogenization method using the fine mesh at the global scale and the coarse mesh at the micro scale (mesh C1). For the case of the homogenized model, the responses of three unit cells around the notched area are presented as well. The three cells correspond to integration points located at the left, underneath and right of the notch as indicated in Figure 6.29b. The geometries of the models presented in the figure are magnified to show the kinematics of the deformed models. The one-scale FE and the homogenized models at the global scale are magnified 200 times (x200) meanwhile that the unit cells are magnified using a factor of 50 (x50).

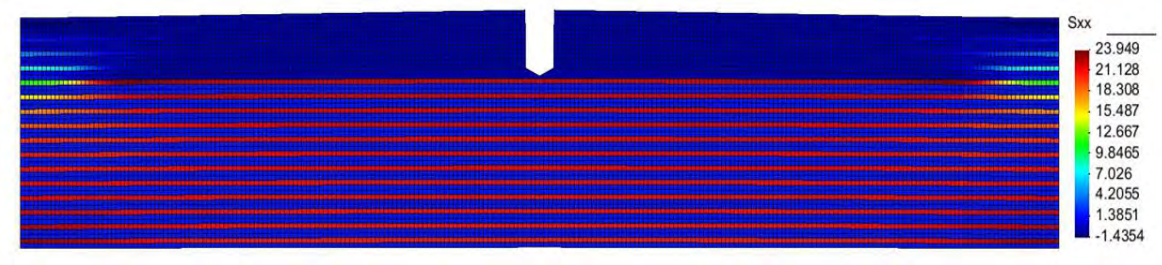

(a) One-scale FEM stress distribution (MPa). Deformed geometry (x200).

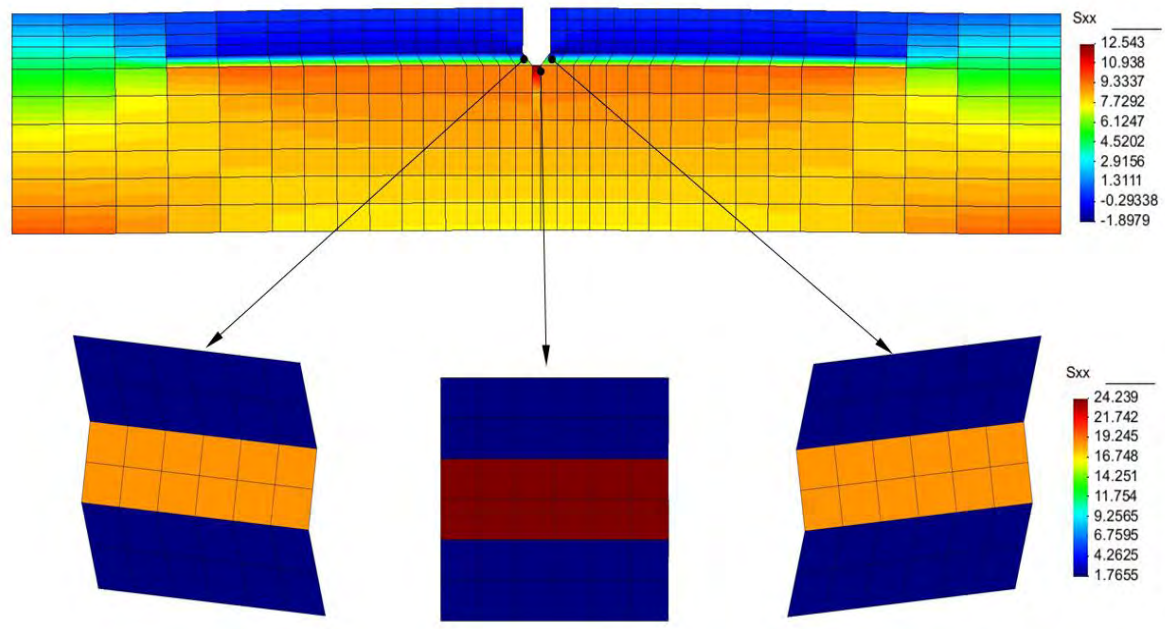

(b) Global and local scale stress distribution (MPa). Deformed geometry of global scale (x200) and local scale (x50).

Figure 6.29: Stress distribution obtained with the classical one-scale FEM and the two-scale homogenization method (fine mesh at the global scale and coarse mesh at the local scale).

Figure 6.30 presents the same information than Figure 6.29 for the case of the damage

index distribution.

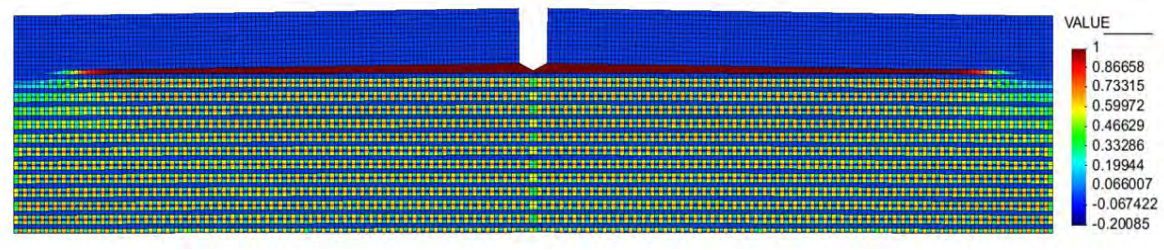

(a) One-scale FEM damage index distribution. Deformed geometry (x200).

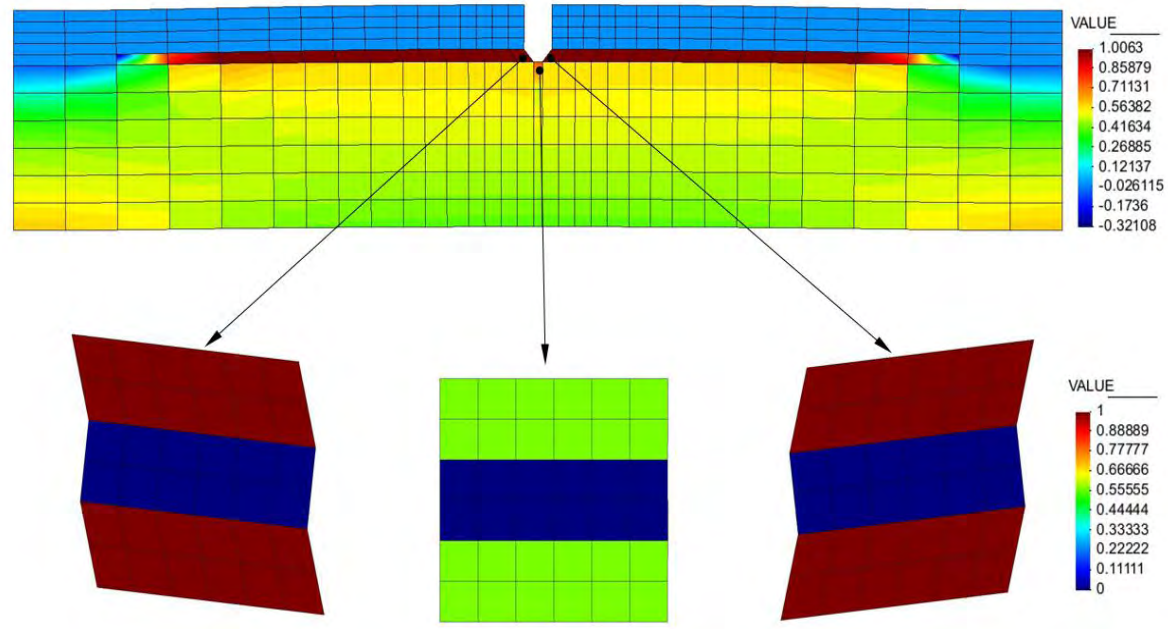

(b) Global and local scale damage index distribution. Deformed geometry of global scale (x200) and local scale (x50).

Figure 6.30: Damage index distribution obtained with the classical one-scale FEM and the two-scale homogenization method (fine mesh at the global scale and coarse mesh at the local scale).

From the results presented in Figure 6.29a, it is observed that on the classical one-scale FE model, the stress concentration is found on most of the fibers of the composite. The areas with the highest stress concentration are two: 1) the fiber located right below the notch, excepting the areas next to the extreme boundaries; and 2) the fibers situated at the areas located at the corners at the bottom of the plate. On the other hand, the fibers located along the height of the notch do not present any stress concentration, since these fibers do not take almost any of the of the axial displacement load. On the homogenized model at the macro scale, presented in the upper part of Figure 6.29b, the stresses obtained as the equivalent to the average of the volumetric participation of the constituents

of the composite obtained at the local scale solution, reproduce in an averaged sense the behavior found at the one-scale FE model. The two high stress concentration areas are located below the notch and at the bottom corners of the plate. Also the areas located at the same height of the notch do not present any high stress concentration in the homogenized model. However, a transition zone is found among the highest and lowest concentration areas which corresponds to the strip located at the bottom of the notch in which a mean stress concentration is found due to the nature of the homogenization method. On the other hand, at the local scale it is found that the stress distribution at the unit cell located underneath the notch perfectly matches the results obtained with the classical one-scale FE model at the matrix and fibers. In the case at the unit cells located at the left and right of the notch, they reproduce the behavior of the transition zone.

For the case of damage index presented in Figure 6.30, the highest value found on the one-scale FE model is located on the strip of matrix material located at the bottom of the notch, almost on the entire length of the strip excepting the areas next to the extreme boundaries. Meanwhile, on the two-scale homogenized model at the macro scale, the damage index matches in an averaged sense the behavior found at the one-scale FEM model and gives an accurate description of the global state of the structure in terms of the damage criteria. At the micro scale, the damage index of the three unit cells depicted corresponding to the integration points around the notch perfectly match the results obtained with the one-scale FE model. Furthermore, the unit cells perfectly reproduce the kinematics of the notch deformation for the entire load history.

Computational effort comparison among the classical one-scale FE method and the two-scale homogenization method in the analysis of the notched composite plate

As in the previous example, a comparison of the computational effort among the classical one-scale FE method and the two-scale homogenization method is presented for this example in Figure 6.31.

The comparison is made taking into account the two different meshes used at the global scale and the two mesh densities used at the local scale (meshes C1 and C2) on the two-scale homogenization method. The results presented for the case of the two-scale homogenized solution were computed using a total of 8 processors in parallel. Also, in the solution process the homogenized non-linear tangent tensor was computed according to the method described in Sections 3.5.5 and 4.4.2.

From the results presented it was calculated that the total computing time (the accumulated time along the computing process) of the classical one-scale FE method (FEM) all along the calculation process is faster 1.4 times than the two-scale homogenized solution with the fine mesh at the global level and coarse mesh at the local level (HOM-Fine mesh-C1). In contrast, the two-scale homogenized solution for the case of the coarse mesh

at the global scale and coarse mesh at the local level (HOM-Coarse mesh-C1) is 4.7 times faster than the classical one-scale FE solution (FEM).

On the other hand, for the case of mesh refinement at the local scale it was calculated that the total computing time of the classical one-scale FE method (FEM) is faster 8.5 times than the two-scale homogenized solution with the fine mesh at the global scale and the fine mesh at the local level (HOM-Fine mesh-C2). On the contrary, the two-scale homogenized solution for the case of the coarse mesh at the global scale and fine mesh at the local level (HOM-Coarse mesh-C2) is 5.6 times faster than the classical one-scale FE solution (FEM).

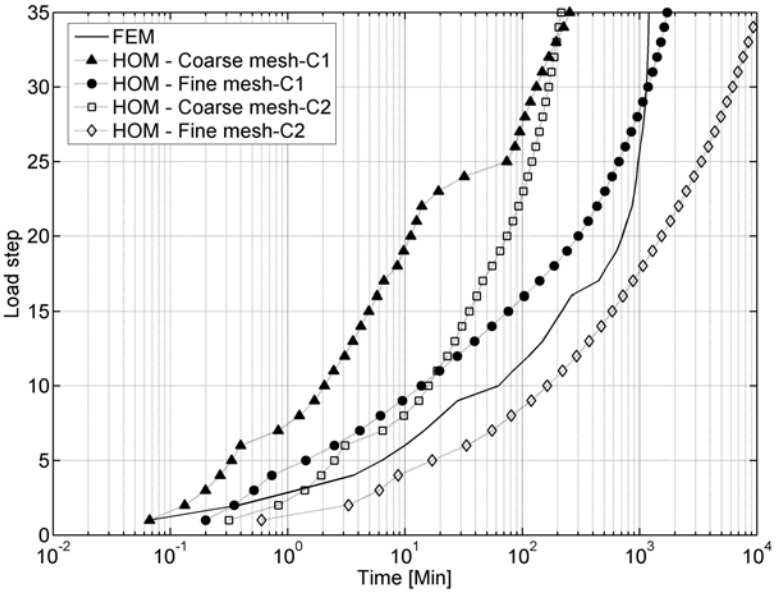

Figure 6.31: Convergence time for each load step for the classical one-scale FE method and the two-scale homogenization method for the notched composite plate analysis.

In this example it is observed that the mesh refinement in the two-scale homogenization method has a great impact on the computational effort when performed at any of the two scales. However, it must be remarked that the mesh refinement performed at the micro scale on the unit cells of this example has little impact on the overall response of the composite, in contrast to the case when the refinement is made at the macro scale, which gives a better approximation with respect to the reference one-scale FEM solution according to the information previously presented in Figure 6.27. Therefore in order to maintain a practical computational effort (time), unnecessary mesh refinement at the micro scale must be avoided when possible.

6.2 Homogenization method applied to composites with several periodic domains

The examples shown in the following paragraphs are presented to demonstrate the applicability of the two-scale homogenization method proposed when applied to the analysis of composite structures with several periodic domains. In the first example the composite structure is analyzed first by means of the classical one-scale FEM by using the program PLCd [19] and then by using the multi-domain (multi-cell) homogenization formulation in two scales proposed in this research. On the second example presented in this section, the same structure of the first example is strengthened by using only the two-scale multi-domain homogenization formulation.

6.2.1 Analysis of a reinforced concrete frame

The example consists of a reinforced concrete (RC) frame composed by concrete and steel, acting under the action of a lateral load P. The geometry dimensions and the steel reinforcement details of the RC frame are presented in Figure 6.32.

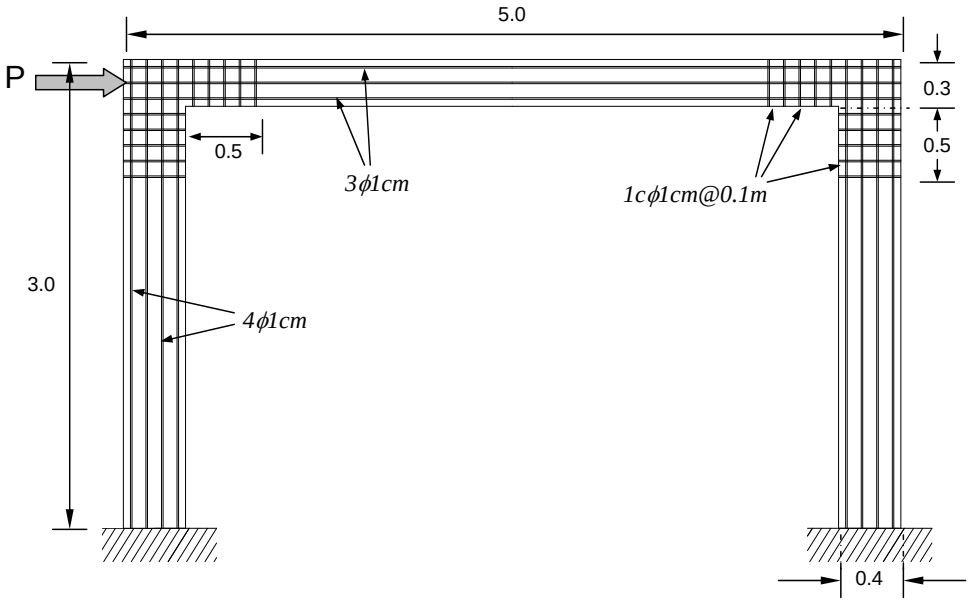

Figure 6.32: Schematic representation of the geometry and boundary conditions of the RC frame (units in m).

The entire frame has a cross section of 0.4 m. The concrete material is modeled assuming damage behavior meanwhile that for the reinforcement steel bars a perfect elasto-plastic model is used. Both constitutive models are described in Appendix A and B, respectively. The constituents material properties are the same than those specified in Table 6.1 used

at the example presented in Section 6.1.1 with a different value of the energy of fracture. The actual values are, $Gf = 0.025mN/m$ for the energy in tension and $Gc = 2.6mN/m$ for the corresponding compression value.

The frame is clamped at the bottom of the columns, and the horizontal load is applied on the left side of the frame at 2.9 m from the bottom of the column. The RC frame is analyzed first by means of the classical one-scale FEM in order to use it as the reference solution and then by using the multi-domain homogenized method in two scales proposed in this study. In both cases the RC frame model was created taking advantage of the symmetry of the structure, since only the symmetric left part of the frame is analyzed. The aim of this example is to apply the multi-domain homogenization formulation presented in this thesis to analyze a structure commonly found on the field of structural analysis.

Analytical models at the classical one-scale FEM and at the multi-domain homogenization method in two scales

The classical one-scale FE model mesh of the RC frame was created using rectangular elements. The load was applied in terms of a lateral force applied on the left side of the frame at a node located at 2.9 m from the bottom of the column. The classical one-scale FE of the RC frame consisted on 1239 elements with 1367 nodes. A schematic representation of the one-scale FE model mesh is presented in Figure 6.33.

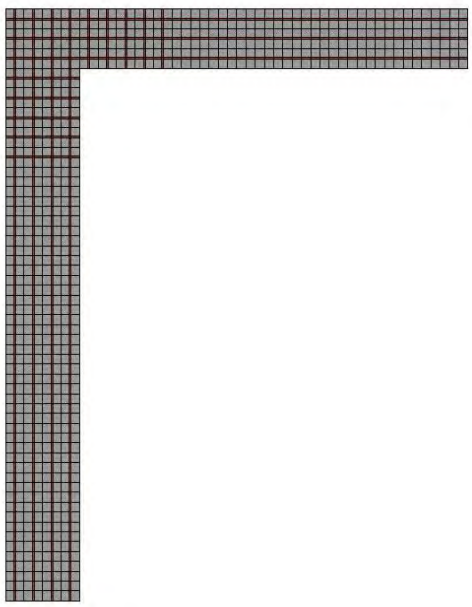

Figure 6.33: Classical one-scale FE model mesh of the RC frame.

On the other hand, the multi-domain homogenized solution has to take into account the different periodic arrangements that conform the structure. Therefore, the first step in

the multi-domain homogenization process is to identify these periodic subdomains, since each one of them will be represented by a different unit cell. The schematic representation made in Figure 6.34 presents the different periodic zones (or periodic subdomains) found within the RC frame. A total of three different periodic subdomains where identified on the structure. The first periodic subdomain corresponds to the column, the second one to the beam-column union and the third one to the horizontal beam.

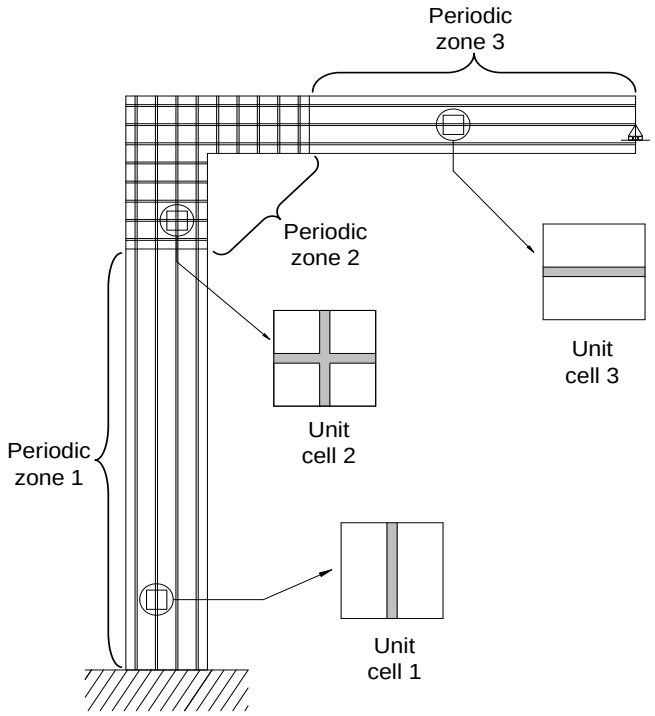

Figure 6.34: Division of the RC frame in periodic subdomains.

The multi-domain homogenized mesh model at the global scale was created using quadrilateral elements with the three different periodic subdomains identified previously in Figure 6.34. The mesh model consisted on 360 elements with 427 nodes. The load was applied the same way as in the one-scale FE model in terms of a lateral force on the left side of the frame at the node located at 2.9 m from the bottom of the column. The different subdomains are identified using different colors on the global mesh model as depicted in Figure 6.35.

In order to represent the internal structure of the RC frame by means of the multi-domain homogenization method, one unit cell is needed to represent each of the periodic subdomains in which the frame is divided. The mesh models of the unit cells consisted on 36 elements with 49 nodes. However, each cell has a different configuration in the arrangement of the material components that conforms them. Figures 6.36a, b and c represent

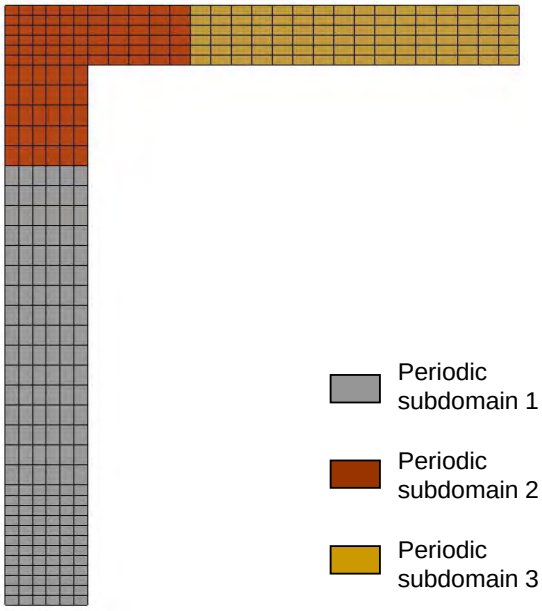

Figure 6.35: Model mesh for the homogenization method global scale with different periodic subdomains.

the internal structure of the periodic subdomains 1, 2 and 3 respectively. The three cells have the same length and height equal to 0.1 m and a thickness equal to 0.4 m.

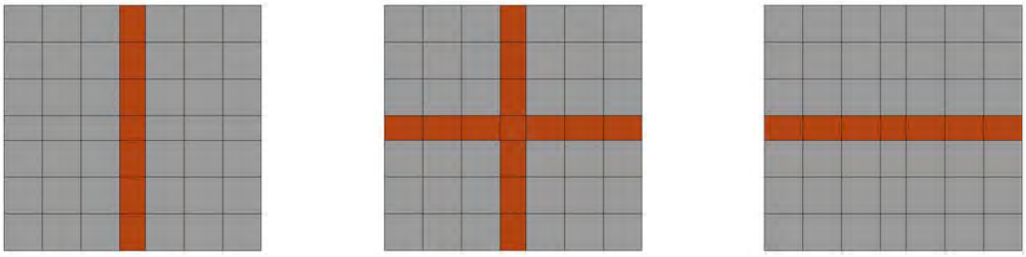

(a) unit cell 1 (b) unit cell 2 (c) unit cell 3

Figure 6.36: FE meshes of the unit cells of the three periodic subdomains of the RC frame homogenized model

Results

One-scale FEM and two-scale homogenization method computations were carried out on the RC frame model for the force described on the paragraphs above. Figure 6.37 presents the capacity curve (force applied versus displacement) for the classical one-scale FE method (FEM) and the multi-domain homogenization analysis in two scales (HOM).

Figure 6.38 presents the same information than Figure 6.37 in terms of displacement field distributions (at the two-scale homogenized solution only the global scale is depicted).

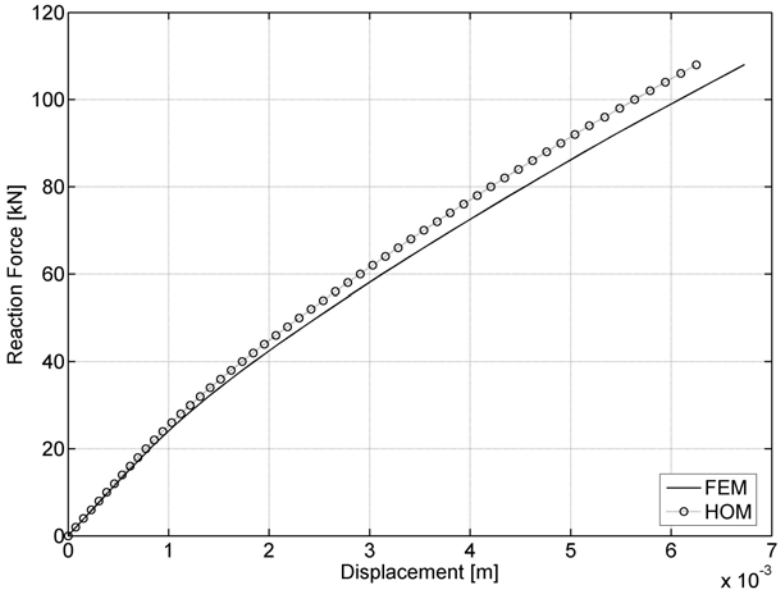

Figure 6.37: Capacity curves of the RC frame for the classical one-scale FEM and the multi-domain homogenization analysis in two scales.

From the information presented in Figures 6.37 and 6.38 it can be stated that the global response of the RC frame computed with the multi-domain homogenized model in two scales matches with great approximation the reference solution obtained with the one-scale FE method in terms of the capacity curves and the displacement field distributions.

The information presented in Figure 6.39 corresponds to the one-scale FEM and the multi-domain homogenized response in terms of stresses in the X-direction. Figure 6.39a presents the information obtained with the classical one-scale FE method for the entire frame and zoomed details of two zones of the structure: 1) the union of the beam and column ($P1$); and 2) the bottom of the beam, at the end of the beam-column reinforcement ($P2$). Meanwhile on Figure 6.39b, presents the homogenized values for the entire structure at the global scale and the response obtained with the unit cells at the local scale at the same two points of interest ($P1$ and $P2$) mentioned at the one-scale FE case. Two different scale vectors are depicted on Figure 6.39b: a) one that corresponds to the homogenized values of the entire structure at the global scale (HOM); and b) another scale that corresponds to the unit cells stress values (RVE) at the local scale. Figure 6.40 presents the same information than Figure 6.39 for the case of the Y-direction. In this case the two points of interest where details are presented are: 1) the union of the beam and column ($P1$); and 2) the bottom left side of the column ($P3$).

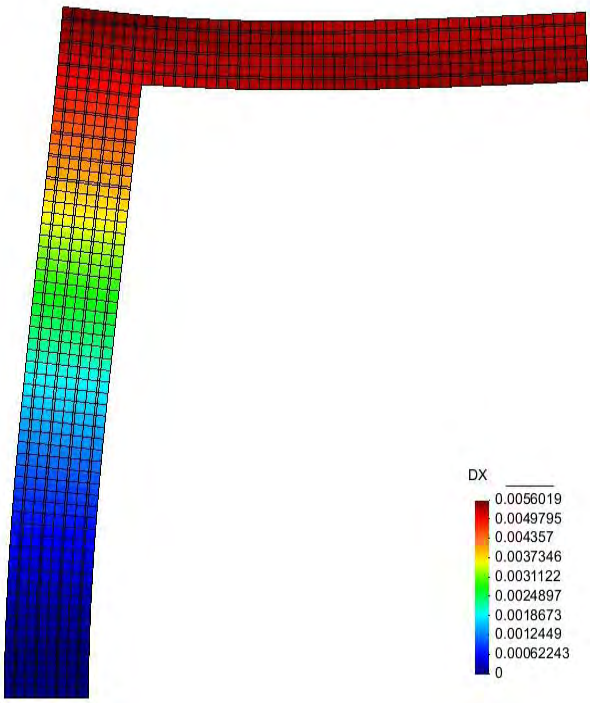

(a) One-scale FEM

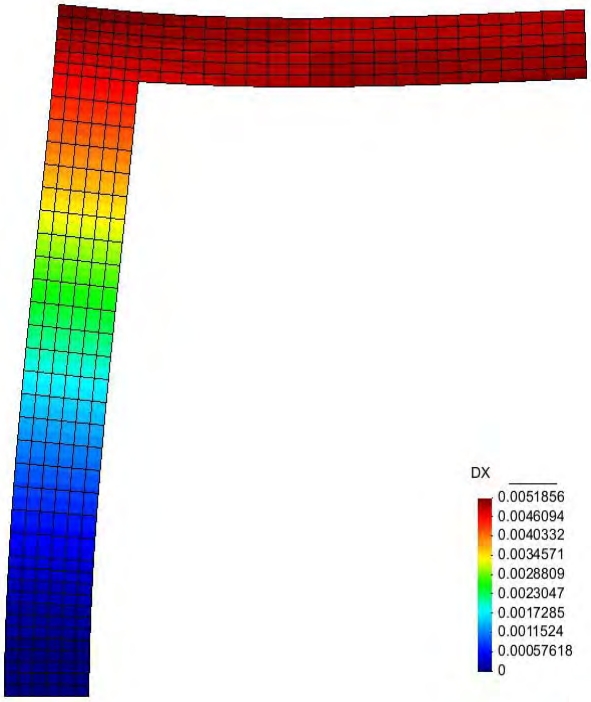

(b) Two-scale homogenization

Figure 6.38: Displacement field distribution obtained with the classical one-scale FEM and the multi-domain homogenization method in two scales on the X-direction. Deformed geometry of the one-scale FEM and global scale of the homogenization method (x50)). Units (cm).

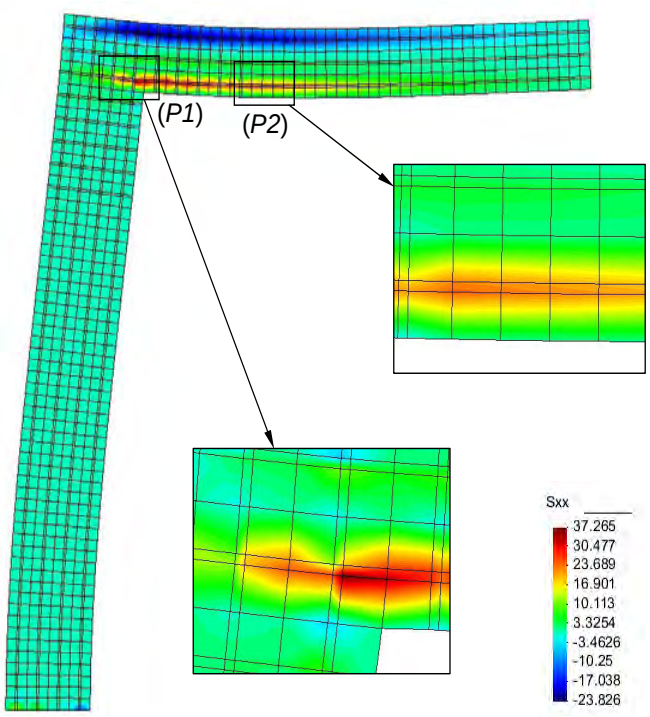

(a) One-scale FEM

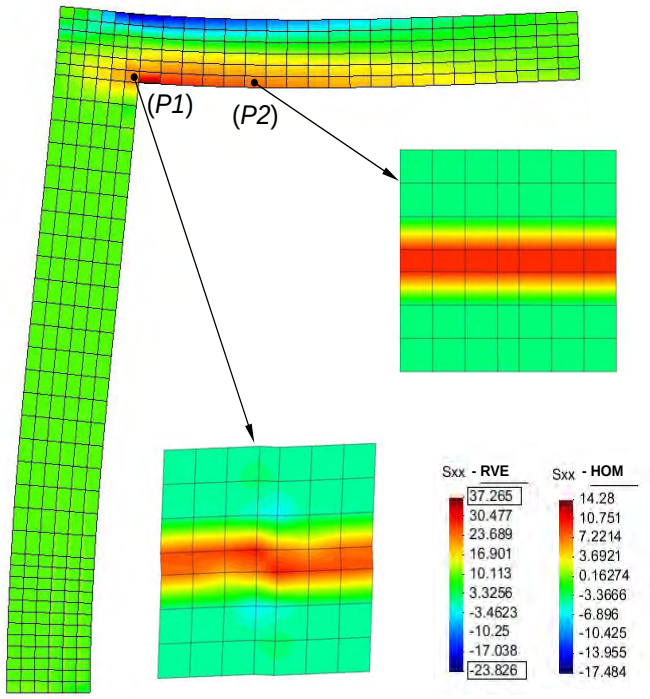

(b) Two-scale homogenization

Figure 6.39: Stress distribution obtained with the classical one-scale FEM and the multi-domain homogenization method in two scales on the X-direction. Deformed geometry of the one-scale FEM and global scale of the homogenization method (x50); local scale (x200). Units (MPa).

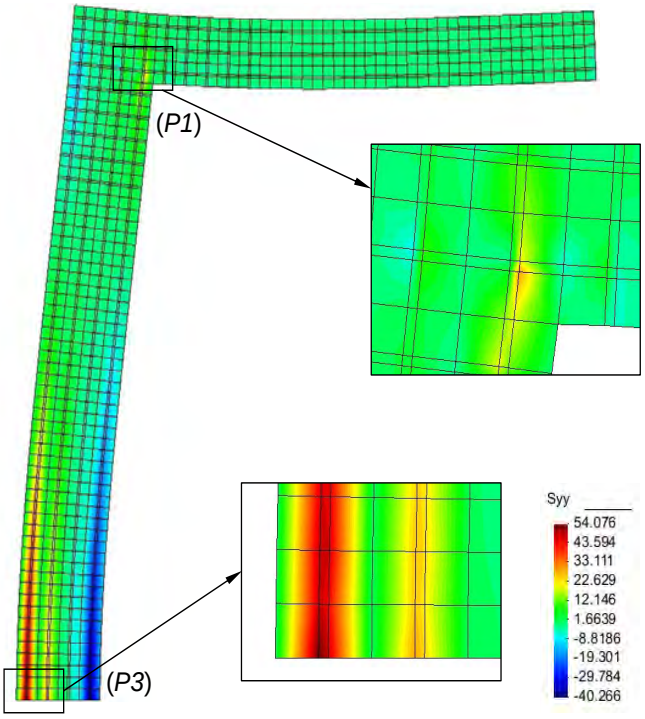

(a) One-scale FEM

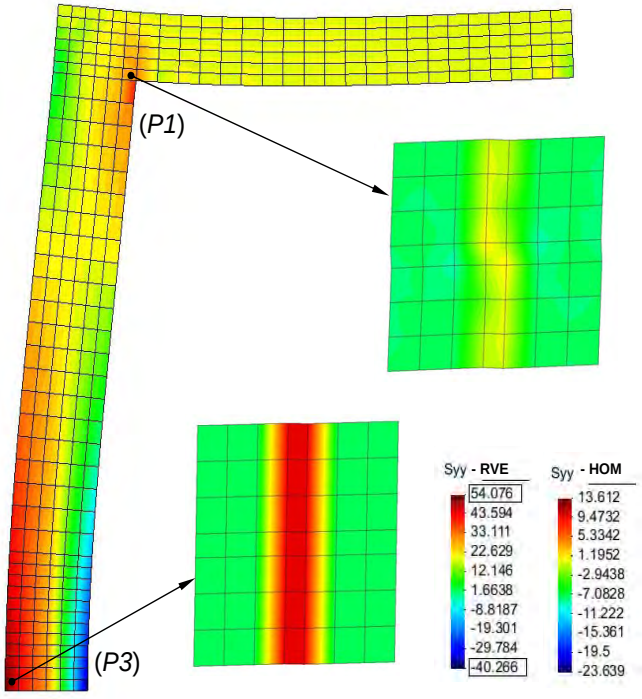

(b) Two-scale homogenization

Figure 6.40: Stress distribution obtained with the classical one-scale FEM and the multi-domain homogenization method in two scales on the Y-direction. Deformed geometry of the one-scale FEM and global scale of the homogenization method (x50); local scale (x200). Units (MPa).

From the results presented in Figure 6.39 for the case of stress distribution at the X-direction, it is observed on the one-scale FE model that the highest tensional stress is found at the lower horizontal steel bar around the beam-column union, meanwhile that for the case in compression it is located at the upper steel bar. On the other hand, on the two-scale homogenized model, at the macro scale, both high stress zones, in tension and compression, are well identified in terms of average stress values. Meanwhile on the micro scale, the stress distribution on the two unit cells that represent the two points of interest ($P1$) located at the union of the beam and the column and ($P2$) located at the bottom of the beam at the end of the beam-column reinforcement, match with great approximation the results obtained with the one-scale FE model.

For the case of the stress distribution at the Y-direction presented in Figure 6.40, the highest tensional stress at the one-scale FE model is found at the left steel bar at the bottom of the column, meanwhile that for the case in compression it is located at the right steel bar also at the bottom of the column. Again, at the macro scale on the two-scale homogenized model, the two high stress zones in tension and compression, are well identified in terms of average stress values. On the micro scale, the stress distribution on the two unit cells that represent the two points of interest ($P1$) located at the union of the beam and column and ($P3$) located at the bottom left side of the column also reproduce with great accuracy the results obtained with the classical one-scale FE model.

Figure 6.41 presents the classical one-scale FEM and the two-scale homogenized response in terms of damage index following the same pattern than in Figures 6.39 and 6.40. In this case, three points of interest are depicted, which correspond to: 1) the union of the beam and column ($P1$); 2) the bottom of the beam at the end of the beam-column reinforcement ($P2$); and 3) the bottom left side of the column ($P3$). On the other hand Figure 6.42 presents the index damage evolution for the same three points of interest for both methods.

For the case of damage index presented in Figure 6.41, the highest value found on the classical one-scale FE model is located on the bottom of the column at the left side and on the union of the beam and column (node of the frame). On the two-scale homogenized model at the macro scale, the damage index perfectly matches the results obtained with the classical one-scale FEM model and gives an accurate description of the global state of the structure in terms of the damage criteria, demonstrating the effectiveness of the method proposed to compute the homogenized internal variables. At the micro scale, the damage index of the three unit cells depicted corresponding to the points of interest ($P1$),($P2$) and ($P3$) matches perfectly the results obtained with the classical one-scale FEM model.

Moreover, the evolution of the index damage of the three points of interest ($P1$),($P2$) and ($P3$) presented on Figure 6.42 demonstrates that the homogenized response reproduces with great accuracy the results used as reference solution obtained with the classical one-scale FE method throughout the loading process.

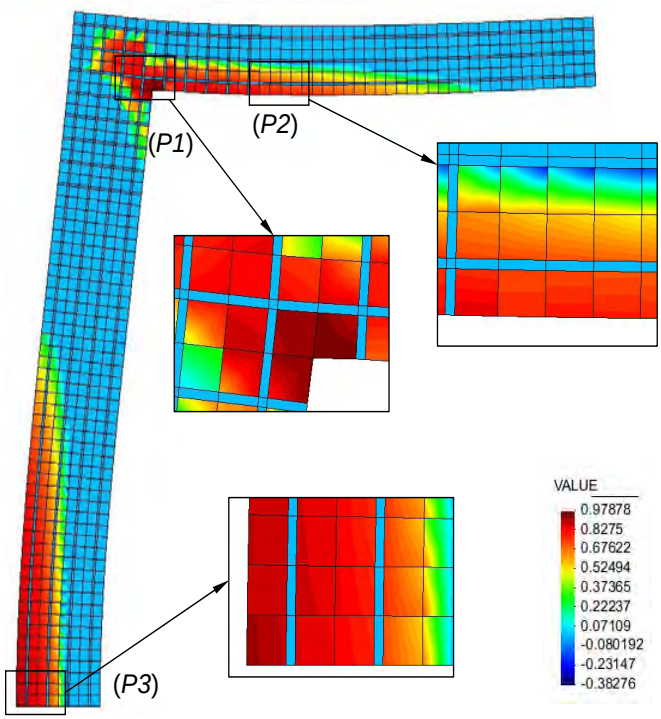

(a) One-scale FEM

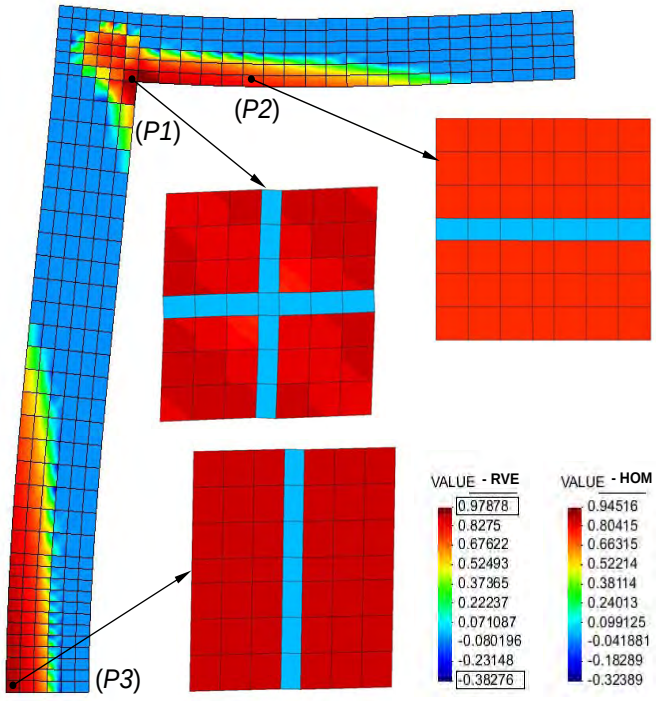

(b) Two-scale homogenization

Figure 6.41: Damage distribution obtained with the classical one-scale FEM and the multi-domain homogenization method in two scales. Deformed geometry of the one-scale FEM and global scale of the homogenization method (x50); local scale (x200).

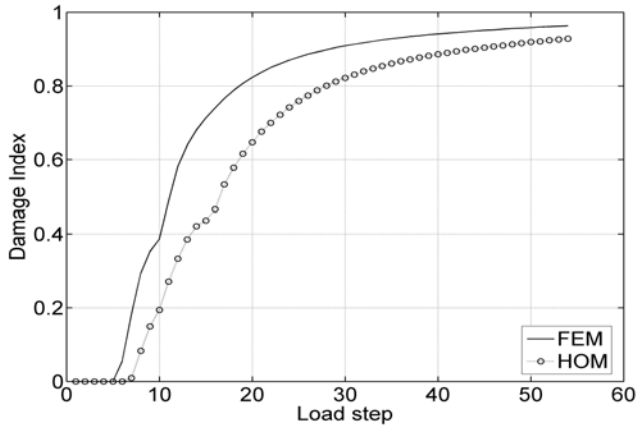

(a) Union of the beam and column ($P1$)

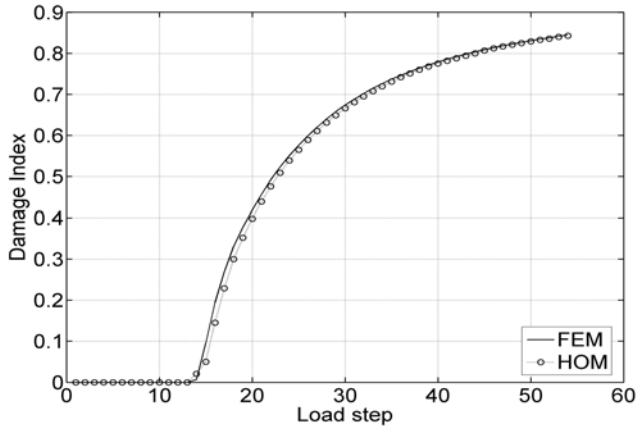

(b) Bottom of the beam at the end of the beam-column reinforcement ($P2$)

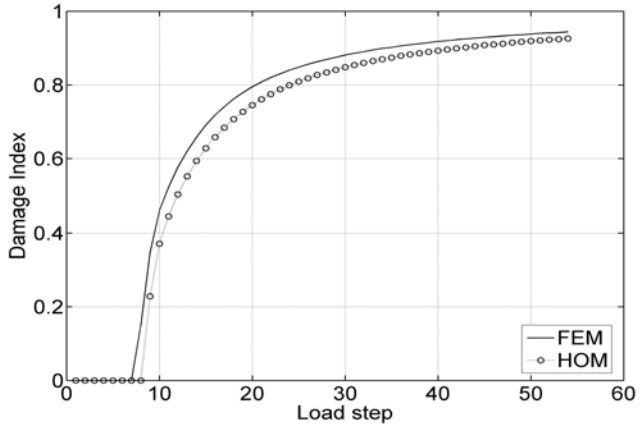

(c) Bottom left side of the column ($P3$)

Figure 6.42: Damage evolution obtained with the classical one-scale FE and the two-scale homogenization method.

The results obtained in this example demonstrated that the proposed multi-domain homogenization method in two-scales reproduces the one-scale FEM results at the global level with great approximation in terms of capacity curves and damage index. Even more, at the local level the results show with great detail the contribution of each of the components on the structural response in terms of stresses and damage distribution. The outcome obtained demonstrates the advantages of the multi-domain homogenization method in two scales to model and compute the response of structures commonly found in engineering that can be represented by different periodic subdomains.

Computational effort comparison among the classical one-scale FE method and the multi-domain homogenization method in two scales in the analysis of the RC frame

The comparison of the computational effort among the classical one-scale FE method (FEM) and the multi-domain homogenization method in two scales (HOM) is presented for this example in Figure 6.43. The results presented for the case of the two-scale homogenized solution were computed using a total of 8 processors in parallel. Also, in the solution process the homogenized non-linear tangent tensor was computed according to the method described in Sections 3.5.5 and 4.4.2.

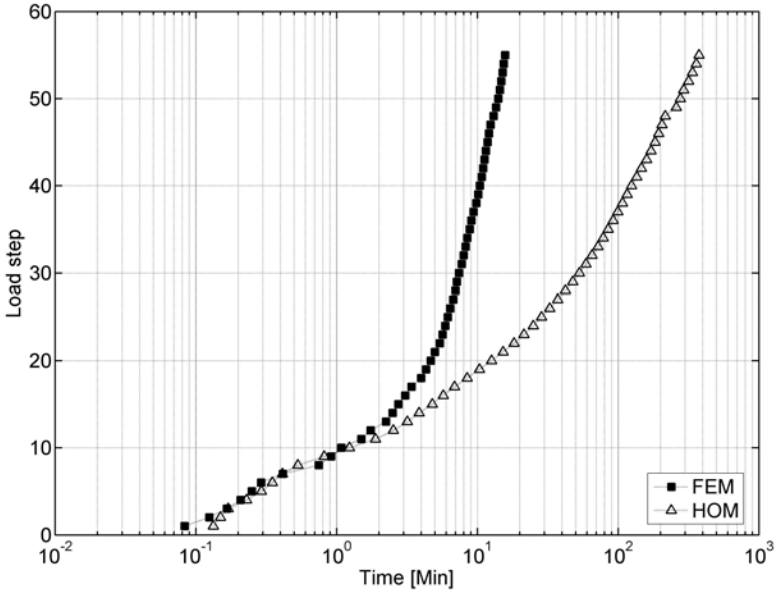

Figure 6.43: Convergence time for each load step for the classical one-scale FE method and the two-scale homogenization method for the RC frame analysis.

From the results obtained it was calculated that the total computing time (the accumulated time along the computing process) of the classical one-scale FEM all along the calculation

process is faster almost 24 times than the two-scale homogenized solution. This example shows a considerable difference in the computational effort to obtain the solution of the RC frame by using the multi-domain homogenization method in two scales with respect to the classical one-scale FE method.

Nevertheless, it must be remarked that the homogenization procedure proposed in this research does not arise with the purpose of improving the speed in the solution process with respect to the traditional methods of analysis, but rather as an alternative procedure in cases when those methods can not be applied in the solution of problems in composite materials and structures because of their characteristics and configuration. Therefore, the computational procedure performed using the multi-scale homogenization technique it is expected to be more expensive in computational terms (computational time, memory, etc.), especially for the case when the structure is composed by several periodic subdomains.

6.2.2 Strengthening of the RC frame

In the previous section it was demonstrated the usefulness of the multi-domain homogenization method in the analysis of structures commonly found on the engineering practice such as it was the case of the RC frame. In this section, the method will be applied to strengthening the frame with the purpose of improving its performance acting under the same load applied of the previous example.

Let us assume that, since the damage index on the RC frame presented in the previous section can compromise the structural integrity of the same, it is desired to retrofit the frame in order to diminish the damage and the structural response in general. The frame is strengthened on the beam-column union and on the bottom of the column according to a traditional structural analysis design, in order to reduce the structural damage in these areas. High stress and damage concentration in these areas it is undesirable since they could result in the total loss of the structural capacity in the case of severe load forces or in damage that is not suitable for retrofitting in the case of less severe actions, being both consequences undesirable from the structural point of view. Therefore, a review of the proposed design should be made be means of a structural analysis method. In this case the method proposed to perform this task is the multi-domain homogenization method presented in this research.

Analytical model on the homogenization method

As part of the RC frame strengthening, the separation between the steel bars at the beam-column union is reduced to a distance of 0.05m. The same steel reinforcement is placed at the bottom of the column up to a height of 0.3m. The rest of the steel reinforcements are maintained as in the original RC frame configuration. Therefore, the periodic subdomains 1 and 3 remain without change, meanwhile that the periodic zone 2 reflects the proposed

structural changes. The modifications on the strengthened RC frame and the division of the RC frame in periodic subdomains are depicted on the schematic representation made in Figure 6.44. In this figure only the new unit cell employed to represent the periodic subdomain 2 is depicted. The unit cells that represent the periodic subdomains 1 and 3 are the same than those used on the example presented in Section 6.2.1. The material properties remain without change as in the mentioned example.

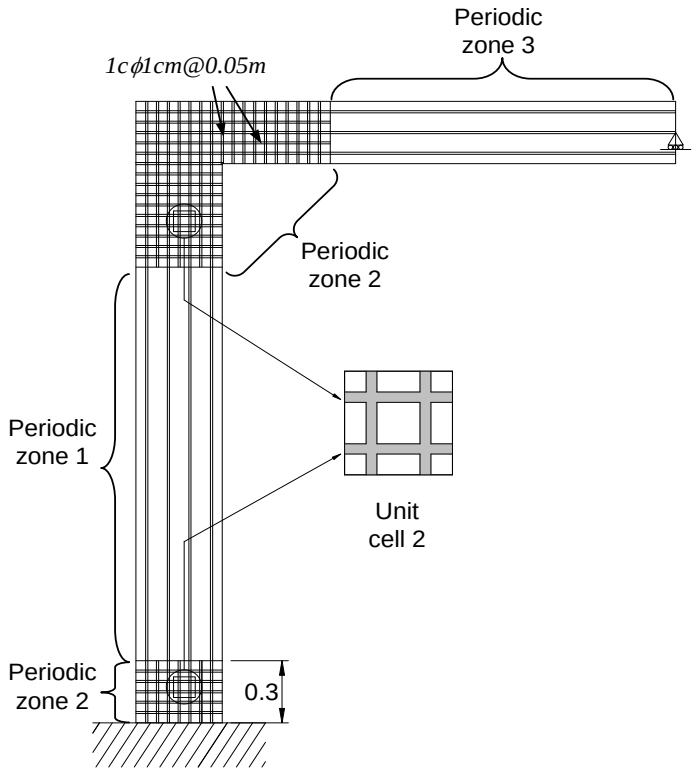

Figure 6.44: Division of the strengthened RC frame in periodic subdomains.

The homogenized model at the global level was created using the same mesh model as in the example presented in Section 6.2.1 with the three different periodic subdomains identified previously in Figure 6.44. The difference in the assignation of the periodic subdomains with the previous example is that in this case the structural configuration of the bottom of the column corresponds to the periodic subdomain 2 (corresponding to the strengthened subdomain). The mesh model consisted on 360 elements with 427 nodes. The load was applied the same way as in the previous example by means of a lateral force on the left side of the frame at the node located at 2.9 m from the bottom of the column.

The different periodic subdomains are identified using different colors on the global mesh of the homogenized model as depicted in Figure 6.45.

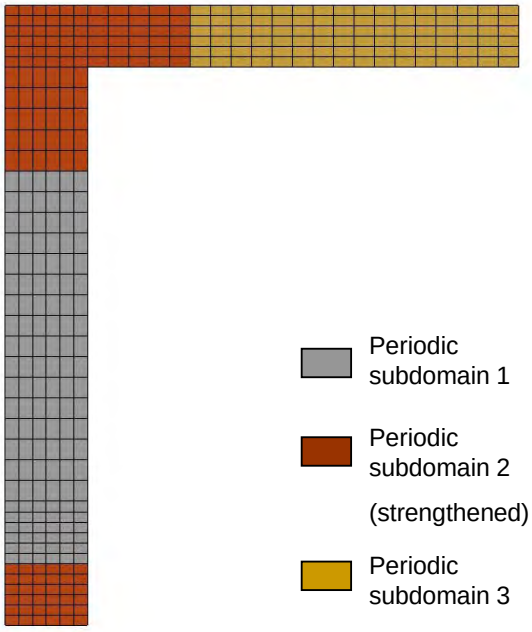

Figure 6.45: Mesh used in the homogenization method with different periodic subdomains.

Figure 6.46 depicts the mesh model of the unit cell that represents the internal structure of the periodic subdomain 2. The mesh model of the unit cell consisted on 100 elements with 121 nodes. The cell has the same length and height equal to 0.1 m and a thickness equal to 0.4 m. The other two cells corresponding to the periodic subdomains 1 and 3 remained without change from those used in the example of Section 6.2.1, as mentioned previously.

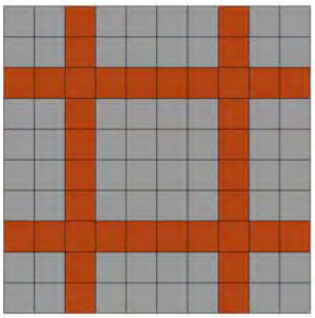

Figure 6.46: FE mesh of the unit cells corresponding to the periodic subdomain 2 of the strengthened RC frame homogenized model

Results

Figure 6.47 presents the capacity curves for the RC frame presented in the previous example in Section 6.2.1 and the strengthened frame, as described in the previous paragraphs, obtained with the multi-domain homogenized method in two scales.

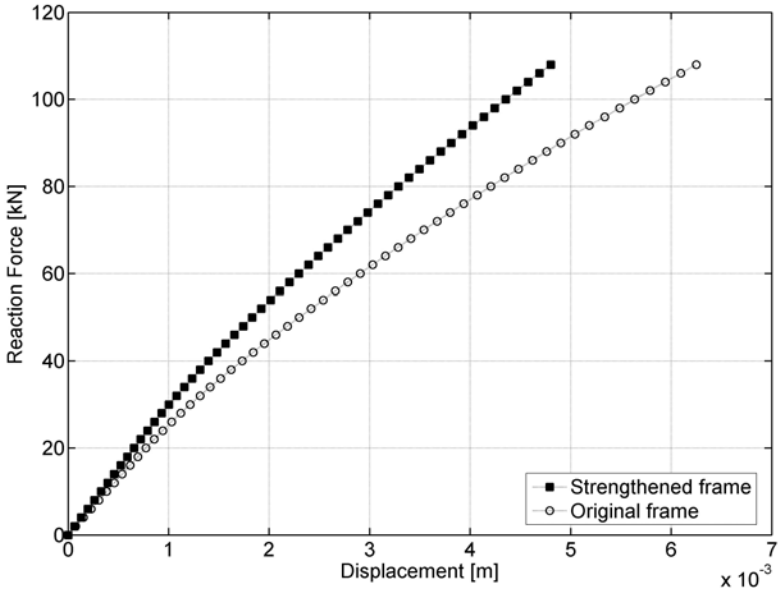

Figure 6.47: Capacity curves of the strengthened and original RC frame obtained with the multi-domain homogenized method in two scales.

Based on the information presented in Figure 6.47 it can be observed that the modifications made on the strengthened RC frame reduce the global response in a 23% approximately with respect to the original RC frame response according to the capacity curves obtained with the multi-domain homogenized method in two scales presented in this figure.

The information presented in Figure 6.48 corresponds to homogenized response in terms of stresses in the X and Y-direction of the strengthened RC frame. The figure presents the homogenized values for the entire structure and the response obtained at the local scale with the unit cells at the same 3 points of interest mentioned on the previous example presented in Section 6.2.1 (the union of the beam and column ($P1$), the bottom of the beam at the end of the beam-column reinforcement ($P2$) and the bottom left side of the column ($P3$)). In this case the two different scale vectors depicted on the figure corresponds to: a) the homogenized values of the entire structure obtained on this analysis (HOM) and b) the scale that corresponds to the unit cells stress values (RVE) presented at the previous example on the original RC frame. This scale modification is established here for comparative purposes.

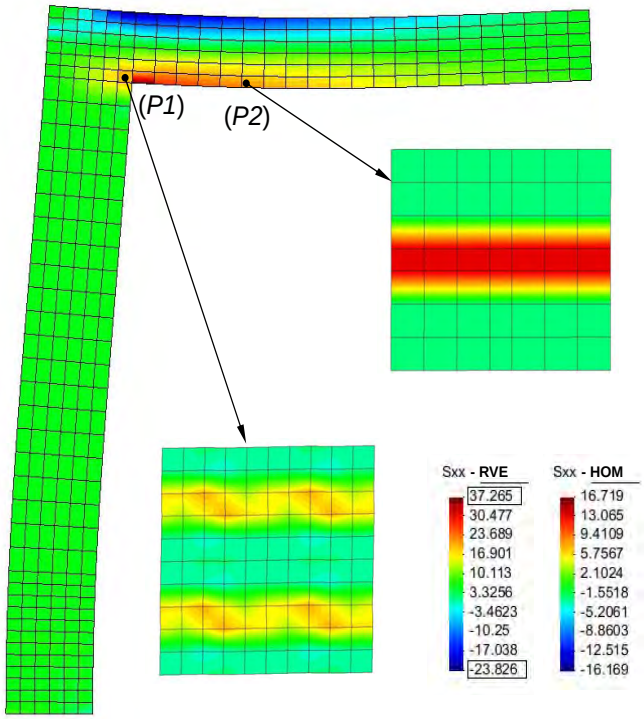

(a) X-direction

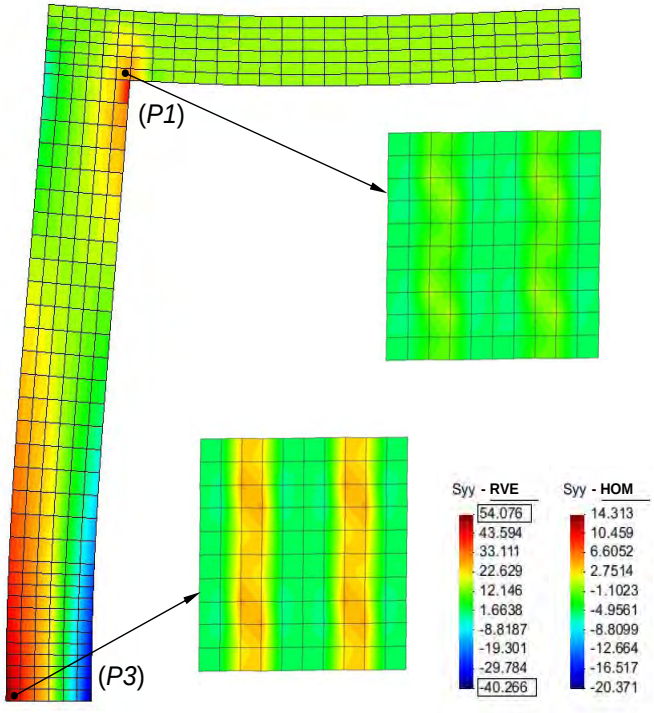

(b) Y-direction

Figure 6.48: Stress distribution obtained with the multi-domain homogenization method in two scales. Deformed geometry of the global scale of the homogenization method (x50); local scale (x200). Units (MPa).

Figure 6.49 presents the homogenized response in terms of damage index. In this case two scale vectors presented correspond to the scale values of the homogenized structure established on the previous example (HOM) and the other scale corresponds to the damage index values of unit cells (RVE) also established at the previous example. The modification on the scale values with respect to the RC frame without strengthening was performed in order to compare the response of both frame configurations. Figure 6.50 presents the damage index evolution for the three interest points of interest ($P1$), ($P2$) and ($P3$) of the frame for the case of the strengthened RC frame and the original configuration obtained with the multi-domain homogenization method.

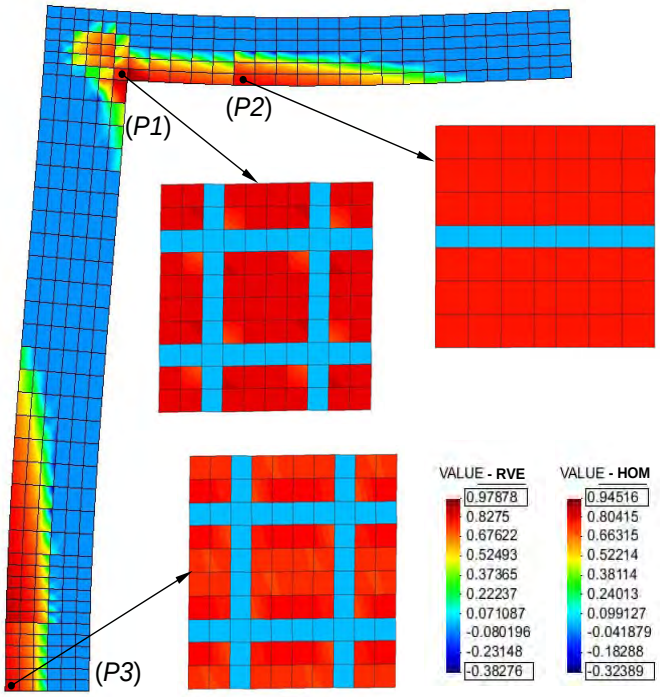

Figure 6.49: Damage distribution obtained with the multi-domain homogenization method in two scales. Deformed geometry of the global scale of the homogenization method (x50); local scale (x200).

From the results presented in Figure 6.48 for the case of stress distribution at the X-direction, it is observed that on the unit cell that represents the union of the beam and column ($P1$), the stress has diminish with respect to the original RC frame configuration, meanwhile that for the case of the cell that represents the point at the beam ($P2$) it does not present any major changes apparently on the stress distribution. For the case at the Y-direction, it is observed that the stress distribution has diminished with respect to the original RC frame configuration at the unit cell that represents the union of the beam and column ($P1$), meanwhile that for the cell with strengthened configuration that represents

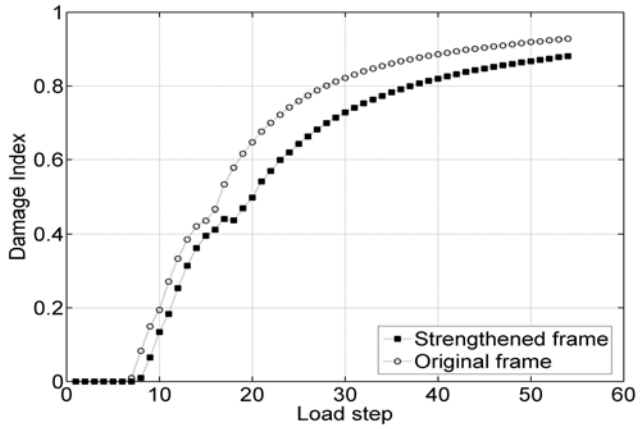

(a) Union of the beam and column ($P1$)

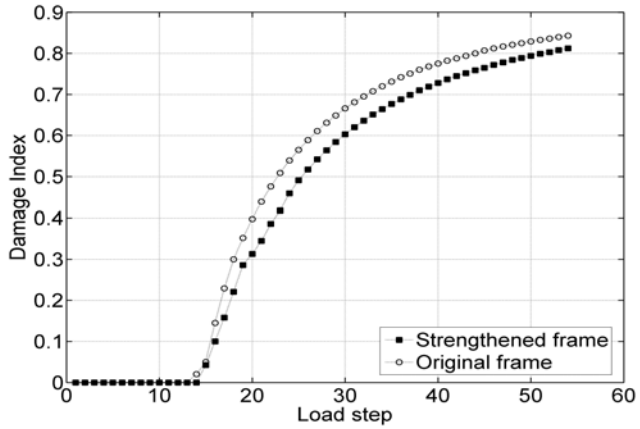

(b) Bottom of the beam at the end of the beam-column reinforcement ($P2$)

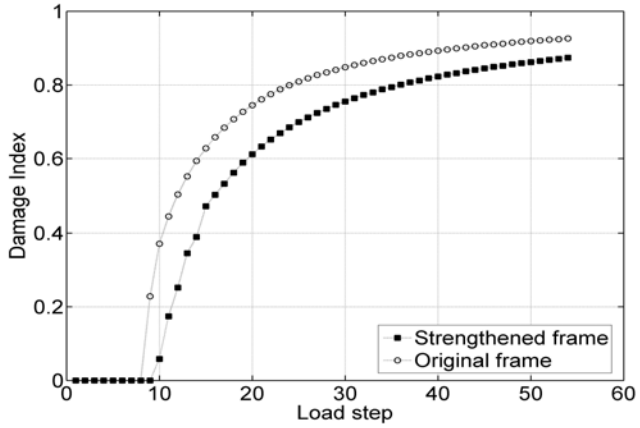

(c) Bottom left side of the column ($P3$)

Figure 6.50: Damage evolution obtained with the multi-domain homogenization method in two scales for the strengthened RC frame and the original design.

the point at the bottom left side of the column ($P3$), the stress distribution has diminished considerably with respect to the cell in the original configuration presented in Figure 6.40b.

For the case of the damage index presented in Figure 6.49 the homogenized values show a reduction on the union of the beam and column of the RC frame ($P1$) and on the bottom of the column ($P3$). The damage on the structure appears to be shifted away from these two critical structural areas, which is desirable from the structural point of view. In this case, according to the homogenized damage index, the largest damage concentration appears on the beam at the end of the beam-column reinforcement ($P2$) and at the column where the strengthened area ends as well. The unit cells that represent the three points of interest ($P1$), ($P2$) and ($P3$) of the RC strengthened frame present a minor damage distribution with respect to the cells corresponding to the original RC frame configuration, however on the colored scale response is difficult to give an proper assessment of this reduction factor. To verify this reduction, a numerical comparison of the damage index is presented in Figure 6.50.

According to the curves presented in Figure 6.50 it is observed that the RC frame strengthened configuration clearly reduces damage index for the three points of interest with respect to the original configuration. The damage index is reduced in a 15% approximately with respect to the original configuration.

The results obtained in this example demonstrate the usefulness that the multi-domain homogenization method in two scales has in computing the response in cases of structures that can be represented by several subperiodic means. In the case of this example, this advantage is demonstrated since no re-meshing at the global scale was needed in order to perform the strengthening of the RC frame. This is a major advantage with respect to a conventional one-scale FEM analysis in which any modification at the geometry or arrangement of the components requires a mesh modification.

Furthermore, the method is capable of dealing adequately with the strain gradients that may appear at the interfaces between the different subperiodic means. Therefore, it can be affirmed that the method represents a convenient and a practical tool to compute the response of structures commonly used on the engineering practice that are composed by different periodic subdomains.

Chapter 7

Conclusions and final remarks

In this chapter the main findings of this study are given in terms of a brief summary and in terms of recommendations and conclusions. Future lines of study and future developments are suggested based on the work presented and on the main difficulties found while developing this research.

7.1 Summary

A multi-domain homogenization method has been proposed and developed in this thesis based on a two-scale technique. The method is capable of analyzing composite structures with several periodic distributions by partitioning the entire domain of the composite into substructures making use of the classical homogenization theory following a first-order standard continuum mechanics formulation. The need to develop the multi-domain homogenization method arose because current homogenization methods are based on the assumption that the entire domain of the composite is represented by one periodic or quasi-periodic distribution. However, in some cases the structure or composite may be formed by more than one type of periodic domain distribution, making the existing homogenization techniques not suitable to analyze this type of cases in which more than one recurrent configuration appears.

The decision of following a first-order computational scheme over using a high-order approximation was adopted based on the fact that high-order methods generally involve elements that make use of a larger number of nodes, degrees of freedom and boundary conditions, which may result in an increment of the computational effort with respect to the first-order formulation. Furthermore, the selection of higher-order boundary conditions is rather an arbitrary task, giving a solution not fully consistent in all cases, since this selection is a matter of choice.

The theoretical principles used in the multi-domain homogenization method were applied to assemble a computational tool based on two nested boundary value problems

represented by a finite element code in two scales: a) one global scale, which treats the composite as an homogeneous material and deals with the boundary conditions, the loads applied and the different periodic (or quasi-periodic) subdomains that may exist in the composite; and b) one local scale, which obtains the homogenized response of the representative volume element or unit cell, that deals with the geometry distribution and with the material properties of the constituents.

The method is based on the local periodicity hypothesis arising from the periodicity of the internal structure of the composite. The numerical implementation of the restrictions on the displacements and forces corresponding to the degrees of freedom of the domain's boundary derived from the periodicity requirement (i.e. the periodic boundary conditions) was performed by means of the Lagrange multipliers method.

The formulation included a method to compute the homogenized non-linear tangent constitutive tensor once the threshold of nonlinearity of any of the unit cells has been surpassed. The procedure is based in performing a numerical derivation applying a perturbation technique. The tangent constitutive tensor is computed for each load increment and for each iteration of the analysis once the structure has entered in the non-linear range. The perturbation method was applied at the global and local scales in order to analyze the performance of the method at both scales. A simple average method of the constitutive tensors of the elements of the cell was also explored for comparison purposes.

A parallelization process was implemented on the multi-domain homogenization method in order to speed-up the computational process due to the huge computational cost that the nested incremental-iterative solution embraces. The parallelization scheme was implemented following a very simple and straightforward approach using a programming interface for parallelization (*OpenMP*).

The effect of softening in two-scale homogenization was investigated following a smeared cracked approach. Mesh objectivity was discussed first within the classical one-scale FE formulation and then the concepts exposed were extrapolated into the two-scale homogenization framework. The importance of the element characteristic length in a multi-scale analysis was highlighted in the computation of the specific dissipated energy when strain-softening occurs.

Various examples were presented to evaluate and explore the capabilities of the computational approach developed in this research. Several aspects were studied, such as analyzing different composite arrangements that include different types of materials, composites that present softening after the yield point is reached (e.g. damage and plasticity) and composites with zones that present high strain gradients. The examples were carried out in composites with one and with several periodic domains using different unit cell configurations. The examples are compared to benchmark solutions obtained with the classical one-scale FE method.

7.2 Conclusions

The following conclusions and recommendations are given based on the assessment of the performance of the multi-domain homogenization method presented in this research.

- In first-order homogenization the size of the cell is commonly considered as irrelevant, since the state variables are obtained assuming uniformity of the macroscopic deformation over the entire microstructural cell. However, this assumption is completely valid only in the linear-elastic or in cases where no strain-softening occurs. In order to ensure that the same energy is being dissipated at the macro structural point and at the corresponding unit cell or RVE in the case where strain-softening occurs, the energy dissipation process that occurs at the microscale has to be 'normalized' with respect to the macroscopic zone where the non-linear behavior actually happens (i.e. the element length at the macroscale in the load direction in a 2D uniaxial case).

- It was demonstrated that the method to obtain the homogenized tangent constitutive tensor applying a perturbation technique at the micro scale was more efficient than a simple average method of the constitutive tensors of the elements of the unit cell or RVE, especially for elevated stages of nonlinearity. Despite that the application of the perturbation method at the macrostructure gave correct results, it was considered not suitable from the point of view of computational cost.

- From the evaluation of the parallelization method presented it was shown that the scheme scaled adequately the speedup values when adding more processors to the computing process. On the other hand, the efficiency values obtained seem reasonable according to the straightforwardness of the parallelization scheme implemented and to the several non-parallelizable (sequential) parts that the two-scale code has at the global and local scales.

- In all the examples presented, the stress and damage distribution at the unit cells representative of the periodic continuum reproduced the behavior accurately of the models developed with the classical one-scale FE method. Furthermore, the unit cells reproduced the kinematics of the deformed geometries obtained with the one-scale FE models in all cases.

- The effectiveness of the method proposed to reproduce the internal variables, such as the damage index, by means of the two-scale homogenization method was demonstrated with great success, even in terms of homogenized values at the global scale.

- For the case of a structure perfectly periodic, the global response computed with the two-scale homogenized method, perfectly matches the reference solution obtained with the classical one-scale FEM. The mesh refinement at the global scale in the two-scale homogenized model does not affect the solution, since similar results are obtained with different mesh densities in the case of stress or damage distribution along the periodic continuum. The change of the size of the unit cell does not affect

the response in terms of the capacity curves at the global scale nor in the case of stress or damage distribution in the global and local scale.

- In the case where high strain gradient appears on the periodic continuum it was observed that the mesh modification at the global scale in the homogenized model does affect the response, since a better approximation to the reference one-scale FEM solution is obtained with a refined mesh. The refinement on the global mesh modified the rapidly changing variational field into a slower change of the macroscopic variables, diminishing the error with respect to the reference solution.

- From the response obtained with the homogenization method applied to the analysis of composite structures with several periodic domains it was demonstrated that method reproduces the global response of the RC frame with great approximation to the reference solution obtained with the classical one-scale FE method. The zones where high stress concentration was present were well identified in terms of average stress values on the homogenized model. Moreover, on the microscale the stress distribution on the unit cells that represented all the points of interest selected, reproduced with great accuracy the results obtained with the classical one-scale FE model. On the other hand, the homogenized damage index perfectly matched the results obtained with the one-scale FE model and gave an accurate description of the global state of the structure in terms of the damage criteria. At the microscale, the damage index of the unit cells that represented the interest points of the structure matched perfectly the results obtained with the classical one-scale FE model.

- The computational effort required when using the multi-scale homogenization technique is more expensive than the classical one-scale FEM in computational terms (computational time, memory, etc.), especially for the case when the structure is composed by several periodic subdomains. Nevertheless, it must be remarked that the homogenization procedure proposed in this research does not arise with the purpose of improving the speed in the solution process with respect to the traditional methods of analysis, but rather as an alternative procedure in cases when those methods can not be applied in the solution of problems in composite materials and structures because of their characteristics and configuration.

- The application of the multi-domain homogenization method in two scales as analysis tool to compute the structural response in cases like the one presented in the strengthened RC frame example, demonstrates one of the main advantages this technique, since no remeshing of the whole structure had to be performed to compute the strengthened response of the RC frame.

- The examples presented demonstrated the usefulness of the multi-domain homogenization method to be used as a practical tool to obtain the response of structures commonly used on the engineering practice that can be represented by different periodic subdomains.

7.3 Future work and future lines of study

The multi-domain homogenization method presented in this research investigation required the conjunction of several formulations. Some of these formulations involved in the developing process of the method still have, naturally, some room for improvement since this approach represents one of the first attempts to represent structures with multiple periodic domains by means of the homogenization method. Among these improvements, the author considers the following ones the most important:

- Extend the formulation into a tridimensional environment since most of the structural arrangements found on the common practice are better represented and described in 3D. This would explode even more the capabilities of the method, since mores structures could be represented by the multi-domain homogenization method than the ones that can be found in 2D. However, in order to expand the formulation, a modification of the Lagrange multipliers method should be made, or a different formulation should be investigated to impose the periodicity conditions, in order to reduce the number of extra degrees of freedom that may be produced on the stiffness matrix of the unit cell representative of the tridimensional volume.

- Improve the efficiency of the parallelization process in order to get a fully optimized formulation. A more comprehensive algorithm should be investigated as the main subject of study in a different research project.

- Perform a parametrization study of the relationship between the two scales in order to investigate if there are limits among the dimensions of the global continuum (characteristic wavelength of the macroscopic problem) and the dimension of the unit cell (period of the characteristic wavelength in the microstructure) when the 'normalization' process is performed at the microscale when strain-softening occurs.

- Investigate the possibility of using a high-order instead of the first-order formulation in order to simulate microstructural effects. However, some improvements on the number of degrees of freedom should be made in order to reduced them, since first-order multi-scale homogenization is already an expensive computational process. Another improvement before using the high-order formulation should be made on the selection of the boundary conditions imposed.

- Investigate the possibility of implementing a large strain formulation approach in multiple scale problems.

- Investigate the use of a model reduction method in multi-scale analysis in order to alleviate the complexity of the problem and to reduce significantly the computational effort.

This page is intentionally left blank.

Appendix A

Damage constitutive model

The continuum damage mechanics theory [106, 86, 84] is based on the definition of the effective stress $\bar{\boldsymbol{\sigma}}$, which can be computed in terms of the total strain tensor $\boldsymbol{\varepsilon}$ as:

$$\bar{\boldsymbol{\sigma}} = \mathbf{C} : \boldsymbol{\varepsilon} \tag{A.1}$$

where $\mathbf{C}$ is the usual (fourth order) isotropic linear-elastic constitutive tensor, and (:) denotes the double contraction. The constitutive equation for the damage model is defined as:

$$\boldsymbol{\sigma} = (1-d)\,\bar{\boldsymbol{\sigma}} = (1-d)\,\mathbf{C} : \boldsymbol{\varepsilon} \tag{A.2}$$

where d is the damage index, whose definition and evolution is given below.

The complete definition of the constitutive equation requires of the following requirements:

1. Definition of the variables of the problem:
   - free variable: $\boldsymbol{\varepsilon}$
   - internal variable: d
2. Establishment of a potential, in this case the free energy is defined as:

$$\Psi(\boldsymbol{\varepsilon}, d) = (1-d)\,\Psi^0(\boldsymbol{\varepsilon}) \quad ; \quad \Psi^0(\boldsymbol{\varepsilon}) = \frac{1}{2}\varepsilon_{ij} C_{ijkl} \varepsilon_{kl} \tag{A.3}$$

3. Determination of thermo-mechanical requirements. This is done using the inequality of Clasius-Planck, valid for thermo-mechanical problems decoupled, as:

$$D = \left(\sigma_{ij} - \frac{\partial \Psi}{\partial \varepsilon_{ij}}\right)\dot{\varepsilon}_{ij} - \frac{\partial \Psi}{\partial d}\dot{d} \geq 0 \tag{A.4}$$

with:

$$\sigma_{ij} = \frac{\partial \Psi}{\partial \varepsilon_{kl}} = (1-d)\, C_{ijkl}\varepsilon_{kl} \tag{A.5}$$

$$D = \frac{\partial \Psi}{\partial d}\dot{d} \geq 0 \tag{A.6}$$

Since $\partial\Psi/\partial d = -\Psi^0$, then the dissipation stays as:

$$D = \Psi^0 \dot{d} \tag{A.7}$$

4. The definition of the norm τ of the strain tensor $\boldsymbol{\varepsilon}$ or alternatively of the undamaged stress tensor $\boldsymbol{\sigma}^0$. This norm is also called equivalent deformation and is used to compare different stages of the material. Therefore, it is possible to distinguish the loading and unloading process. Different alternatives to characterize the material behavior are given:

   - Symmetric elastic model: The norm is defined in terms of elastic energy Ψ^0. The elastic domain is represented by an ellipsoid centered at the origin in the space of strains or stresses.

$$\tau = \sqrt{2\Psi^0} = \sqrt{\boldsymbol{\varepsilon} : \mathbf{C} : \boldsymbol{\varepsilon}} = \sqrt{\boldsymbol{\sigma} : \mathbf{C} : \boldsymbol{\sigma}} = \sqrt{\boldsymbol{\sigma} : \boldsymbol{\varepsilon}} \tag{A.8}$$

   - Model subjected to simple traction: This model is useful when the damage criterion occurs only by traction. The norm is determined by the ramp function (expressed by the Macaulay brackets $\langle . \rangle$). Therefore it takes only positive values, which corresponds to the principal stresses.

$$\tau = \sqrt{\boldsymbol{\sigma} : \langle \boldsymbol{\varepsilon} \rangle} \tag{A.9}$$

   - Not symmetric model: Used to represent materials in which the elastic domain in tension differs from the compression one. This domain is characterized as follows.

$$\tau = \left(\varsigma + \frac{1-\varsigma}{n} \right) \sqrt{\boldsymbol{\sigma} : \boldsymbol{\varepsilon}} \tag{A.10}$$

   where n is the ratio of the strength in compression and the strength in tension and ς is a weight function that depends on the stress state $\boldsymbol{\sigma}^0$. This function is defined as:

$$\varsigma = \frac{\sum_{i=1}^{3} \langle \boldsymbol{\sigma}_i \rangle}{|\boldsymbol{\sigma}_i|} \tag{A.11}$$

   where i denotes each of the stress principal directions.

5. Damage criterion. Introduced as:

$$\Phi(\tau, r) = \tau - r \leq 0 \tag{A.12}$$

where r is an internal stress-like variable representing the current damage threshold, as its value controls the size of the (monotonically) expanding damage surface. The initial value of the damage threshold is $r_0 = \boldsymbol{\sigma}_0$, where $\boldsymbol{\sigma}_0$ is the initial uniaxial damage stress.

The expansion of the damage bounding surface for loading, unloading and reloading conditions is controlled by the KuhnTucker relations and the damage consistency condition, which are:

$$\dot{r} \geq 0; \quad \Phi(\tau, r) \leq 0; \quad \dot{r}\Phi(\tau, r) = 0 \tag{A.13}$$

Which leads to the loading condition:

$$\dot{r} = \dot{\tau} \tag{A.14}$$

Which in turn, leads to the explicit definition of the current values of the internal variable r in the form:

$$r = max\{r_0, max(\tau)\} \tag{A.15}$$

This equation allows to compute the current values for r in terms of the current value of τ, which depends explicitly on the current total strains.

Finally, the damage index $d = d(r)$ is explicitly defined in terms of the corresponding current value of the damage threshold, so that it is a monotonically increasing function such that $0 \leq d \leq 1$.

In this work, the following functions are used:

- Linear softening

$$d(r) = \begin{cases} (1 + H_S)\left(1 - \frac{r_0}{r}\right); & r_0 \leq r \leq r_u = r_0\left(1 - \frac{1}{H_S}\right) \\ 1; & r \leq r_u \end{cases} \tag{A.16}$$

- Exponential softening

$$d(r) = 1 - \frac{r_0}{r}\exp\left\{-2H_S\left(\frac{r - r_0}{r_0}\right)\right\}; \quad r_0 \leq r \tag{A.17}$$

where H_S is softening modulus

6. Mechanical dissipation. The mechanical free energy term for the damage model is defined in the form:

$$W = (1-d)W^e(\boldsymbol{\varepsilon}) = (1-d)\left[\frac{1}{2}\boldsymbol{\varepsilon} : \mathbf{C} : \boldsymbol{\varepsilon}\right] \geq 0 \tag{A.18}$$

Thus, the rate of mechanical dissipation can be expressed as:

$$\dot{\mathscr{D}} = W^e \dot{d} \geq 0 \tag{A.19}$$

Provided that the damage index increases monotonically, $\dot{d} \geq 0$.

7. Strain-softening and fracture energy release. The specific dissipated energy $\mathscr{D}$ is scaled in order to avoid lack of objectivity of the response independently of the element size. This is done as follows:

$$\mathscr{D} l_{ch} = G_f \tag{A.20}$$

where l_{ch} is the element characteristic length, G_f is the mode I fracture energy of the material, regarded to be a material property. This makes the softening modulus H_S, which defines the softening response, dependent on the element size. It also sets a maximum size for the elements that can be used in the analysis.

The procedure is as follows: consider an ideal uniaxial tensile experiment in which the tensile strain increases monotonically and quasi-statically from an initial unstressed state to another in which full degradation takes place. The specific energy dissipated in the process is:

$$\mathscr{D} = \int_{t=0}^{t=\infty} \dot{\mathscr{D}} dt = \int_{t=0}^{t=\infty} W^e \dot{d} dt = \frac{1}{2E} \int_{r=r_0}^{r=\infty} r^2 d' dr \tag{A.21}$$

where E is the Youngs modulus and the rate of damage has been expressed as $\dot{d} = d'\dot{r}$. The expressions for the linear and exponential softening stays as:

- Linear softening. Using Equation (A.16), $d' = (1+H_S)r_0/r^2$, for $r_0 \leq r \leq r_u$, with $r_u = r_0(1+1/H_S)$, and $d' = 0$, otherwise. Recalling that $r_0 = \sigma_0$ and integrating:

$$\mathscr{D} = \left(1 + \frac{1}{H_S}\right)\frac{\boldsymbol{\sigma}_0^2}{2E} \tag{A.22}$$

and equating $\mathscr{D} = G_f/l_{ch}$, we have:

$$H_S = \frac{\bar{H}_S\, l_{ch}}{1 - \bar{H}_S\, l_{ch}} \geq 0 \tag{A.23}$$

where $H_S = \boldsymbol{\sigma}_0^2/(2EG_f)$ depends only on the material properties, as G_f is the mode I fracture energy per unit area, $\boldsymbol{\sigma}_0$ is the uniaxial strength and E is the Youngs modulus.

- Exponential softening. Using Equation (A.17), $d' = (r_0 + 2H_S r)\exp\left\{-2H_S\left(\frac{r-r_0}{r_0}\right)\right\}/r^2$, for $r_0 \leq r \leq \infty$. Recalling that $r_0 = \boldsymbol{\sigma}_0$ and integrating, the same expression as the one in Equation (A.22) is obtained.

8. Tangent operator. The tangent constitutive tensor $\mathbf{C}^{tan}$ can be obtained explicitly. The stress increment is given by:

$$\begin{aligned} \dot{\boldsymbol{\sigma}} &= \mathbf{C}^{\tan} : \boldsymbol{\varepsilon} \\ &= (1-d)\mathbf{C} : \dot{\boldsymbol{\varepsilon}} - \dot{d}C : \boldsymbol{\varepsilon} \\ &= (1-d)\mathbf{C} : \dot{\boldsymbol{\varepsilon}} - \dot{d}\sigma \end{aligned} \tag{A.24}$$

In the elastic regime, the stress rate is expressed as:

$$\dot{\boldsymbol{\sigma}} = (1-d)\mathbf{C} : \dot{\boldsymbol{\varepsilon}} \quad ; \quad \dot{d} = 0 \tag{A.25}$$

Recalling that the rate of the damage index has been expressed as $\dot{d} = d'\dot{r}$ and that in the loading direction $\dot{r} = \dot{\tau}$, then the stress increment can be expressed as:

$$\dot{\boldsymbol{\sigma}} = (1-d)\mathbf{C} : \dot{\boldsymbol{\varepsilon}} - \frac{d'}{\tau}\boldsymbol{\sigma} \otimes \boldsymbol{\sigma} : \dot{\boldsymbol{\varepsilon}} \tag{A.26}$$

$$\dot{\boldsymbol{\sigma}} = \left[(1-d)\mathbf{C} - \frac{d'}{\tau}\boldsymbol{\sigma} \otimes \boldsymbol{\sigma}\right]\dot{\boldsymbol{\varepsilon}} \tag{A.27}$$

And the tangent constitutive tensor stays as:

$$\mathbf{C}^{\tan} = (1-d)\mathbf{C} - \frac{d'}{\tau}\boldsymbol{\sigma} \otimes \boldsymbol{\sigma} \tag{A.28}$$

This page is intentionally left blank.

Appendix B

Plasticity

The equations of classical rate-independent plasticity within the classical framework of response functions formulated in stress space are presented in this Appendix following the formulation presented in [107].

B.1 General formulation

The stress-space governing equations are set as follows.

1. Additive decomposition of the strain tensor. One assumes that the strain tensor $\boldsymbol{\varepsilon}$ can be decomposed into an elastic and plastic part, denoted by $\boldsymbol{\varepsilon}^e$ and $\boldsymbol{\varepsilon}^p$, respectively, according to the relationship:

$$\boldsymbol{\varepsilon} = \boldsymbol{\varepsilon}^e + \boldsymbol{\varepsilon}^p \tag{B.1}$$

   Since $\boldsymbol{\varepsilon}$ is regarded as an independent variable and the evolution of $\boldsymbol{\varepsilon}^p$ is defined through the flow rule, Equation (B.1) should be viewed as a definition of the elastic strain tensor as $\boldsymbol{\varepsilon}^e := \boldsymbol{\varepsilon} - \boldsymbol{\varepsilon}^p$.

2. Elastic stress response. The stress tensor $\boldsymbol{\sigma}$ is related to the elastic strain $\boldsymbol{\varepsilon}^e$ by means of a stored-energy function $W : \mathcal{B} \times \mathbb{S} \to \mathbb{R}$ according to the (hyperelastic) relationship:

$$\boldsymbol{\sigma}(x,t) = \frac{\partial W\left[x, \boldsymbol{\varepsilon}^e(x,t)\right]}{\partial \boldsymbol{\varepsilon}^e} \tag{B.2}$$

   For linearized elasticity, W is a quadratic form in the elastic strain, i.e., $W = \frac{1}{2}\boldsymbol{\varepsilon}^e : \mathbf{C} : \boldsymbol{\varepsilon}^e$, where $\mathbf{C}$ is the tensor of elastic moduli which is assumed constant. Then Equations (B.1) and (B.2) imply that:

$$\boldsymbol{\sigma} = \mathbf{C} : [\boldsymbol{\varepsilon}^p - \boldsymbol{\varepsilon}] \tag{B.3}$$

We observe that Equations (B.2)-(B.3) and the decomposition (B.1) are local. Therefore, although the total strain is the (symmetric) gradient of the displacement field, the elastic strain is not in general the gradient of an elastic displacement field. Note further that $\boldsymbol{\varepsilon}^p$ and, consequently, $\boldsymbol{\varepsilon}^e$ are assumed to be symmetric at the outset, i.e., $\boldsymbol{\varepsilon}^p \in \mathbb{S}$. Thus, the notion of a plastic spin plays no role in classical plasticity.

3. Elastic domain and yield condition.We define a function $f : \mathbb{S} \times \mathbb{R}^m \to \mathbb{R}$ called the yield criterion and constrain the admissible states $\{\boldsymbol{\sigma}, \boldsymbol{q}\} \in \mathbb{S} \times \mathbb{R}^m$ in stress space to lie in the set $\mathbb{E}_\sigma$ defined as:

$$\mathbb{E}_\sigma = \{(\boldsymbol{\sigma}, \boldsymbol{q}) \in \mathbb{S} \times \mathbb{R}^m | (\boldsymbol{\sigma}, \boldsymbol{q}) \leq 0\} \tag{B.4}$$

One refers to the interior of $\mathbb{E}_\sigma$, denoted by $int(\mathbb{E}_\sigma)$ and given by:

$$int(\mathbb{E}_\sigma) := \{(\boldsymbol{\sigma}, \boldsymbol{q}) \in \mathbb{S} \times \mathbb{R}^m | (\boldsymbol{\sigma}, \boldsymbol{q})0\} \tag{B.5}$$

as the elastic domain; whereas the boundary of $\mathbb{E}_\sigma$, denoted by $\partial\mathbb{E}_\sigma$ and defined as:

$$\partial\mathbb{E}_\sigma := \{(\boldsymbol{\sigma}, \boldsymbol{q}) \in \mathbb{S} \times \mathbb{R}^m | (\boldsymbol{\sigma}, \boldsymbol{q}) = 0\} \tag{B.6}$$

is called the yield surface in stress space. As in the one-dimensional case $\partial\mathbb{E}_\sigma = int(\mathbb{E}_\sigma) \bigcup \partial\mathbb{E}_\sigma$. Note that states $(\boldsymbol{\sigma}, \boldsymbol{q})$ outside $\mathbb{E}_\sigma$ are nonadmissible and are ruled out in classical plasticity.

4. Flow rule and hardening law. Loading/unloading conditions. Now we introduce the notion of irreversibility of plastic flow by the following (nonsmooth) equations of evolution for $\{\boldsymbol{\varepsilon}^p, \boldsymbol{q}\}$, called flow rule and hardening law, respectively;

$$\begin{aligned} \dot{\boldsymbol{\varepsilon}}^p &= \gamma r(\boldsymbol{\sigma}, \boldsymbol{q}) \\ \dot{\boldsymbol{q}} &= -\gamma h(\boldsymbol{\sigma}, \boldsymbol{q}) \end{aligned} \tag{B.7}$$

Here $r : \mathbb{S} \times \mathbb{R}^m \to \mathbb{S}$ and $h : \mathbb{S} \times \mathbb{R}^m \to \mathbb{R}^m$ are prescribed functions which define the direction of plastic flow and the type of hardening. The parameter $\gamma \geq 0$ is a nonnegative function, called the consistency parameter, which is assumed to obey the following Kuhn-Tucker complementarity conditions:

$$\begin{aligned} \gamma \geq 0, \quad \boldsymbol{\sigma}(\boldsymbol{\sigma}, \boldsymbol{q}) &\leq 0 \\ \gamma f(\boldsymbol{\sigma}, \boldsymbol{q}) &= 0 \end{aligned} \tag{B.8}$$

In addition to conditions B.8 $\gamma \geq 0$ satisfies the consistency requirement:

$$\gamma \dot{f}(\boldsymbol{\sigma}, \boldsymbol{q}) = 0 \tag{B.9}$$

In the classical literature, conditions B.8 and B.9 go by the names loading/un-loading and consistency conditions, respectively.

5. Consistency condition and elastoplastic tangent moduli. To exploit condition B.9, we start out by evaluating the time derivative of f at $(\boldsymbol{\sigma}, \boldsymbol{q}) \in \mathbb{E}_\sigma$. Using the chain rule, along with the rate forms of the stress-strain relationship B.4, the flow rule, and the hardening law in B.7, we find that:

$$\begin{aligned} \dot{f} &= \partial_\sigma f : \dot{\boldsymbol{\sigma}} + \partial_q f \cdot \dot{\boldsymbol{q}} \\ &= \partial_\sigma f : \mathbf{C} : [\dot{\boldsymbol{\varepsilon}} - \dot{\boldsymbol{\varepsilon}}^p] + \partial_q f \cdot \dot{\boldsymbol{q}} \\ &= \partial_\sigma f : \mathbf{C} : \dot{\boldsymbol{\varepsilon}} - \gamma \left[\partial_\sigma f : \mathbf{C} : r + \partial_q f \cdot h\right] \leq 0 \end{aligned} \tag{B.10}$$

Assuming that for associative perfect plasticity:

$$\dot{f} = 0 \Leftrightarrow \gamma = \frac{\langle \partial_\sigma f : \mathbf{C} : \dot{\boldsymbol{\varepsilon}} \rangle}{\partial_\sigma f : \mathbf{C} : r + \partial_q f \cdot h} \tag{B.11}$$

where the norm is determined by the ramp function (expressed by the Macaulay brackets $\langle . \rangle$).

Finally, according to Equations (B.4) and (B.7):

$$\dot{\boldsymbol{\sigma}} = \mathbf{C} : [\dot{\boldsymbol{\varepsilon}} - \dot{\boldsymbol{\varepsilon}}^p] = \mathbf{C} : [\dot{\boldsymbol{\varepsilon}} - \gamma r] \tag{B.12}$$

Then substituting (B.11) in (B.12) then yields the rate of change of $\boldsymbol{\sigma}$ in terms of the total strain rate $\dot{\varepsilon}$ as:

$$\dot{\boldsymbol{\sigma}} = \mathbf{C}^{tan} : \dot{\boldsymbol{\varepsilon}} \tag{B.13}$$

where $\mathbf{C}^{tan}$ is the so-called tensor of tangent elastoplastic moduli given by the expression:

$$\mathbf{C}^{tan} = \begin{cases} \mathbf{C} & if \quad \gamma = 0 \\ \mathbf{C} - \dfrac{\mathbf{C} : r \otimes \mathbf{C} : \partial_\sigma f}{\partial_\sigma f : \mathbf{C} : r + \partial_q f \cdot h} & if \quad \gamma > 0 \end{cases} \tag{B.14}$$

Note that $\mathbf{C}^{tan}$ is generally nonsymmetric for arbitrary $r(\boldsymbol{\sigma}, \boldsymbol{q})$, except in the case for which:

$$r(\boldsymbol{\sigma}, \boldsymbol{q}) = \partial_\sigma f(\boldsymbol{\sigma}, \boldsymbol{q}) \tag{B.15}$$

which has special significance and is called an associative flow rule.

B.2 J2 Flow theory with isotropic/kinematic hardening

A choice of internal plastic variables which is typically of metal plasticity is $\boldsymbol{q} := \{\alpha, \beta\}$. Here, α is the equivalent plastic strain that defines isotropic hardening of the von Mises yield surface, and β defines the center of the von Mises yield surface in stress deviator space. The resulting J_2-plasticity model has the following yield condition flow rule and hardening law:

$$\eta : = dev\left[\boldsymbol{\sigma}\right] - \bar{\beta}, tr\left[\bar{\beta}\right] := 0 \tag{B.16}$$

$$f(\boldsymbol{\sigma}, \boldsymbol{q}) = \|\eta\| - \sqrt{\frac{2}{3}} K\left(\alpha\right) \tag{B.17}$$

$$\dot{\boldsymbol{\varepsilon}}^p = \gamma \frac{\eta}{\|\eta\|} \tag{B.18}$$

$$\dot{\bar{\beta}} = \gamma \frac{2}{3} H'\left(\alpha\right) \frac{\eta}{\|\eta\|} \tag{B.19}$$

$$\dot{\alpha} = \gamma \sqrt{\frac{2}{3}} \tag{B.20}$$

The functions $K'\left(\alpha\right)$ and $H'\left(\alpha\right)$ are called the isotropic and kinematic hardening modulus, respectively. Since $\|\dot{\boldsymbol{\varepsilon}}^p\|$, relationship (B.20) implies that:

$$\alpha(t) := \int_0^t \sqrt{\frac{2}{3}} \left\|\dot{\boldsymbol{\varepsilon}}^p(\tau)\right\| d\tau \tag{B.21}$$

which agrees with the usual definition of equivalent plastic strain.

Now, the plastic consistency parameter given by (B.11) in the general case takes the explicit form:

$$\gamma = \frac{\langle n : \dot{\boldsymbol{\varepsilon}} \rangle}{1 + \frac{H' + K'}{3\mu}} \tag{B.22}$$

where:

$$n = \frac{\eta}{\|\eta\|} \tag{B.23}$$

Note that since $tr[n] = 0$, it follows that $n : \dot{\boldsymbol{\varepsilon}} \equiv n : dev\left[\dot{\boldsymbol{\varepsilon}}\right]$. Finally, for $\langle\gamma\rangle = \gamma 0$, i.e., for plastic loading, the elastoplastic tangent moduli are obtained from (B.14) as:

$$\mathbf{C}^{tan} = \kappa 1 \otimes 1 + 2\mu \left[I - \frac{1}{3} 1 \otimes 1 - \frac{n \otimes n}{1 + \frac{H' + K'}{3\mu}} \right], \quad for \quad \gamma > 0 \tag{B.24}$$

References

[1] Adkins, J. E. Non-linear diffusion I. diffusion and flow of mixtures of fluids. *Philosophical Transactions of the Royal Society of London. Series A, Mathematical and Physical Sciences 255*, 1064 (1963), pp. 607–633.

[2] Anthoine, A. Derivation of the in-plane elastic characteristics of masonry through homogenization theory. *International Journal of Solids and Structures 32*, 2 (1995), 137 – 163.

[3] Aymerich, F., and Serra, M. Prediction of fatigue strength of composite laminates by means of neural network. *Key Eng Mater 144* (1998), 231240.

[4] Badillo, H., and Oller, S. Numerical simulation of composite materials and structures using the unit cell homogenization approach. In *V International Conference on Science and Technology of Composite Materials* (2009).

[5] Bathe, K. J. *Finite Element Procedures*. Prentice-Hall, New Jersey, 1996.

[6] Bazant, Z., and Oh, B. Crack band theory for fracture of concrete. *Materials and Structures 16* (1983), 155–177. 10.1007/BF02486267.

[7] Bensoussan, A., Lions, J., and Papanicolaou, G. *Asymptotic Analysis for Periodic Structures*. North-Holland, Amsterdam, 1978.

[8] Beran, M., and Molyneux, J. E. Use of classical variational principles to determine bounds for the effective bulk modulus in heterogeneous media. *Q. Appl. Math. 24* (1966), 107–118.

[9] Bowen, R. M., and Wiese, J. C. Diffusion in mixtures of elastic materials. *International Journal of Engineering Science 7*, 7 (1969), 689 – 722.

[10] Brisard, S., and Dormieux, L. FFT-based methods for the mechanics of composites: A general variational framework. *Computational Materials Science 49*, 3 (2010), 663 – 671.

[11] Brockenbrough, J., Suresh, S., and Wienecke, H. Deformation of metal-matrix composites with continuous fibers: geometrical effects of fiber distribution and shape. *Acta Metallurgica et Materialia 39*, 5 (1991), 735 – 752.

[12] Budiansky, B. On the elastic moduli of some heterogeneous materials. *Journal of the Mechanics and Physics of Solids 13*, 4 (1965), 223 – 227.

[13] Car, E. *Modelo constitutivo continuo para el estudio del comportamiento mecánico de los materiales compuestos (in Spanish)*. PhD thesis, Strength of materials and structures in engineering department. Technical University of Catalonia, 2000.

[14] Car, E., Oller, S., and Oñate, E. An anisotropic elastoplastic constitutive model for large strain analysis of fiber reinforced composite materials. *Computer Methods in Applied Mechanics and Engineering 185*, 2-4 (2000), 245 – 277.

[15] Cartraud, P., and Messager, T. Computational homogenization of periodic beam-like structures. *International Journal of Solids and Structures 43*, 3-4 (2006), 686 – 696.

[16] Cervera, M., and Chiumenti, M. Mesh objective tensile cracking via a local continuum damage model and a crack tracking technique. *Computer Methods in Applied Mechanics and Engineering 196*, 1-3 (2006), 304 – 320.

[17] Chandrashekhara, K., Okafor, A. C., and Jiang, Y. P. Estimation of contact force on composite plates using impact-induced strain and neural networks. *Composites Part B: Engineering 29*, 4 (1998), 363 – 370.

[18] Christensen, R. M., and Lo, K. H. Solutions for effective shear properties in three phase sphere and cylinder models. *Journal of the Mechanics and Physics of Solids 27*, 4 (1979), 315 – 330.

[19] CIMNE. *PLCd - Non-linear thermomechanic finite element code*. International Center of Numerical Methods in Enginering, (1991-2008). Finite element code oriented to PhD student education.

[20] Coenen, E., Kouznetsova, V., and Geers, M. Computational homogenization for heterogeneous thin sheets. *International Journal for Numerical Methods in Engineering 83*, 8-9 (2010), 1180 – 1205.

[21] De Bellis, M. L. *A Cosserat based Multi-Scale Technique for Masonry Structures*. PhD thesis, Universit di Roma Sapienza, 2009.

[22] Devries, F., Dumontet, H., Duvaut, G., and Lene, F. Homogenization and damage for composite structures. *Int. J. Numer. Meth. Engng. 27*, 2 (1989), 285–298.

[23] Drugan, W. J., and Willis, J. R. A micromechanics-based nonlocal constitutive equation and estimates of representative volume element size for elastic composites. *Journal of the Mechanics and Physics of Solids 44*, 4 (1996), 497 – 524.

[24] Dumontet, H. Study of a boundary layer problem in elastic composite materials. *RAIRO. Mathematical Modelling and Numerical Analysis. 20* (1986), 265–286.

[25] Eager, D., Zahorjan, J., and Lazowska, E. Speedup versus efficiency in parallel systems. *Computers, IEEE Transactions on 38*, 3 (mar 1989), 408 –423.

[26] Eshelby, J. The determination of the elastic field of an ellipsoidal inclusion and related problems. In *Proceedings of The Royal Society* (1957), vol. 241, pp. 376–396.

[27] Feyel, F., and Chaboche, J.-L. Fe2 multiscale approach for modelling the elastoviscoplastic behaviour of long fibre sic/ti composite materials. *Computer Methods in Applied Mechanics and Engineering 183*, 3-4 (2000), 309 – 330.

[28] Fish, J., and Belsky, V. Multi-grid method for periodic heterogeneous media part 2: Multiscale modeling and quality control in multidimensional case. *Computer Methods in Applied Mechanics and Engineering 126*, 1-2 (1995), 17 – 38.

[29] Fish, J., and Wagiman, A. Multiscale finite element method for a locally nonperiodic heterogeneous medium. *Computational Mechanics 12* (1993), 164–180. 10.1007/BF00371991.

[30] Fish, J., Yu, Q., and Shek, K. Computational damage mechanics for composite materials based on mathematical homogenization. *Int. J. Numer. Meth. Engng. 45*, 11 (1999), 1657–1679.

[31] Forest, S., Pradel, F., and Sab, K. Asymptotic analysis of heterogeneous cosserat media. *International Journal of Solids and Structures 38*, 26-27 (2001), 4585 – 4608.

[32] Galli, M., Botsis, J., and Janczak-Rusch, J. An elastoplastic three-dimensional homogenization model for particle reinforced composites. *Computational Materials Science 41*, 3 (2008), 312 – 321.

[33] Ghosh, S., Lee, K., and Moorthy, S. Multiple scale analysis of heterogeneous elastic structures using homogenization theory and voronoi cell finite element method. *International Journal of Solids and Structures 32*, 1 (1995), 27 – 62.

[34] Ghosh, S., Lee, K., and Moorthy, S. Two scale analysis of heterogeneous elastic-plastic materials with asymptotic homogenization and voronoi cell finite element model. *Computer Methods in Applied Mechanics and Engineering 132*, 1-2 (1996), 63 – 116.

[35] Ghosh, S., and Liu, Y. Voronoi cell finite element model based on micropolar theory of thermoelasticity for heterogeneous materials. *Int. J. Numer. Methods Eng. 38*, 8 (1995), 1361–1398.

[36] Ghosh, S., and Moorthy, S. Elastic-plastic analysis of arbitrary heterogeneous materials with the voronoi cell finite element method. *Computer Methods in Applied Mechanics and Engineering 121*, 1-4 (1995), 373 – 409.

[37] Ghosh, S., and Mukhopadhyay, S. A two-dimensional automatic mesh generator for finite element analysis for random composites. *Computers & Structures 41*, 2 (1991), 245 – 256.

[38] Ghosh, S., and Mukhopadhyay, S. N. A material based finite element analysis of heterogeneous media involving dirichlet tessellations. *Computer Methods in Applied Mechanics and Engineering 104*, 2 (1993), 211 – 247.

[39] Gitman, I., Askes, H., and Sluys, L. Representative volume: Existence and size determination. *Engineering Fracture Mechanics 74*, 16 (2007), 2518 – 2534.

[40] Gonzlez, C., and LLorca, J. A self-consistent approach to the elasto-plastic behaviour of two-phase materials including damage. *Journal of the Mechanics and Physics of Solids 48*, 4 (2000), 675 – 692.

[41] Green, A. E., and Adkins, J. E. A contribution to the theory of non-linear diffusion. *Archive for Rational Mechanics and Analysis 15* (1964), 235–246. 10.1007/BF00275633.

[42] Green, A. E., and Naghdi, P. M. A dynamical theory of interacting continua. *International Journal of Engineering Science 3*, 2 (1965), 231 – 241.

[43] Guedes, J. M., and Kikuchi, N. Preprocessing and postprocessing for materials based on the homogenization method with adaptive finite element methods. *Computer Methods in Applied Mechanics and Engineering 83*, 2 (1990), 143 – 198.

[44] Haj-Ali, R., Kilic, H., and Muliana, A. Nested nonlinear micromechanical and structural models for the analysis of thick-section composite materials and structures. *Composites Science and Technology 67*, 10 (2007), 1993 – 2004.

[45] Haj-Ali, R., and Kim, H.-K. Nonlinear constitutive models for frp composites using artificial neural networks. *Mechanics of Materials 39*, 12 (2007), 1035 – 1042.

[46] Haj-Ali, R. M., and Muliana, A. H. A micromechanical constitutive framework for the nonlinear viscoelastic behavior of pultruded composite materials. *International Journal of Solids and Structures 40*, 5 (2003), 1037 – 1057.

[47] Haj-Ali, R. M., and Muliana, A. H. A multi-scale constitutive formulation for the nonlinear viscoelastic analysis of laminated composite materials and structures. *International Journal of Solids and Structures 41*, 13 (2004), 3461 – 3490.

[48] Hami, A. E., and Radi, B. Some decomposition methods in the analysis of repetitive structures. *Computers & Structures 58*, 5 (1996), 973 – 980.

[49] Hashin, Z. The elastic moduli of heterogeneous materials. *Journal of Applied Mechanics 29* (1962), 143150.

[50] Hashin, Z., and Shtrikman, S. On some variational principles in anisotropic and nonhomogeneous elasticity. *Journal of the Mechanics and Physics of Solids 10*, 4 (1962), 335 – 342.

[51] Hill, R. A self-consistent mechanics of composite materials. *Journal of the Mechanics and Physics of Solids 13* (1965), 213–222.

[52] Hughes, T. J. R. *The Finite Element Method: Linear Static and Dynamic Finite Element Analysis*. Dover Publications, 2000.

[53] Jardak, M., and Ghanem, R. G. Spectral stochastic homogenization of divergence-type pdes. *Computer Methods in Applied Mechanics and Engineering 193*, 6-8 (2004), 429 – 447.

[54] Kaczmarczyk, L., Pearce, C. J., and Biani, N. Scale transition and enforcement of rve boundary conditions in second-order computational homogenization. *International Journal for Numerical Methods in Engineering 74*, 3 (2008), 506–522.

[55] Kaczmarczyk, L., Pearce, C. J., and Bicanic, N. Studies of microstructural size effect and higher-order deformation in second-order computational homogenization. *Computers & Structures In Press, Corrected Proof* (2008), –.

[56] Kadi, H. E. Modeling the mechanical behavior of fiber-reinforced polymeric composite materials using artificial neural networks–a review. *Composite Structures 73*, 1 (2006), 1 – 23.

[57] Kaminski, M., and Kleiber, M. Perturbation based stochastic finite element method for homogenization of two-phase elastic composites. *Computers & Structures 78*, 6 (2000), 811 – 826.

[58] Kouznetsova, V., Geers, M., and Brekelmans, W. Multi-scale second-order computational homogenization of multi-phase materials: a nested finite element solution strategy. *Computer Methods in Applied Mechanics and Engineering 193*, 48-51 (2004), 5525 – 5550. Advances in Computational Plasticity.

[59] Kouznetsova, V., Geers, M. G. D., and Brekelmans, W. A. M. Multi-scale constitutive modelling of heterogeneous materials with a gradient-enhanced computational homogenization scheme. *International Journal for Numerical Methods in Engineering 54*, 8 (2002), 1235–1260.

[60] Kröner, E. Elastic moduli of perfectly disordered composite materials. *Journal of the Mechanics and Physics of Solids 15*, 5 (1967), 319 – 329.

[61] Ladevèze, P. New approaches and non-incremental methods of calculation. In *Nonlinear Computational Structural Mechanics*, Mechanical Engineering Series. Springer Verlag, 1999.

[62] Ladevèze, P. Multiscale modelling and computational strategies for composites. *International Journal for Numerical Methods in Engineering 60*, 1 (2004), 233–253.

[63] Ladevèze, P., Loiseau, O., and Dureisseix, D. A micro macro and parallel computational strategy for highly heterogeneous structures. *International Journal for Numerical Methods in Engineering 52*, 1-2 (2001), 121–138.

[64] Ladevèze, P., Néron, D., and Gosselet, P. On a mixed and multiscale domain decomposition method. *Computer Methods in Applied Mechanics and Engineering 196*, 8 (2007), 1526 – 1540. Domain Decomposition Methods: recent advances and new challenges in engineering.

[65] Ladevèze, P., and Nouy, A. On a multiscale computational strategy with time and space homogenization for structural mechanics. *Computer Methods in Applied Mechanics and Engineering 192*, 28-30 (2003), 3061 – 3087. Multiscale Computational Mechanics for Materials and Structures.

[66] Lahellec, N., and Suquet, P. On the effective behavior of nonlinear inelastic composites: I. incremental variational principles. *Journal of the Mechanics and Physics of Solids 55*, 9 (2007), 1932 – 1963.

[67] Lahellec, N., and Suquet, P. On the effective behavior of nonlinear inelastic composites: Ii: A second-order procedure. *Journal of the Mechanics and Physics of Solids 55*, 9 (2007), 1964 – 1992.

[68] Lee, J. A., Almond, D. P., and Harris, B. The use of neural networks for the prediction of fatigue lives of composite materials. *Composites Part A: Applied Science and Manufacturing 30*, 10 (1999), 1159 – 1169.

[69] Lee, K., Moorthy, S., and Ghosh, S. Multiple scale computational model for damage in composite materials. *Computer Methods in Applied Mechanics and Engineering 172*, 1-4 (1999), 175 – 201.

[70] Lefik, M., Boso, D., and Schrefler, B. Artificial neural networks in numerical modelling of composites. *Computer Methods in Applied Mechanics and Engineering 198*, 21-26 (2009), 1785 – 1804. Advances in Simulation-Based Engineering Sciences - Honoring J. Tinsley Oden.

[71] Martinez, X., Oller, S., Rastellini, F., and Barbat, A. H. A numerical procedure simulating rc structures reinforced with frp using the serial/parallel mixing theory. *Computers & Structures 86*, 15-16 (2008), 1604 – 1618.

[72] Mercier, S., Jacques, N., and Molinari, A. Validation of an interaction law for the eshelby inclusion problem in elasto-viscoplasticity. *International Journal of Solids and Structures 42*, 7 (2005), 1923 – 1941.

[73] Mercier, S., and Molinari, A. Homogenization of elastic-viscoplastic heterogeneous materials: Self-consistent and mori-tanaka schemes. *International Journal of Plasticity 25*, 6 (2009), 1024 – 1048.

[74] Michel, J., Moulinec, H., and Suquet, P. Effective properties of composite materials with periodic microstructure: a computational approach. *Computer Methods in Applied Mechanics and Engineering 172*, 1-4 (1999), 109 – 143.

[75] Miehe, C. Numerical computation of algorithmic (consistent) tangent moduli in large-strain computational inelasticity. *Computer Methods in Applied Mechanics and Engineering 134*, 3-4 (Aug. 1996), 223–240.

[76] Molinari, A. Averaging models for heterogeneous viscoplastic and elastic viscoplastic materials. *Journal of Engineering Materials and Technology 124*, 1 (2002), 62–70.

[77] Mori, T., and Tanaka, K. Average stress in matrix and average elastic energy of materials with misfitting inclusions. *Acta Metallurgica 21*, 5 (1973), 571 – 574.

[78] Moulinec, H., and Suquet, P. A fast numerical method for computing the linear and nonlinear properties of composites. *C.R. Acad. SC. II-318* (1994), 1417–1423.

[79] Moulinec, H., and Suquet, P. A fftbased numerical method for computing the mechanical properties of composites from images of their microstructure. In *Microstructure-Property Interactions in Composite Materials*, R. Pyrz, Ed. Kluwer Academic, 1995, pp. 235–246.

[80] Moulinec, H., and Suquet, P. A numerical method for computing the overall response of nonlinear composites with complex microstructure. *Computer Methods in Applied Mechanics and Engineering 157*, 1-2 (1998), 69 – 94.

[81] Nouy, A., and Ladevèze, P. Multiscale computational strategy with time and space homogenization: A radial-type approximation technique for solving microproblems. *International Journal for Multiscale Computational Engineering 2*, 4 (2004), 18.

[82] Oñate, E., Neamtu, L., and Oller, S. Un modelo constitutivo para el análisis por el mef para materiales compuestos. In *J. Gemes & C. Navarro (Eds.), Materiales Compuestos 97* (1997), pp. 206–211.

[83] Oliver, J. A consistent characteristic length for smeared cracking models. *International Journal for Numerical Methods in Engineering 28*, 2 (1989), 461–474.

[84] Oliver, J., Cervera, M., Oller, S., and Lubliner, J. Isotropic damage models and smeared crack analysis of concrete. In *Second International Conference on Analysis and Design of Concrete Structures* (1990), vol. 2, p. 945958.

[85] Oliver, J., Huespe, A. E., Pulido, M. D. G., and Chaves, E. From continuum mechanics to fracture mechanics: the strong discontinuity approach. *Engineering Fracture Mechanics 69*, 2 (2002), 113 – 136.

[86] Oller, S. *Un Modelo de Daño Continuo para Materiales Friccionales*. PhD thesis, Strength of materials and structures in engineering department. Technical University of Catalonia, 1988.

[87] Oller, S. *Fractura mecánica. Un enfoque global*. Centro Internacional de Métodos Numéricos en Ingeniería - CIMNE, 2001.

[88] Oller, S. *Simulación numérica del comportamiento mecánico de los materiales compuestos*. Centro Internacional de Métodos Numéricos en Ingeniería - CIMNE, 2003.

[89] Oller, S., Botello, S., Miquel, J., and Oñate, E. An anisotropic elastoplastic model based on an isotropic formulation. *Engineering Computations 12*, 3 (1995), 245–262.

[90] Oller, S., Canet, J. M., and Zalamea, F. Composite material behavior using a homogenization double scale method. *Journal of Engineering Mechanics 131*, 1 (2005), 65–79.

[91] Oller, S., Neamtu, L., and Oñate, E. Una generalización de la teoría de mezclas clásica para el tratamiento de compuestos en serie/paralelo. In *Congreso Nacional de Materiales Compuestos* (1995), pp. 433–438.

[92] Ortiz, M., and Popov, E. A physical model for the inelasticity of concrete. In *Proceedings of The Royal Society* (1982), vol. A383, pp. 101–125.

[93] Ortiz, M., and Popov, E. P. Plain concrete as a composite material. *Mechanics of Materials 1*, 2 (1982), 139 – 150.

[94] Ostoja-Starzewski, M. Random field models of heterogeneous materials. *International Journal of Solids and Structures 35*, 19 (1998), 2429 – 2455.

[95] Pidaparti, R., and Palakal, M. Material model for composites using neural networks. Tech. Rep. 31:15335, AIAA J, 1993.

[96] Ponte Castañeda, P. New variational principles in plasticity and their application to composite materials. *Journal of the Mechanics and Physics of Solids 40*, 8 (1992), 1757 – 1788.

[97] Ponte Castañeda, P. Exact second-order estimates for the effective mechanical properties of nonlinear composite materials. *Journal of the Mechanics and Physics of Solids 44*, 6 (1996), 827 – 862.

[98] Rastellini, F. *Modelización numérica de la no-linealidad constitutiva de laminados compuestos(in Spanish)*. PhD thesis, Strength of materials and structures in engineering department. Technical University of Catalonia, 2006.

[99] Rastellini, F., Oller, S., Salomón, O., and nate., E. O. Composite materials non-linear modelling for long fibre-reinforced laminates: Continuum basis, computational aspects and validations. *Computers & Structures 86*, 9 (2008), 879 – 896. Composites.

[100] Renard, J., and Marmonier, M. Etude de léinitiation de léendommagement dans la matrice déun matériau composite par une méthode d´homogénisation. *Aerosp. Sci. Technol. 6* (1987), 3751.

[101] Reuss, A. Calculation of the flow limits of mixed crystals on the basis of the plasticity of mono-crystals. *Z. Anger. Math. Mech. 9* (1929), 49–58.

[102] Sakata, S., Ashida, F., Kojima, T., and Zako, M. Three-dimensional stochastic analysis using a perturbation-based homogenization method for elastic properties of composite material considering microscopic uncertainty. *International Journal of Solids and Structures 45*, 3-4 (2008), 894 – 907.

[103] Sanchez-Palencia, E. Non-homogeneous media and vibration theory. In *Lecture Notes in Physics*, vol. 127. Springer-Verlag, Berlin, 1980.

[104] Sanchez-Palencia, E. Homogenization method for the study of composite media. In *Asymptotic Analysis II* , F. Verhulst, Ed., vol. 985 of *Lecture Notes in Mathematics*. Springer Berlin / Heidelberg, 1983, pp. 192–214. 10.1007/BFb0062368.

[105] Sanchez-Palencia, E. Homogenization in mechanics. a survey of solved and open problems. In *Rend. Sem. Mat. Univ. Politec. Torino* (1986), vol. 44, pp. 1–45.

[106] Simo, J., and Ju, J. Strain- and stress-based continuum damage models - i. formulation. *International Journal of Solids and Structures 23*, 7 (1987), 821 – 840.

[107] Simo, J. C., and Hughes, T. J. R. *Computational Inelasticity*, vol. 7 of *Interdisciplinary Applied Mathematics*. Springer, 1998.

[108] Smit, R. J. M., Brekelmans, W. A. M., and Meijer, H. E. H. Prediction of the mechanical behavior of nonlinear heterogeneous systems by multi-level finite element modeling. *Computer Methods in Applied Mechanics and Engineering 155*, 1-2 (1998), 181 – 192.

[109] Spitzig, W., Kelly, J., and Richmond, O. Quantitative characterization of second-phase populations. *Metallography 18*, 3 (1985), 235 – 261.

[110] Suquet, P. Local and global aspects in the mathematical theory of plasticity. In *Plasticity Today - Modeling Methods and Applications*, A. Sawczuk and G. Bianchi, Eds. Elsevier, London, 1985.

[111] Swan, C. C. Techniques for stress- and strain-controlled homogenization of inelastic periodic composites. *Computer Methods in Applied Mechanics and Engineering 117*, 3-4 (1994), 249 – 267.

[112] Swan, C. C., and Cakmak, A. S. Homogenization and effective elastoplasticity models for periodic composites. *Communications in Numerical Methods in Engineering 10*, 3 (1994), 257–265.

[113] Takano, N., and Okuno, Y. Three-scale finite element analysis of heterogeneous media by asymptotic homogenization and mesh superposition methods. *International Journal of Solids and Structures 41*, 15 (2004), 4121 – 4135.

[114] Takano, N., Uetsuji, Y., Kashiwagi, Y., and Zako, M. Hierarchical modelling of textile composite materials and structures by the homogenization method. *Modelling and Simulation in Materials Science and Engineering 7*, 2 (1999), 207.

[115] Talbot, D. R. S., and Willis, J. R. Bounds of third order for the overall response of nonlinear composites. *Journal of the Mechanics and Physics of Solids 45*, 1 (1997), 87 – 111.

[116] Terada, K., Hori, M., Kyoya, T., and Kikuchi, N. Simulation of the multi-scale convergence in computational homogenization approaches. *International Journal of Solids and Structures 37*, 16 (2000), 2285 – 2311.

[117] Todoroki, A. The effect of number of electrodes and diagnostic tool for monitoring the delamination of cfrp laminates by changes in electrical resistance. *Composites Science and Technology 61*, 13 (2001), 1871 – 1880.

[118] Tootkaboni, M., and Graham-Brady, L. A multi-scale spectral stochastic method for homogenization of multi-phase periodic composites with random material properties. *Int. J. Numer. Meth. Engng. 83*, 1 (2010), 59–90.

[119] Truesdell, C. Mechanical basis of diffusion. *The Journal of Chemical Physics 37*, 10 (1962), 2336–2344.

[120] Truesdell, C., and Toupin, R. *The classical Field Theories. Handbuch der Physik III/I*. Springer Verlag, Berlin, 1960.

[121] Unger, J. F., and Könke, C. Coupling of scales in a multiscale simulation using neural networks. *Computers & Structures 86*, 21-22 (2008), 1994 – 2003.

[122] Walpole, L. On bounds for the overall elastic moduli of inhomogeneous systems–i. *Journal of the Mechanics and Physics of Solids 14*, 3 (1966), 151 – 162.

[123] Wellmann, C., Lillie, C., and Wriggers, P. Homogenization of granular material modeled by a three-dimensional discrete element method. *Computers and Geotechnics 35*, 3 (2008), 394 – 405.

[124] Xu, X., and Graham-Brady, L. A stochastic computational method for evaluation of global and local behavior of random elastic media. *Computer Methods in Applied Mechanics and Engineering 194*, 42-44 (2005), 4362 – 4385.

[125] Yuan, Z., and Fish, J. Hierarchical model reduction at multiple scales. *Int. J. Numer. Meth. Engng. 79*, 3 (2009), 314–339.

[126] Zalamea, F. *Tratamiento numérico de materiales compuestos mediante la teoría de homogeneización(in Spanish)*. PhD thesis, Strength of materials and structures in engineering department. Technical University of Catalonia, 2000.

[127] Zeman, J., Vondrejc, J., Novk, J., and Marek, I. Accelerating a fft-based solver for numerical homogenization of periodic media by conjugate gradients. *Journal of Computational Physics 229*, 21 (2010), 8065 – 8071.

[128] Zhang, Z., and Friedrich, K. Artificial neural networks applied to polymer composites: a review. *Composites Science and Technology 63*, 14 (2003), 2029 – 2044. Polymer Composites: Design, Materials, Manufacturing, Dedicated to Professor M. Neitzel.

[129] Zienkiewicz, O., and Taylor, R. *The Finite Element Method, Volumes 1 and 2*. Mc Graw Hill, 1988.

Happy Xmas. The war is over!